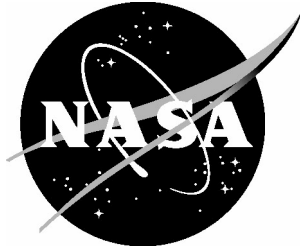


NASA/TM-2005-213529



Measurements of Flow Turbulence in the NASA Langley Transonic Dynamics Tunnel

*Carol D. Wieseman and Robert K. Sleeper
Langley Research Center, Hampton, Virginia*

February 2005

The NASA STI Program Office . . . in Profile

Since its founding, NASA has been dedicated to the advancement of aeronautics and space science. The NASA Scientific and Technical Information (STI) Program Office plays a key part in helping NASA maintain this important role.

The NASA STI Program Office is operated by Langley Research Center, the lead center for NASA's scientific and technical information. The NASA STI Program Office provides access to the NASA STI Database, the largest collection of aeronautical and space science STI in the world. The Program Office is also NASA's institutional mechanism for disseminating the results of its research and development activities. These results are published by NASA in the NASA STI Report Series, which includes the following report types:

- **TECHNICAL PUBLICATION.** Reports of completed research or a major significant phase of research that present the results of NASA programs and include extensive data or theoretical analysis. Includes compilations of significant scientific and technical data and information deemed to be of continuing reference value. NASA counterpart of peer-reviewed formal professional papers, but having less stringent limitations on manuscript length and extent of graphic presentations.
- **TECHNICAL MEMORANDUM.** Scientific and technical findings that are preliminary or of specialized interest, e.g., quick release reports, working papers, and bibliographies that contain minimal annotation. Does not contain extensive analysis.
- **CONTRACTOR REPORT.** Scientific and technical findings by NASA-sponsored contractors and grantees.

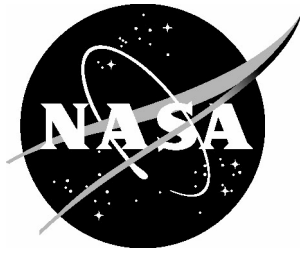
- **CONFERENCE PUBLICATION.** Collected papers from scientific and technical conferences, symposia, seminars, or other meetings sponsored or co-sponsored by NASA.
- **SPECIAL PUBLICATION.** Scientific, technical, or historical information from NASA programs, projects, and missions, often concerned with subjects having substantial public interest.
- **TECHNICAL TRANSLATION.** English-language translations of foreign scientific and technical material pertinent to NASA's mission.

Specialized services that complement the STI Program Office's diverse offerings include creating custom thesauri, building customized databases, organizing and publishing research results ... even providing videos.

For more information about the NASA STI Program Office, see the following:

- Access the NASA STI Program Home Page at <http://www.sti.nasa.gov>
- E-mail your question via the Internet to help@sti.nasa.gov
- Fax your question to the NASA STI Help Desk at (301) 621-0134
- Phone the NASA STI Help Desk at (301) 621-0390
- Write to:
NASA STI Help Desk
NASA Center for AeroSpace Information
7121 Standard Drive
Hanover, MD 21076-1320

NASA/TM-2005-213529



Measurements of Flow Turbulence in the NASA Langley Transonic Dynamics Tunnel

*Carol D. Wieseman and Robert K. Sleeper
Langley Research Center, Hampton, Virginia*

National Aeronautics and
Space Administration

Langley Research Center
Hampton, Virginia 23681-2199

February 2005

Available from:

NASA Center for AeroSpace Information (CASI)
7121 Standard Drive
Hanover, MD 21076-1320
(301) 621-0390

National Technical Information Service (NTIS)
5285 Port Royal Road
Springfield, VA 22161-2171
(703) 605-6000

Abstract

An assessment of the flow turbulence in the NASA Langley Transonic Dynamics Tunnel (TDT) was conducted during calibration activities following the facility conversion from a Freon-12 heavy-gas test medium to an R134a heavy-gas test medium. Total pressure, static pressure, and acoustic pressure levels were measured at several locations on a sting-mounted rake. The test measured wall static pressures at several locations although this paper presents only those from one location. The test used two data acquisition systems, one sampling at 1000 Hz and the second sampling at 125 000 Hz, for acquiring time-domain data. This paper presents standard deviations and power spectral densities of the turbulence points throughout the wind tunnel envelope in air and R134a. The objective of this paper is to present the turbulence characteristics for the test section. No attempt is made to assess the causes of the turbulence. The present paper looks at turbulence in terms of pressure fluctuations. Reference 1 looked at tunnel turbulence in terms of velocity fluctuations.

Introduction

Wind tunnels, like other engineering devices, require calibration in order to provide reliable and accurate information. A wind tunnel calibration involves determining the mean values and uniformity of various flow parameters in the tunnel test section. For a low-speed tunnel that operates at Mach numbers of 0.5 and below, the calibration typically involves determining the distribution of dynamic pressure, static pressure, total pressure, temperature, turbulence, and flow angularity. The calibration of tunnels that operate in the transonic and supersonic regions (Mach numbers from 0.8 to 5.0) is focused on determining the distribution of Mach numbers along the test section centerline. A good distribution of Mach numbers along the test section of a transonic tunnel is generally indicative of smooth flow (ref. 2); however, the assessment should still determine flow angularity and turbulence for completeness.

Wind tunnel calibrations are typically conducted on a regular basis to monitor flow conditions or after any changes or modifications have been made to the facility. In the case of the Langley Transonic Dynamics Tunnel (TDT), a calibration was conducted following a facility modification. This report documents the tunnel turbulence in the TDT.

The TDT is a closed-circuit, continuous-flow, slotted test section, transonic wind tunnel, specifically designed to conduct dynamic tests associated with aeroelastic research. This research includes the study of flutter, buffet, aerodynamic loads, forced response, and active control using aeroelastic models (refs. 3–7).

The TDT has a 16- by 16-ft slotted test section and is capable of Mach numbers from near 0 to 1.2. Stagnation pressures from near vacuum to atmospheric pressure and dynamic pressures from near 0 to 550 psf are possible, depending on the test medium. Tests in the TDT can be conducted in air or in a heavy-gas test medium. The heavy-gas testing offers advantages for testing aeroelastically scaled models.

The TDT is a unique facility for testing aeroelastic models large enough to allow the accurate scaling of mass and stiffness distributions from the full-scale vehicle to the model. Besides matching such important model structural and mass properties, it is imperative for high subsonic and transonic flutter models that full-scale Mach numbers be matched because of compressibility effects. In addition, other dimensionless quantities, such as reduced frequency and Froude number, must also be matched for the model at wind tunnel test conditions to adequately represent the airplane at full-scale flight conditions. Using typical model design techniques, it is not possible to match Mach number, Froude number, and reduced frequency simultaneously using air as the test medium in a wind tunnel. However, it is sometimes possible to match these dimensionless parameters by using heavy gas as the test medium.

In 1997, the TDT underwent a conversion from a Freon-12 test medium to an R134a test medium for environmental purposes. Reference 8 describes the TDT heavy-gas conversion process. Because of the change in test medium, it was necessary to determine the TDT performance envelope and document various test section flow parameters before regular testing resumed. Over the period of a year, an exhaustive calibration effort took place involving sidewall pressures (ref. 9), survey rake measurements of flow angularity (ref. 10), centerline measurements of Mach number distribution, boundary layer measurements, and survey rake measurements of flow turbulence.

The objective of this paper is to present the turbulence data for the test section in terms of standard deviation and spectral characteristics of pressures.

Nomenclature

ASC	all slots closed
BPF	blade passing frequency, Hz (=RPM * 47/60)
DAS	data acquisition system
$G_{\bar{p}/q}(f)$	normalized power spectral density function of pressure, per Hz
M	Mach number
P	pressure, psf
PSD	power spectral density
P_t	total pressure, psf
q	dynamic pressure, psf
R	Reynolds number
RMS	root-mean-square
RPM	motor revolutions per minute
T	temperature, °F

TDT	Transonic Dynamics Tunnel
TS	tunnel station, ft
WSC	wall slots closed
$\sigma_{\tilde{p}}$	standard deviation, psf
$\sigma_{\tilde{p}/q}$	normalized standard deviation of pressure, expressed as a percent

Apparatus and Procedures

The apparatus consists of the wind tunnel, rake and probes, and the data acquisition equipment.

Wind Tunnel

The TDT is a continuous-flow, transonic wind tunnel which has many unique features that make it suitable for aeroelastic testing. The facility is capable of attaining Mach numbers between near 0 to 1.2 in either air or R134a as a test medium. Stagnation pressures from near zero to atmospheric pressure are possible, and dynamic pressures up to 550 psf are possible using R134a as a test medium.

Figure 1 shows an aerial photograph of the TDT. Figures 2 and 3 provide detailed drawings of the layout of the TDT. The major components of the TDT include a steel pressure shell, settling chamber, contraction section, slotted test section with plenum chamber, diffuser section, electric drive system with a 47 blade fan, and a high-volume gas handling system for heavy-gas operations. The whole tunnel encloses a volume of about a million cubic feet.

A 60-ft-diameter plenum chamber surrounds the 16- by 16-ft test section that has three slots in both the ceiling and the floor and two slots on each of the walls to provide an adequate area for flow expansion and, therefore, enables transonic testing. The transonic slot shapes provide a nearly gradient free region of flow at transonic speeds in the vicinity of a model.

The test chamber, which can be isolated from the rest of the tunnel using the butterfly and gate valves (fig. 3), is composed of the 16-ft square test section and the 60-ft-diameter plenum chamber that surrounds it. During operations above Mach 0.85, double-hinged reentry flaps in the floor and ceiling are progressively opened to allow flow that exits the test section through the transonic slots to reenter the main flow in the diffuser section. The tunnel flow reentry flaps are outlined in the downstream view in figure 4. This figure also shows the slots located on the walls and ceiling of the test section. The slots on the floor were covered at the time this photo was taken. This photo includes boundary layer rakes mounted on the floor, ceiling, and walls, which were used for another calibration test but were not present in the test section for the turbulence measurement tests. Figure 5 shows a schematic of the reentry flap operation, including the flap schedule.

The flow is powered by a 30 000-hp fan drive motor and enhanced by the reentry flap settings and remotely controlled prerotation vanes. Figure 6 shows the location of the prerotation vanes as directly upstream of the fan blades. The figure also shows a few of the 47 fan blades immediately behind the prerotation vanes. The vanes only pivot about their spanwise axis to change the angle of flow impinging on the fan blades. Smaller prerotation vane angles would attain higher speeds, but greater angles provide

better operating efficiency. The prerotation vanes are only rotated at the upper limits of the tunnel operation when additional speeds are required that cannot be obtained just by increasing tunnel motor power and rotation rate.

Tunnel flow cooling is provided at the turning vanes downstream of the motor to limit temperature to a maximum of 120° to 130°. The tunnel has two screens, one a model debris catch screen upstream of the prerotation vanes and the other a flow-smoothing screen near the downstream tip of the fan motor nacelle.

Figures 7 and 8 show significant portions of the TDT operating envelopes as functions of Mach number and dynamic pressure for air and for R134a. Superimposed on these figures are the open-slot test points at which turbulence data were acquired to be presented in this paper.

Rake and Measurements

A survey rake, 10.5 ft in length with provision for mounting 11 probes, was installed horizontally in the test section. Figure 9 shows how the rake was mounted to a sting. This survey rake was also used to mount probes to measure flow angularity (ref. 10). The rake schematic in figure 10 shows a detailed layout of the rake, identifying the sensors and their locations. A shaped plug filled the unused probe receptacles.

The leading edge of the rake has three different types of pressure probes mounted on it. These pressure probes measured (1) unsteady total pressures at stations 3 and 9 on the rake, (2) fluctuating static pressure at station 5, and (3) sound pressure measured by an acoustic pressure probe (microphone) at station 4.

Langley manufactured the unsteady total pressure probes using 0.25-in-diameter stainless steel tubing and miniature ± 2 psig piezoresistive pressure-differential sensors designed to have a flat frequency response up to 15 KHz. Figure 11(a) shows a total pressure probe, an adapter, and a probe with the adapter installed. Figure 11(b) is a close-up view of the flat face of a total pressure probe tip showing the head of an embedded sensor and a 0.02-in-diameter reference pressure orifice. A 10-ft length of 0.015-in-internal diameter flexible tubing feeds the orifice pressure back to the sensor reference. The tubing provides a damped probe-face pressure for the sensor reference pressure, yielding the fluctuating portion of the unsteady total pressure measurement.

The static pressure probe located at station 5 was similar in design to that described in reference 11. It also has a flat frequency up to 15 KHz. Figure 12 shows the components of the static pressure probe. From top to bottom, they consist of the probe-to-rake adapter and the outer and inner probe components. The sensor is mounted on the inner component. The outer component has a tip with a general ogive shape and a 0.02-in-diameter orifice along its side leading to the sensor of the inner component and located 2.5 in. aft of the tip. The reference tube of the sensor was exposed to the tunnel static pressure during the test. The primary calibrations of the static and total pressure sensors were conducted under laboratory conditions before they were installed into their probe housings. Once installed there was no easy way to calibrate the pressure sensors; however, known pressures were applied to the transducers as a check on their measurements.

The acoustic pressure probe (microphone) was located at station 4. It had a 0.125-in-diameter diaphragm and a nose cone as shown in figure 13(a). Figure 13(b) shows the probe system. The probe calibration curve provided with the instrument showed it to exhibit a flat frequency response from 20 to 50 000 Hz.

Static pressure probes were also mounted flush with the test section walls and centered vertically between the floor and the ceiling. The wall probes were located in the east wall (port) at tunnel stations 43, 76, 87, 95, and 108 and in the west wall (starboard) at station 95, where tunnel stations are measured in feet. This report presents only the port probe measurements at station 43. Station 43 is forward of the typical location of most wind tunnel models; however, it is the closest to the models being tested. The measurement of the wall pressure at tunnel station 76 exhibited low-frequency oscillations and, at times, linear trends within the data record. The linear trends were unexplainable and rendered the data untrustworthy and, therefore, are not included in this report, although these data would have been of interest because of the proximity to where the wall mounted models would be installed. Most wind tunnel models are mounted to be centered at tunnel station 72 in the test section.

Additionally, stations 2, 6, and 10 had hot-wire anemometer X-probes installed on the rake; however, measurement difficulties precluded the derivation of useful data from them.

The rake was equipped with three accelerometers positioned 1 ft aft of the probe tips with lateral locations of -4.84 , -0.16 , and 4.84 ft with respect to the rake center where positive values denote a starboard location. Table 1 provides the modes and frequencies of the rake and sting.

Data Acquisition

The test measured all data as analog signals. As shown in figure 14, the test sampled data using two data acquisition systems (DASs). The DAS associated with Computer 1 sampled all the recorded data at 1000 Hz for 60 s. The DAS associated with Computer 2 sampled selected data channels at 125 000 Hz for 8 s. The National Wind Tunnel Complex Government Industry Team recommended the high sample rate in reference 12.

The processing sequence of the DASs was originally organized to preserve the signal phase for cross-wire measurements. Because the phase response of the high-speed DAS was less accurate than that of the low-speed DAS, first the selected analog signals were gained and sent to the high-speed DAS, and then the high-speed DAS forwarded the corresponding digital signals to the low-speed DAS. The remaining analog signals were sent directly to the low-speed DAS. The analog signals to high-speed DAS were filtered with sixth-order Bessel analog filters at 50 000 Hz and truncated to 20 000 Hz. The analog signals to the low-speed DAS signals were filtered with fourth-order Bessel analog filters at 200 Hz. A 5-V peak-to-peak sinusoidal reference signal having a 4-Hz frequency was provided to each DAS to permit signal synchronizing. The wind-off levels of the signals were subtracted from the data of the low-speed DAS.

Data Processing

Power spectral densities (PSDs) of the time histories were calculated from the time histories of the signals. These were calculated using a MATLAB based software program developed at the NASA Langley Research Center for processing experimental time-domain data (ref. 13). PSDs of these time histories were computed using data block sizes of 32 768 for the high-speed sampling and 4096 for low-speed sampling, while employing the Hanning window function and 50 percent overlap processing. Each data block was detrended prior to calculating the PSD. These specifications imply a spectral frequency resolution of 3.81 Hz for the high-speed DAS and a frequency resolution of 0.244 Hz for the low-speed DAS.

Root-mean-square (RMS) values of the signals were generated from the measurement time histories and were normalized by dynamic pressure. The mean of the entire time history was removed prior to calculating the square root of the variance of the time history signals. This is equivalent to the standard deviation.

Comparisons were made between these RMS values and the square root of the numerical integration of the area under the PSD. Except for those differences identified in table 2 by shaded cells, all comparisons were within 10 percent.

Although the reduced data are included for these quantities at these conditions, the data are suspect.

During testing it was noticed that, at some test conditions, the survey rake underwent small-amplitude up-and-down pitching motions. The authors wondered to what extent this rake pitching motion influenced the turbulence data being acquired by the fluctuating pressures on the rake. To assess this influence, the coherence function was calculated between the acoustic pressure probe and the port accelerometer. The acoustic pressure probe was chosen since it is considered to be the most accurate of the sensors in measuring turbulence. The accelerometer on the rake was the accelerometer closest to the acoustic pressure probe. These results are discussed in detail in the next section.

Results and Discussion

This section of the paper describes and discusses the turbulence characteristics of the TDT test section as measured by the fluctuating pressure instrumentation. The present paper looks at turbulence in terms of pressure fluctuations. Reference 1 looked at tunnel turbulence in terms of velocity fluctuations.

The next subsection discusses test conditions, followed by turbulence intensity (as represented by normalized standard deviation) and turbulence frequency content (as represented by its power spectral density function). This section concludes with a brief examination of the statistical correlation between the turbulence measured on the rake and the vertical acceleration of the rake (as represented by the coherence function relating these two quantities).

Test Conditions

As can be seen from figures 7 and 8, a total of nine combinations of Mach number and dynamic pressure was chosen for the air test medium, while over 40 combinations were chosen for the heavy-gas test medium. These combinations in air corresponded to nominal total pressures of about 100, 400, and 2200 psf over a range of Mach numbers and dynamic pressures. The combinations in heavy gas corresponded to nominal total pressures of about 200, 500, and 1800 psf over a range of Mach numbers and dynamic pressures and at constant nominal dynamic pressure (about 225 psf) over a range of Mach numbers. (Additional combinations were acquired in air at nominal total pressures of about 700 and 1200 psf but are not presented in this paper because of the similarity of those results to corresponding results in air at 2200 psf.) Other variations that occurred during testing were slot conditions with open slots, with wall slots closed and with all slots closed.

Table 2 presents a summary of turbulence levels for 76 test conditions. These results are grouped into 12 sets. Sets 1–3 were conducted in air (showing a value of zero for R134a purity) and the remaining sets were conducted in heavy gas. Sets 1–4, which include only low-speed test points, may be useful for comparisons with other wind tunnels. Set 5 is a full set of test points for which the tunnel total pressure is approximately 500 psf. Set 6 supplements set 5 with a high-speed pass for a similar total pressure. It should be noted, however, that all test points of set 6 have the high-speed reentry flap setting of 4. Set 7

is a full set of test points for which the total pressure is approximately 200 psf. Set 8 includes test points of various total pressures, but where each test has a dynamic pressure of 225 psf. Set 8 may also be useful for comparisons with other wind tunnels. Set 9 consists of test points for which the wall slots are closed and the total pressure is approximately 500 psf. Similarly, set 10 consists of test points for which the wall slots are closed and the total pressure is approximately 200 psf. Set 11 consists of test points for which all slots are closed and the total pressure is approximately 500 psf, and set 12 consists of test points for which all slots are closed and the total pressure is approximately 200 psf. Included in the table are the set number and the run and test point identifiers for each test point.

The following describes the other contents in the table.

Slot configuration. The slot configuration is indicated as open (all wall slot covers, floor slot covers, and ceiling slot covers are open), east wall slots closed (WSC), or all slots closed (ASC).

R134a purity. The purity of R134a indicates the proportion of R134a in the test medium. Any data with a purity that is nonzero are R134a test points. Zero purity corresponds to air.

Tunnel total pressure. The tunnel total pressure is provided. As mentioned earlier, data were acquired in air at nominal total pressures of 100, 400, and 2100 psf. R134a data were acquired at nominal total pressures of 200, 500, and 1800 psf.

Reentry flap settings. The reentry flap settings are indicated by a number from 1–4 which corresponds to the flap schedule which had previously been described and shown in figure 5.

Prerotation vane and motor power. For completeness, the prerotation vane setting is included. The prerotation vanes are set at 19.5° for all cases except for the highest Mach number settings in which the prerotation vane setting is decreased because Mach number cannot be achieved because of limitations on motor rotational speed.

Motor power. For completeness, the motor power is provided.

Mach number. The free-stream Mach number is shown.

Dynamic pressure. The dynamic pressure of each test point is shown.

Other tunnel conditions. The tunnel stagnation temperature and tunnel static pressure measured during testing are given. The test flow velocity and density are also provided. These along with the Reynolds number are determined using a computer program which calculates the isentropic flow properties for mixtures of R134a and air which requires as input the tunnel stagnation and static pressures, the tunnel stagnation temperature, and the purity (ref. 14).

Motor rotational speed. The motor rotational speed for each test point is also provided.

Blade passing frequency (BPF). The BPF is included using

$$\text{BPF} = \text{RPM} \times \frac{47}{60} \quad (1)$$

where RPM is the rotational speed of the drive motor in revolutions per minute, and 47 is the number of fan blades.

Intensity of TDT Turbulence

The normalized standard deviation of fluctuating pressures is taken as the measure of the intensity of the turbulence in the TDT test section. The five right-most columns in table 2 contain these standard deviations, expressed as a percentage of free-stream dynamic pressure acquired from two total pressure transducers, two static pressure transducers, and one sound pressure transducer. Expressed in this way, turbulence levels varied between a minimum of 0.14 percent at a low subsonic Mach number in air and a maximum of 0.89 percent at a transonic Mach number in heavy gas. Figures 15 through 21 present in graphical form the information contained in table 2.

The turbulence levels shown are for the low-speed sampled data only, although standard deviations were also calculated for the high-speed sampled data. The turbulence levels are presented for each of the five pressure measurements. Figure 15 shows the variations of turbulence for approximate total pressures of 100, 400, and 2100 psf in air and for a total pressure of 1800 psf in the heavy gas. The Mach numbers range between 0.2 and 0.7 as contained in sets 1–4 for open slots. Figure 15(a) depicts rather low constant values with a changing Mach number for the rake total pressure probes. The port pressure levels are greater than the starboard pressure levels. Similar results can be seen in figure 15(b) for the rake static pressure and sound coefficients in which the rake static pressures are greater than the sound pressures and in figure 15(c) for the wall static measurements, although figure 15(b) exhibits slightly more scatter. The wall turbulence levels are higher than the static turbulence levels at the lower Mach numbers, but the rake static level is higher than the wall static level at the higher Mach numbers. All turbulence levels remain below 0.7 percent.

Figure 16 shows the turbulence variation for a broader range of Mach numbers conducted in the heavy gas for tunnel total pressures of 200 and 500 psf and encompassing sets 5–7. The port turbulence levels are slightly greater than the static turbulence levels. The turbulence levels measured using the rake static pressures are greater than those measured using the sound pressures. The wall static turbulence level is slightly larger than the rake static levels subsonically and slightly less supersonically.

Figure 17 shows set 8. Once again the port levels are slightly greater than the starboard levels. The rake static level is greater than the sound level and the wall static level is very similar. The rake and sting exhibited an oscillation within the region of $0.76 \leq M \leq 0.85$; therefore, data were not measured in this region. The turbulence levels remained below 1 percent.

Figure 18 shows coefficient variations for sets 9 and 10 for which the wall slots are closed and the tunnel total pressures are, respectively, about 500 and 200 psf. These plots terminate near $M = 1$. As shown in figure 18(a), the port turbulence levels are greater than the starboard turbulence levels, especially in the subsonic range. As shown in figure 18(b), the turbulence levels as measured by the rake static pressures are greater than those from sound pressures. The wall static pressures (fig. 18(c)) are slightly greater than the rake static pressures subsonically.

Figure 19 shows coefficient variations for sets 11 and 12 for which all slots are closed and the tunnel total pressures are, respectively, about 500 and 200 psf. The plots terminate at reduced values near $M = 0.9$. Once again figure 19(a) shows port turbulence slightly above starboard turbulence. Figure 19(b) shows rake static turbulence that is almost double the sound turbulence. Figure 19(c) shows that the wall static turbulence is greater than the rake static turbulence.

Figures 20 and 21 directly compare the effects of closing the slots when the total pressures are 500 and 200 psf, respectively. In figure 20(a), the effect of the slots being closed is minimal subsonically, and

there is a slight decrease in the levels of turbulence transonically. In figure 20(b), the effect of closing all slots is to decrease the turbulence levels transonically. In figure 20(c), the effect of closing all slots is to increase the turbulence at the wall transonically. The results at a total pressure P_t of 200 psf in figure 21 are very similar to the results shown for $P_t = 500$ psf.

Frequency Content of TDT Turbulence

The PSD function of fluctuating pressures is taken as the measure of the frequency content of the turbulence in the TDT test section. The main body of this paper presents low-frequency PSDs (frequencies up to 200 Hz). The appendix to this paper presents high-frequency PSDs (frequencies up to 20 000 Hz).

Figures 22–33 contain plots of PSDs for data acquired for each sensor and for each of the 76 unique test conditions identified in table 2. Each figure pertains to a different data set, beginning with data set 1 for figure 22 and ending with data set 12 for figure 33. Each figure has five parts, (a) through (e), with each pertaining to data acquired by a different fluctuating pressure transducer. Within each part, PSD plots are presented by a Mach number. Thus, data set 1, with only two Mach numbers, contains two PSDs per part, while data set 7, with 12 Mach numbers, contains 12 PSDs per part. These low-frequency spectral data are of most interest to potential customers at the TDT.

In order to present many PSDs on a single plot without the confusion of overlapping PSDs, a multiplication-factor scheme has been employed. Each PSD has been multiplied by a different, even power of 10 so that there is sufficient separation of the PSDs in the figure to avoid overlap. In the key for each figure, the numbers in parentheses following the Mach number indicate the multiplication factor which must be removed from that particular PSD in order to determine its correct magnitude at any given frequency.

Figures 22–33 show the PSDs of the tunnel turbulence for frequencies from near 0 to 200 Hz for each set. The BPF and its harmonics (multiples of the BPF) can be seen on all sensors to a greater or lesser degree.

Figure 22 shows the air cases at the lower Mach numbers. The rake port PSDs and the rake starboard PSDs have very similar shapes and features. The rake static turbulence trend shows a more prominent trough at 60 Hz and a peak at 80 Hz. These exist for the port and starboard total turbulence but are not as obvious. The sound turbulence trend is similar to the rake static turbulence trend. The BPFs for these two points at 135 ($M = 0.3$) and 176 ($M = 0.4$) as shown in table 2 are clearly shown on all the plots. The acoustic turbulence has low-frequency attenuation not present for the others. The PSDs are constant at low frequency with a drop-off at high frequency. This is in common with the von Karman (ref. 15) spectrum. These are true for figures (a), (b), (c), and (e), but not for the acoustic turbulence in (d).

Other PSD figures show some additional differences which are described next. At the lowest Mach number (0.2) and dynamic pressure, there exist large peaks in the PSDs at the high frequencies. These peaks are probably due to the way the data were normalized. The high-frequency asymptote for the Mach 1.0 case has a shallower slope. There are some cases in which the drop-off at low frequencies does not exist for the rake acoustic spectra but actually has an increase in the lowest frequency decade. There are a few cases in which the wall static pressure has an increase at the low frequency.

On average, the slopes of the high-frequency asymptotes are on the order of $-5/3$ for all the sensors and all the data, which are characteristic of the von Karman spectrum. In comparison with previously obtained results (ref. 1), the same general features of the turbulence exist with constant low-frequency behavior and the same slope (on a log-log scale) of the high-frequency asymptote.

One complete set, including extended spectra of the PSDs for all five sensors for air at $P_t = 2100$ psf and R134a at 1800 psf at Mach 0.4, are provided to directly compare these test conditions. Figures 34 and 35 show the comparison of the spectra. For the sake of the completeness of this comparison, figure 35 also shows the PSDs for up to 20 000 Hz. The plots include both the high- and low-frequency data. The axis for the air test point is on the left side of the plot and that for the R134a is on the right side of the plot. The total pressure turbulence spectra followed the same basic trend with peaks associated with the blade passing frequency located at different frequencies. The static pressure spectrum is considerably different. These differences are mostly in the high-frequency range above 200 Hz.

Statistical Correlation Between Rake-Measured Turbulence and Rake Vertical Accelerations

The coherence function, γ^2 , reveals the extent to which two quantities are statistically correlated. The coherence function may assume a value between 0 (indicating no correlation between signals, or the signals are incoherent) and 1 (indicating a one-to-one correlation between signals, or the signals are fully coherent). Intermediate values indicate varying levels of correlation, or coherence.

During testing it was noticed that, at some test conditions, the survey rake underwent small-amplitude up-and-down pitching motions. The authors wondered to what extent this rake pitching motion influenced the turbulence data being acquired by the fluctuating pressures on the rake. To assess this influence, the coherence function between one of the transducers and an accelerometer on the rake was computed.

The coherences were calculated between the acoustic pressure probe and the port accelerometer. The acoustic pressure probe was chosen since it is considered to be the most accurate of the sensors in measuring turbulence. The accelerometer on the rake was the accelerometer closest to the acoustic pressure probe.

Figure 36 consists of coherence functions for $M = 0.5$ to 1.2 at the highest dynamic pressure condition. If correlation exists between the sensors, we would expect to see it at these high dynamic pressure conditions; however, the data in figure 36 show no significant interaction. Figure 36(a) at Mach 0.5 has general levels below 0.2 with a few scattered peaks at approximately 0.3 and 0.4. The spike at 104 Hz corresponds to the BPF. Figure 36(b) has low levels of coherence below 0.2–0.3. The highest peak of approximately 0.48 again corresponds to the BPF at 121 Hz. Figure 36(c) at Mach = 0.7 shows the BPF and another peak, which could correspond to a subharmonic or probably electrical noise of 60 Hz. Figure 36(d) at Mach 0.76 does not show a prominent peak at the BPF but does show a peak at the 60-Hz electrical noise frequency. Figure 36(e) has low levels of coherence, although it shows a few peaks between 50 and 100 Hz and the BPF. Figure 36 (f) which shows the Mach 0.9 case shows the BPF and a peak around 10 Hz which could correspond to a rake vertical mode (table 1). It is unclear what the source of this peak is. Figure 36(g), which shows the Mach 1.0 case, shows the BPF and a subharmonic. Figure 36(h) shows the BPF and its subharmonic for the Mach 1.1 case.

Concluding Remarks

An investigation was conducted in the Langley Transonic Dynamics Tunnel (TDT) to measure the tunnel turbulence at tunnel station 72, the typical location for models tested in the TDT. For this paper turbulence is defined as fluctuating pressures. Flow measurements were made at several lateral locations on a survey rake. Total pressures at two positions, static pressure and acoustic pressure, were measured on the rake, and wall static pressures at one tunnel station were also measured. Measurements were made

for nearly constant tunnel total pressures at Mach numbers and dynamic pressures spanning the wind tunnel test envelope with slots open and with wall slots closed and with all slots closed. This paper has presented the standard deviations and the power-spectral densities of the turbulence without attempting to analyze or assess the reasons or causes for the turbulence. The data are available for future analyses and interpretation.

References

1. Sleeper, R. K.; Keller, Donald F.; Perry, Boyd, III; and Sandford, Maynard: *Characteristics of Vertical and Lateral Turbulence Measured in Air in the Langley Transonic Dynamics Tunnel*. NASA TM 107734, 1993.
2. Pope, Alan: *Wind-Tunnel Testing*. 2nd Ed. John Wiley & Sons, Inc., 1964.
3. Rivera, Jose A.; and Florance, James R.: Contributions of Transonic Dynamics Tunnel Testing to Airplane Flutter Clearance. AIAA 2000-1768, *AIAA Dynamics Specialists Conference*, Atlanta, GA, April 5–6, 2000.
4. Cole, Stanley R.; Keller, Donald F.; and Piatak, David J.: Contributions of the NASA Langley Transonic Dynamics Tunnel Testing To Launch Vehicle and Spacecraft Development. AIAA 2000-1772, *AIAA Dynamics Specialists Conference*, Atlanta, GA, April 5–6, 2000.
5. Perry, Boyd, III; Noll, Thomas E.; and Scott, Robert C.: Contributions of the Transonic Dynamics Tunnel to the Testing of Active Control of Aeroelastic Response. AIAA 2000-1769, *AIAA Dynamics Specialists Conference*, Atlanta, GA, April 5–6, 2000.
6. Schuster, David M.; Edwards, John W.; and Bennett, Robert M.: An Overview of Unsteady Pressure Measurements in the Transonic Dynamics Tunnel. AIAA 2000-1770, *AIAA Dynamics Specialists Conference*, Atlanta, GA, April 5–6, 2000.
7. Cole, Stanley; and Garcia, Jerry L.: Past, Present, and Future Capabilities of the Transonic Dynamics Tunnel From an Aeroelasticity Perspective. AIAA 2000-1767, *AIAA Dynamics Specialists Conference*, Atlanta, GA, April 5–6, 2000.
8. Corliss, James M.; and Cole, Stanley R.: Heavy Gas Conversion of the NASA Langley Transonic Dynamics Tunnel. AIAA 98-2710, *20th AIAA Advanced Measurement and Ground Testing Technology Conference*, Albuquerque, NM, June 15–18, 1998.
9. Florance, James R.; and Rivera, Jose A.: *Sidewall Mach Number Distributions for the NASA Langley Transonic Dynamics Tunnel*. NASA TM 2001-211019, 2001.
10. Yeager, William T.; Wilbur, Matt; Rivera, Jose A.; and Mirick, Paul: Flow Angularity Measurements in the NASA Langley Transonic Dynamics Tunnel, awaiting publication.
11. Jones, Gregory S.: The Measurement of Wind Tunnel Flow Quality at Transonic Speeds. Doctor of Philosophy Dissertation, Virginia Polytechnic and State University, 1991.
12. National Wind Tunnel Complex Government/Industry Team: Flow Quality Requirements for Laminar Flow Testing. Document No. DB-1-026, August 7, 1995.
13. Wieseman, C. D.; and Hoadley, S. T.: Versatile Software Package for Near Real-Time Analysis of Experimental Data. AIAA 98-2722, *20th AIAA Advanced Measurement and Ground Testing Technology Conference*, Albuquerque, NM, June 15–18, 1998.
14. Kvaternik, R. G.: *Computer Programs for Calculating the Isentropic Flow Properties for Mixtures of R134a and Air*. NASA TM 2000-210622, 2000.
15. Houbolt, John C.; Steiner, Roy; and Pratt, Kermit G.: *Dynamic Response of Airplanes to Atmospheric Turbulence Including Flight Data on Input and Response*. NASA TR R-199, 1964.

Table 1. Modal Frequencies of Rake

Frequency, Hz	Description
6.25	First vertical
7.375	First torsion
5.562	First lateral
13.813	Sting/rake vertical

Table 2. Turbulence Levels

Set	Test point	Test conditions														Turbulence levels in percent for pressure sensor					
		Slot configuration	R134a purity	Total pressure, psf	Reentry flaps setting	Prerotatation vane setting, deg	Motor power, megawatts	Mach number	Dynamic pressure, psf	Stagnation temperature, °F	Static pressure, psf	Test flow velocity, fps	Test density, lb/ft ³	Motor rotational speed, rpm	Blade passing frequency, Hz	Reynolds number x1/1000000	Port total pressure	Starboard total pressure	Static pressure	Sound pressure	Wall static pressure
1	39	open	0	2096	1	19.5	8.5	0.30	123	92	1970	340	0.00212	173	135	1.86	0.36	0.33	0.23	0.14	0.32
1	43	open	0	2096	1	19.5	12.8	0.40	207	101	1881	453	0.00202	225	176	2.36	0.36	0.32	0.27	0.17	0.34
2	77	open	0	390	1	19.5	7.1	0.20	10	84	379	226	0.00041	122	95	0.24	0.45	0.34	0.24	0.21	0.35
2	76	open	0	393	1	19.5	7.0	0.30	23	86	370	339	0.00040	178	140	0.36	0.38	0.33	0.25	0.18	0.33
2	75	open	0	399	1	19.5	7.6	0.40	40	88	358	449	0.00039	230	180	0.46	0.36	0.34	0.30	0.19	0.35
3	73	open	0	104	1	19.5	4.2	0.40	10	85	93	451	0.00010	250	196	0.12	0.45	0.43	0.35	0.25	0.37
3	74	open	0	110	1	19.5	5.4	0.64	24	86	83	709	0.00010	358	280	0.19	0.46	0.42	0.58	0.39	0.48
4	307	open	0.97	1802	1	19.5	6.0	0.20	39	88	1763	109	0.00656	54	42	2.79	0.51	0.45	0.24	0.16	0.43
4	306	open	0.97	1822	1	19.5	7.8	0.30	86	90	1734	163	0.00645	80	63	4.10	0.49	0.40	0.25	0.16	0.37
4	305	open	0.97	1849	1	19.5	10.1	0.40	150	92	1693	218	0.00629	105	82	5.33	0.48	0.41	0.38	0.19	0.41
4	304	open	0.97	1879	1	19.5	13.0	0.50	225	95	1639	272	0.00609	127	100	6.44	0.50	0.45	0.40	0.24	0.45
5	105	open	0.97	491	1	19.5	4.3	0.20	11	85	480	110	0.00178	56	44	0.77	0.50	0.40	0.28	0.25	0.53
5	104	open	0.97	495	1	19.5	4.4	0.30	24	87	470	165	0.00174	83	65	1.13	0.45	0.38	0.30	0.19	0.45
5	163	open	0.94	551	1	19.5	5.0	0.40	45	88	504	221	0.00183	109	85	1.57	0.45	0.40	0.35	0.20	0.45
5	164	open	0.94	559	1	19.5	5.5	0.50	68	90	487	277	0.00177	133	104	1.91	0.44	0.41	0.40	0.25	0.48
5	167	open	0.94	570	1	19.5	6.5	0.60	93	91	468	331	0.00171	154	121	2.21	0.47	0.44	0.54	0.34	0.57
5	168	open	0.94	582	1	19.5	7.8	0.70	121	93	445	385	0.00163	172	135	2.46	0.53	0.50	0.71	0.48	0.66
5	169	open	0.94	590	1	19.5	8.5	0.76	138	95	430	418	0.00158	182	142	2.60	0.49	0.48	0.73	0.51	0.69
5	171	open	0.94	603	1	19.5	9.6	0.85	163	97	407	467	0.00150	195	152	2.76	0.43	0.40	0.55	0.45	0.60
5	173	open	0.94	612	2	19.5	10.4	0.90	177	99	394	494	0.00145	202	158	2.84	0.37	0.35	0.37	0.30	0.38
5	178	open	0.94	633	3	19.5	12.4	1.00	205	103	368	550	0.00136	218	171	2.95	0.34	0.33	0.29	0.25	0.17
5	183	open	0.94	656	4	19.5	15.0	1.10	230	109	342	604	0.00126	233	183	3.02	0.34	0.32	0.34	0.28	0.17
6	313	open	0.97	579	4	19.5	5.8	0.50	70	83	505	271	0.00190	132	103	2.04	0.44	0.41	0.42	0.26	0.49
6	314	open	0.97	613	4	19.5	9.2	0.76	143	88	446	412	0.00169	183	143	2.79	0.51	0.49	0.76	0.53	0.75
6	316	open	0.95	654	4	19.5	13.0	1.00	212	97	380	544	0.00143	216	169	3.12	0.36	0.38	0.33	0.25	0.16
6	317	open	0.95	676	4	19.5	15.5	1.10	237	103	352	598	0.00133	232	182	3.18	0.35	0.33	0.34	0.29	0.17

Table 2. Continued

Set	Test point	Test conditions													Turbulence levels in percent for pressure sensor						
		Slot configuration	R134a purity	Total pressure, psf	Reentry flaps setting	Prerotation vane setting, deg	Motor power, megawatts	Mach number	Dynamic pressure, psf	Stagnation temperature, °F	Static pressure, psf	Test flow velocity, fps	Test density, lb/ft ³	Motor rotational speed, rpm	Blade passing frequency, Hz	Reynolds number x1/1000000	Port total pressure	Starboard total pressure	Static pressure	Sound pressure	Wall static pressure
6	318	open	0.95	705	4	19.5	21.0	1.20	261	110	326	652	0.00123	233	182	3.21	0.38	0.38	0.78	0.22	0.18
7	238	open	0.97	205	1	19.5	4.2	0.20	5	81	200	111	0.00075	57	44	0.33	0.50	0.36	0.28	0.44	0.45
7	239	open	0.97	207	1	19.5	3.9	0.30	10	82	197	163	0.00074	83	65	0.47	0.45	0.38	0.27	0.26	0.43
7	240	open	0.97	210	1	19.5	3.5	0.40	17	82	192	218	0.00072	109	85	0.62	0.44	0.40	0.35	0.24	0.48
7	241	open	0.97	213	1	19.5	3.4	0.50	26	83	186	272	0.00070	133	104	0.76	0.45	0.41	0.42	0.26	0.53
7	242	open	0.97	217	1	19.5	3.7	0.60	35	84	179	325	0.00067	154	121	0.87	0.48	0.46	0.55	0.34	0.60
7	243	open	0.97	222	1	19.5	4.2	0.70	46	85	170	379	0.00064	173	135	0.98	0.53	0.49	0.74	0.48	0.67
7	244	open	0.97	225	1	19.5	4.5	0.76	53	86	164	410	0.00062	182	142	1.03	0.50	0.48	0.77	0.52	0.69
7	246	open	0.97	230	1	19.5	4.9	0.85	62	87	155	457	0.00059	195	152	1.10	0.45	0.41	0.59	0.46	0.60
7	247	open	0.97	233	2	19.5	5.2	0.90	68	88	150	484	0.00058	202	158	1.13	0.36	0.33	0.39	0.30	0.41
7	249	open	0.97	241	3	19.5	6.0	1.00	78	91	140	538	0.00054	218	171	1.18	0.34	0.31	0.29	0.23	0.24
7	251	open	0.97	251	4	18.0	7.2	1.10	88	96	130	591	0.00050	233	183	1.22	0.34	0.32	0.34	0.27	0.24
7	253	open	0.97	261	4	2.0	9.5	1.20	97	100	120	645	0.00047	233	183	1.23	0.37	0.36	0.57	0.21	0.25
8	304	open	0.97	1879	1	19.5	13.0	0.50	225	95	1639	272	0.00609	127	100	6.44	0.50	0.45	0.40	0.24	0.45
8	225	open	0.98	1380	1	19.5	12.7	0.60	225	96	1134	326	0.00424	150	117	5.41	0.50	0.45	0.52	0.33	0.56
8	289	open	0.97	1087	1	19.5	12.5	0.70	225	99	832	382	0.00309	169	132	4.61	0.54	0.51	0.69	0.46	0.66
8	208	open	0.94	965	1	19.5	12.4	0.76	226	100	703	420	0.00256	181	142	4.18	0.51	0.48	0.70	0.50	0.70
8	197	open	0.94	832	2	19.5	12.5	0.85	225	103	562	469	0.00205	195	153	3.75	0.44	0.42	0.59	0.48	0.63
8	277	open	0.97	778	2	19.5	12.6	0.90	225	105	501	491	0.00187	200	157	3.61	0.38	0.35	0.39	0.30	0.37
8	276	open	0.97	733	2	19.5	12.6	0.95	225	106	450	517	0.00168	206	161	3.44	0.36	0.35	0.30	0.22	0.23
8	186	open	0.94	696	3	19.5	13.4	1.00	225	107	406	550	0.00149	218	171	3.22	0.36	0.33	0.32	0.25	0.17
8	274	open	0.97	669	3	19.5	14.0	1.05	226	108	370	570	0.00139	223	175	3.14	0.34	0.32	0.32	0.26	0.16
8	159	open	0.94	643	4	17.5	14.6	1.10	225	110	337	602	0.00124	234	183	2.95	0.34	0.32	0.33	0.28	0.17
8	255	open	0.97	624	4	15.0	16.2	1.15	225	110	307	622	0.00116	233	183	2.89	0.34	0.35	0.40	0.48	0.17
8	254	open	0.97	607	4	7.0	18.4	1.20	225	110	281	648	0.00107	233	182	2.79	0.38	0.37	0.65	0.22	0.19

Table 2. Concluded

Set	Test point	Test conditions														Turbulence levels in percent for pressure sensor					
		Slot configuration	R134a purity	Total pressure, psf	Reentry flaps setting	Prerotatation vane setting, deg	Motor power, megawatts	Mach number	Dynamic pressure, psf	Stagnation temperature, °F	Static pressure, psf	Test flow velocity, fps	Test density, lb/ft ³	Motor rotational speed, rpm	Blade passing frequency, Hz	Reynolds number x1/1000000	Port total pressure	Starboard total pressure	Static pressure	Sound pressure	Wall static pressure
9	335	WSC	0.95	541	1	19.5	4.6	0.20	12	83	529	109	0.00194	54	43	0.83	0.50	0.40	0.26	0.18	0.51
9	336	WSC	0.95	552	1	19.5	5.0	0.40	45	84	505	221	0.00186	107	84	1.61	0.44	0.39	0.35	0.21	0.43
9	337	WSC	0.95	571	1	19.5	6.4	0.60	94	86	468	329	0.00174	150	118	2.26	0.46	0.42	0.51	0.33	0.55
9	338	WSC	0.95	583	1	19.5	7.7	0.70	121	88	445	383	0.00166	168	132	2.52	0.49	0.47	0.67	0.45	0.64
9	339	WSC	0.95	590	1	19.5	8.5	0.76	138	90	431	414	0.00161	178	139	2.64	0.48	0.45	0.70	0.50	0.68
9	340	WSC	0.95	604	2	19.5	9.5	0.85	164	92	407	464	0.00152	190	149	2.81	0.42	0.40	0.56	0.46	0.60
9	341	WSC	0.95	612	1	19.5	10.3	0.90	178	94	394	491	0.00147	197	154	2.89	0.35	0.34	0.36	0.30	0.39
9	343	WSC	0.95	631	3	19.5	12.4	1.00	204	98	367	544	0.00138	213	167	3.01	0.34	0.33	0.29	0.22	0.17
10	325	WSC	0.95	203	1	19.5	4.2	0.20	4	82	198	111	0.00073	56	44	0.32	0.51	0.38	0.30	0.28	0.45
10	326	WSC	0.95	207	1	19.5	3.5	0.40	17	82	189	220	0.00070	109	85	0.61	0.46	0.39	0.36	0.22	0.46
10	327	WSC	0.95	214	1	19.5	3.7	0.60	35	84	176	328	0.00065	154	120	0.85	0.46	0.43	0.53	0.33	0.59
10	328	WSC	0.95	219	1	19.5	4.2	0.70	46	85	167	382	0.00062	172	135	0.95	0.49	0.46	0.71	0.45	0.65
10	329	WSC	0.95	222	1	19.5	4.6	0.76	52	86	162	413	0.00061	182	142	1.00	0.48	0.45	0.74	0.50	0.69
10	330	WSC	0.95	226	2	19.5	5.0	0.85	61	87	153	462	0.00058	195	152	1.07	0.44	0.39	0.59	0.46	0.59
10	331	WSC	0.95	229	1	19.5	5.4	0.90	67	88	148	488	0.00056	201	158	1.10	0.35	0.32	0.37	0.30	0.42
10	333	WSC	0.95	236	3	19.5	6.2	1.00	77	90	137	542	0.00052	219	171	1.15	0.33	0.31	0.27	0.20	0.26
11	359	ASC	0.97	540	2	19.5	4.6	0.20	12	84	528	110	0.00196	54	42	0.84	0.50	0.42	0.29	0.17	0.49
11	360	ASC	0.97	552	2	19.5	4.9	0.40	45	85	505	218	0.00188	104	82	1.62	0.44	0.39	0.35	0.19	0.46
11	361	ASC	0.97	570	2	19.5	6.2	0.60	93	87	468	326	0.00176	148	116	2.27	0.44	0.40	0.47	0.28	0.53
11	362	ASC	0.97	582	2	19.5	7.4	0.70	121	89	445	380	0.00168	166	130	2.53	0.44	0.42	0.58	0.37	0.66
11	363	ASC	0.97	590	2	19.5	8.1	0.76	138	91	430	412	0.00162	176	138	2.66	0.42	0.39	0.63	0.43	0.76
11	364	ASC	0.97	603	2	19.5	9.1	0.85	163	93	407	460	0.00154	188	148	2.83	0.36	0.33	0.52	0.42	0.78
11	365	ASC	0.97	611	2	19.5	9.8	0.90	177	95	393	487	0.00149	195	153	2.91	0.27	0.23	0.23	0.15	0.51
12	355	ASC	0.95	234	2	19.5	5.0	0.85	64	89	157	465	0.00059	195	153	1.10	0.38	0.35	0.58	0.45	0.89
12	356	ASC	0.95	237	2	19.5	5.3	0.90	69	90	153	489	0.00058	200	157	1.13	0.28	0.23	0.22	0.15	0.56



Figure 1. Aerial view of NASA Langley Transonic Dynamics Tunnel.

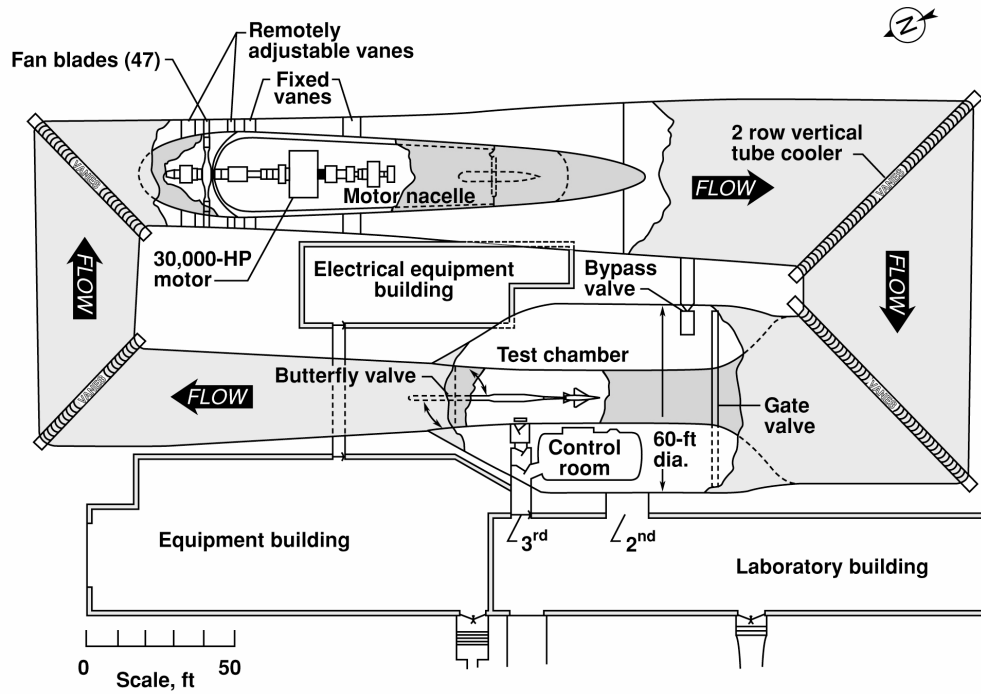


Figure 2. Plan view drawing of NASA Langley Transonic Dynamics Tunnel.

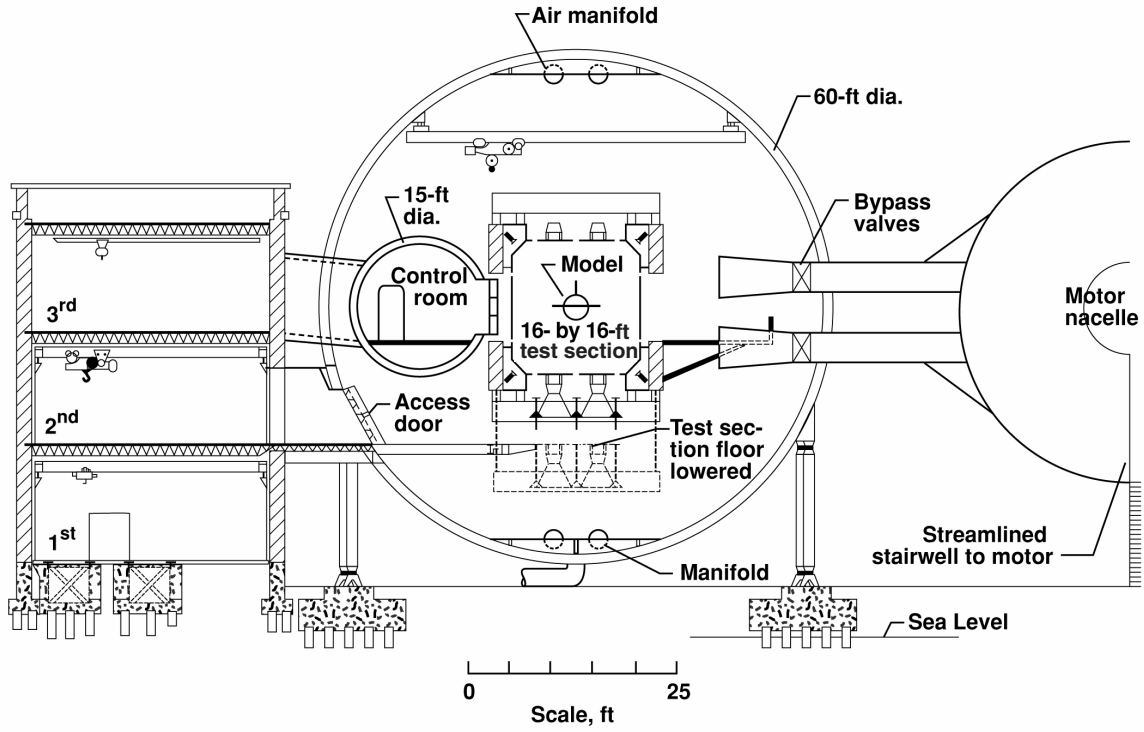


Figure 3. Cross section of TDT through model testing location.

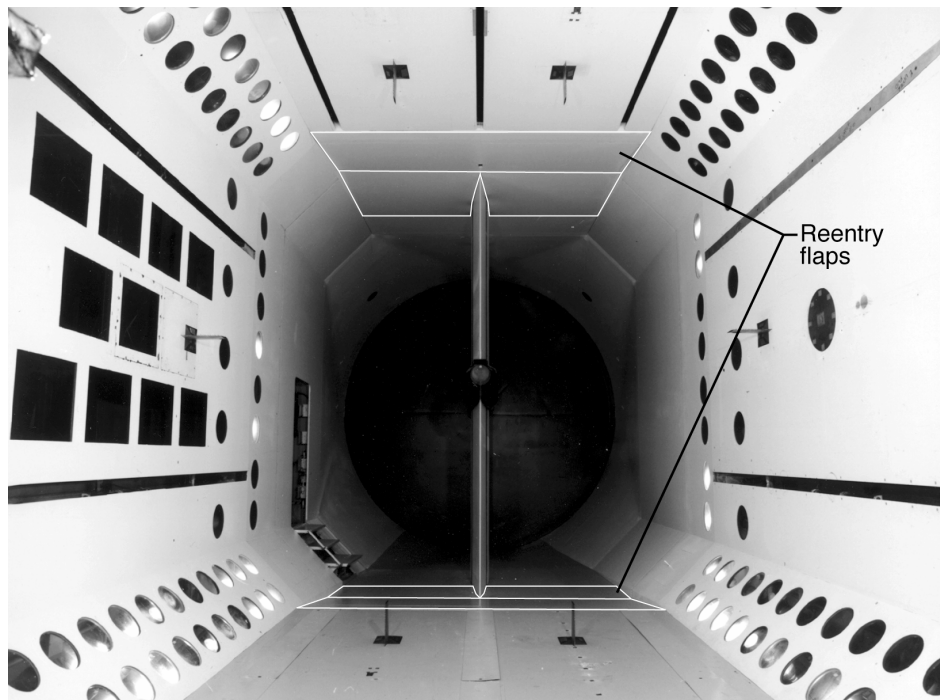


Figure 4. Photo showing position of reentry flaps in TDT test section.

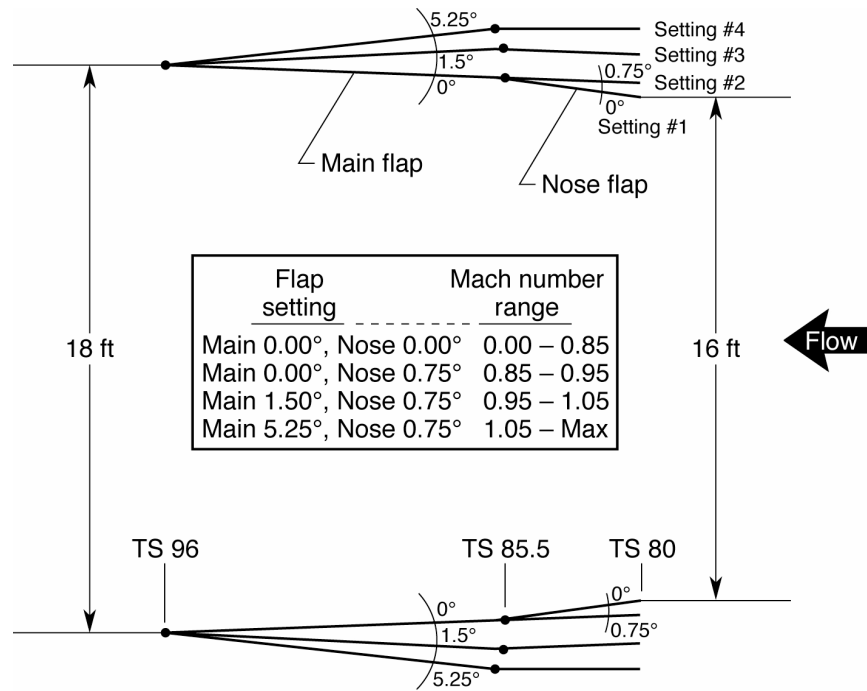


Figure 5. Schematic of reentry flap operation and reentry flap schedule.

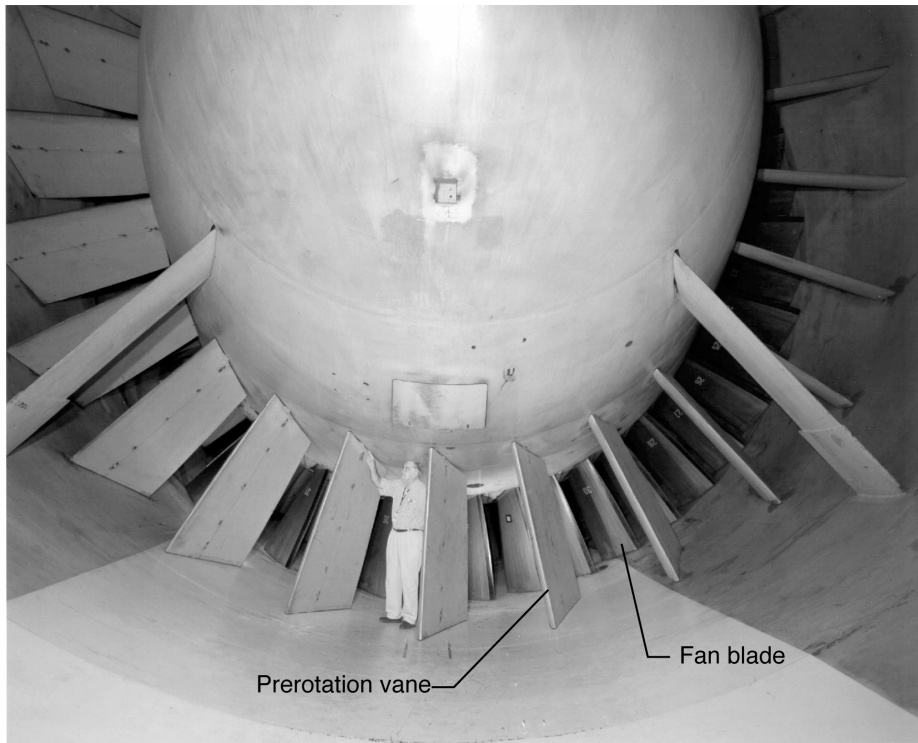


Figure 6. Photograph of prerotation vanes and fan blades.

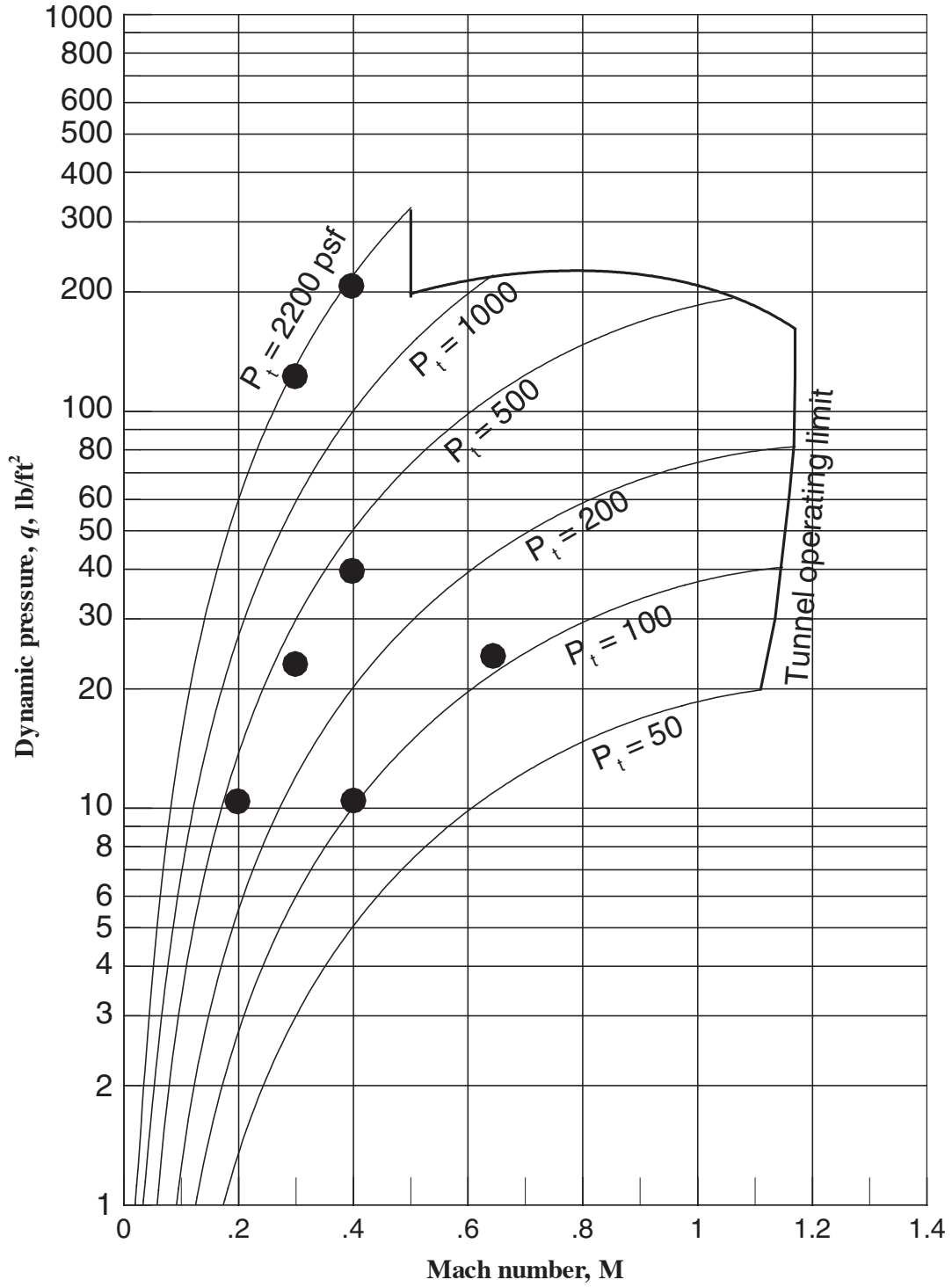


Figure 7. Significant portion of TDT operating boundary in air with test points superimposed.

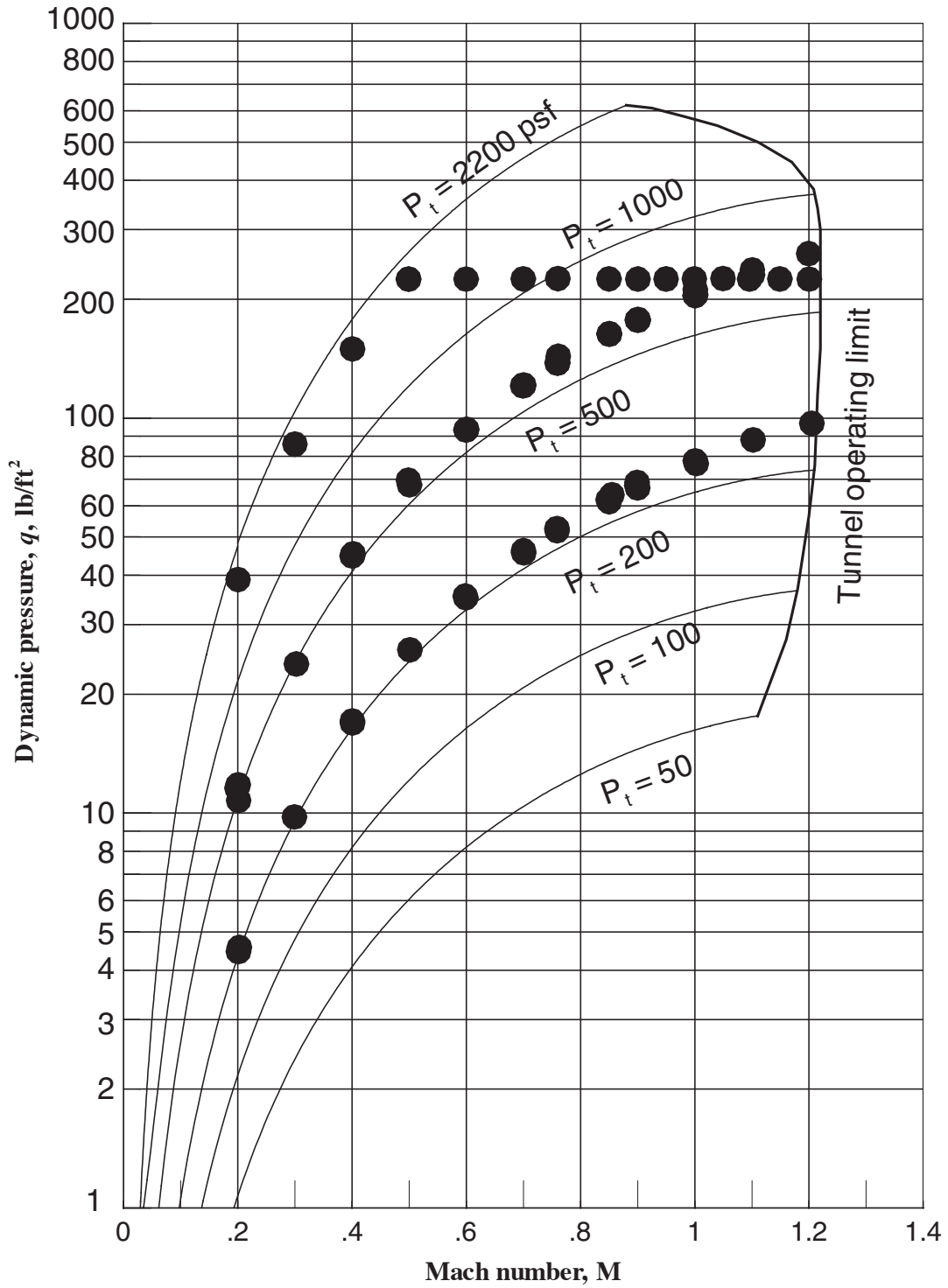


Figure 8. Significant portion of TDT operating boundary in R134a with test points superimposed.

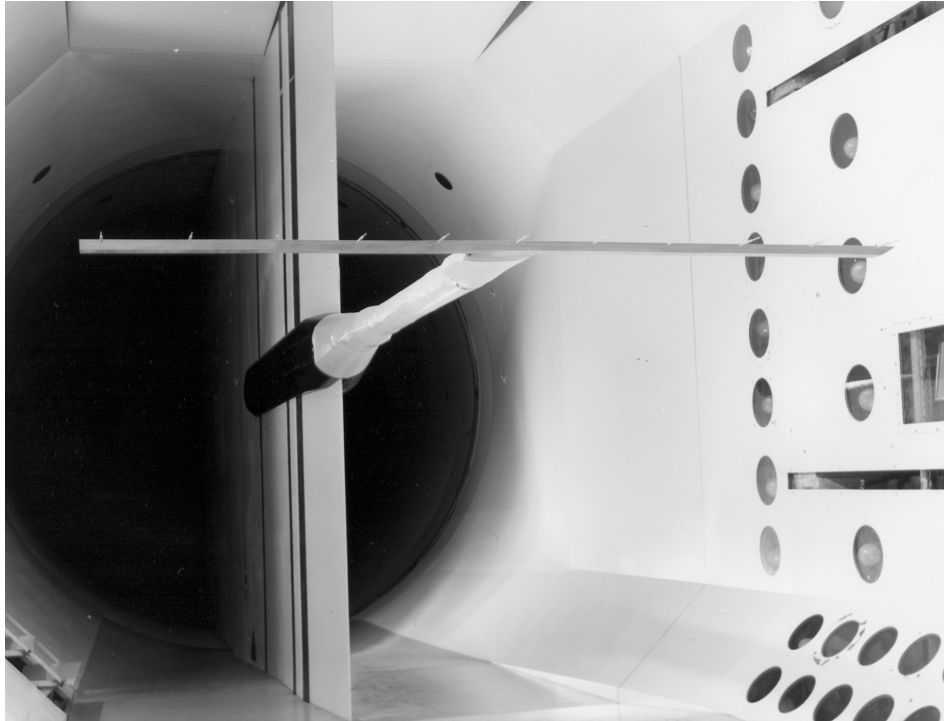
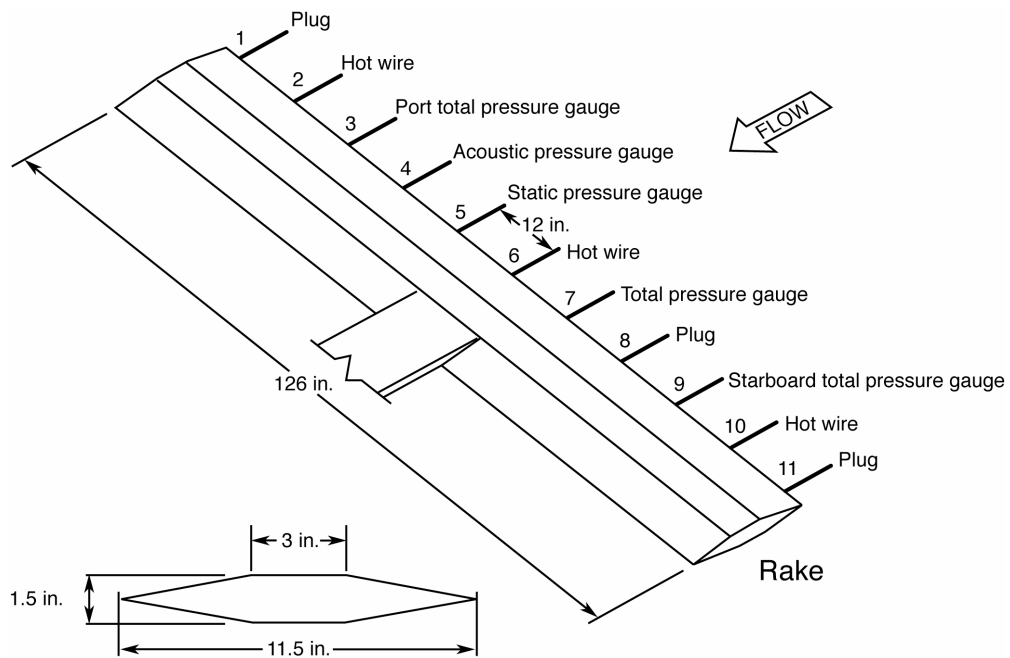
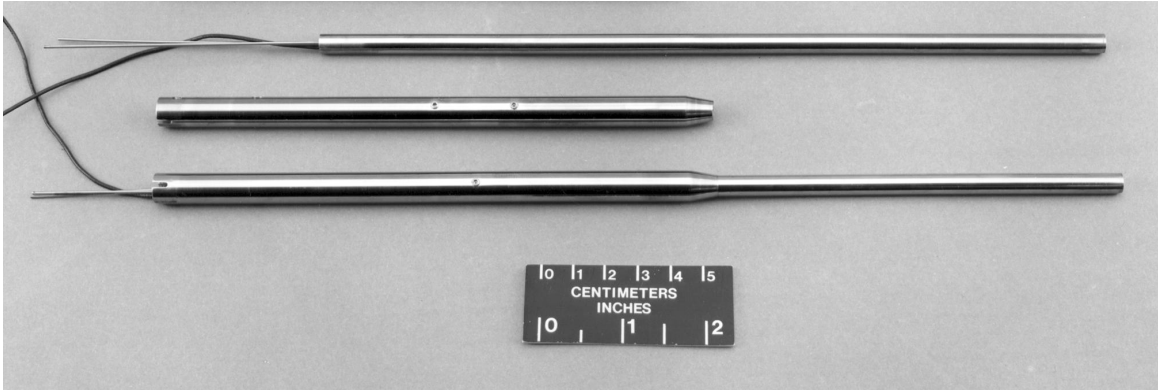


Figure 9. Flow survey rake installed on sting in TDT test section.

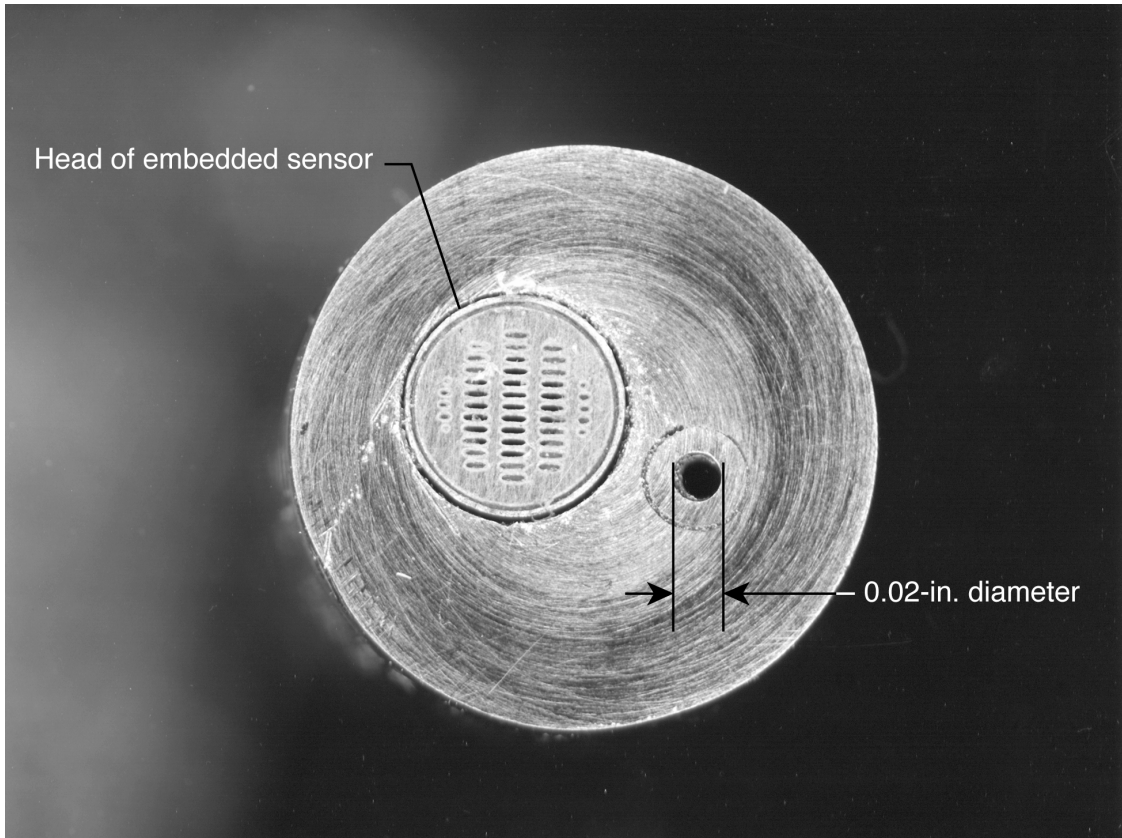


Rake cross section

Figure 10. Rake schematic showing locations of pressure probes.



(a) Overall view.



(b) Magnified view of total pressure probe tip.

Figure 11. Total pressure probe.

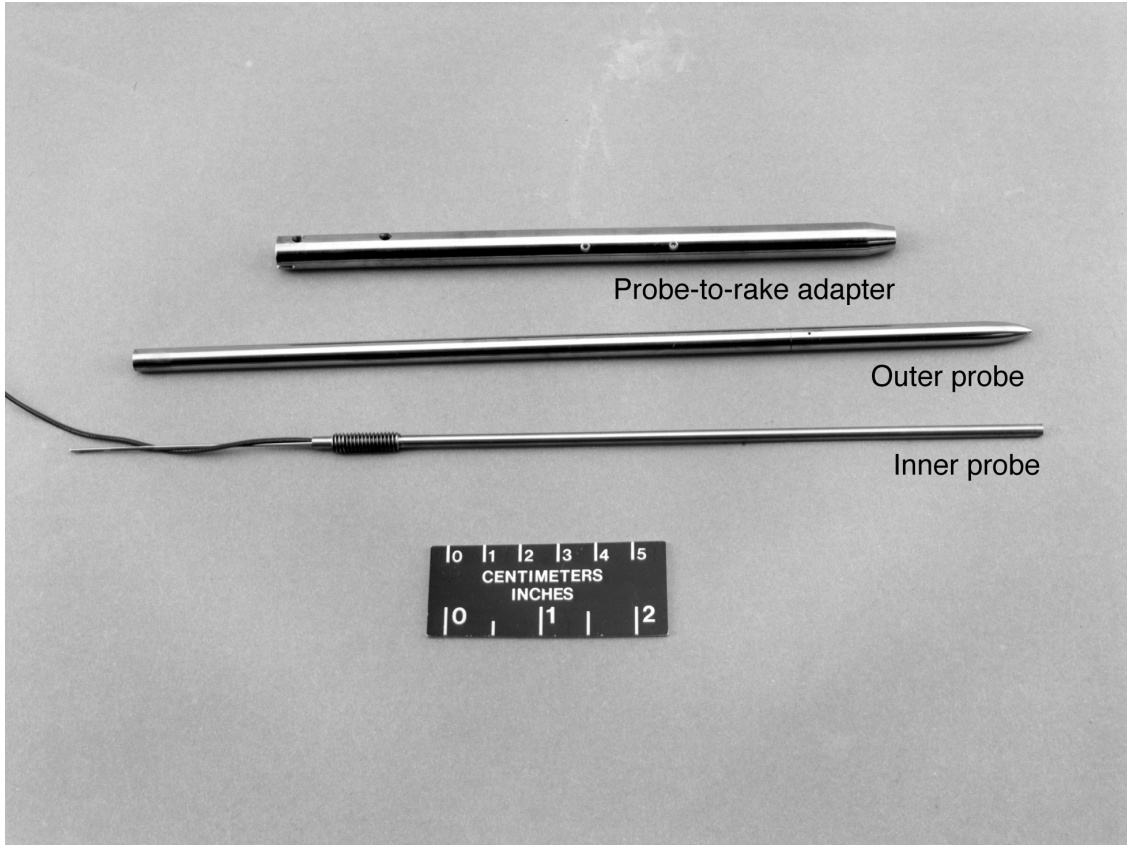
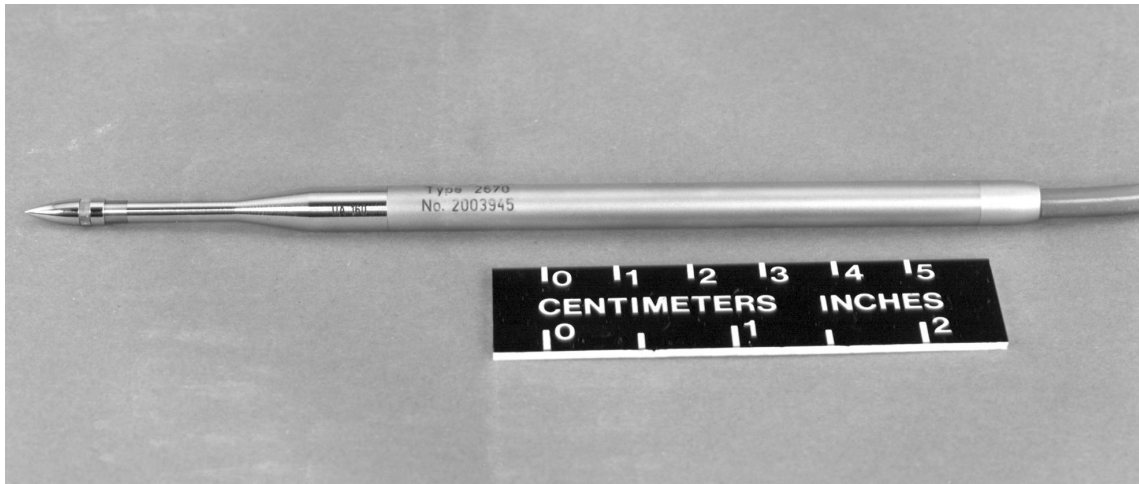
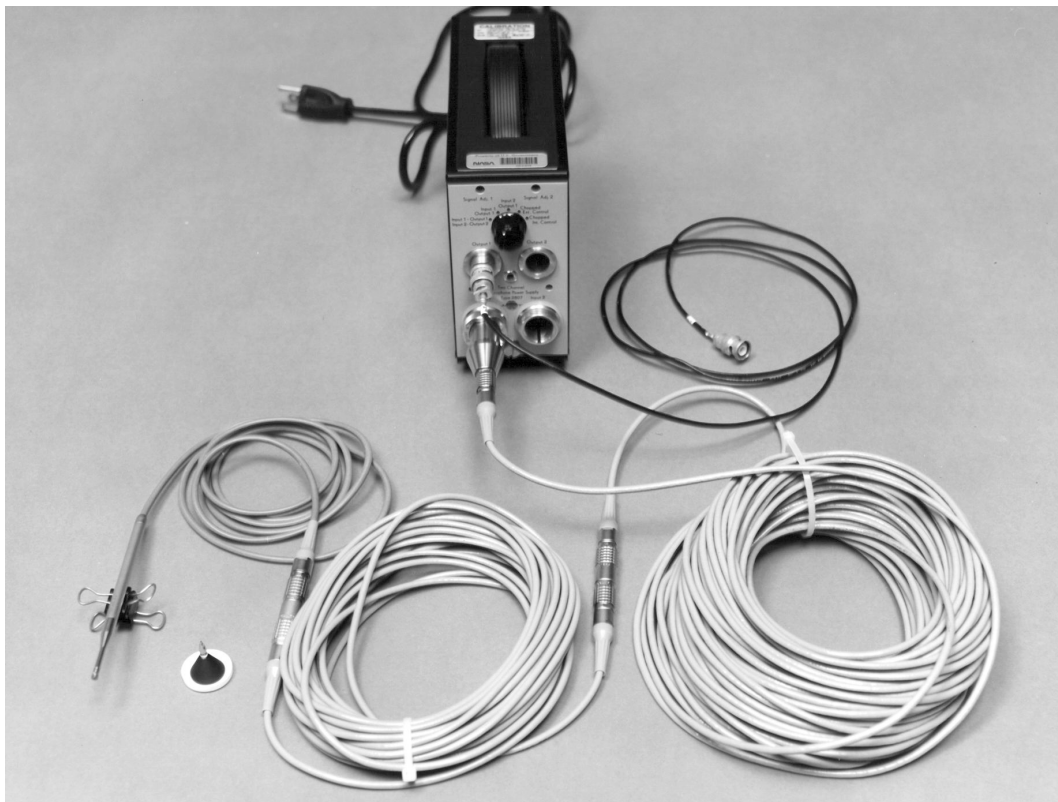


Figure 12. Static pressure probe.



(a) Acoustic pressure probe.



(b) Acoustic probe system.

Figure 13. Acoustic pressure measurement system.

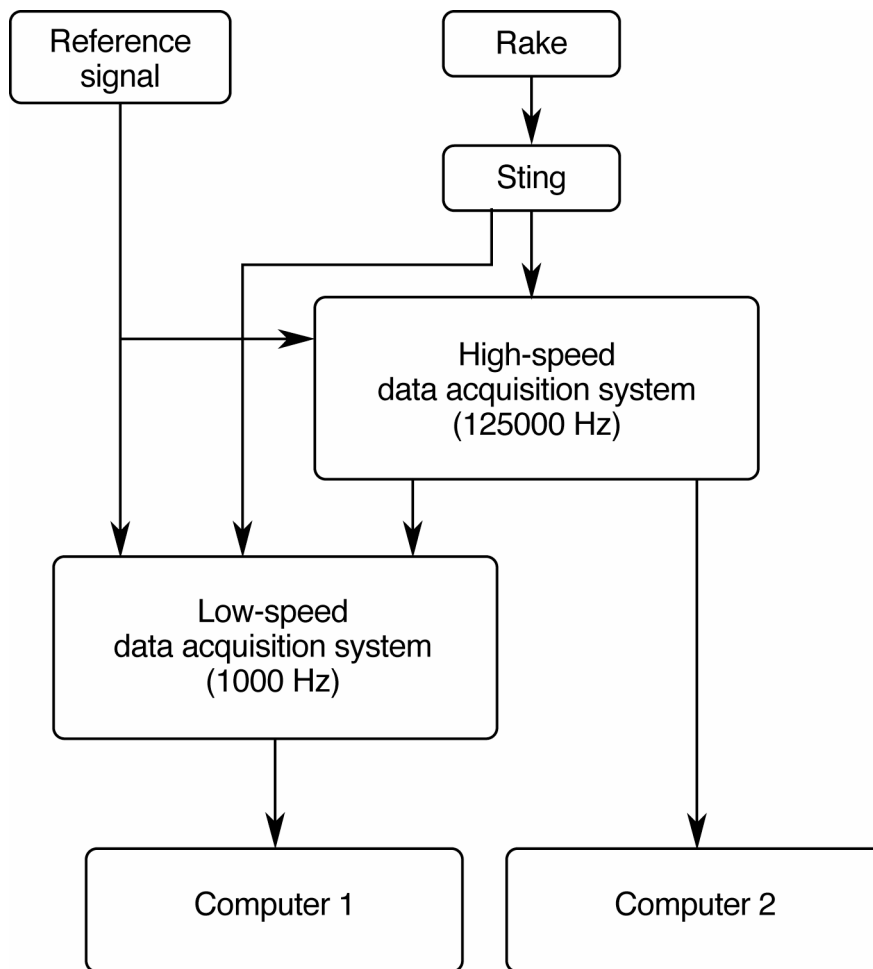
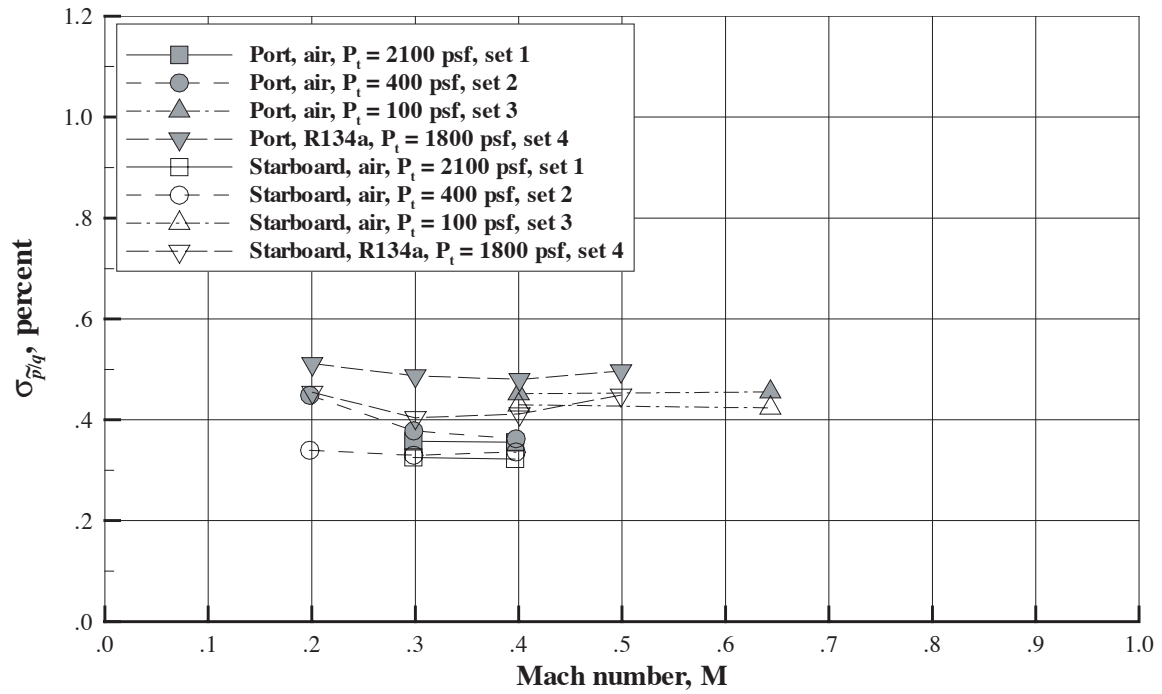
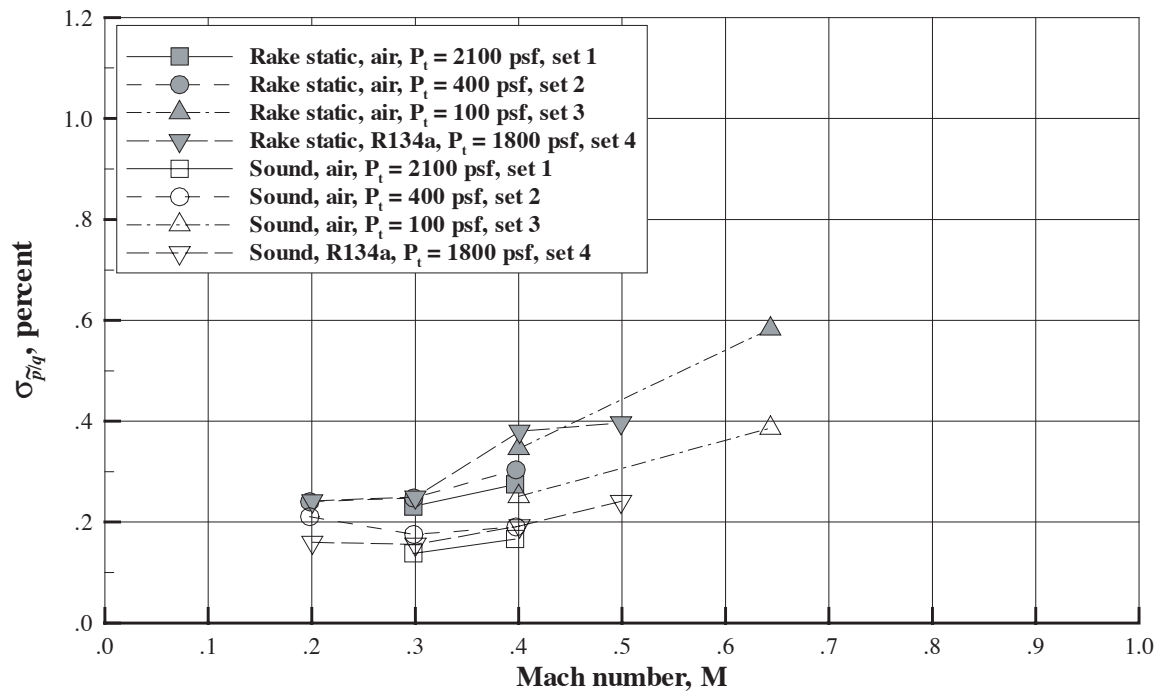


Figure 14. Data flow schematic.

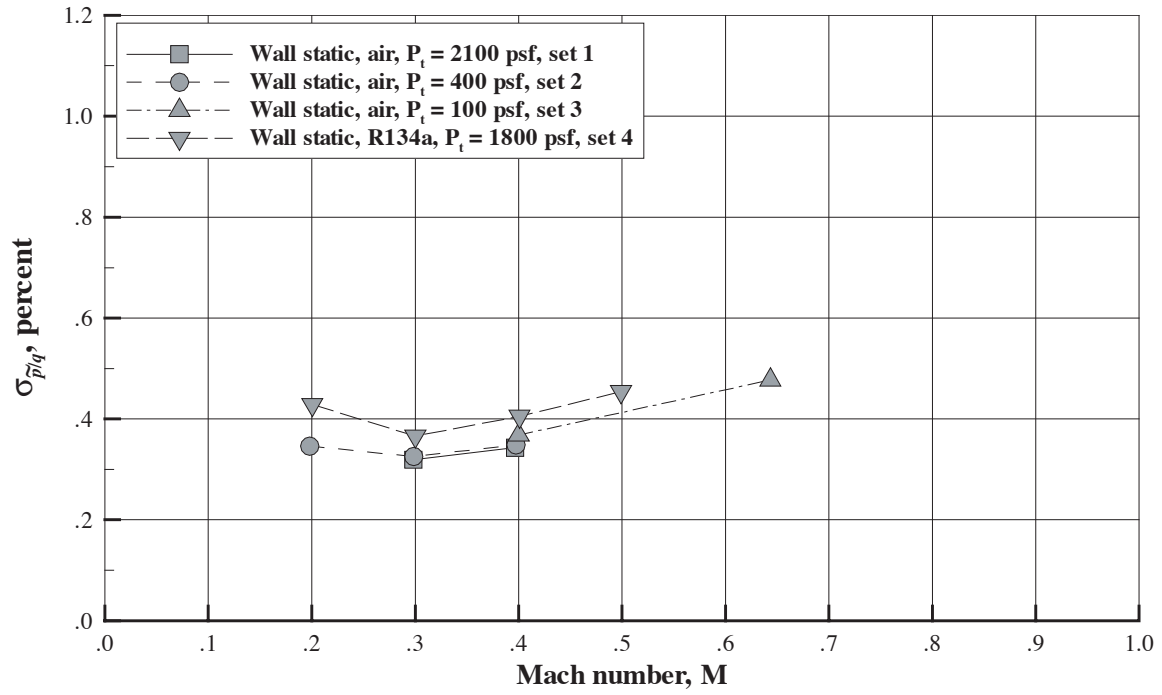


(a) Rake total pressures.



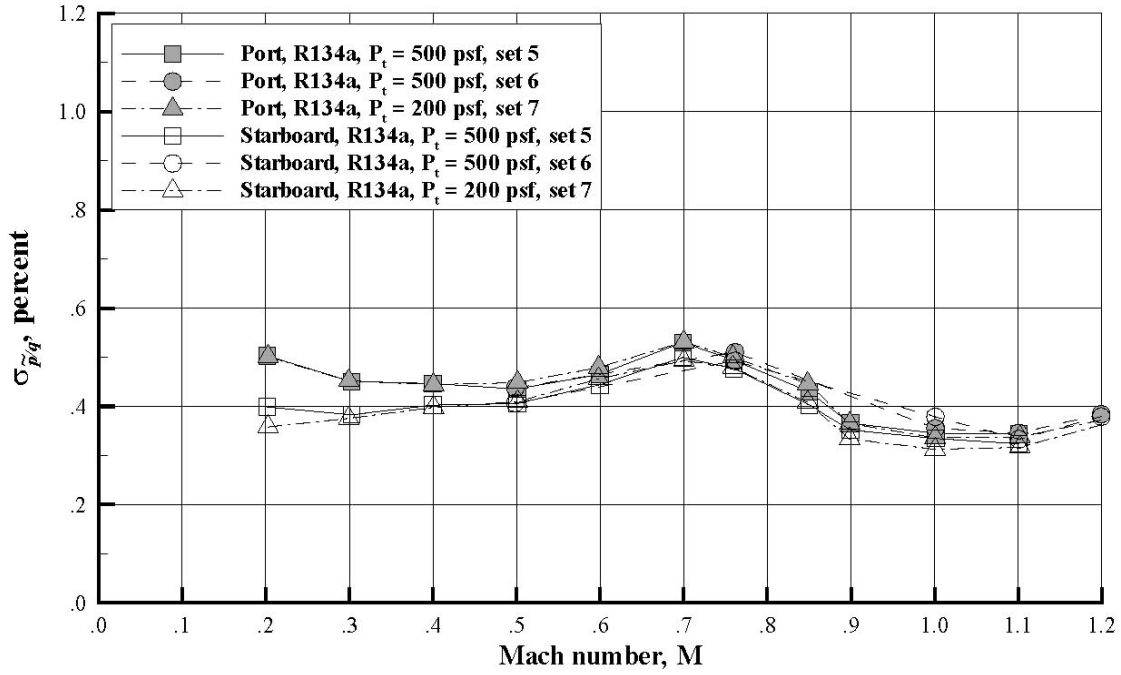
(b) Rake static and acoustic pressures.

Figure 15. Variation of turbulence levels with Mach number at low speed in air and R134a, open slots.

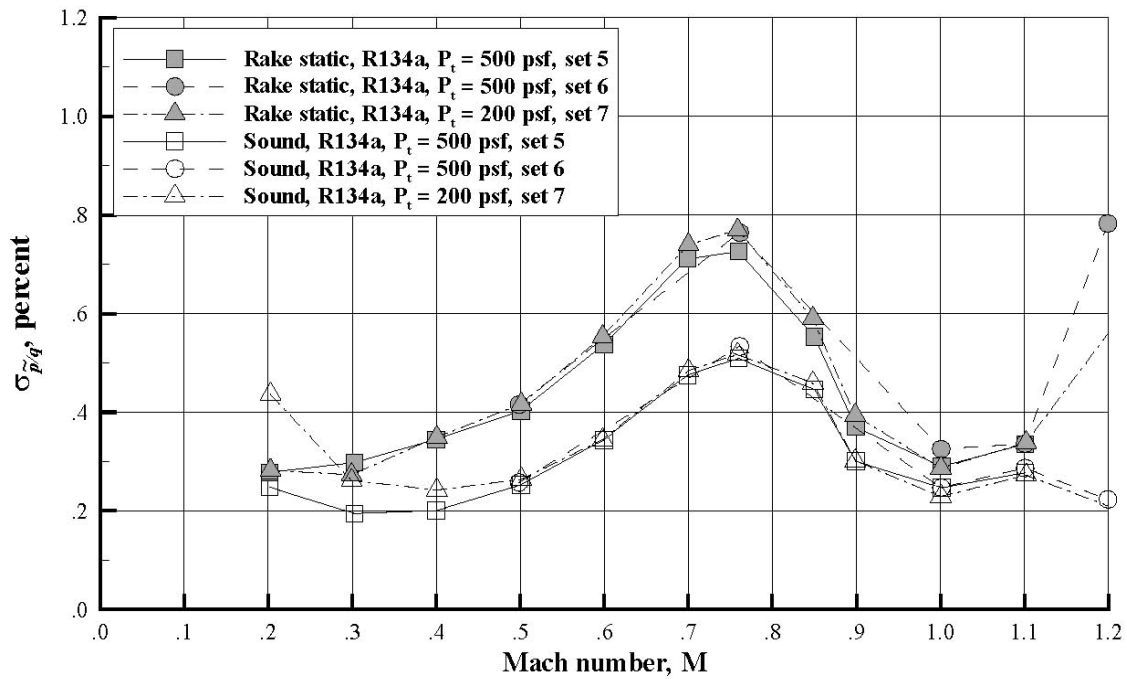


(c) Wall static pressures.

Figure 15. Concluded.

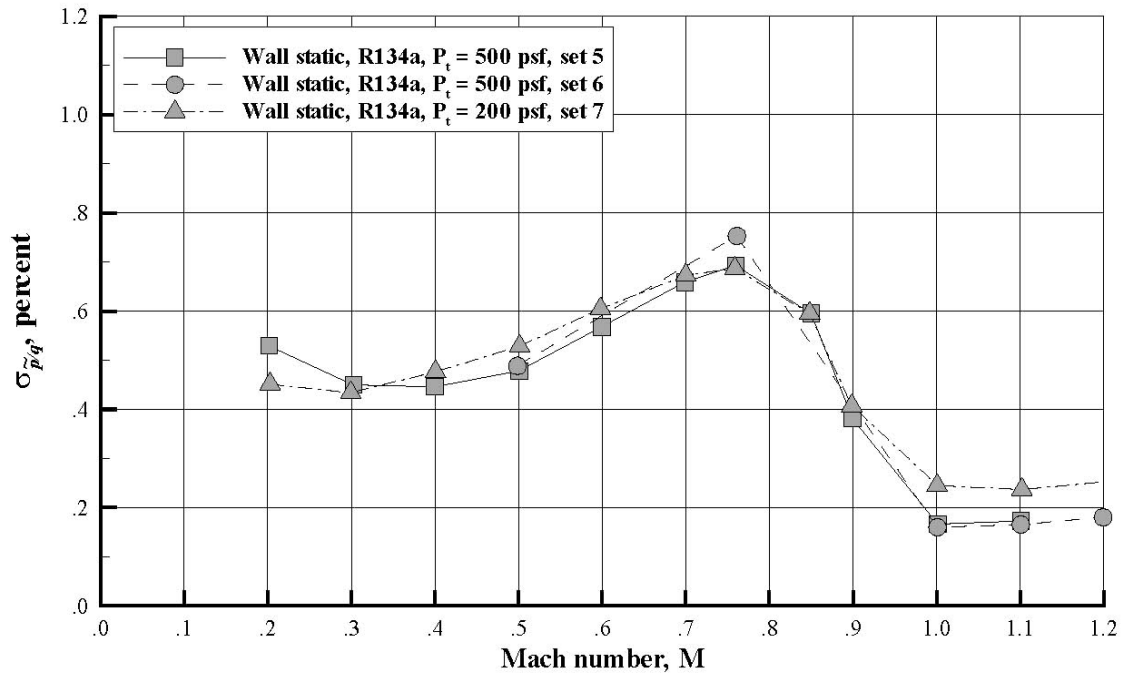


(a) Rake total pressures.



(b) Rake static and acoustic pressures.

Figure 16. Variation of turbulence levels with Mach number in R134a, open slots, $P_t = 200$ and 500 psf.



(c) Wall static pressures.

Figure 16. Concluded.

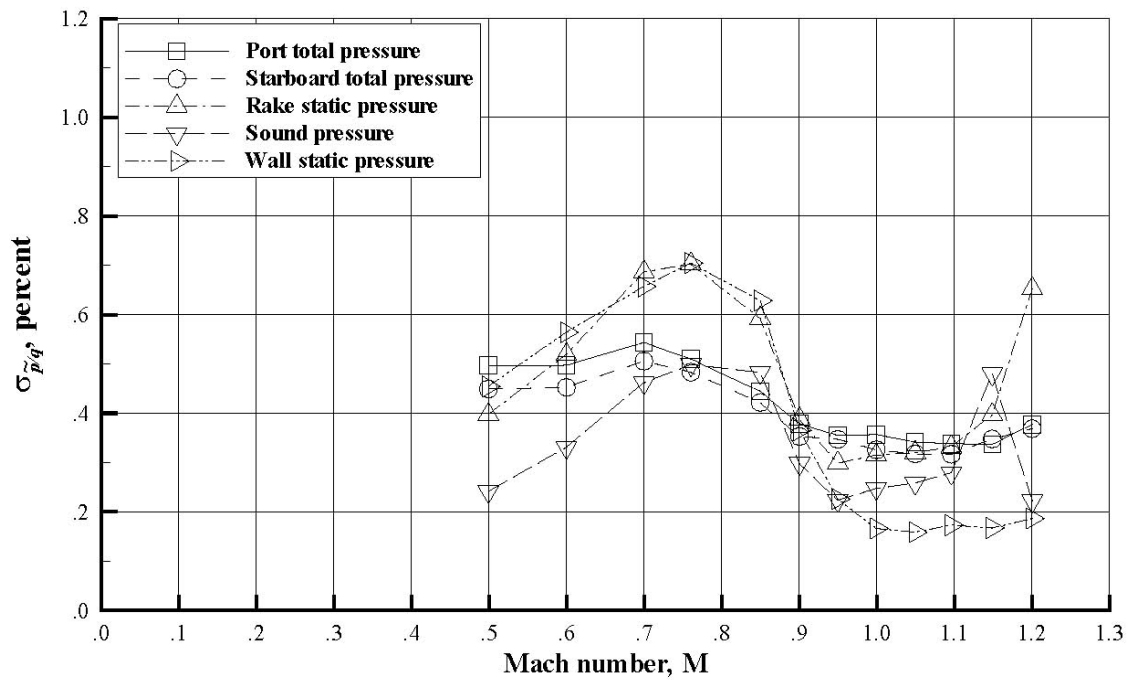
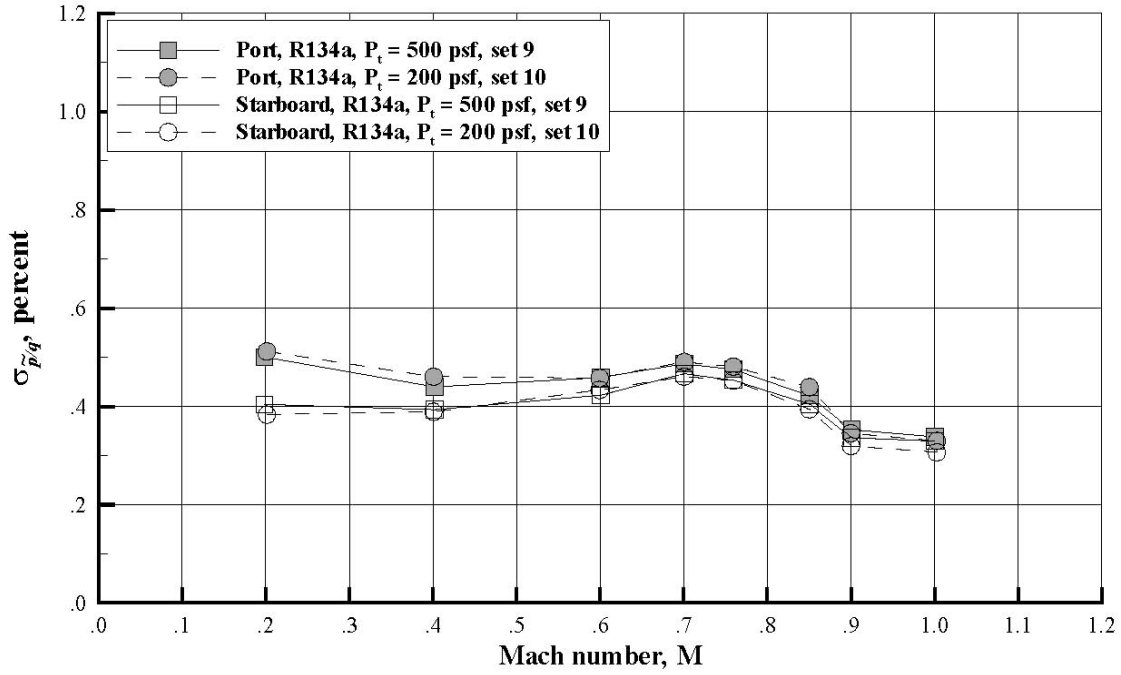
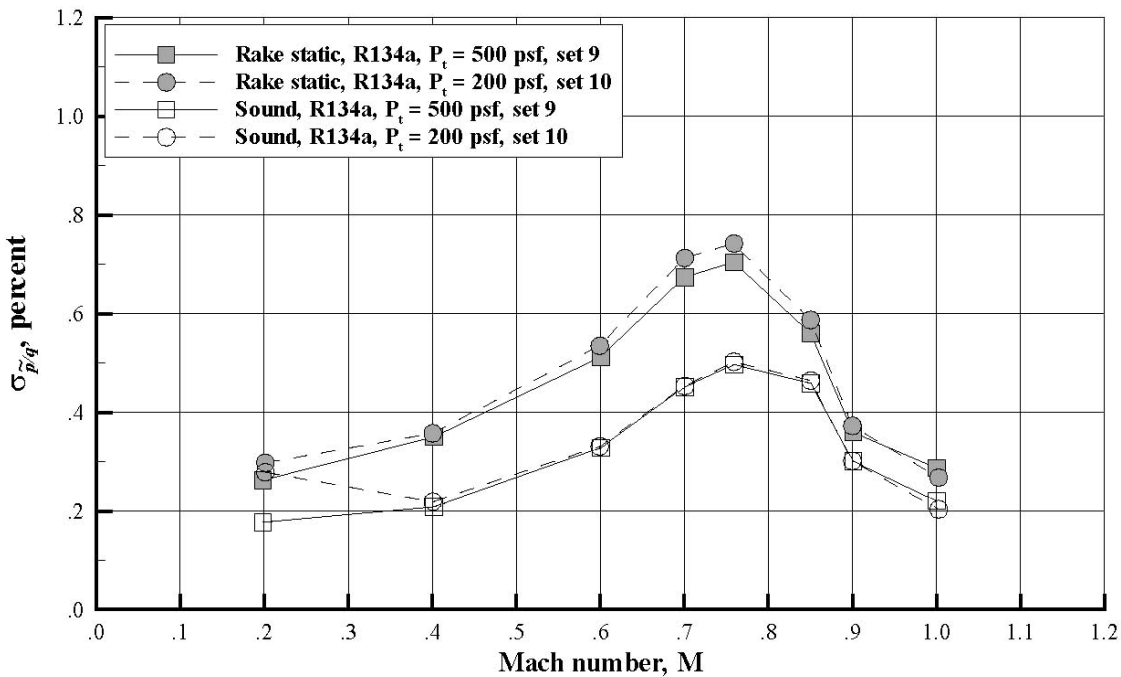


Figure 17. Variation of turbulence levels with Mach number in R134a for various P_t , open slots, $q = 225$ psf.

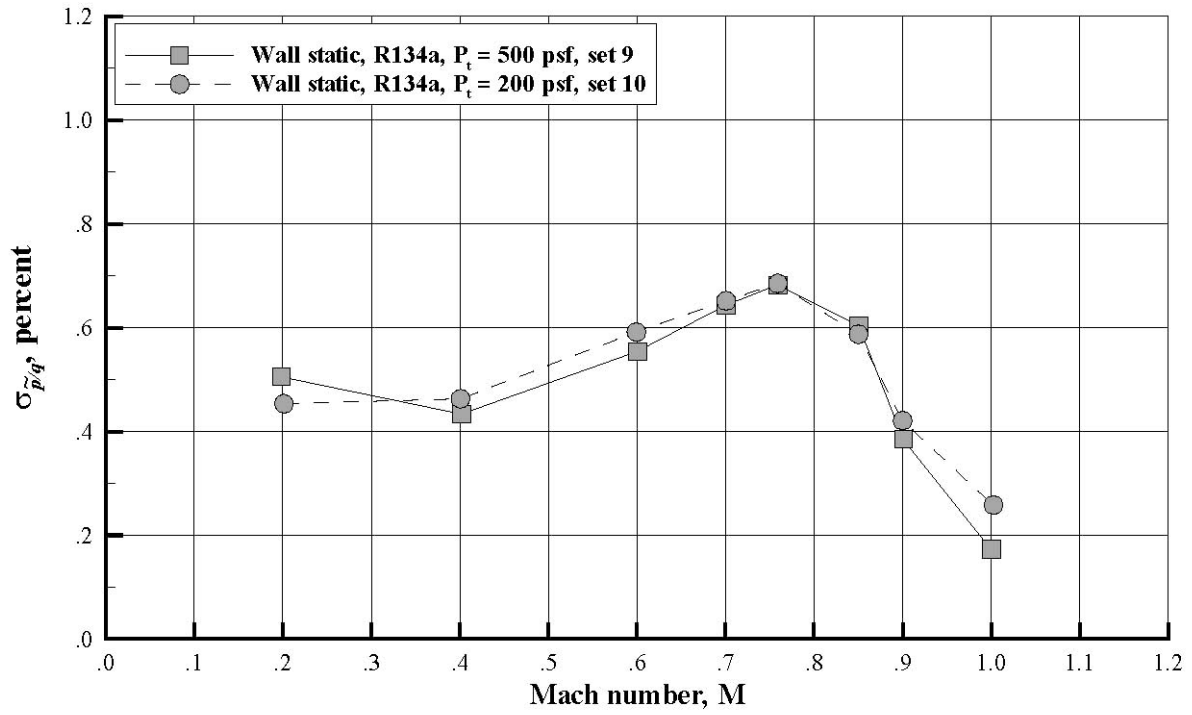


(a) Rake total pressures.



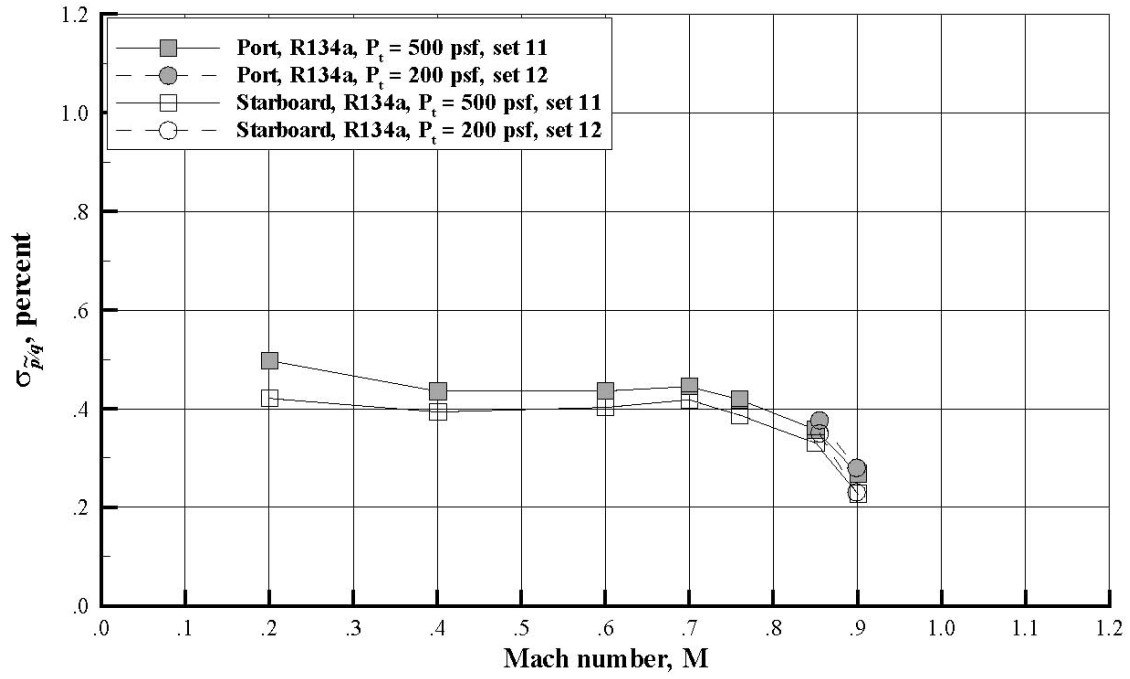
(b) Rake static and acoustic pressures.

Figure 18. Effect of covered wall slots on turbulence levels with Mach number in R134a, $P_t = 500$ and 200 psf.

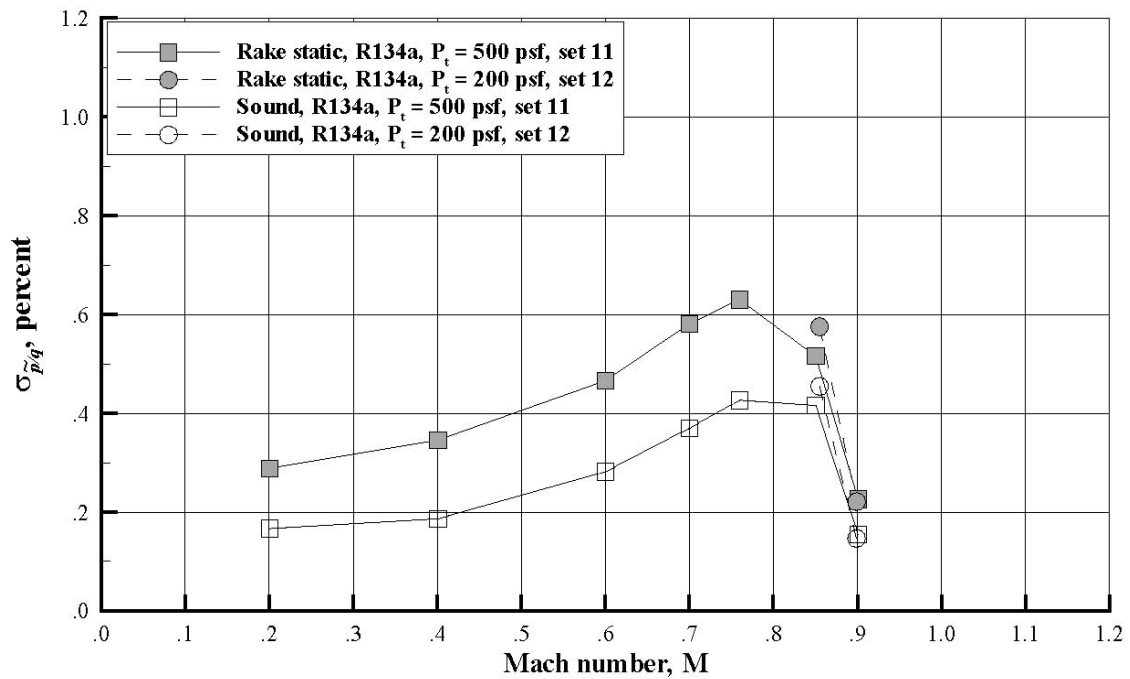


(c) Wall static pressures.

Figure 18. Concluded.

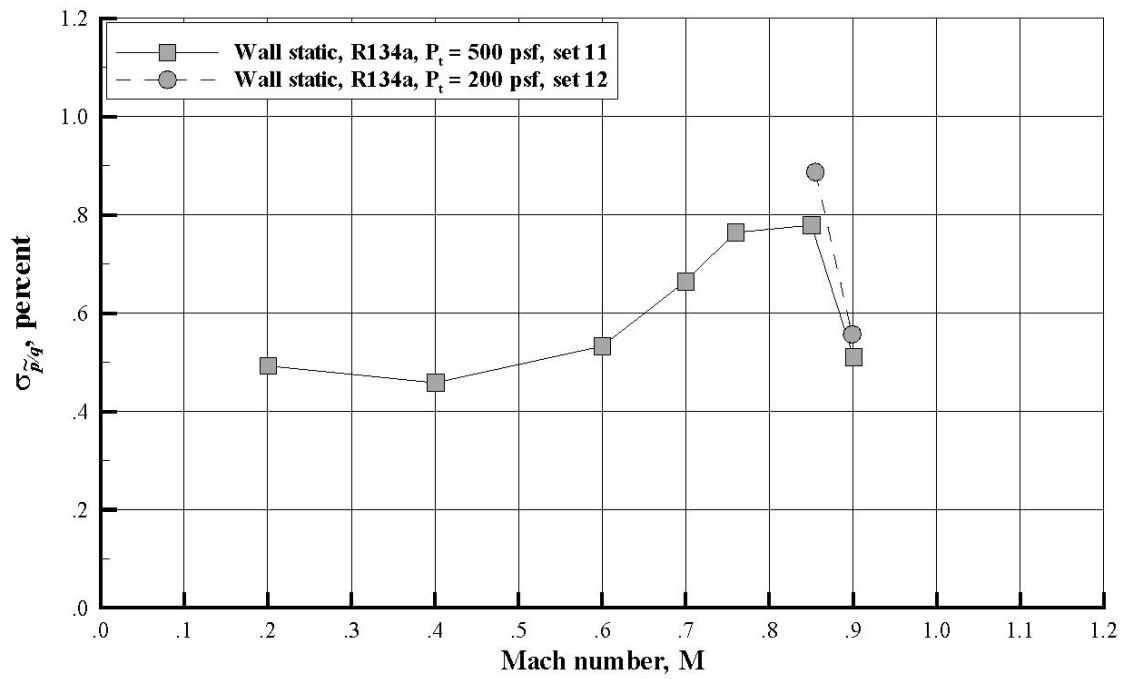


(a) Rake total pressures.



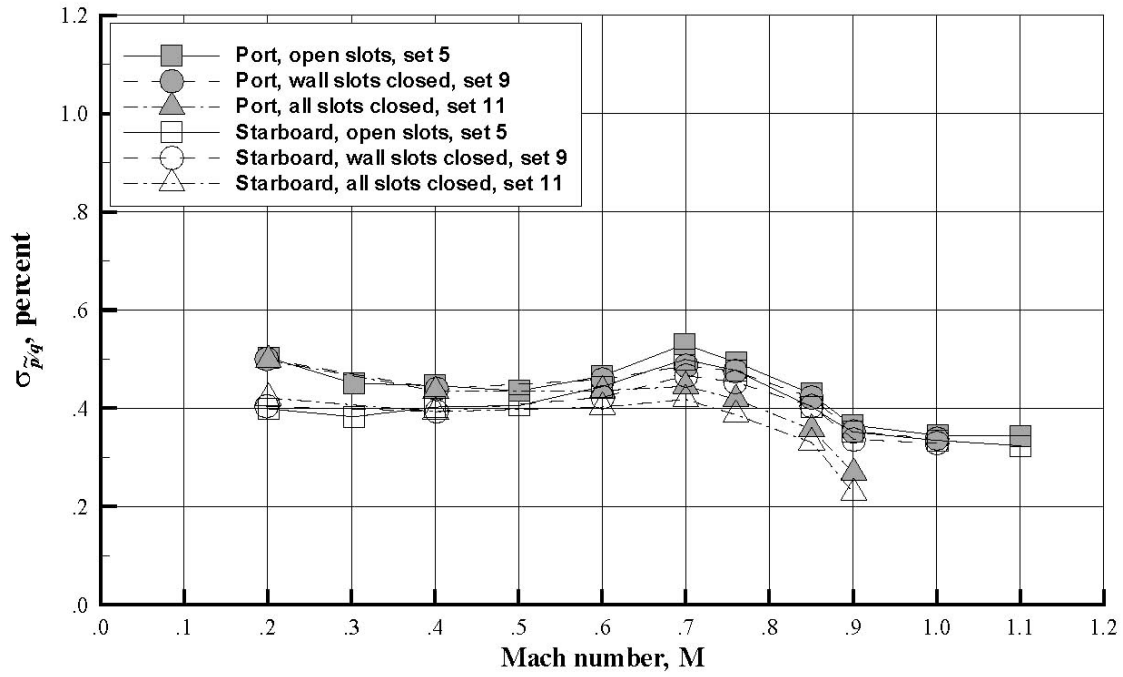
(b) Rake static and acoustic pressures.

Figure 19. Effect of slot covering on turbulence levels in R134a, $P_t = 500$ and 200 psf.

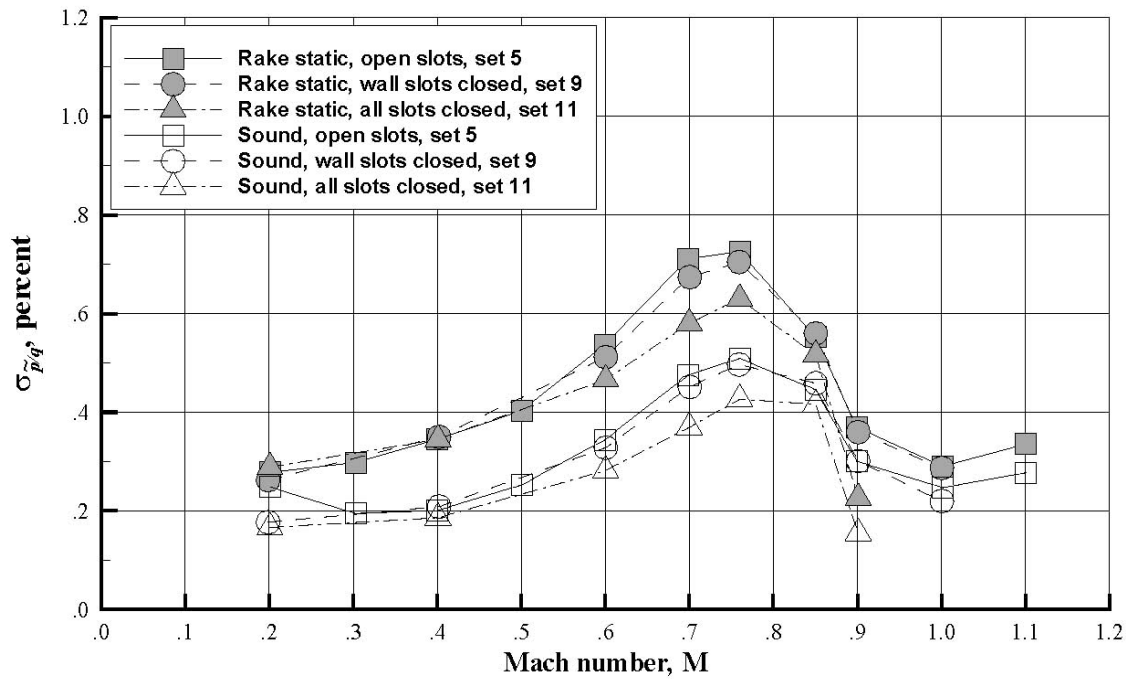


(c) Wall static pressures.

Figure 19. Concluded.

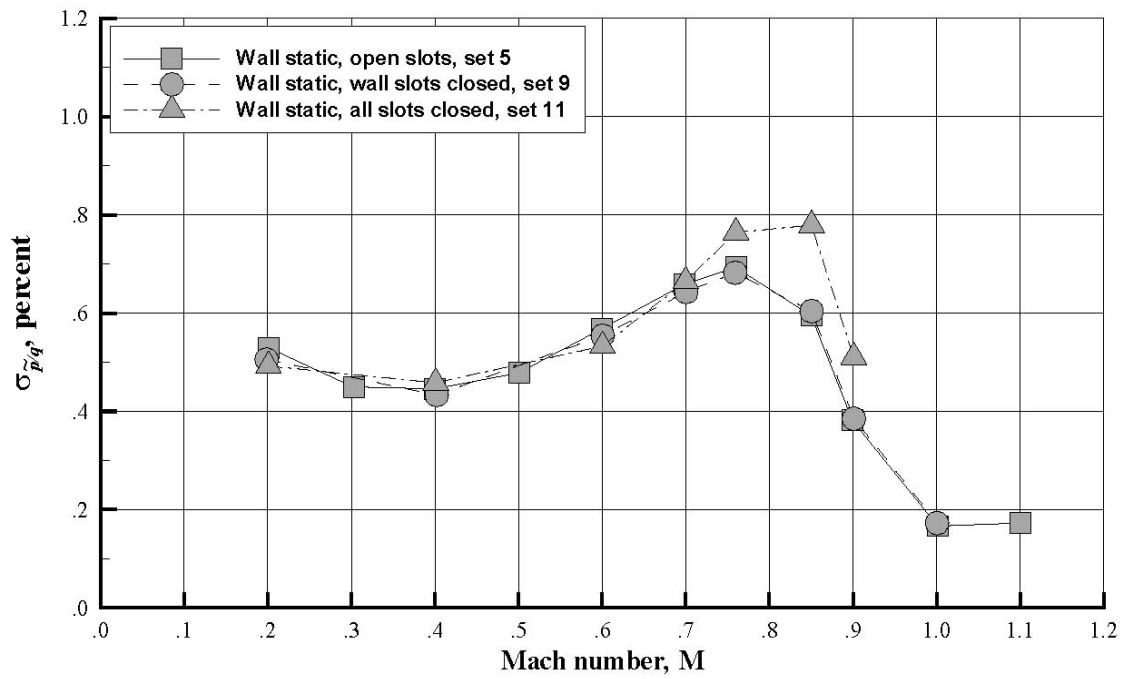


(a) Rake total pressures.



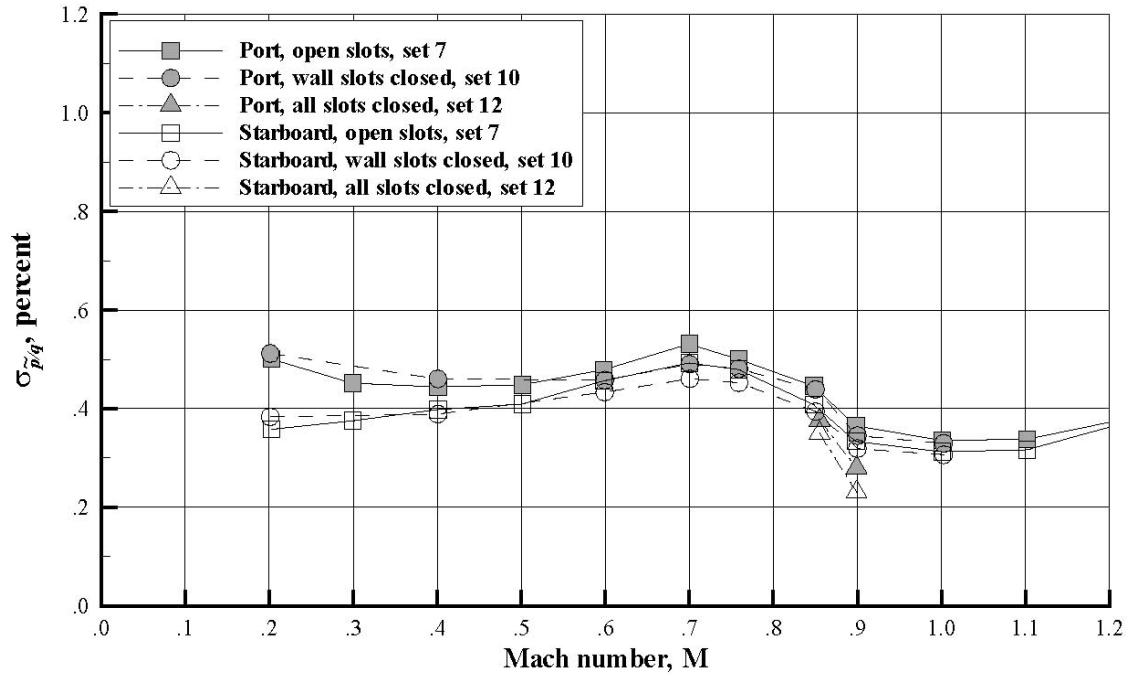
(b) Rake static and acoustic pressures.

Figure 20. Effect of slot covering on turbulence levels in R134a, $P_t = 500$ psf.

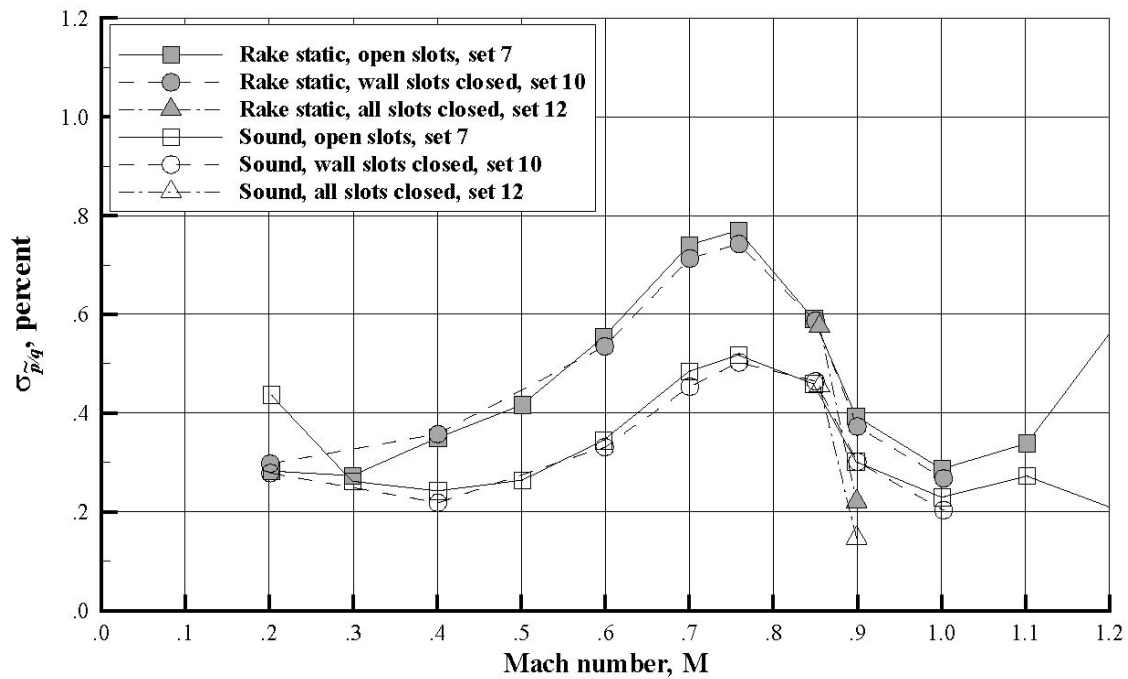


(c) Wall static pressures.

Figure 20. Concluded.

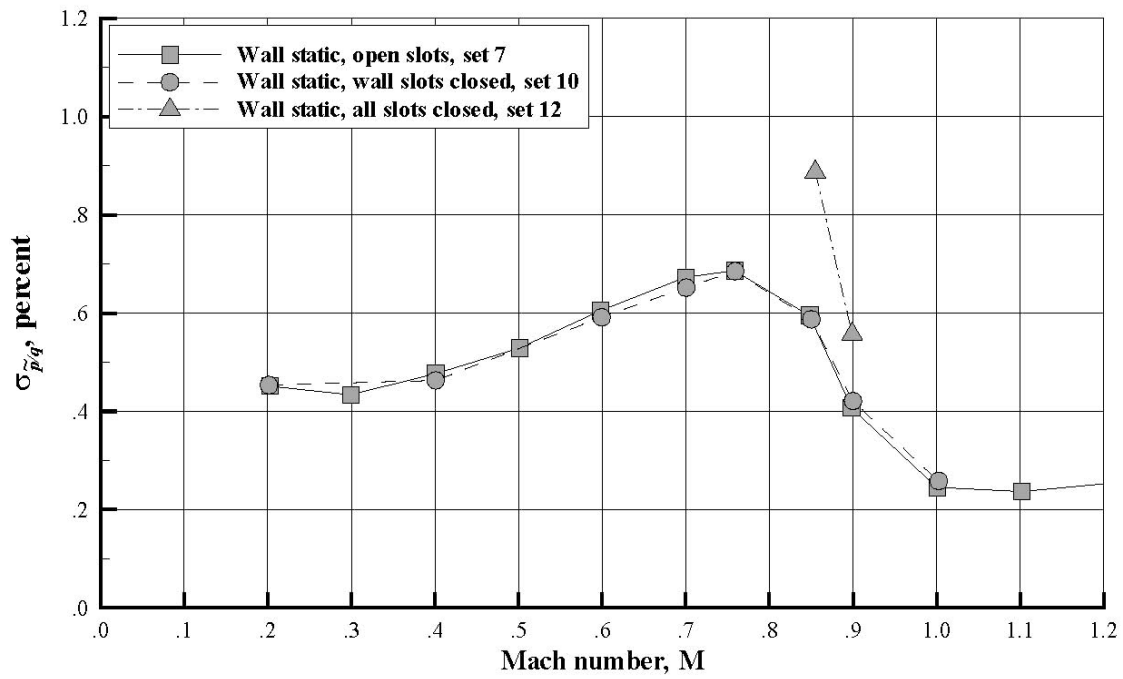


(a) Rake total pressures.



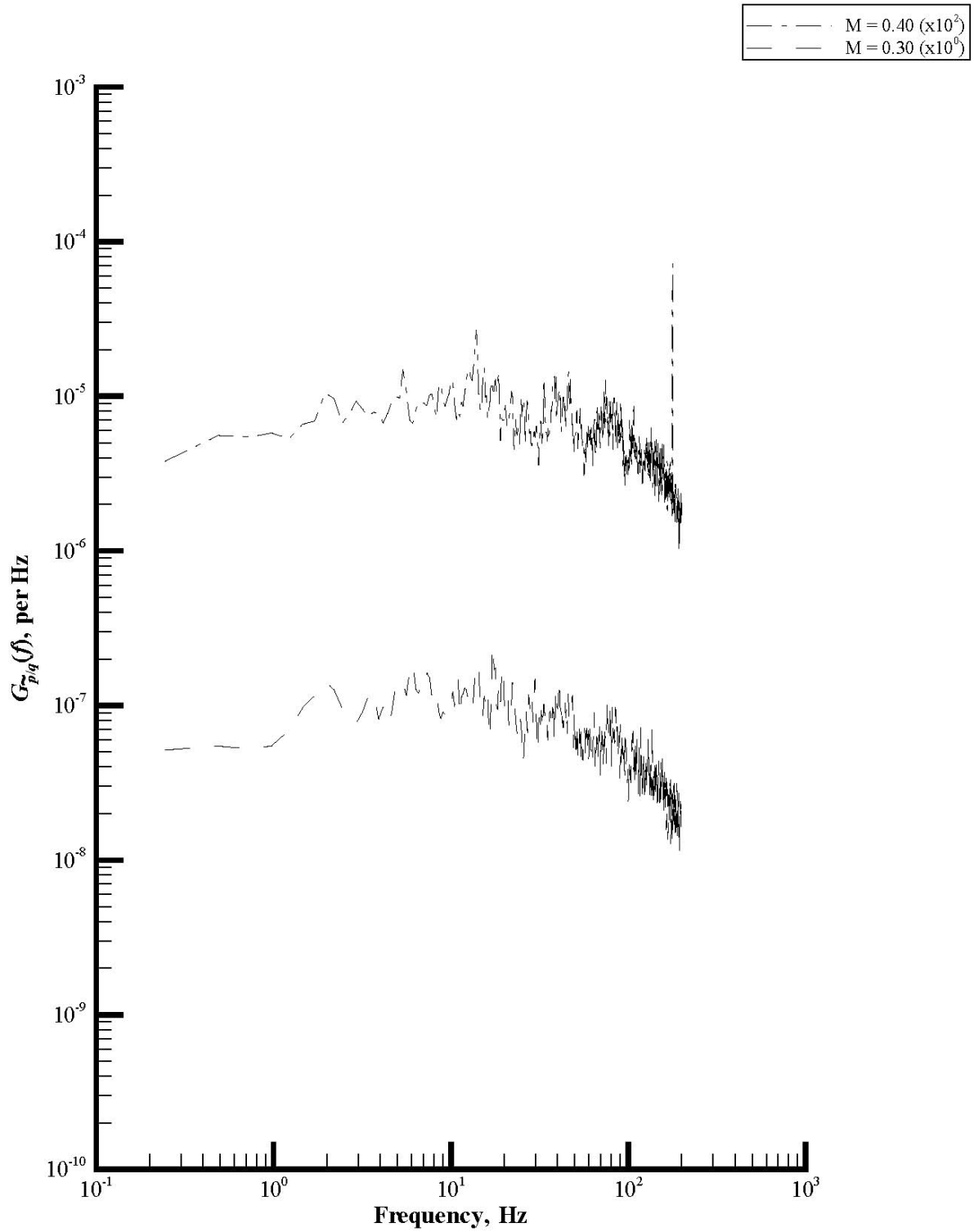
(b) Rake static and acoustic pressures.

Figure 21. Effect of slot covering on turbulence levels in R134a; $P_t = 200$ psf.



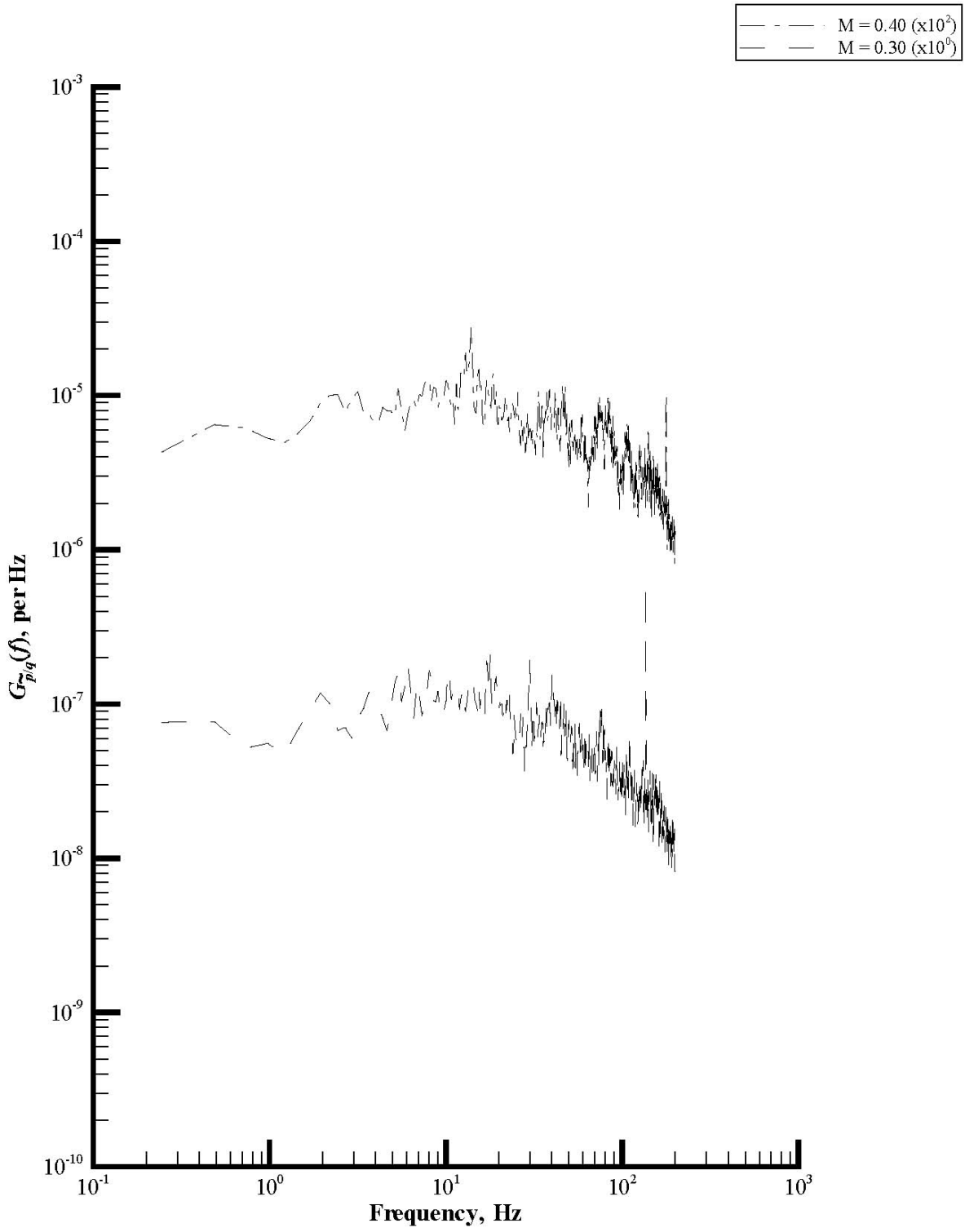
(c) Wall static pressures.

Figure 21. Concluded.



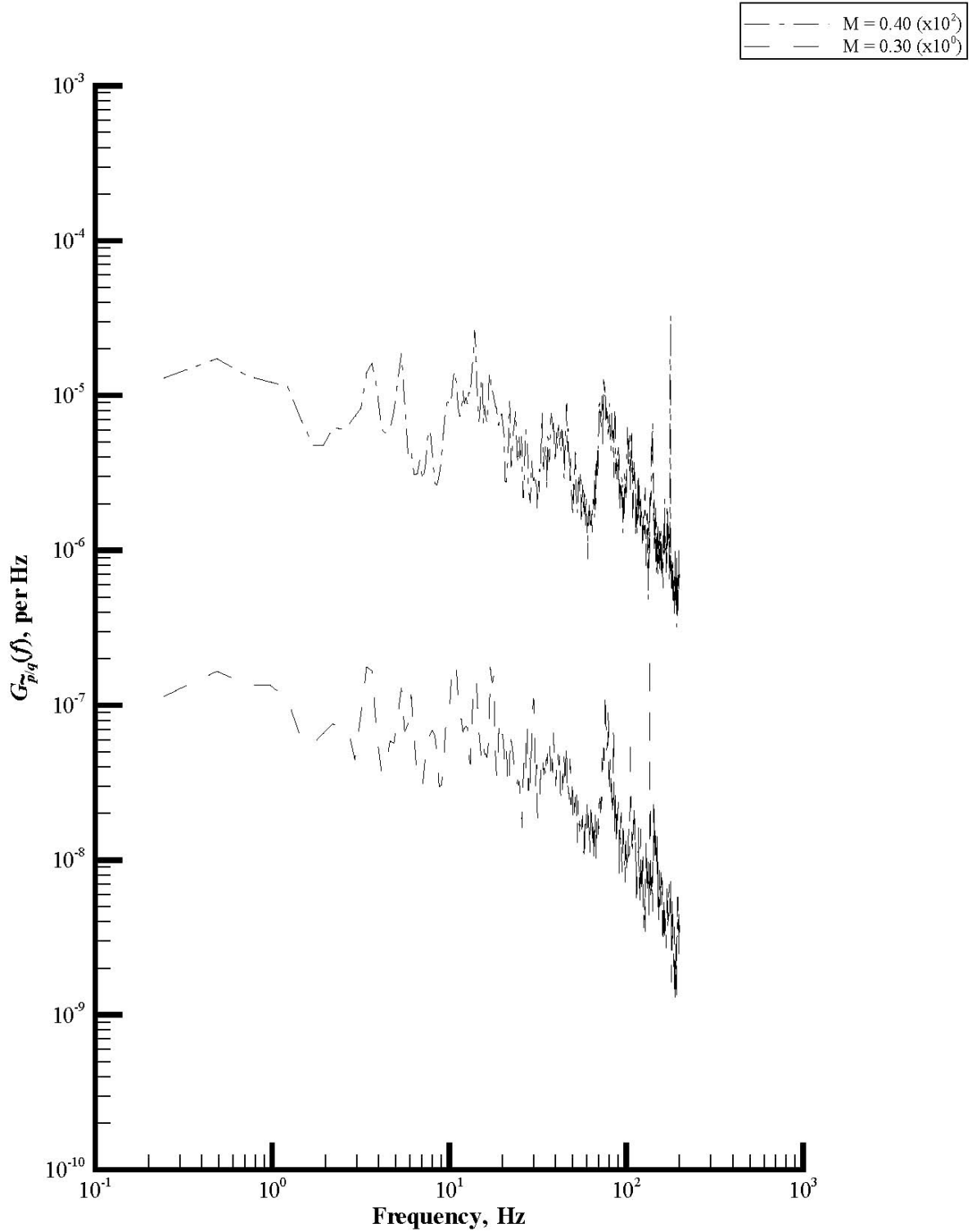
(a) Rake port total pressure.

Figure 22. Plots of power spectral density functions of set 1.



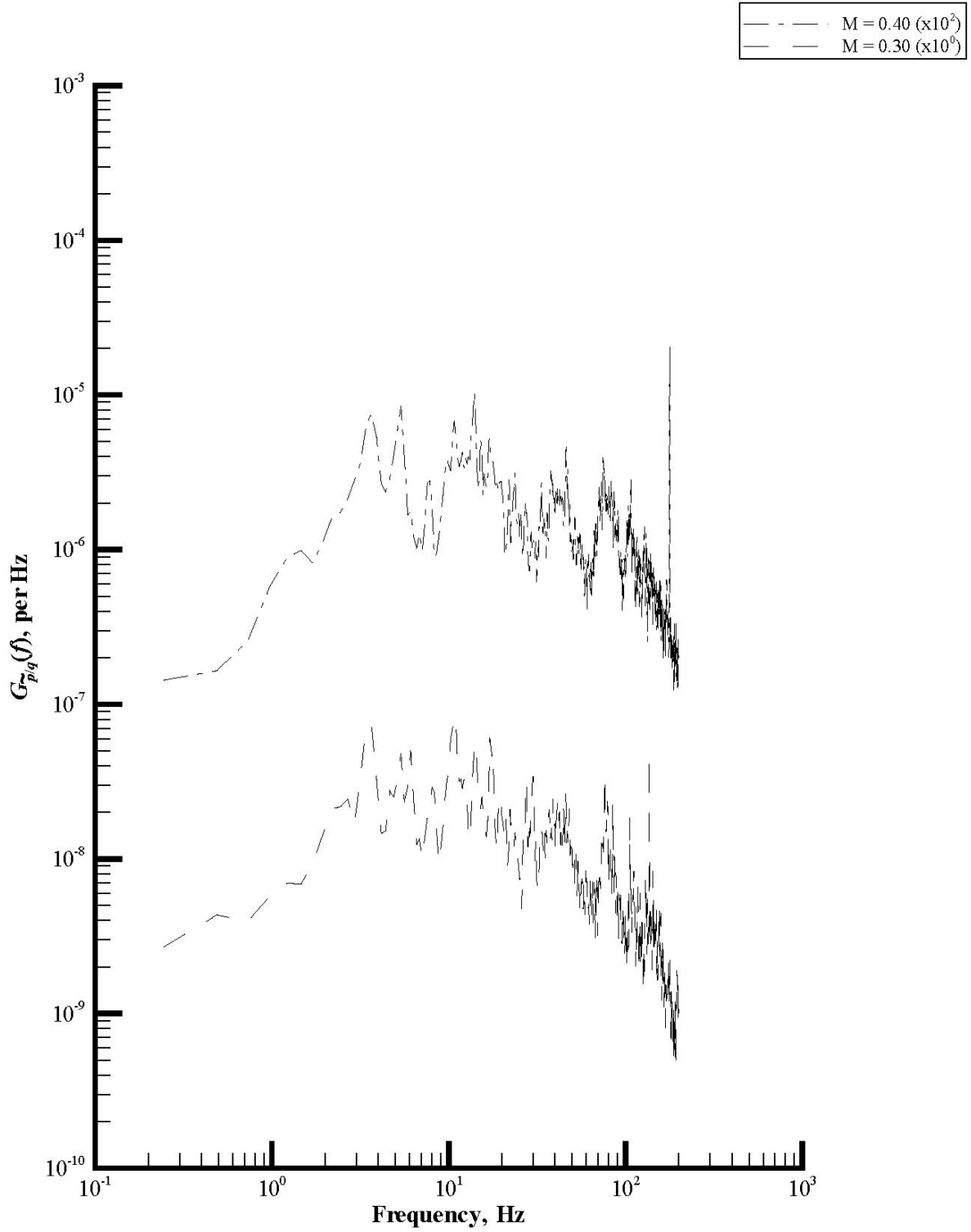
(b) Rake starboard total pressure.

Figure 22. Continued.



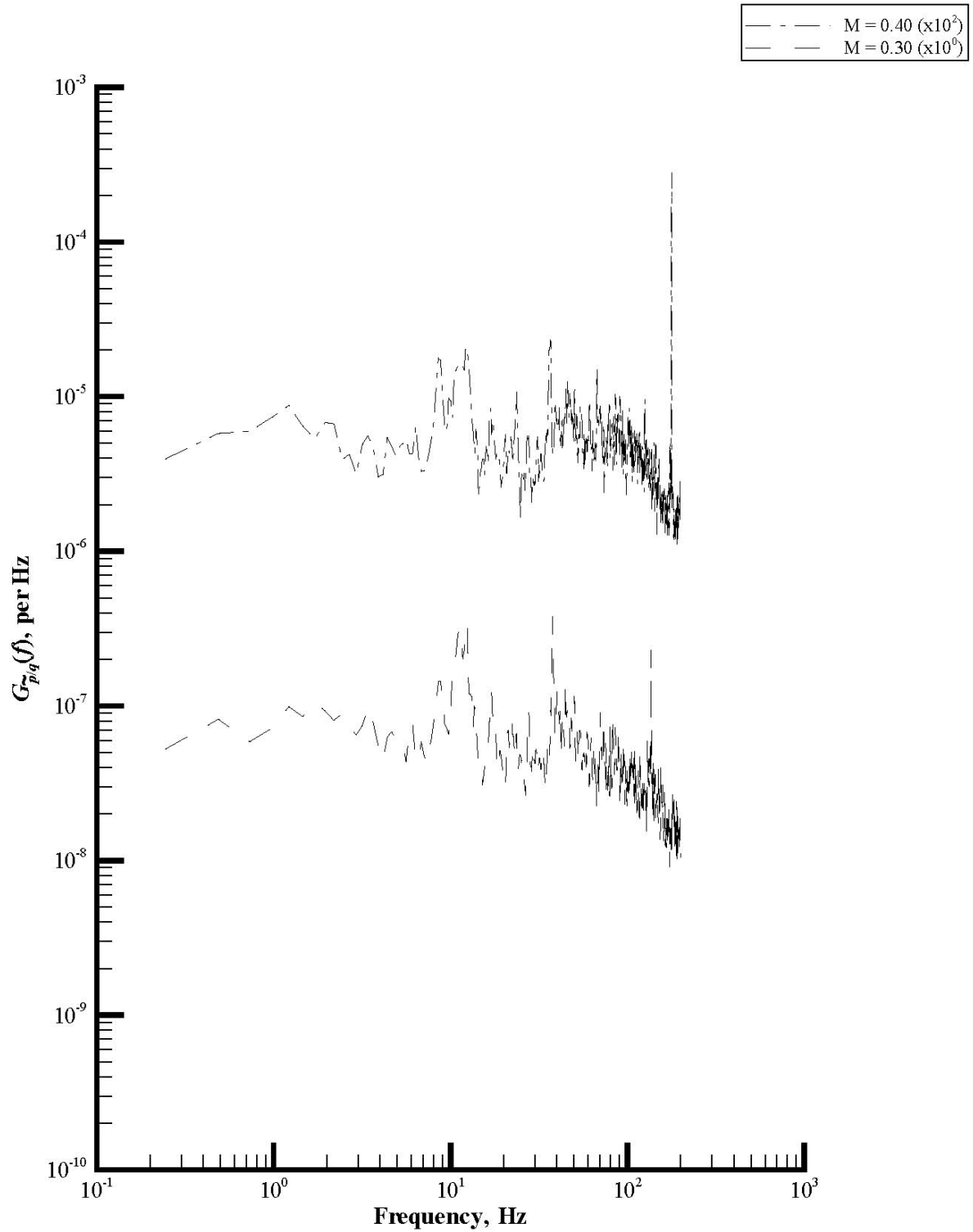
(c) Rake static pressure.

Figure 22. Continued.



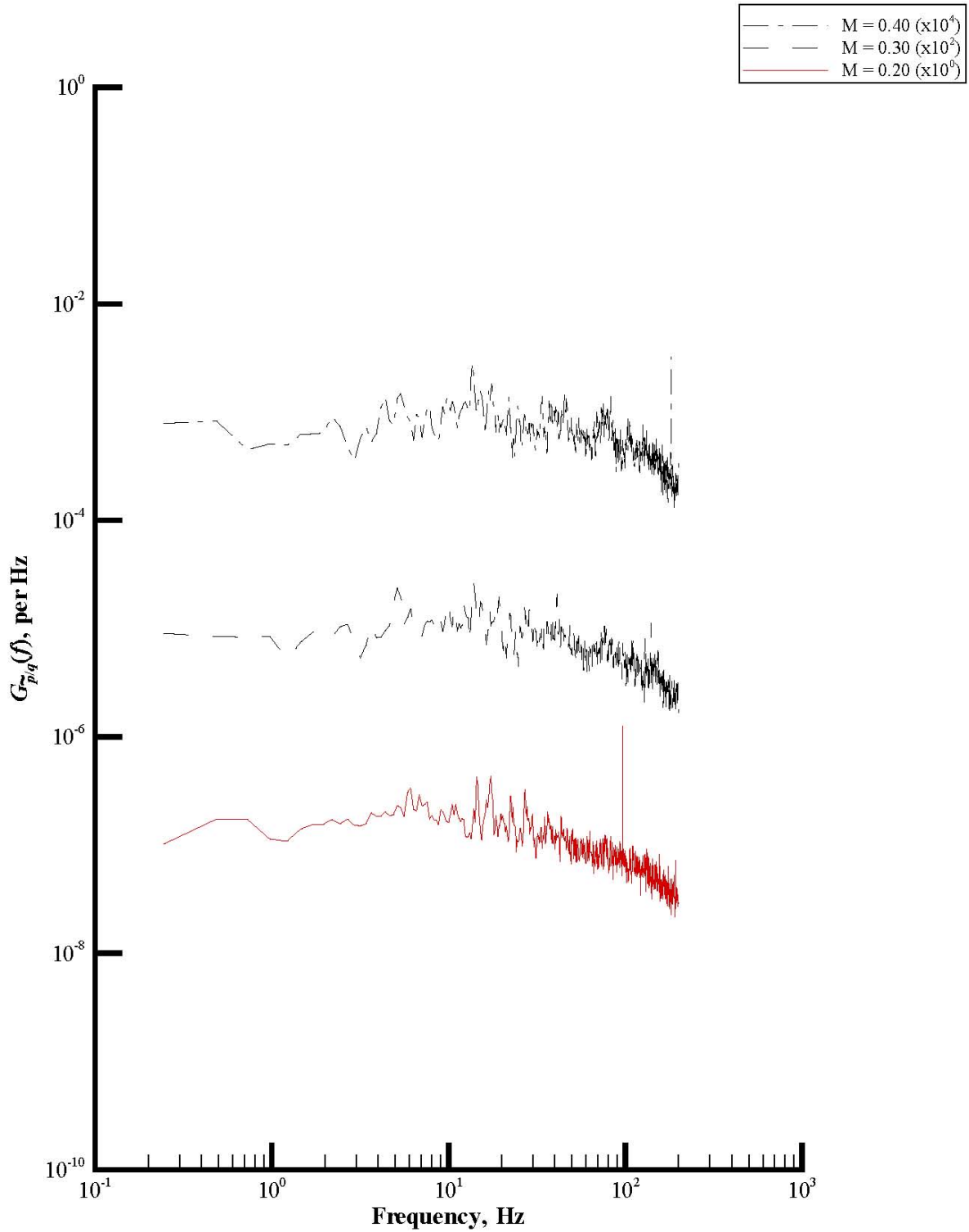
(d) Rake acoustic pressure.

Figure 22. Continued.



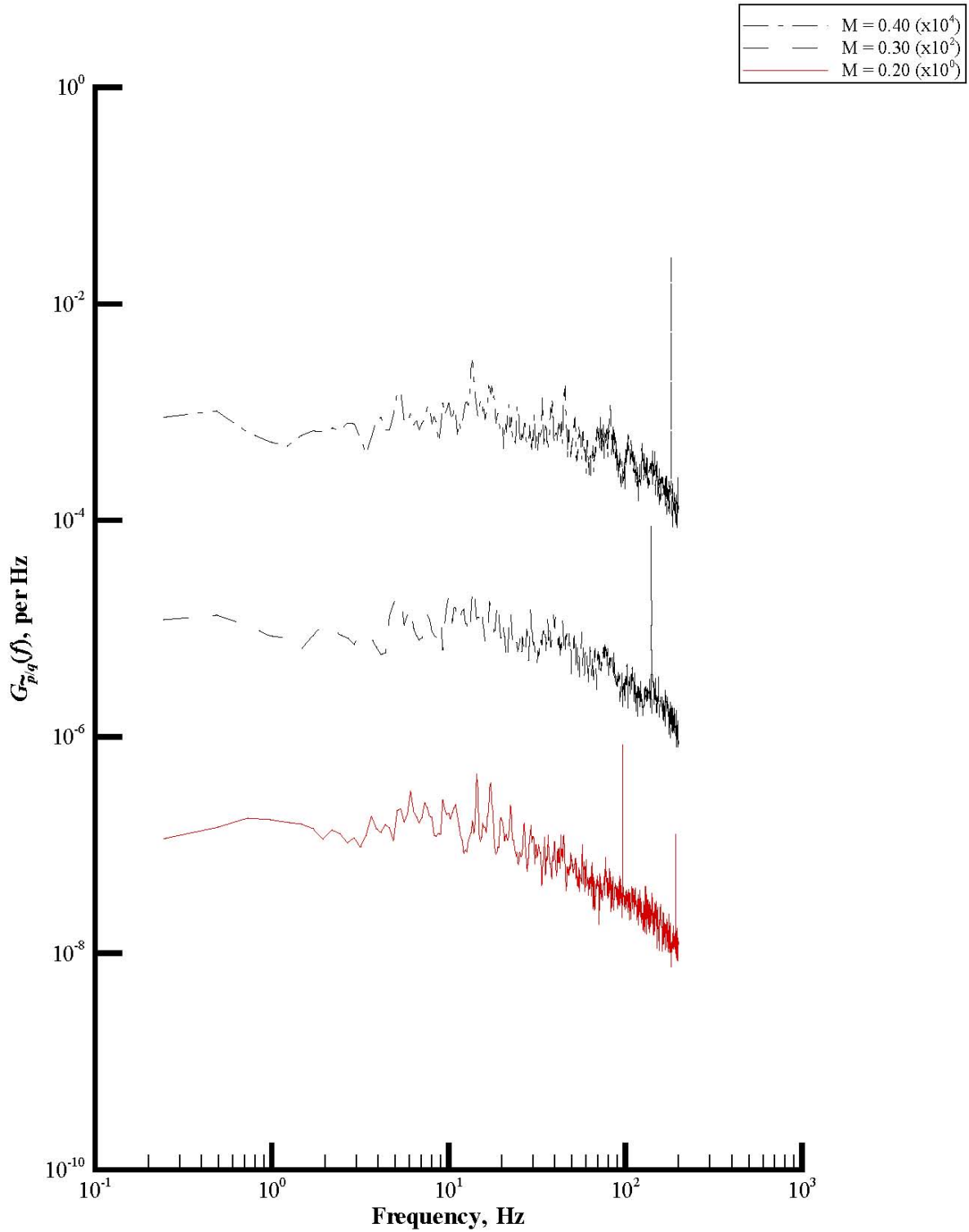
(e) Wall static pressure.

Figure 22. Concluded.



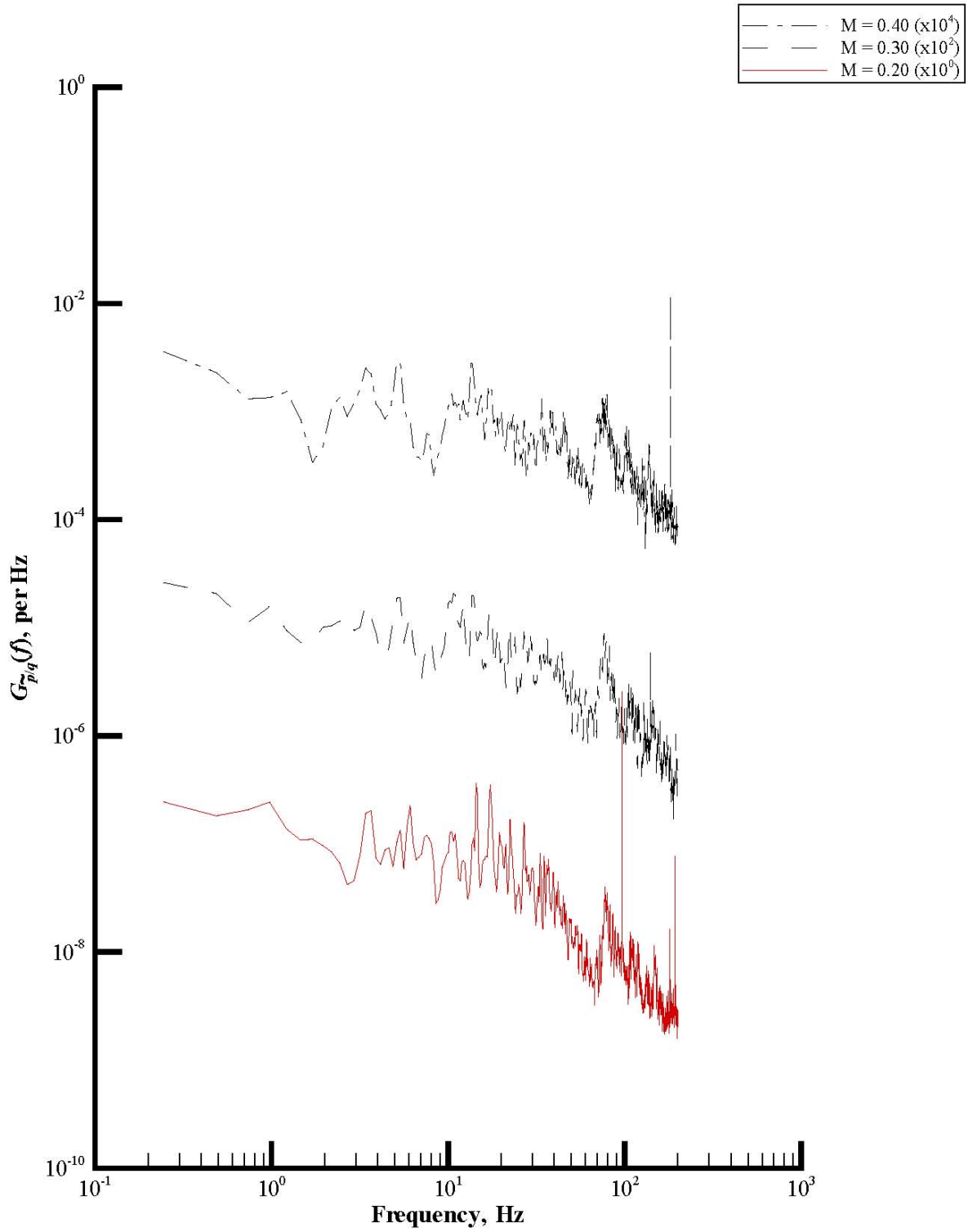
(a) Rake port total pressure.

Figure 23. Plots of power spectral density functions of set 2.



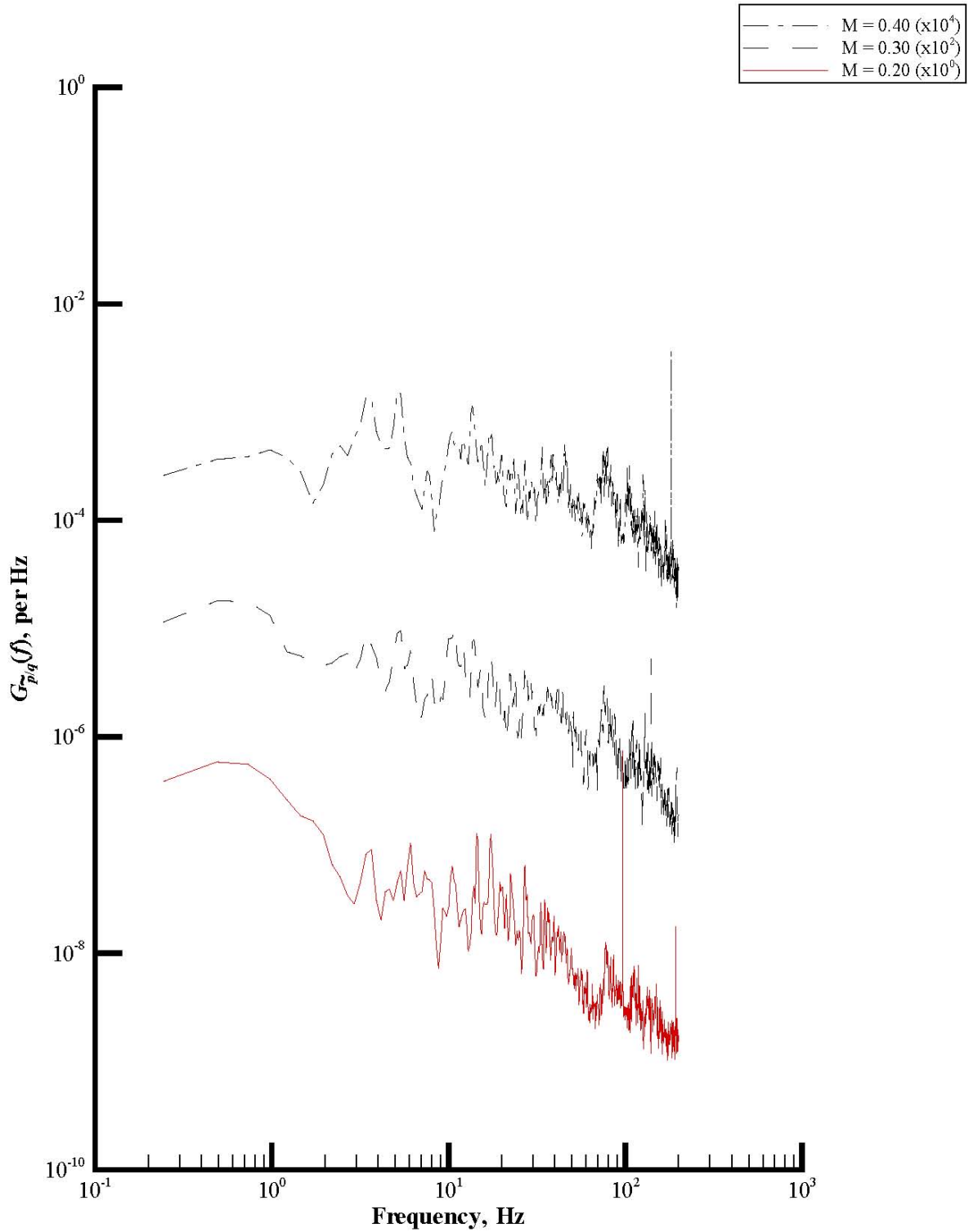
(b) Rake starboard total pressure.

Figure 23. Continued.



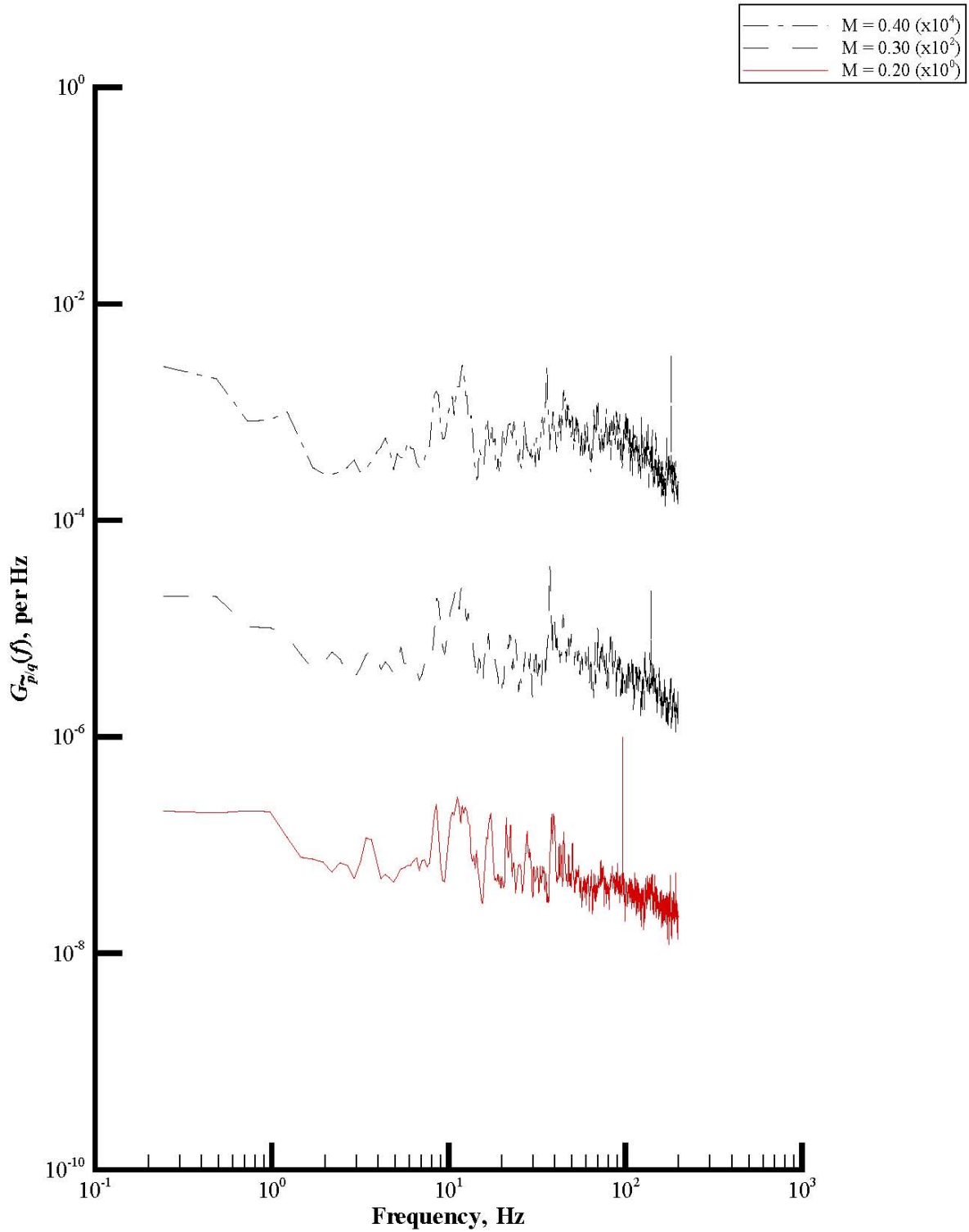
(c) Rake static pressure.

Figure 23. Continued.



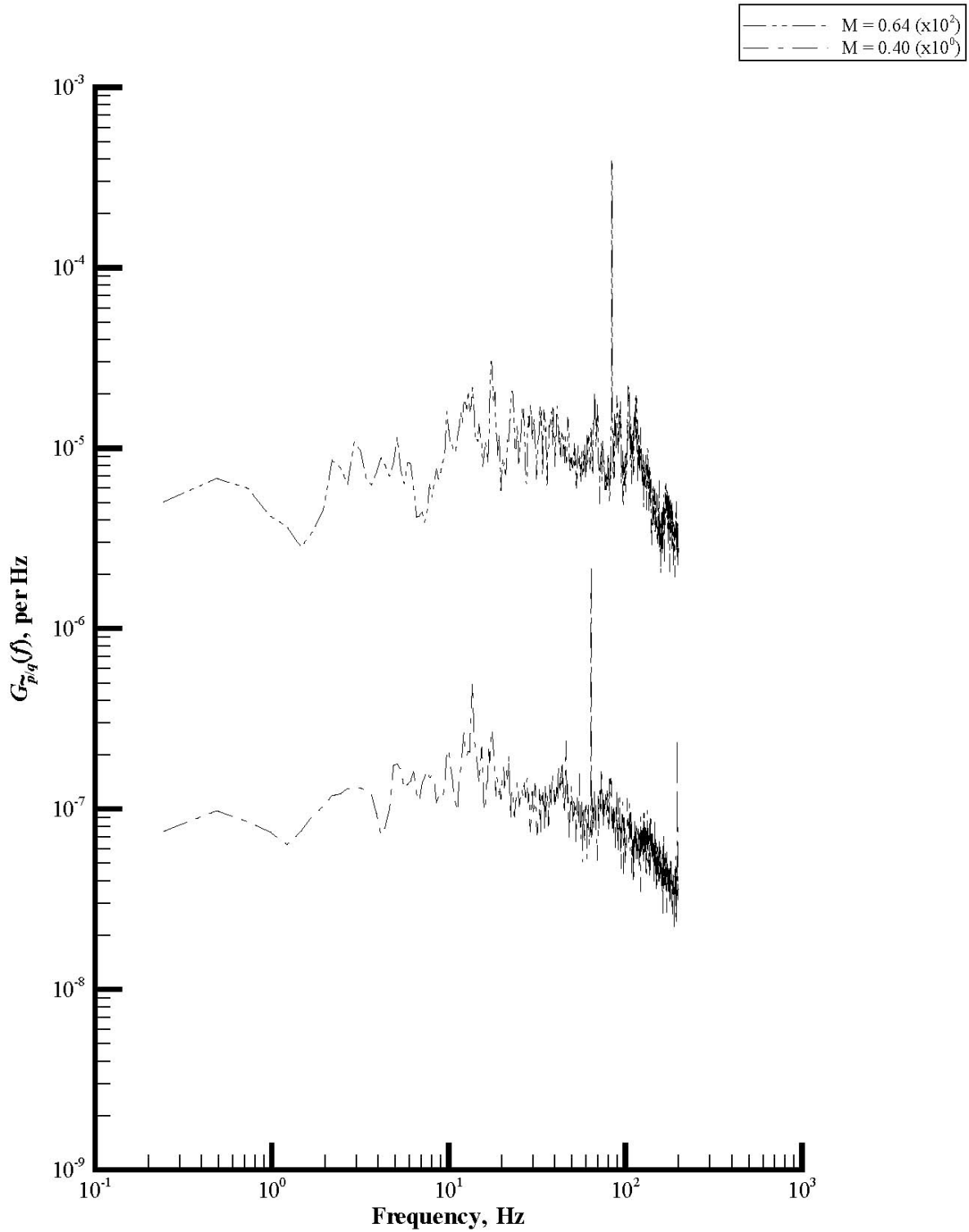
(d) Rake acoustic pressure.

Figure 23. Continued.



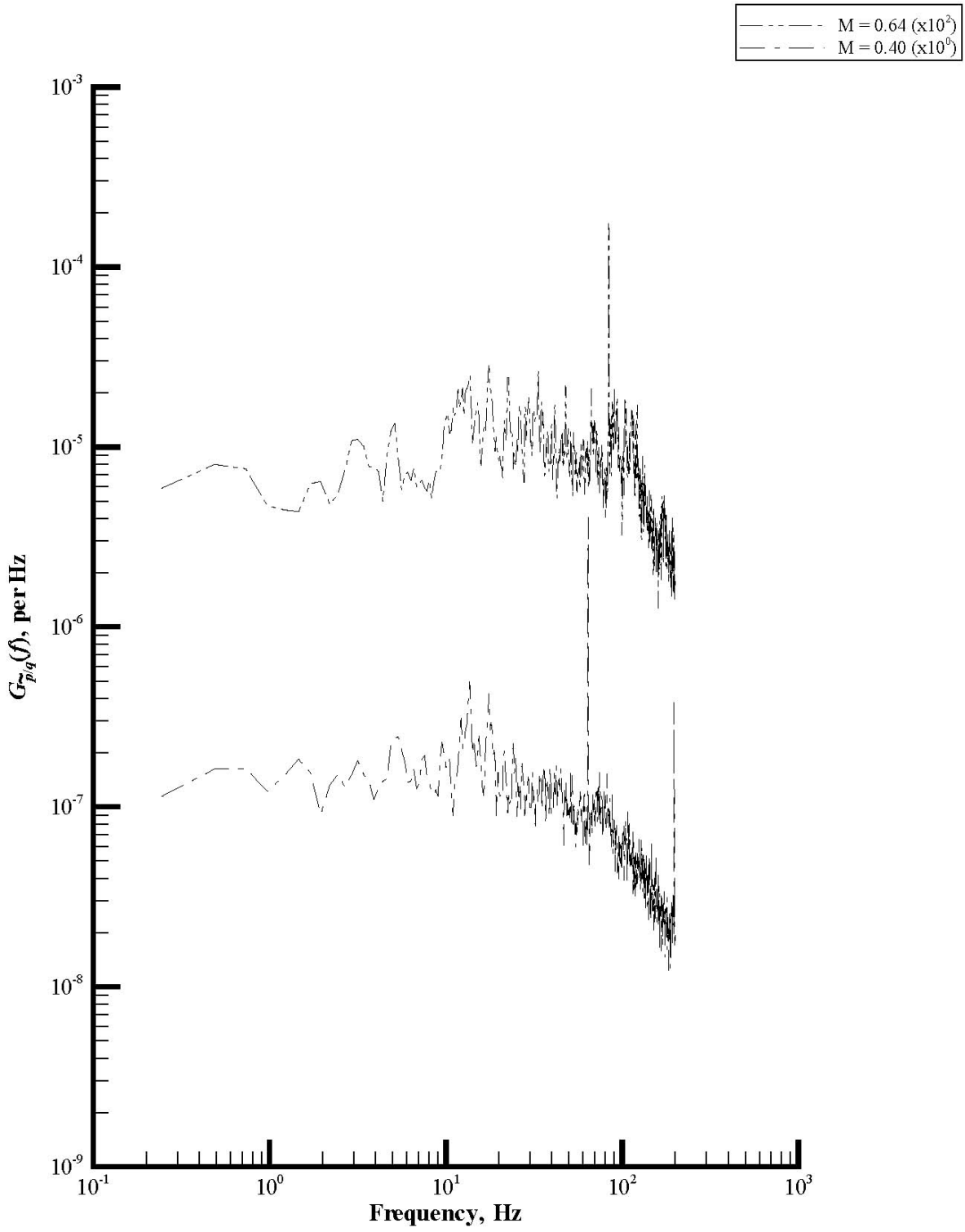
(e) Wall static pressure.

Figure 23. Concluded.



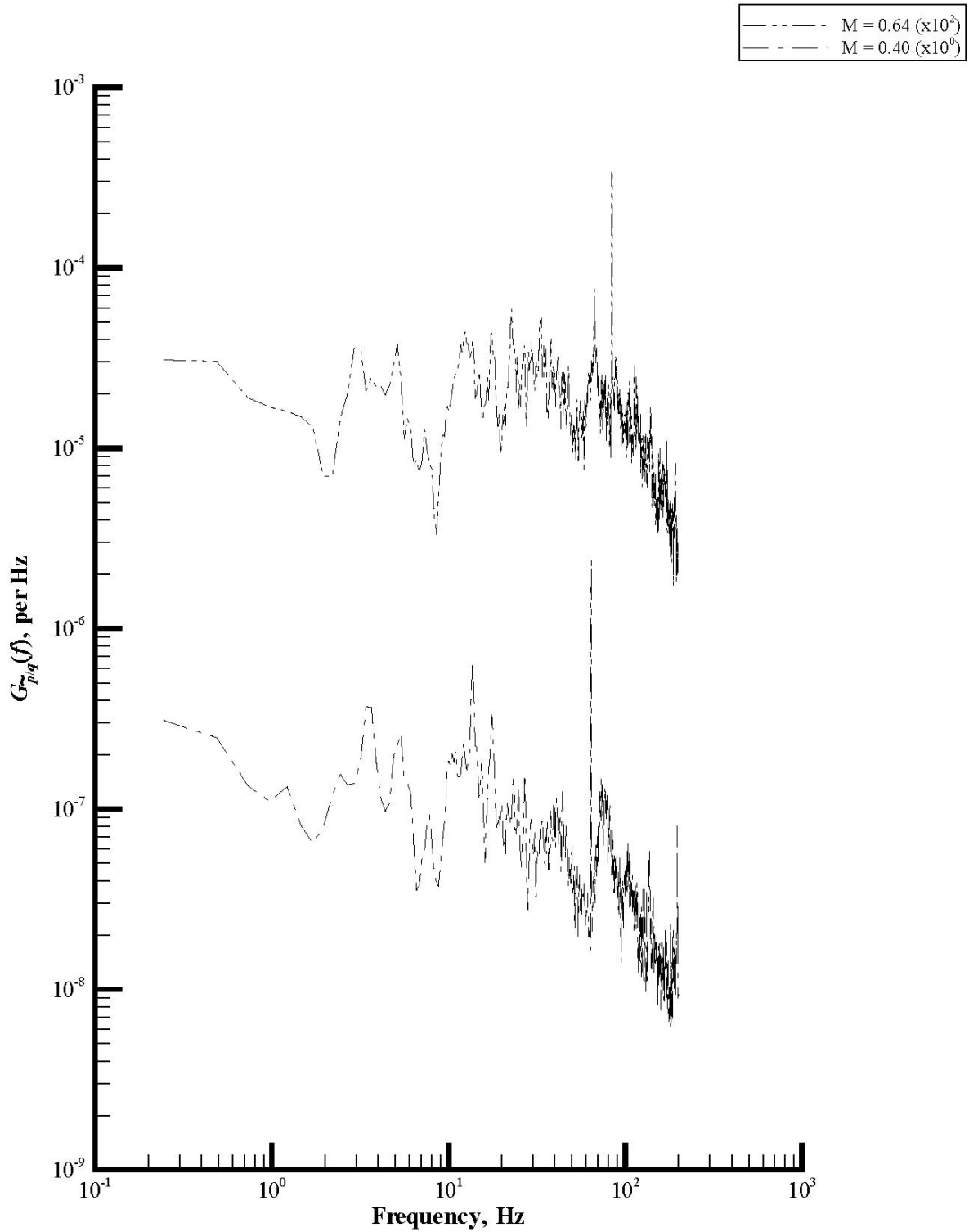
(a) Rake port total pressure.

Figure 24. Plots of power spectral density functions of set 3.



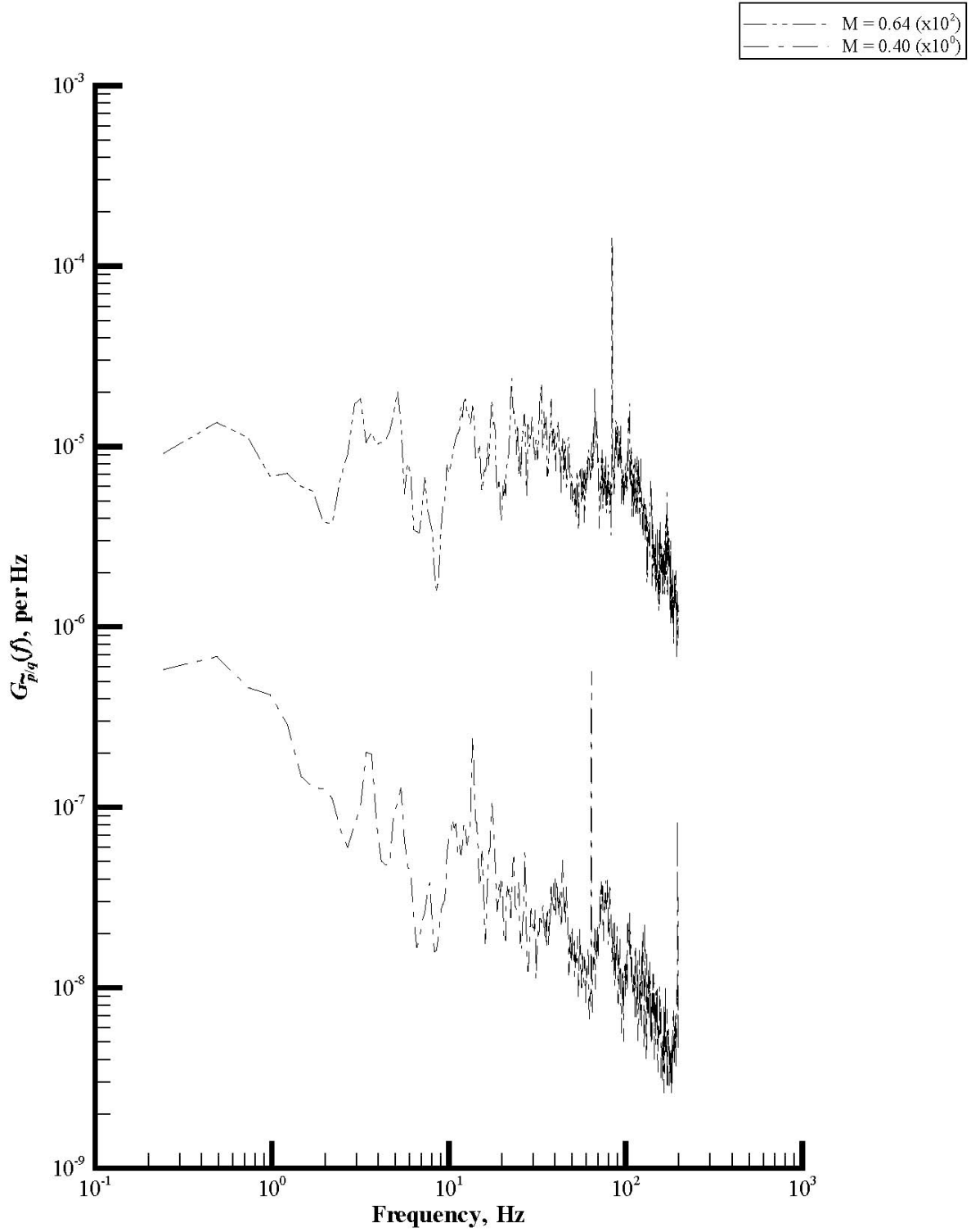
(b) Rake starboard total pressure.

Figure 24. Continued.



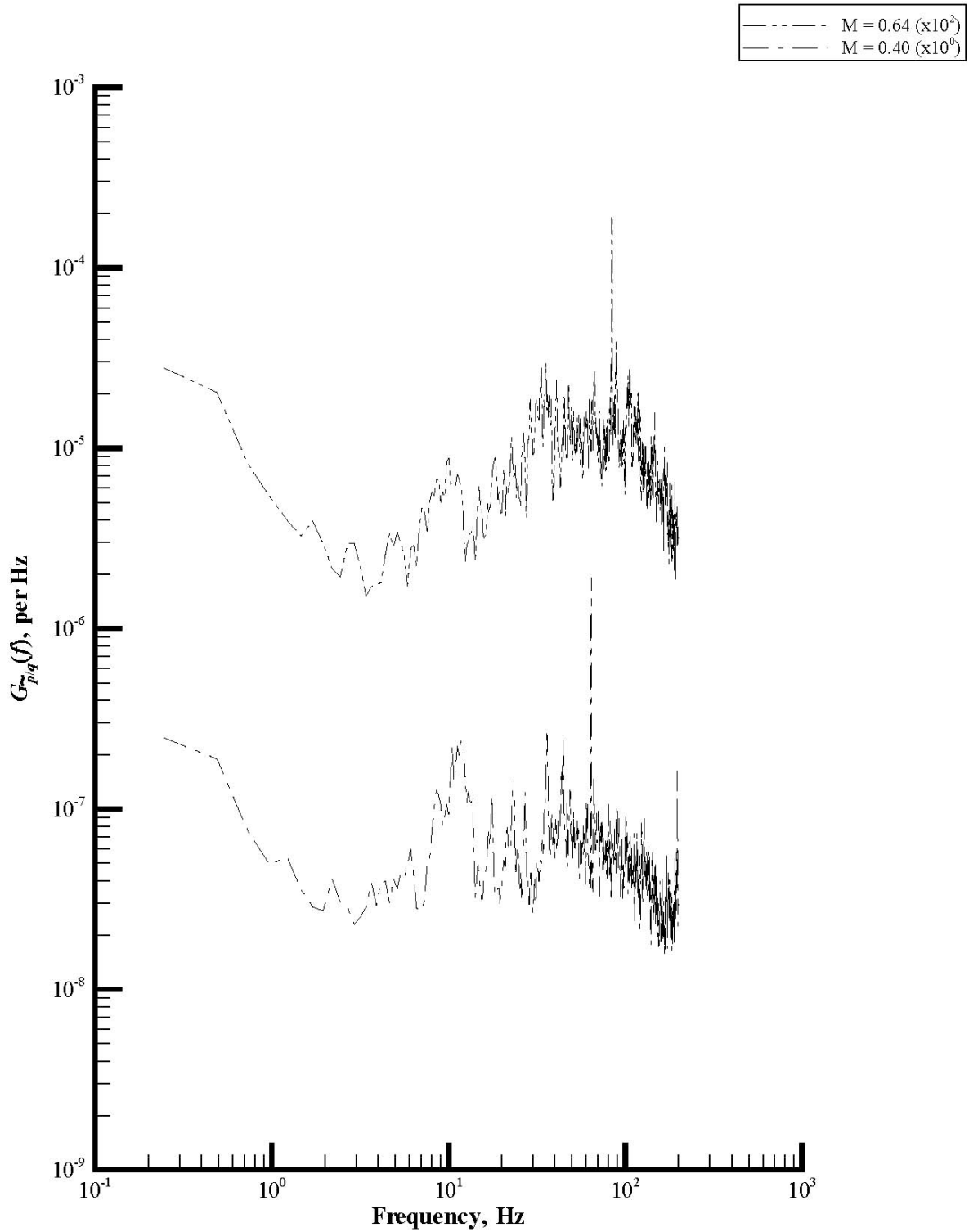
(c) Rake static pressure.

Figure 24. Continued.



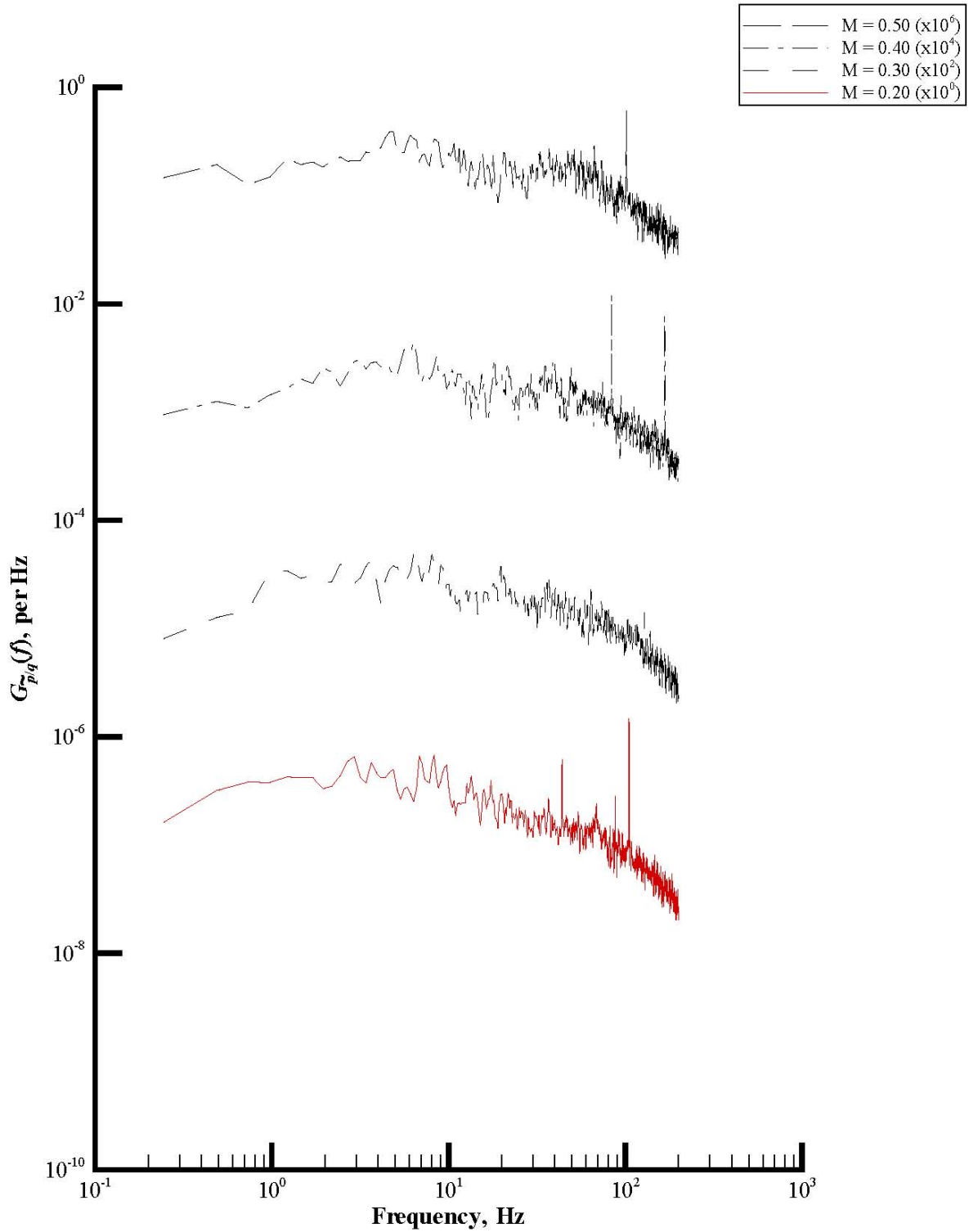
(d) Rake acoustic pressure.

Figure 24. Continued.



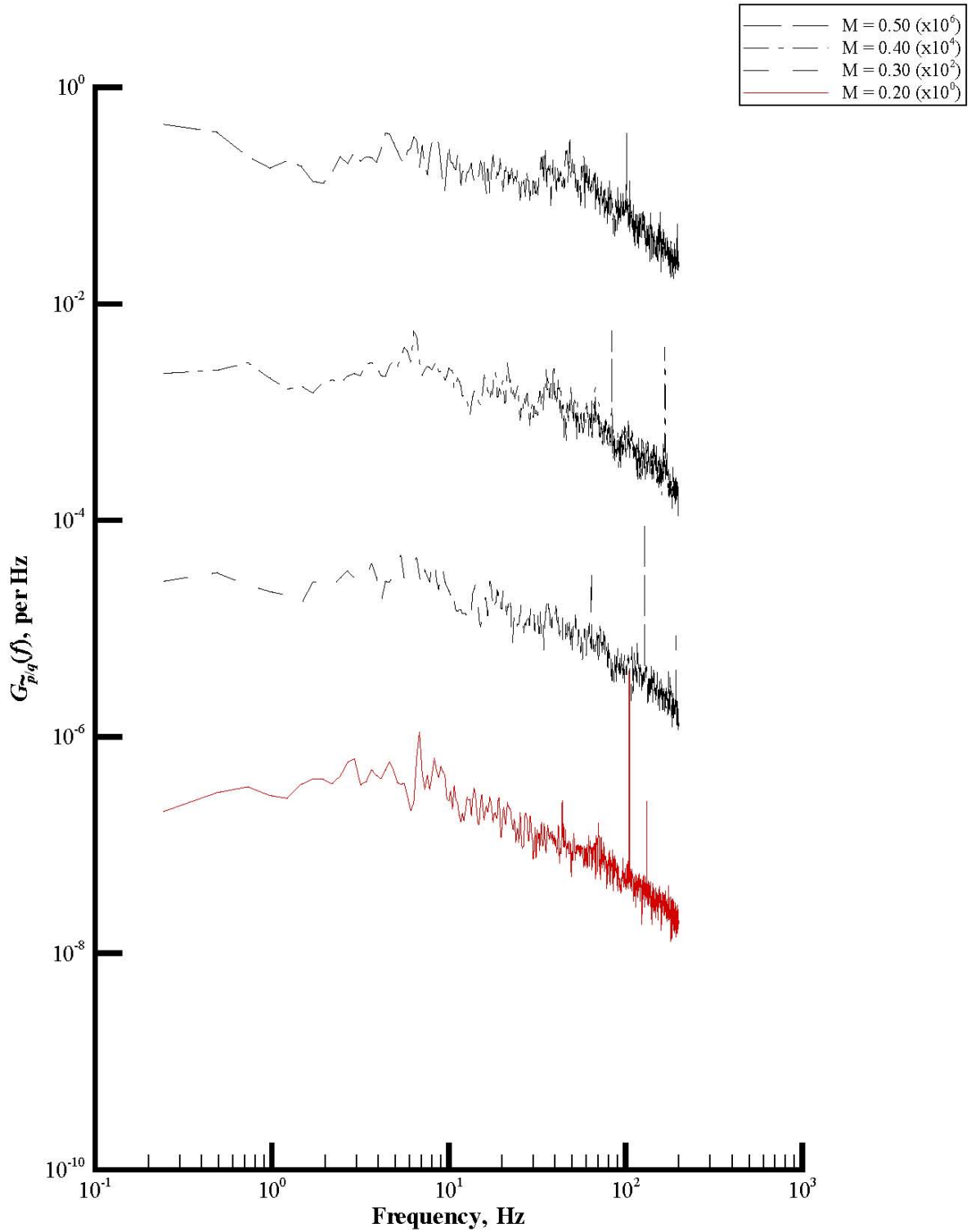
(e) Wall static pressure.

Figure 24. Concluded.



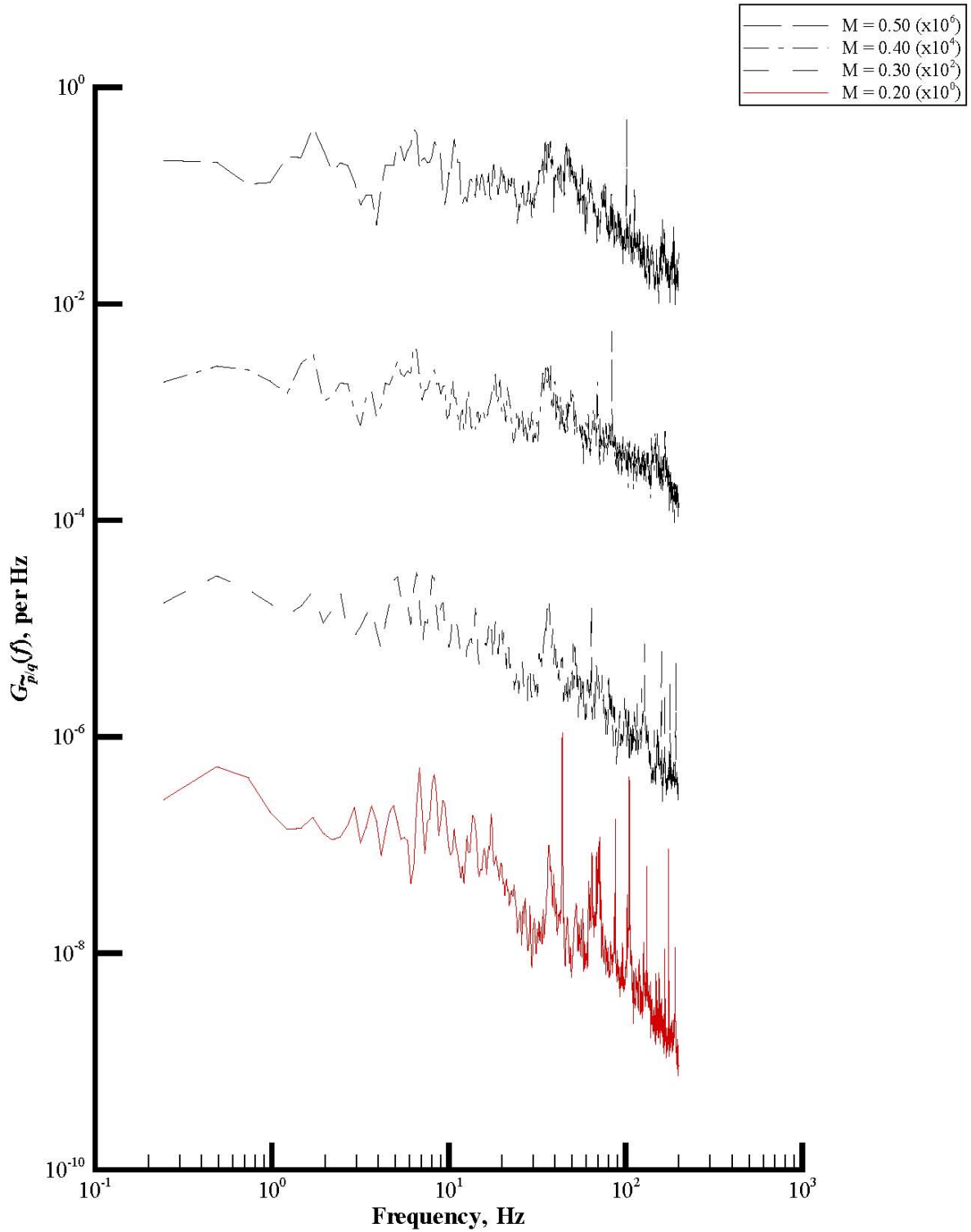
(a) Rake port total pressure.

Figure 25. Plots of power spectral density functions of set 4.



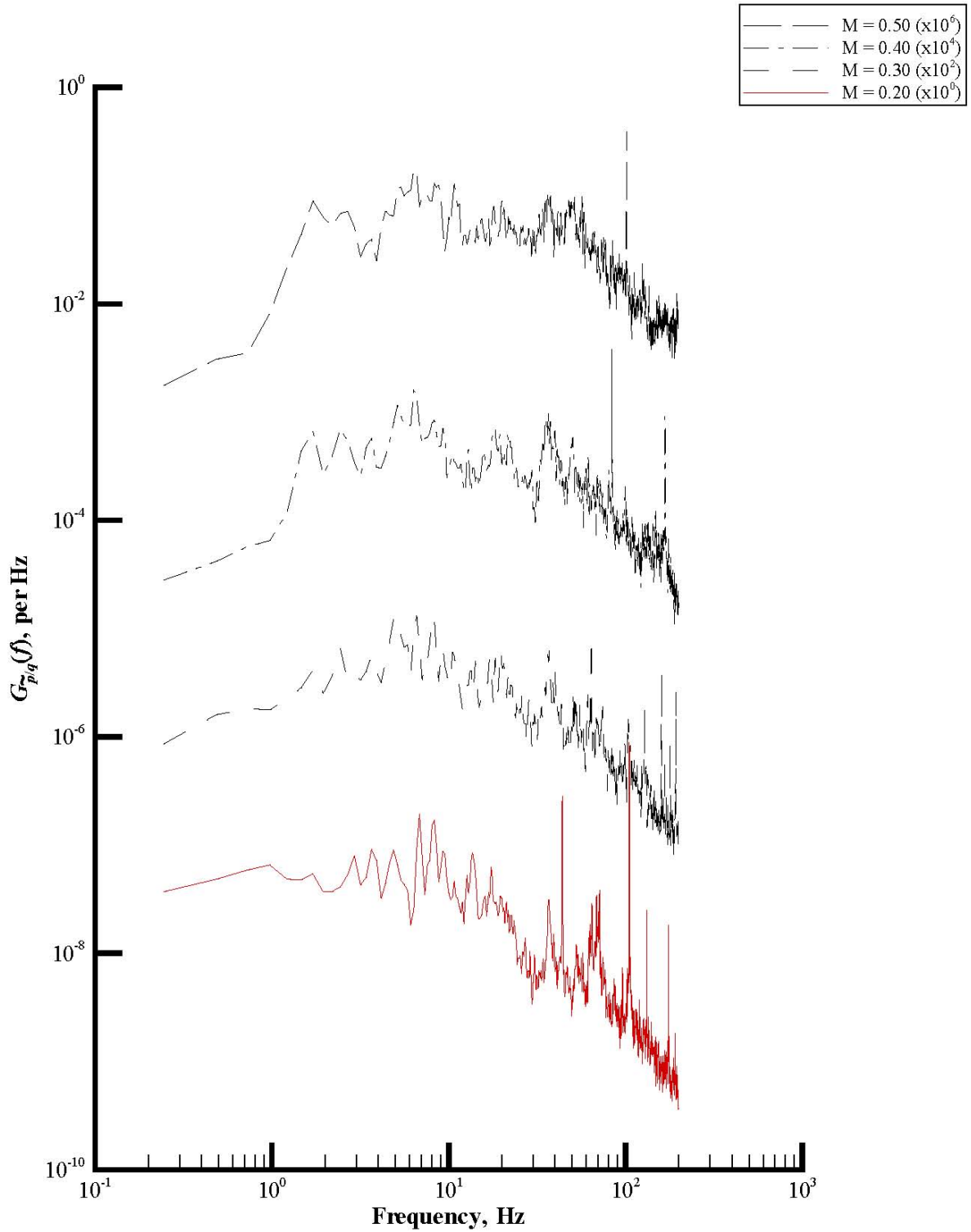
(b) Rake starboard total pressure.

Figure 25. Continued.



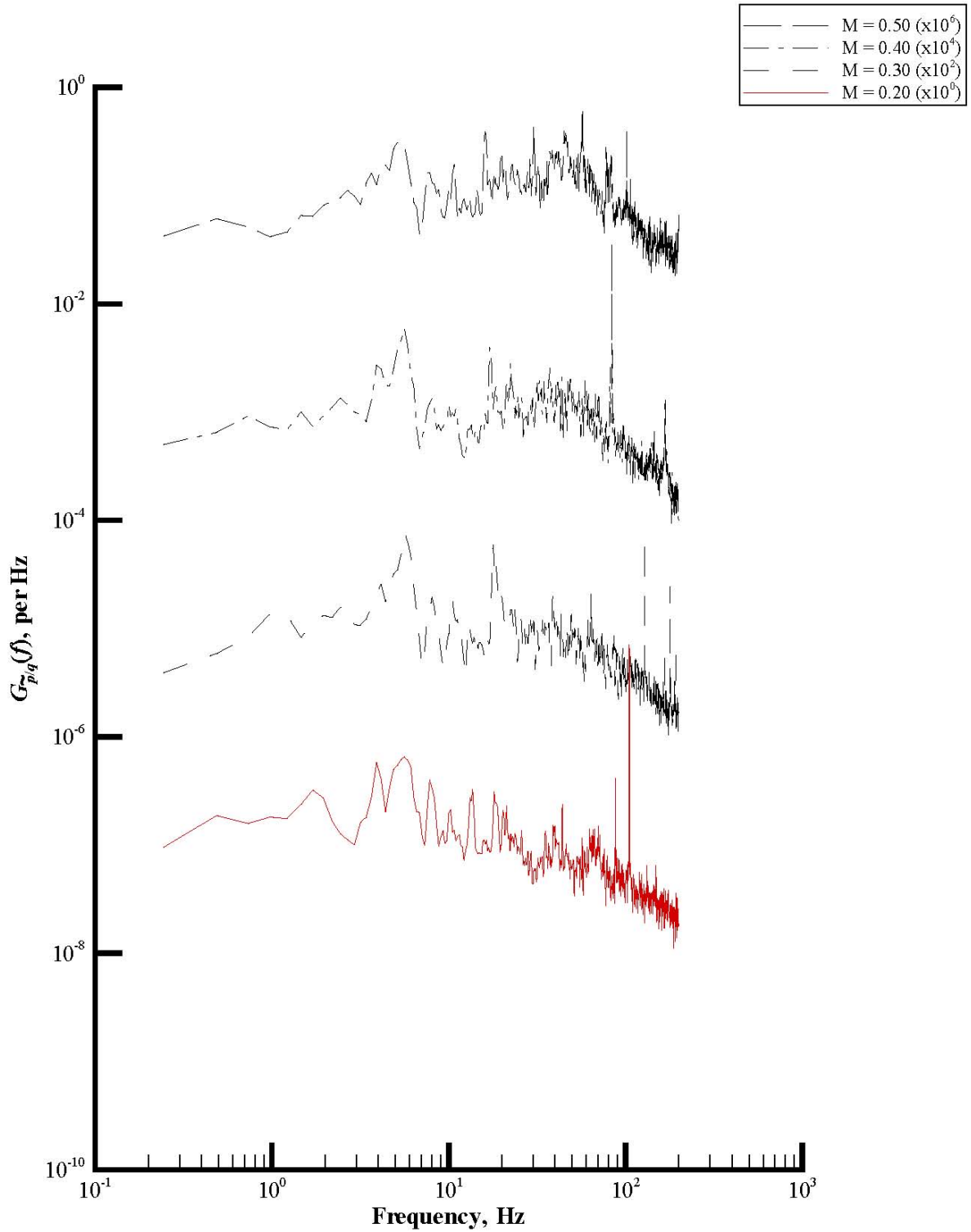
(c) Rake static pressure.

Figure 25. Continued.



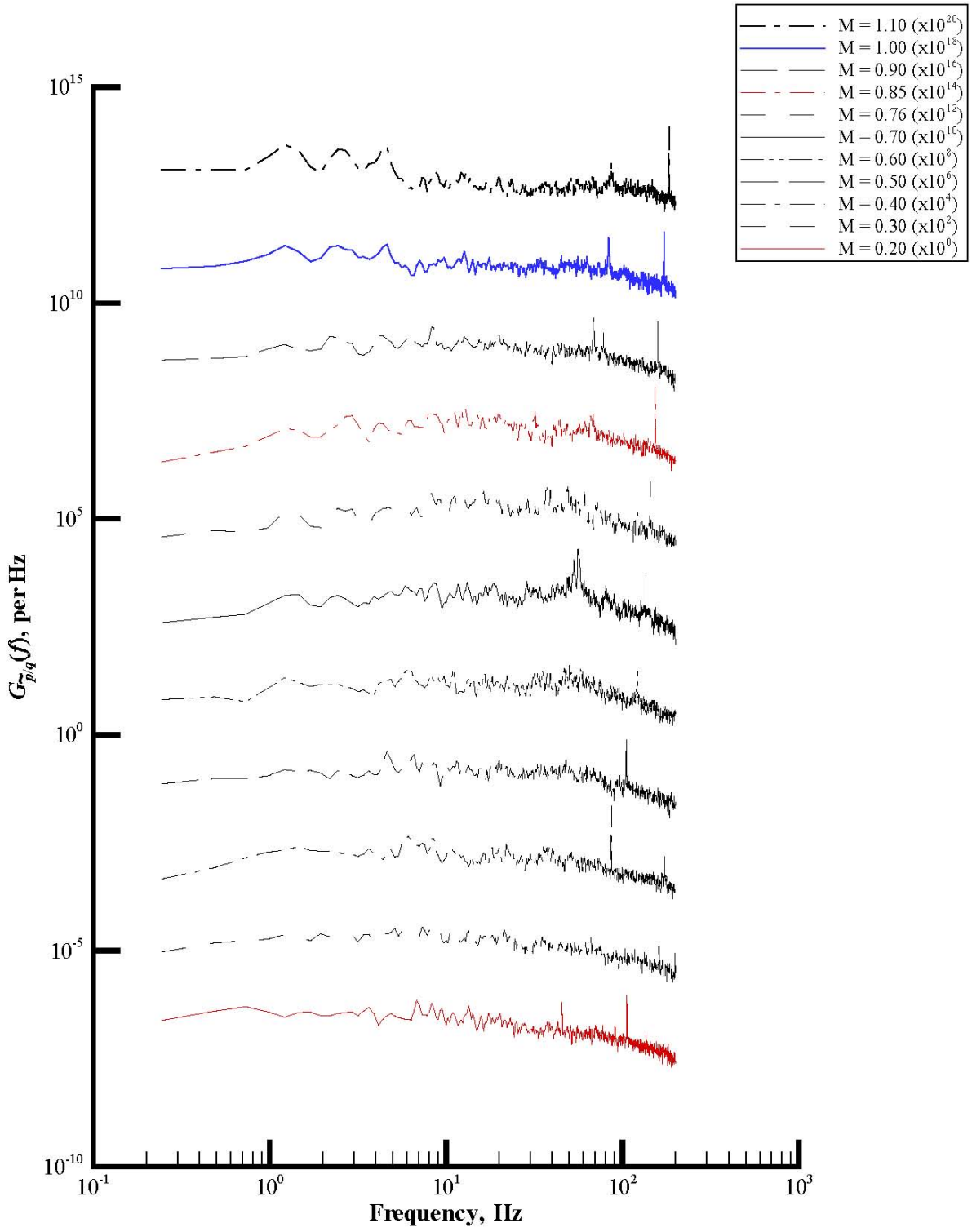
(d) Rake acoustic pressure.

Figure 25. Continued.



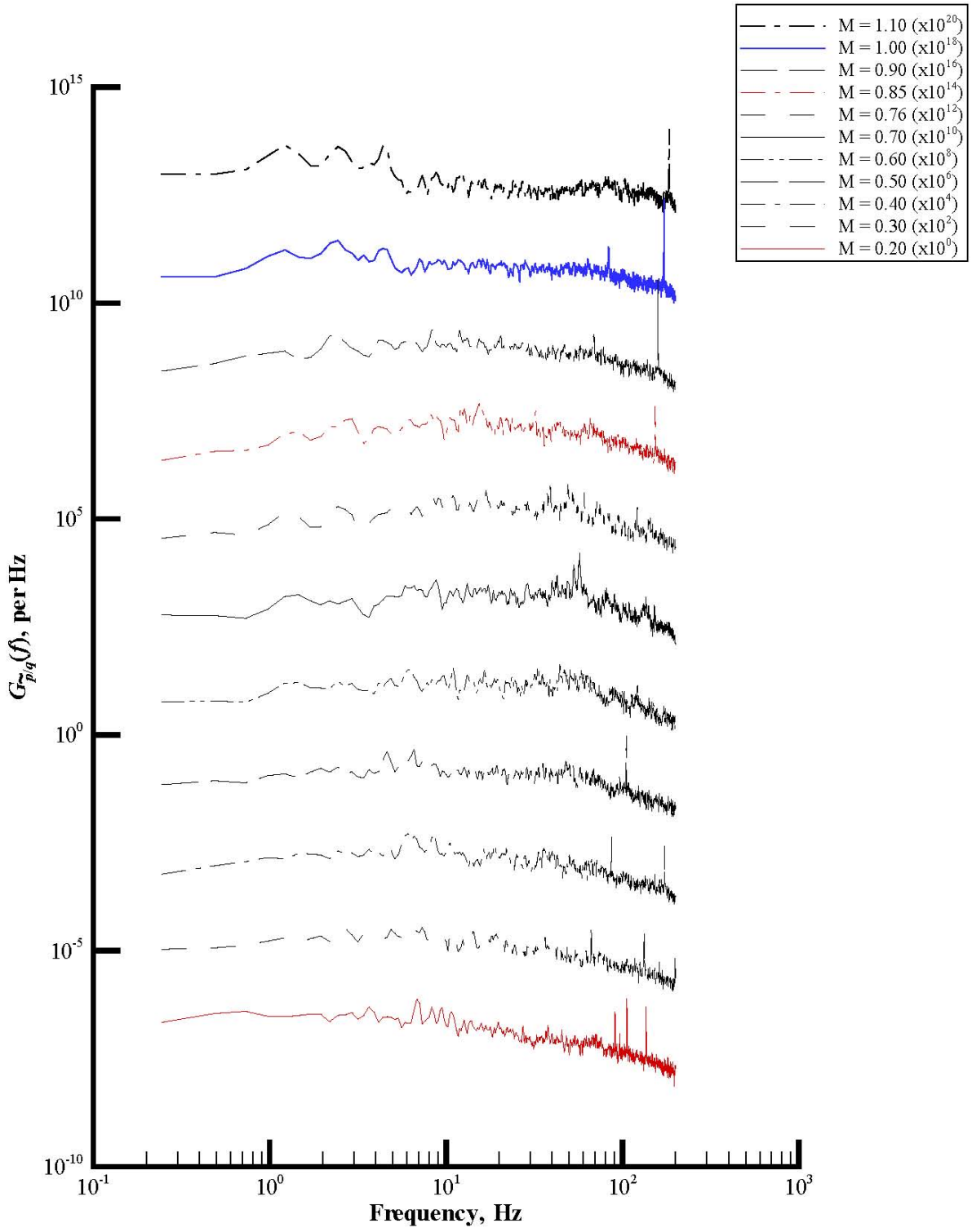
(e) Wall static pressure.

Figure 25. Concluded.



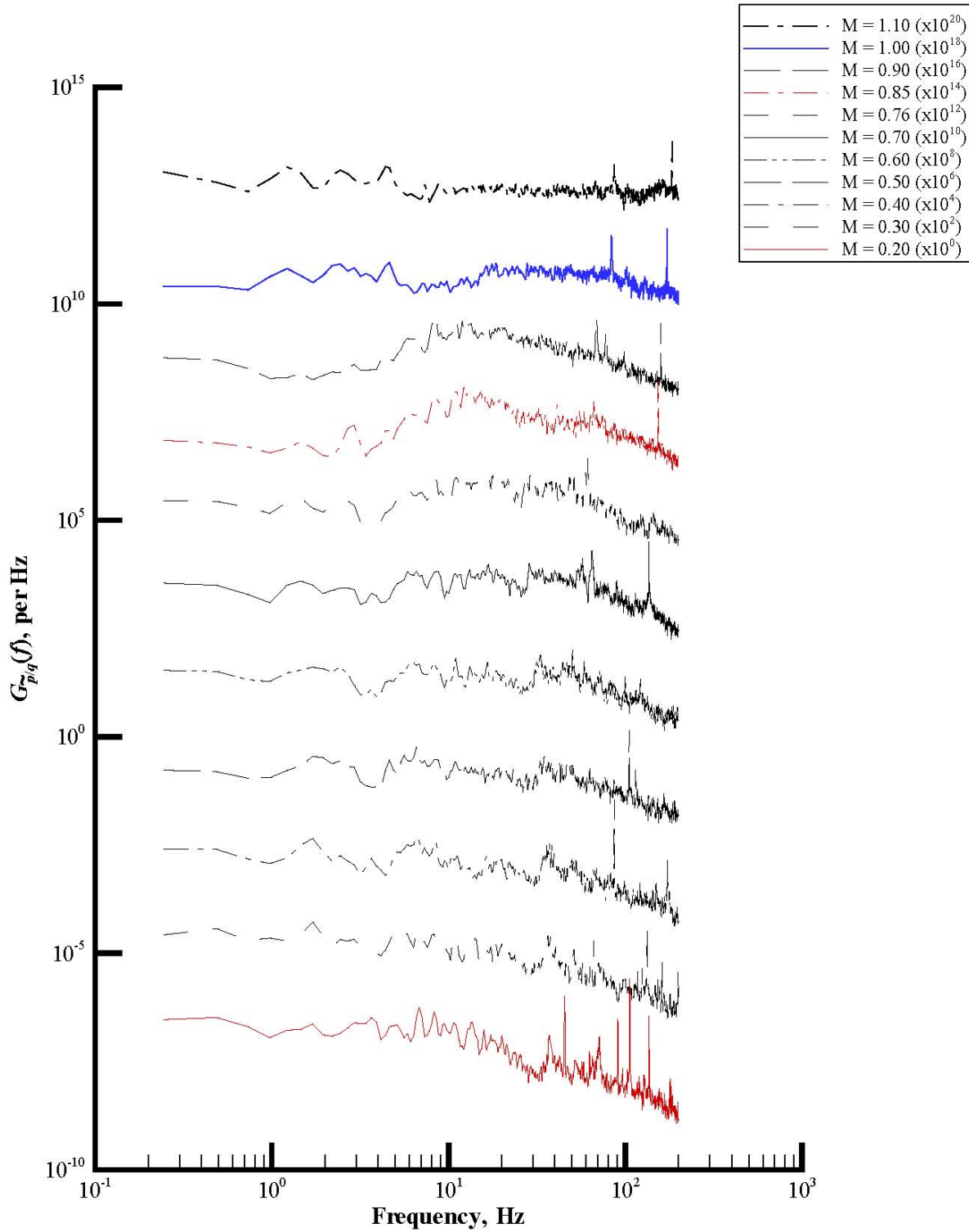
(a) Rake port total pressure.

Figure 26. Plots of power spectral density functions of set 5.



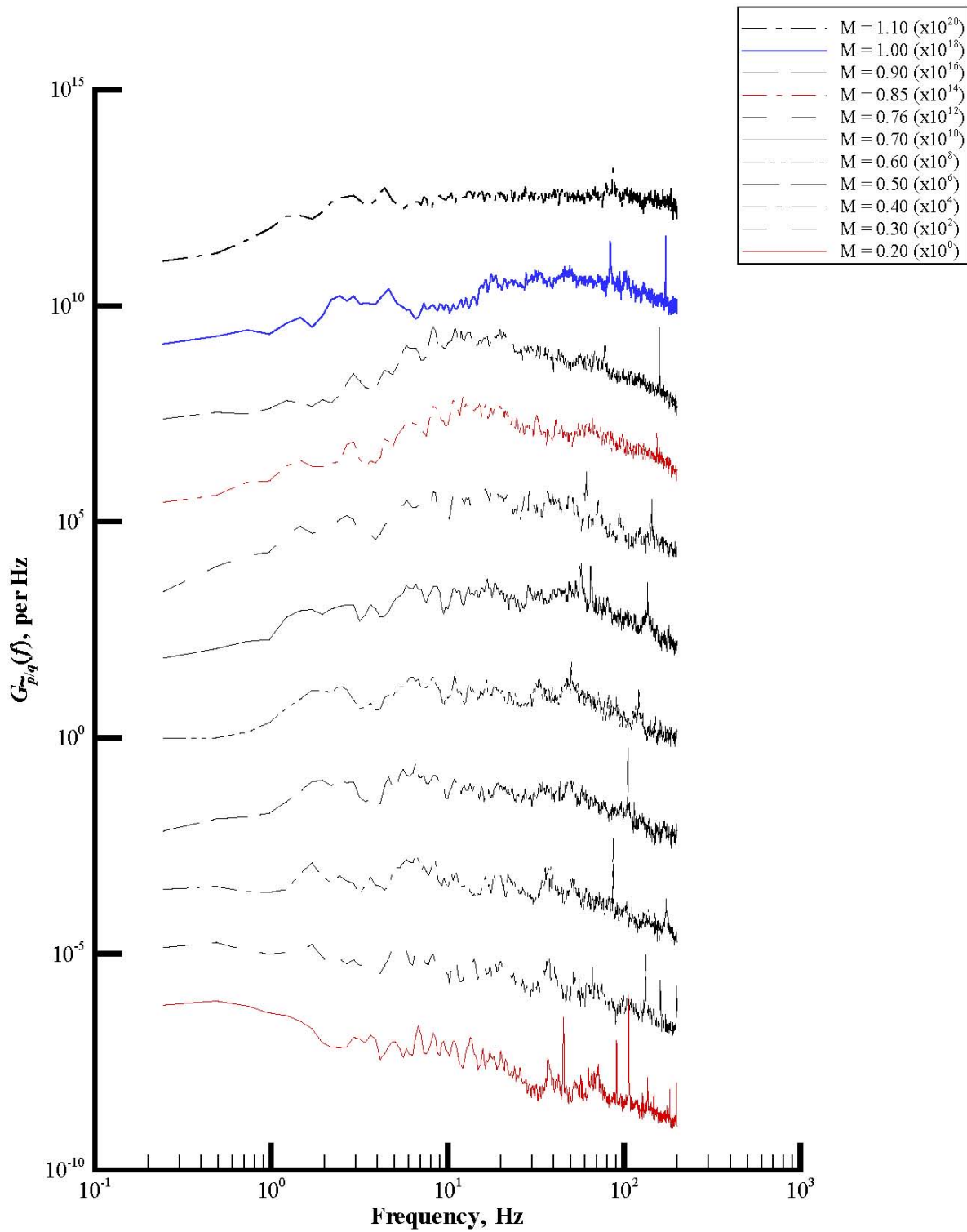
(b) Rake starboard total pressure.

Figure 26. Continued.



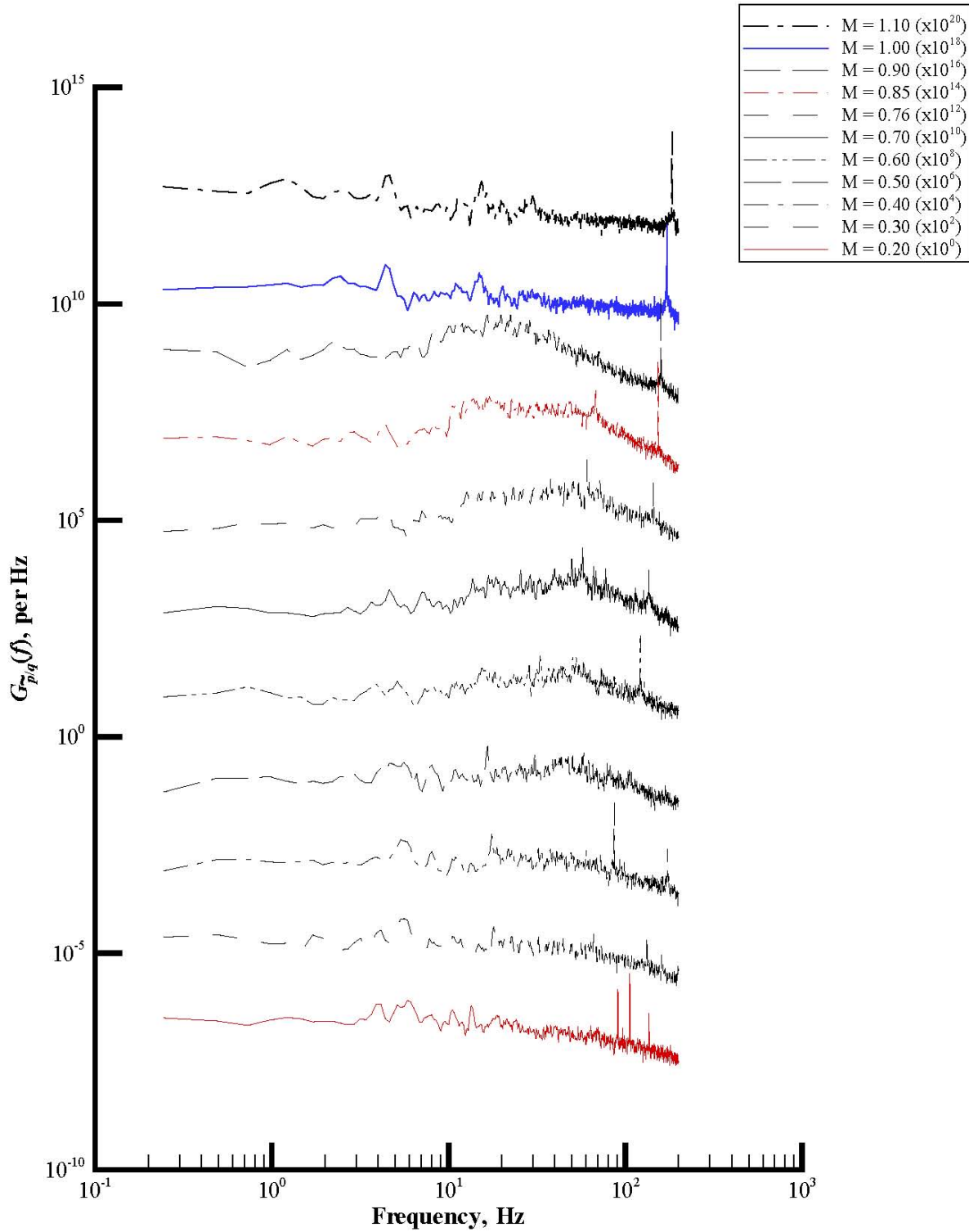
(c) Rake static pressure.

Figure 26. Continued.



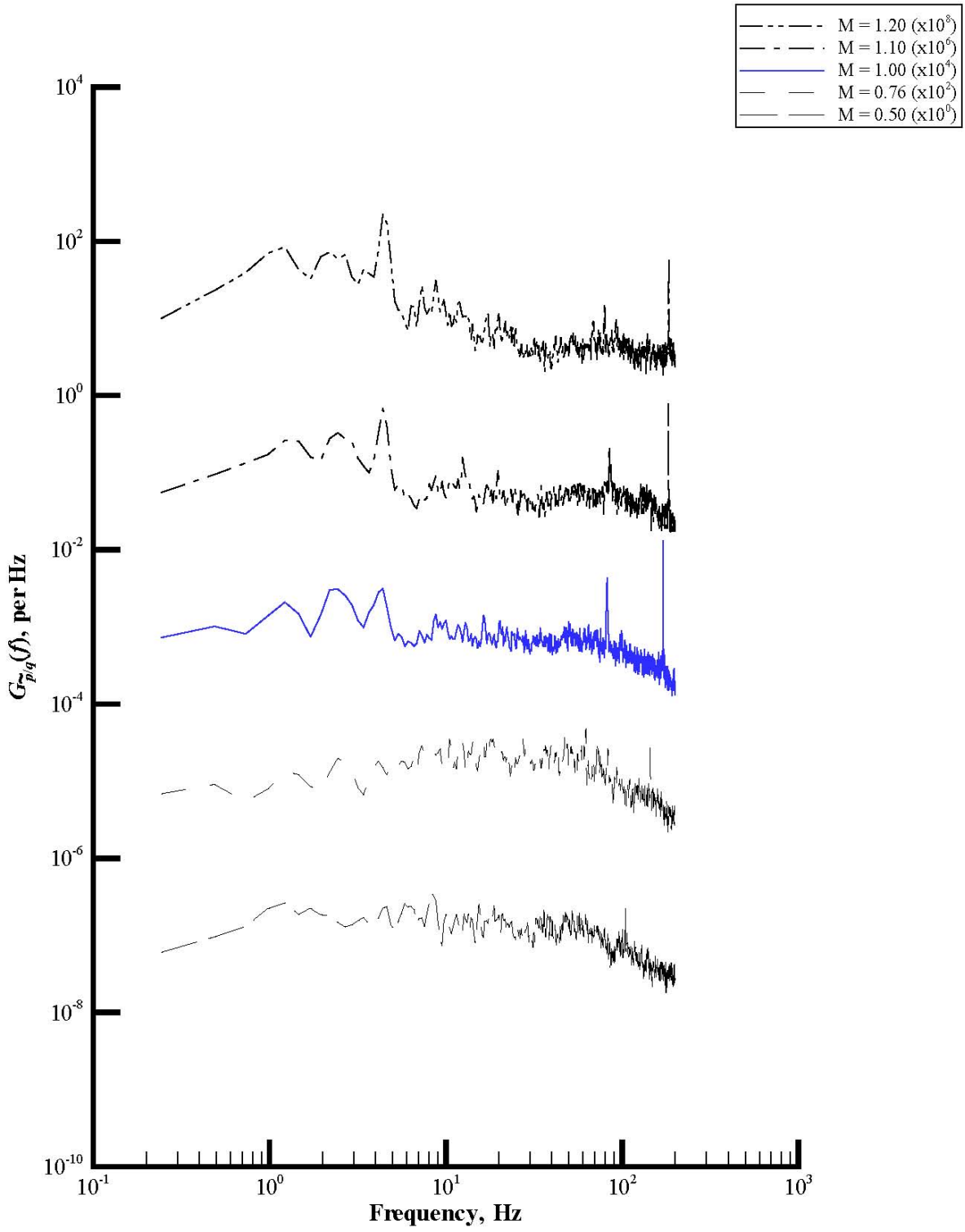
(d) Rake acoustic pressure.

Figure 26. Continued.



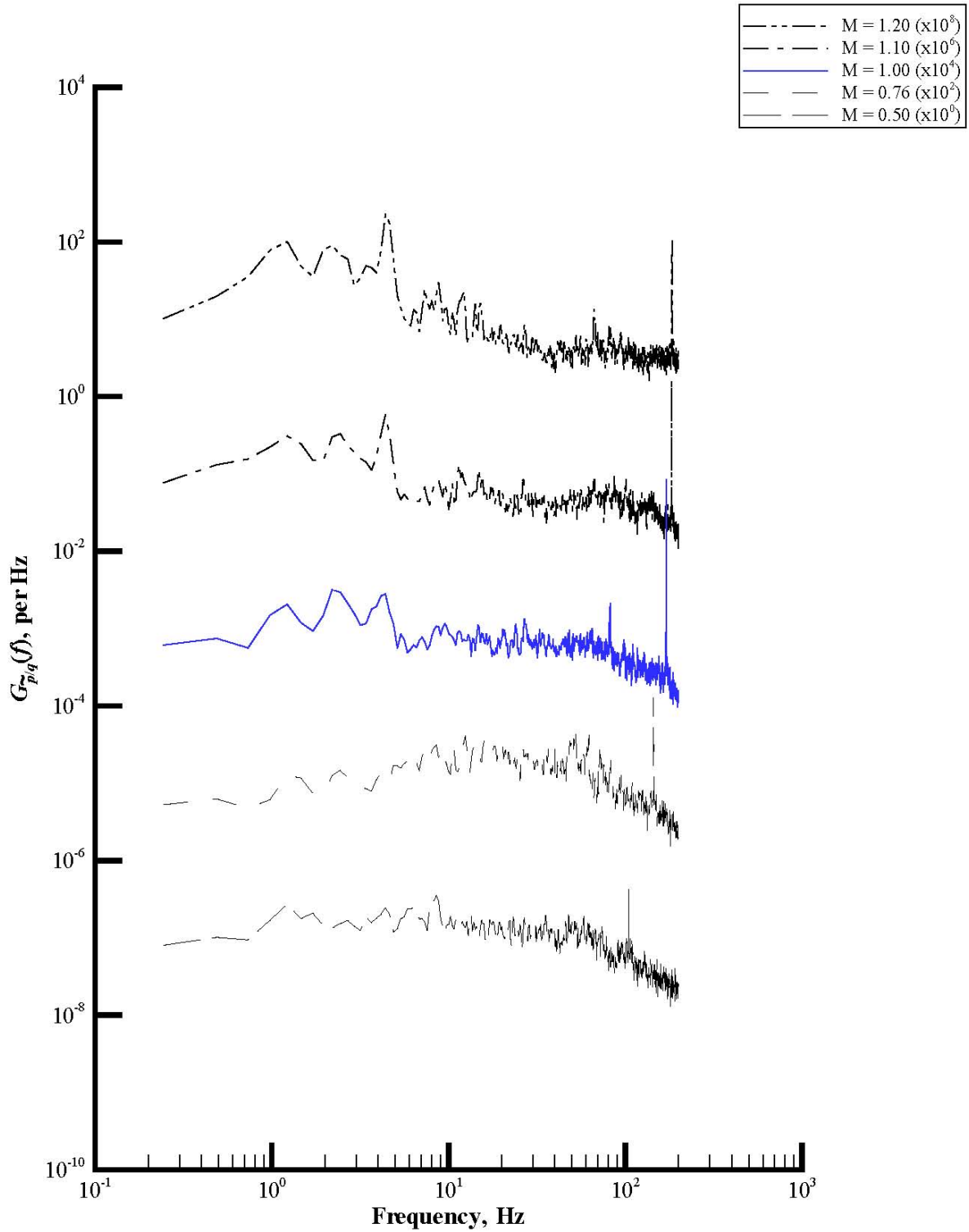
(e) Wall static pressure.

Figure 26. Concluded.



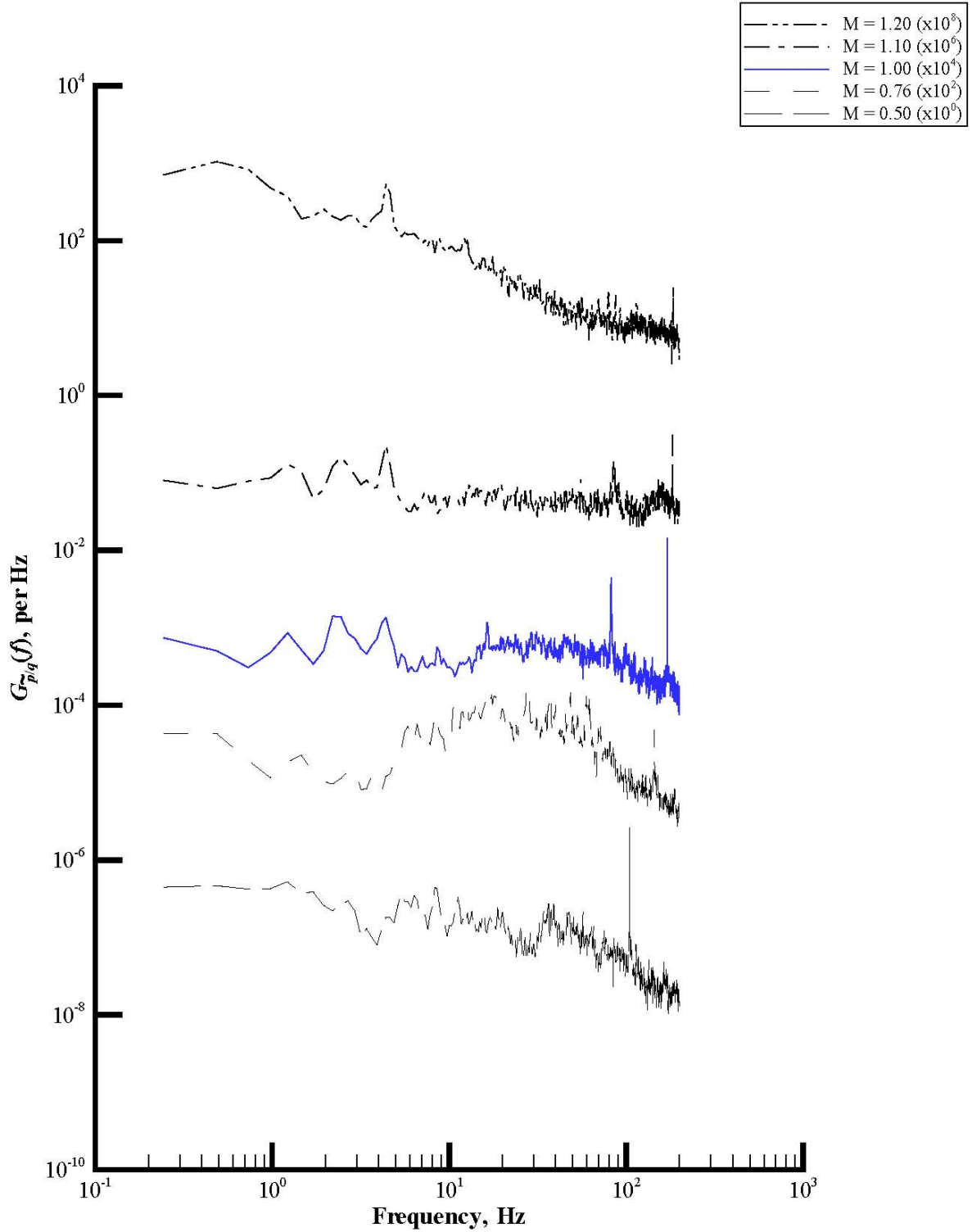
(a) Rake port total pressure.

Figure 27. Plots of power spectral density functions of set 6.



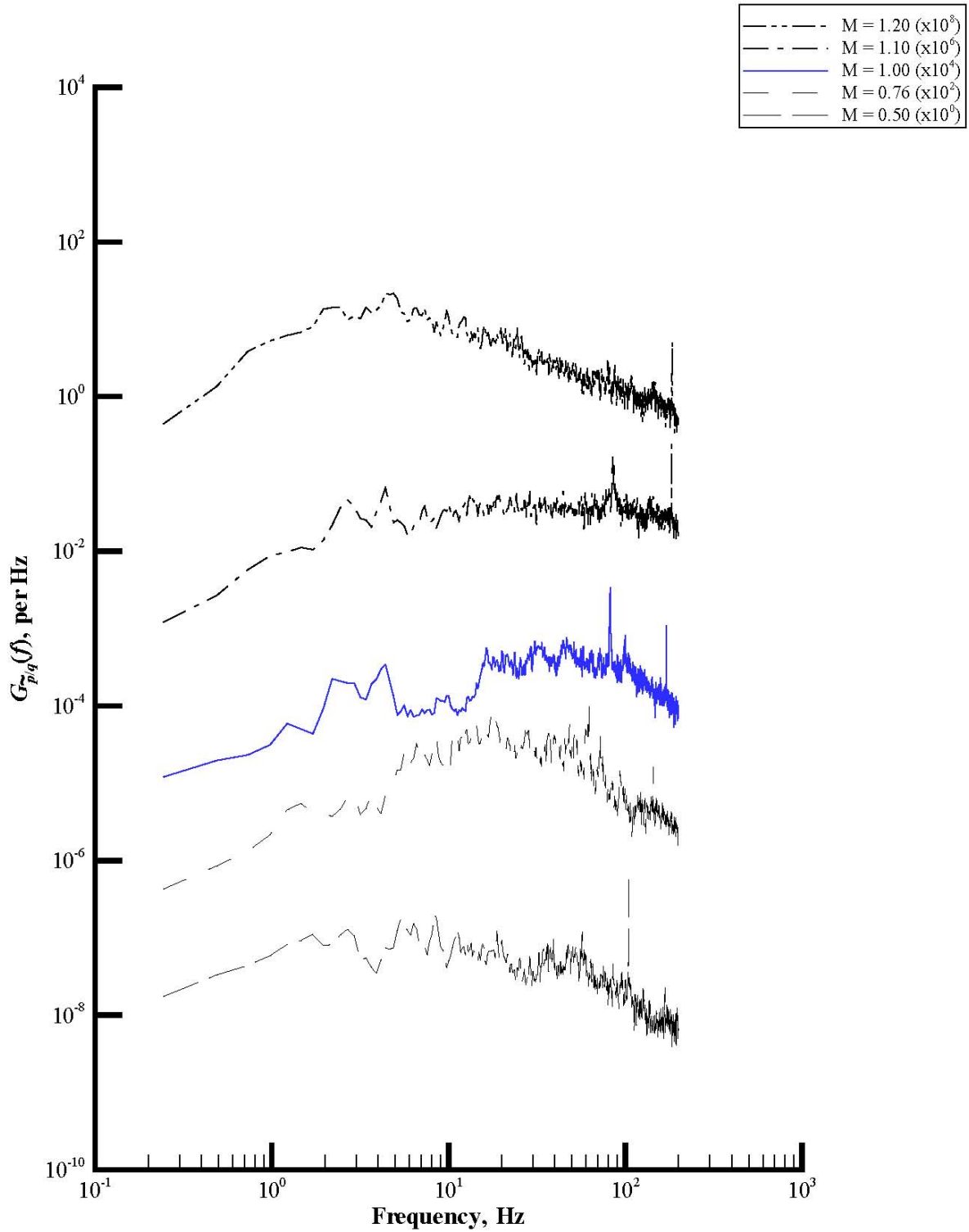
(b) Rake starboard total pressure.

Figure 27. Continued.



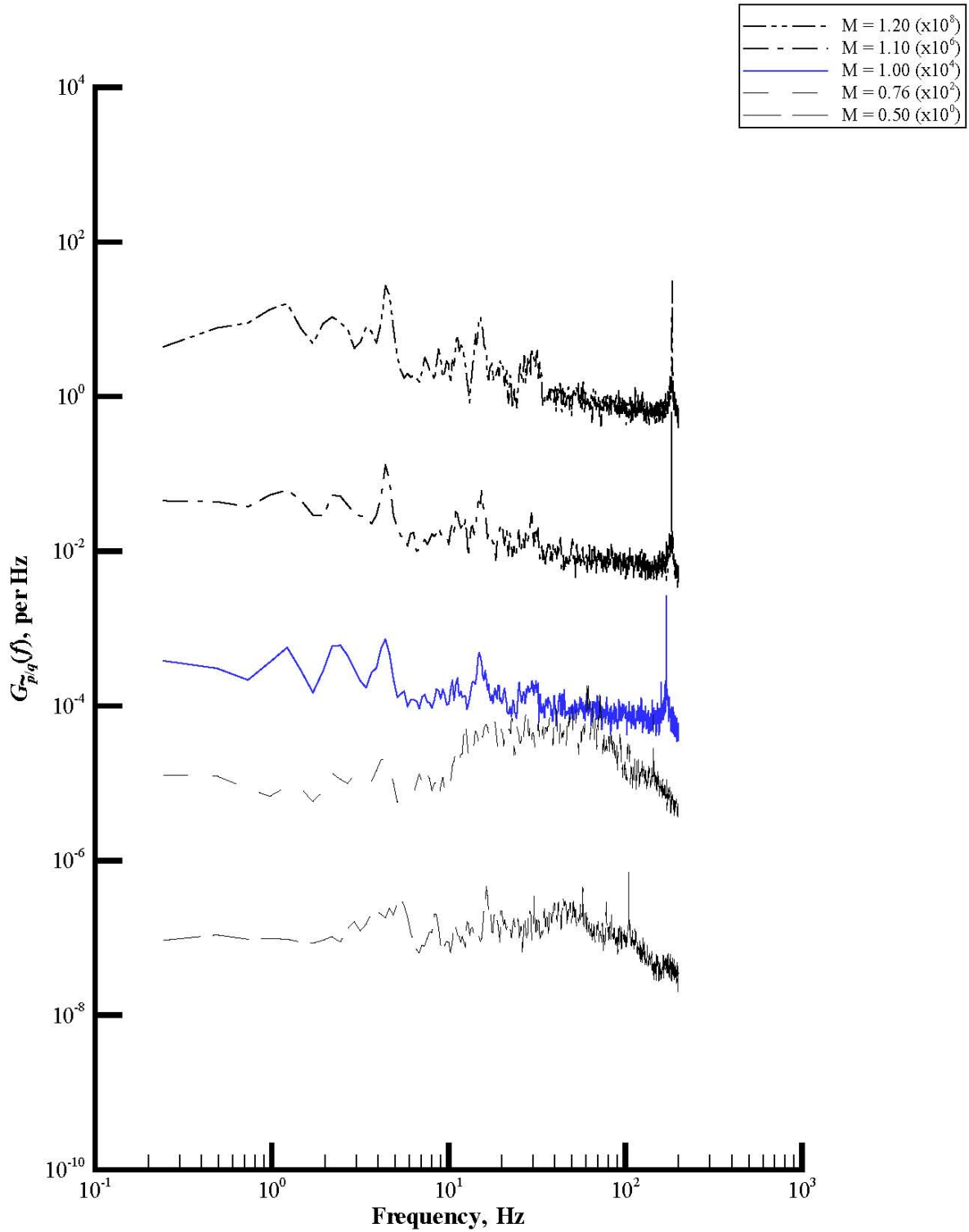
(c) Rake static pressure.

Figure 27. Continued.



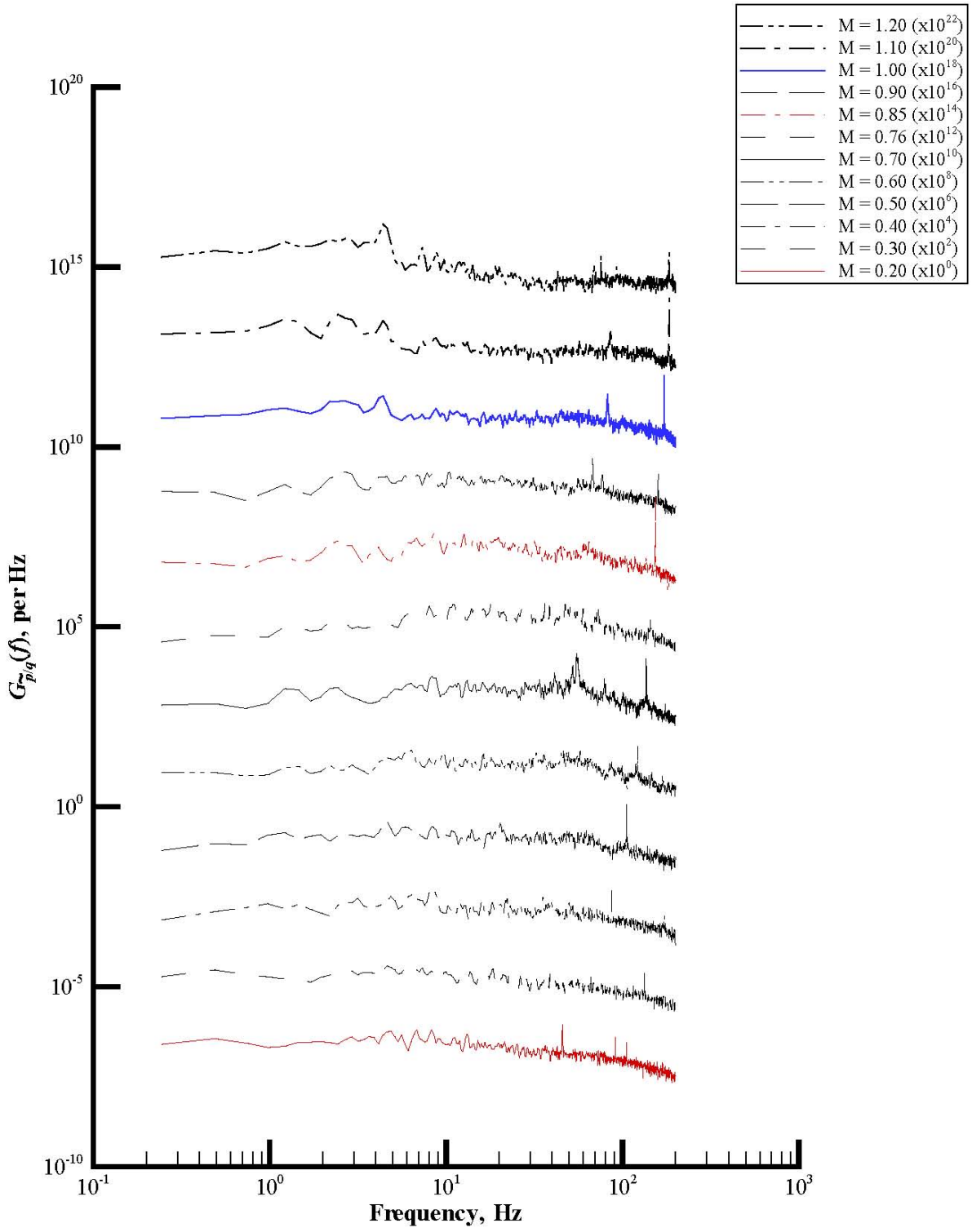
(d) Rake acoustic pressure.

Figure 27. Continued.



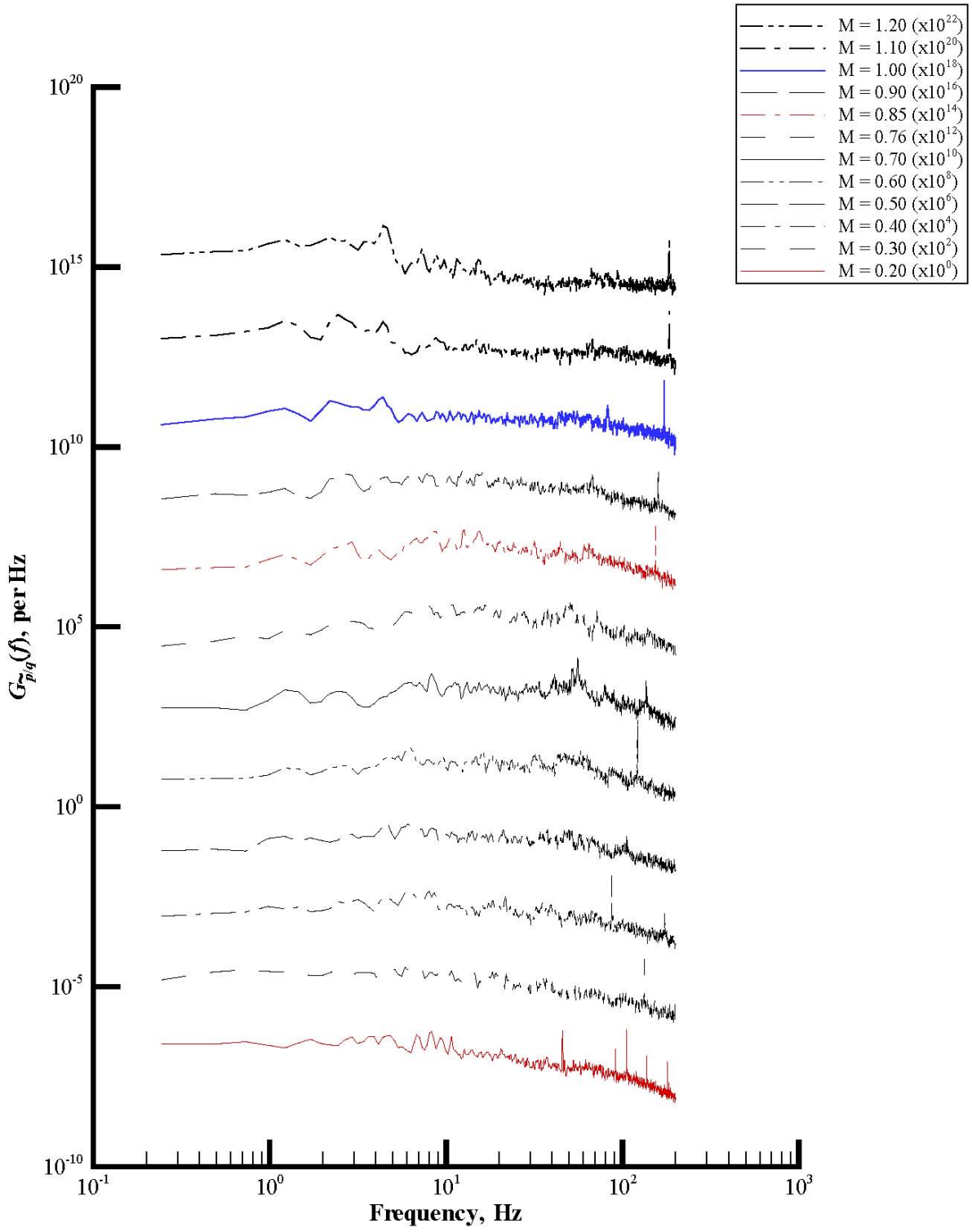
(e) Wall static pressure.

Figure 27. Concluded.



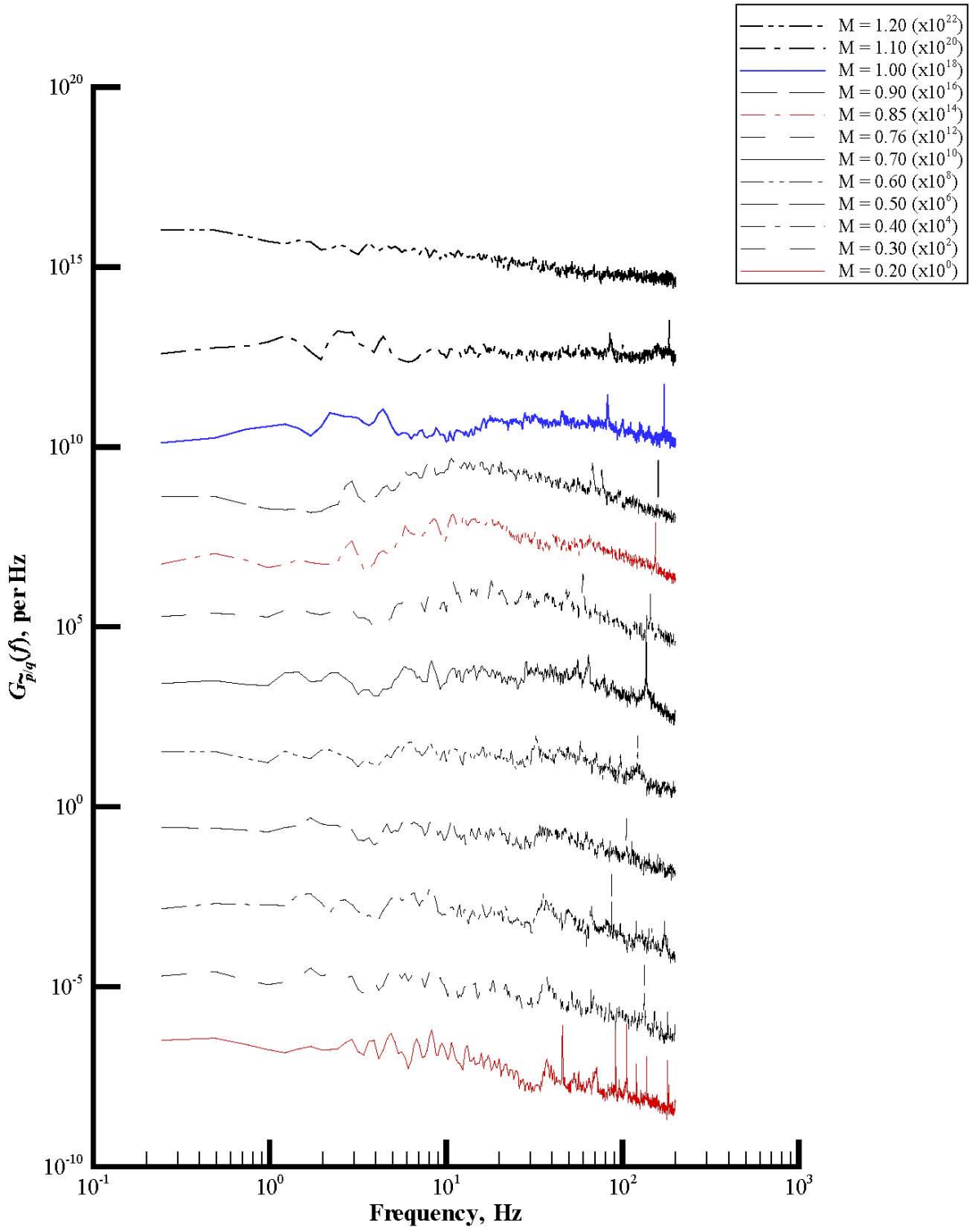
(a) Rake port total pressure.

Figure 28. Plots of power spectral density functions of set 7.



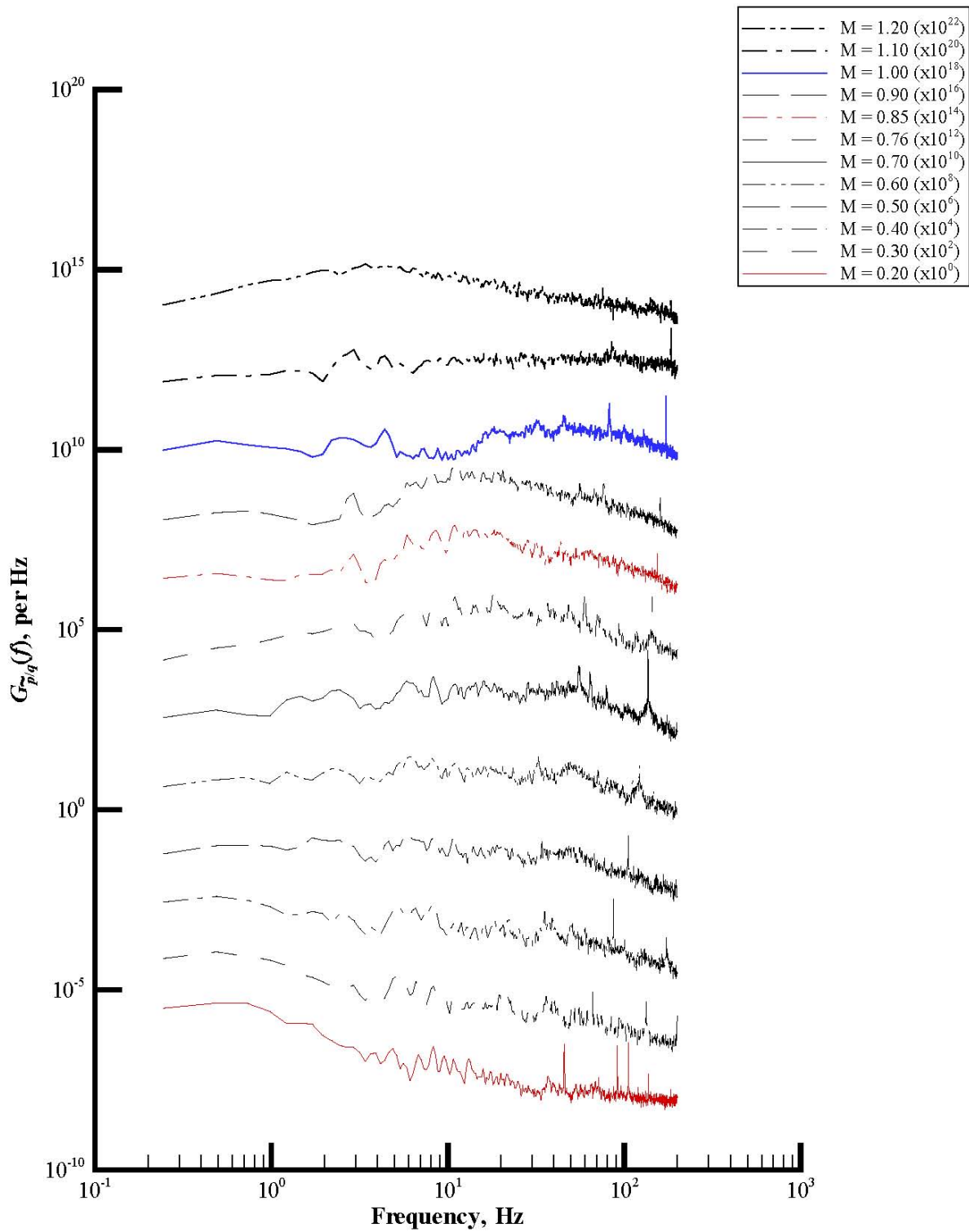
(b) Rake starboard total pressure.

Figure 28. Continued.



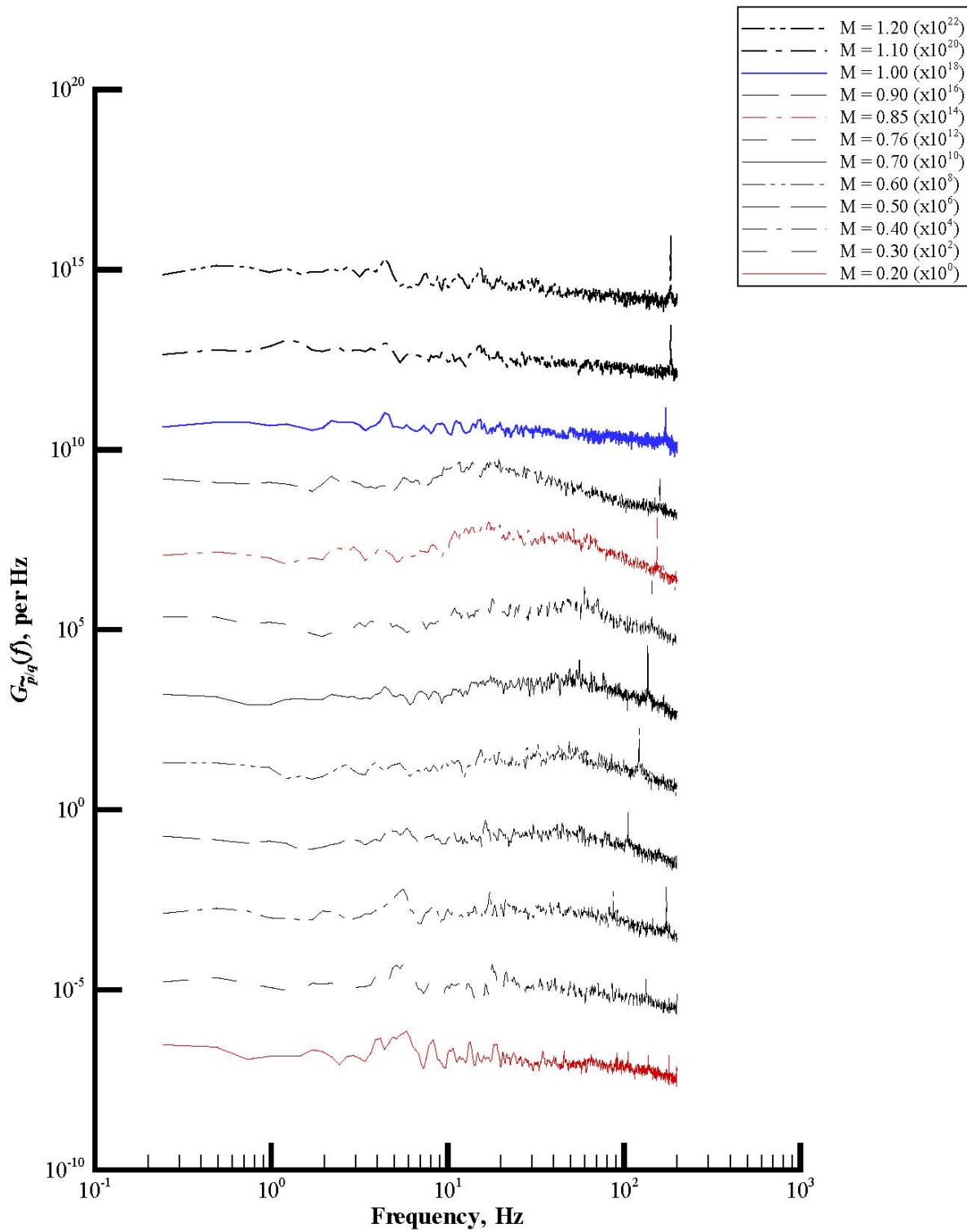
(c) Rake static pressure.

Figure 28. Continued.



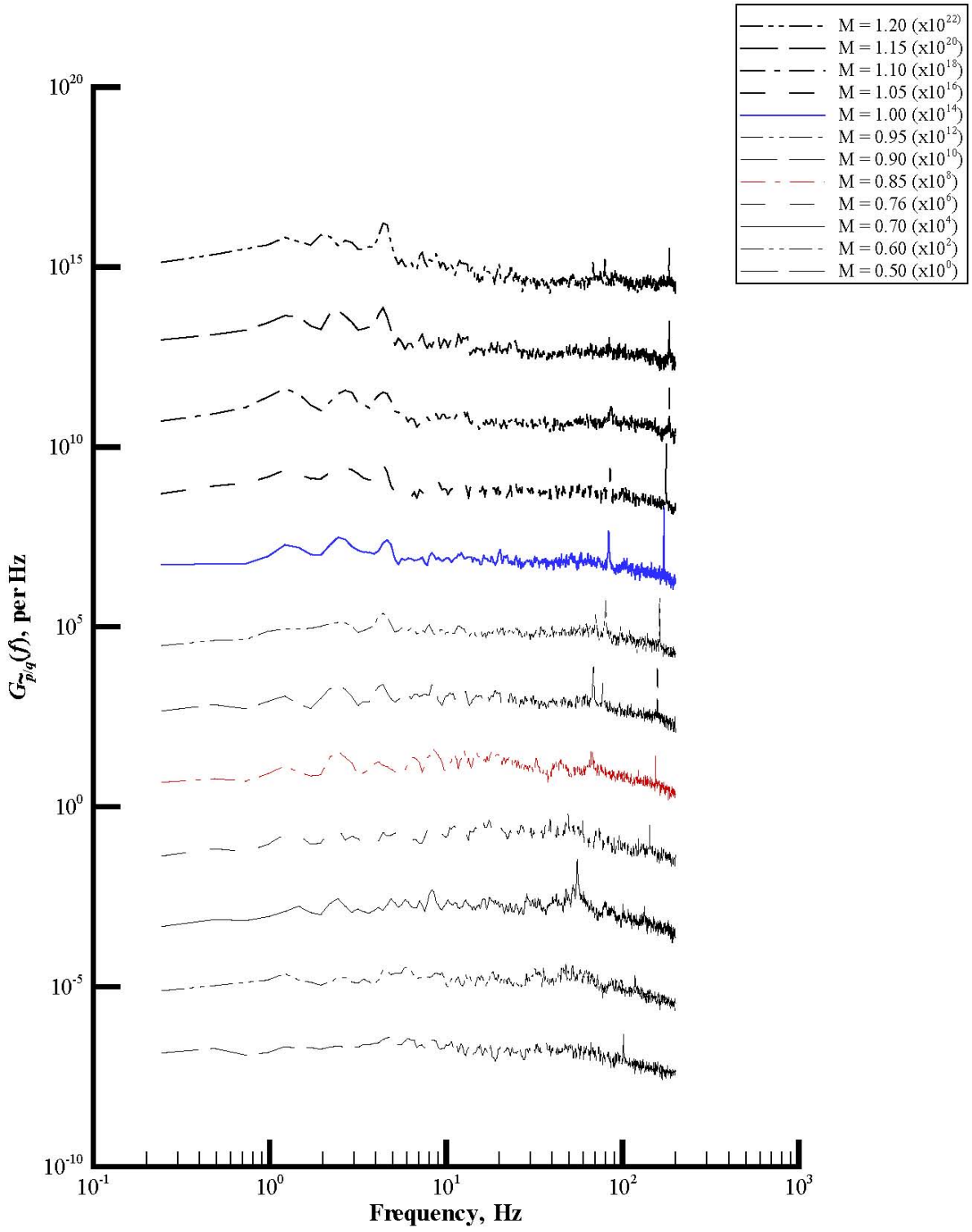
(d) Rake acoustic pressure.

Figure 28. Continued.



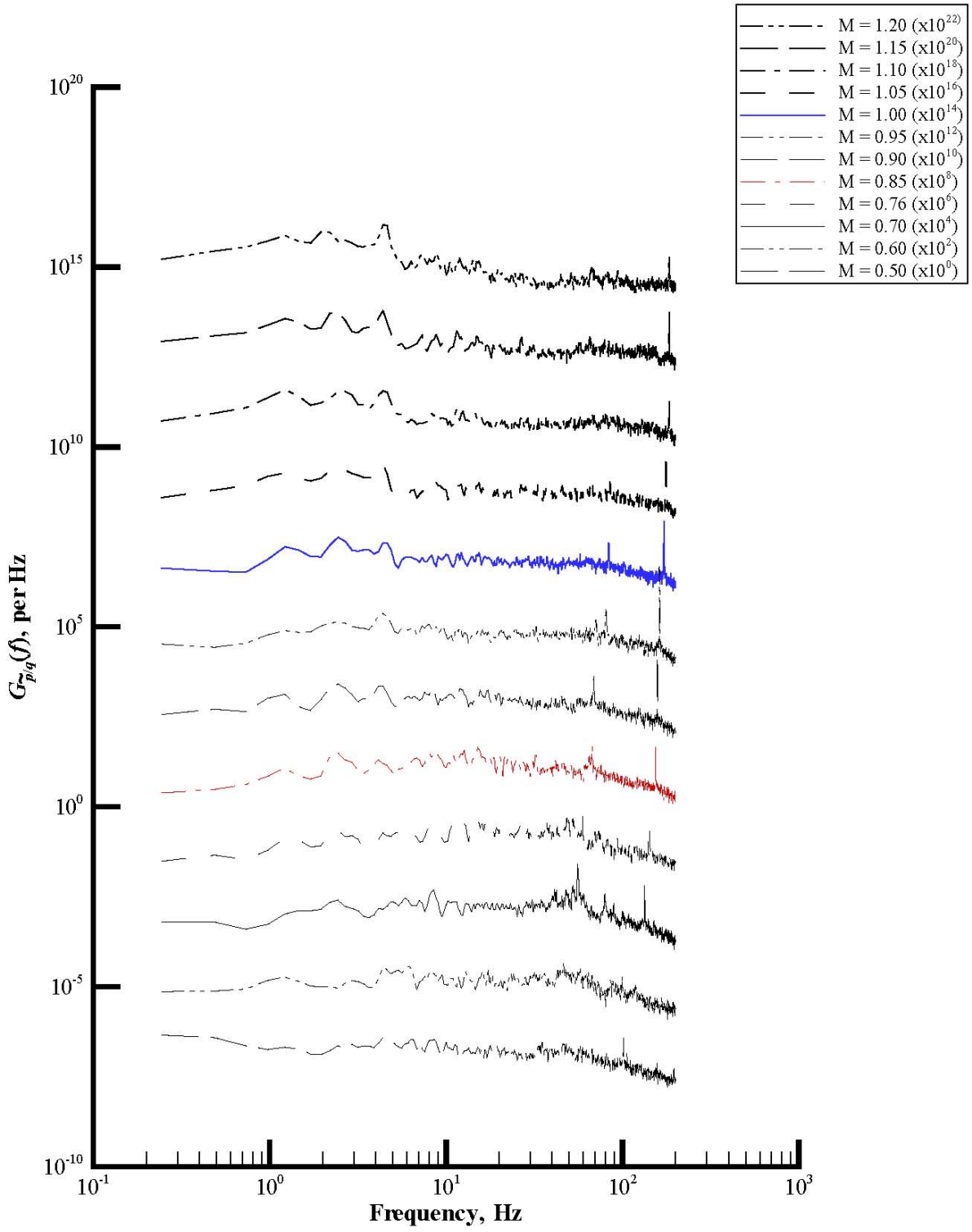
(e) Wall static pressure.

Figure 28. Concluded.



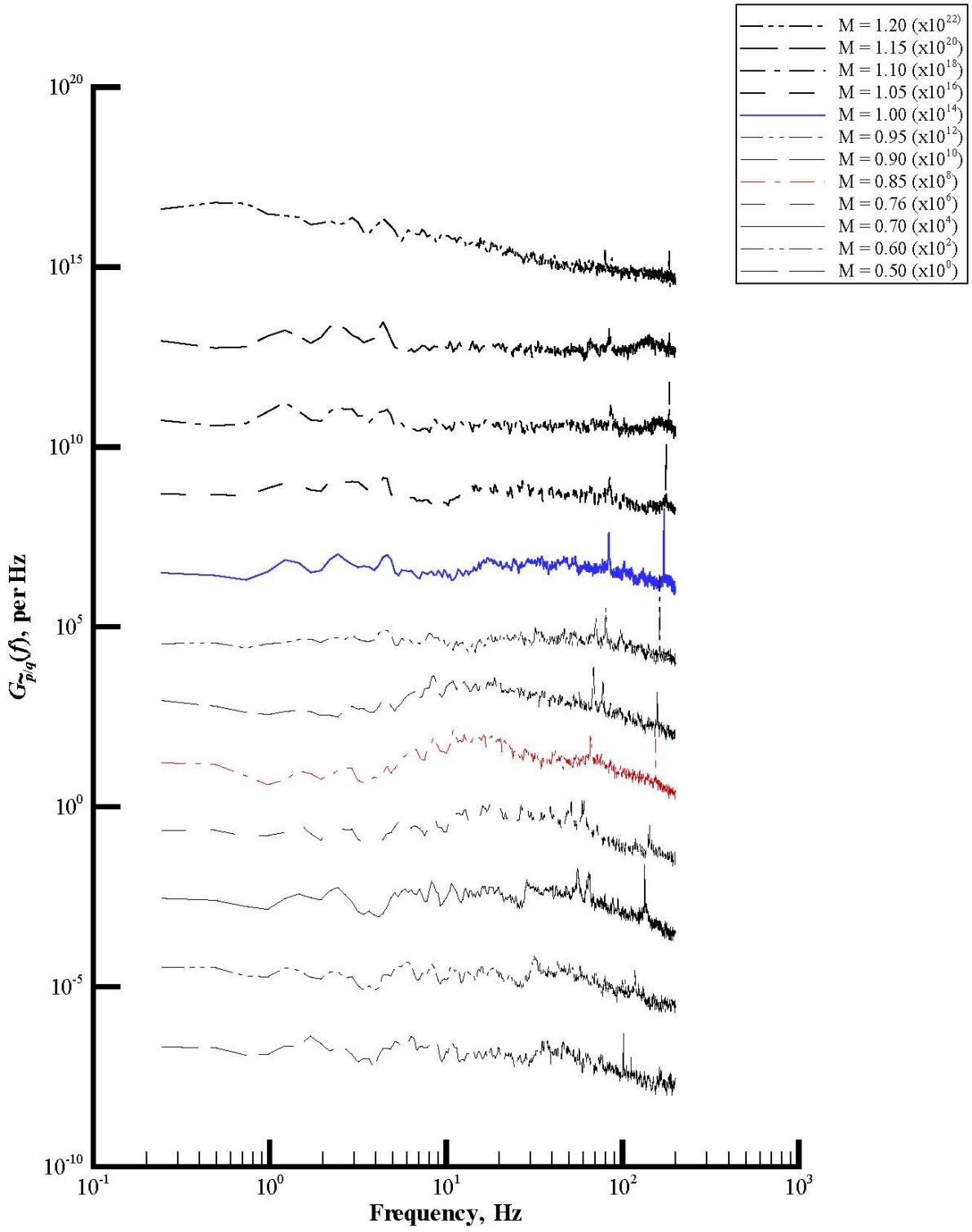
(a) Rake port total pressure.

Figure 29. Plots of power spectral density functions of set 8.



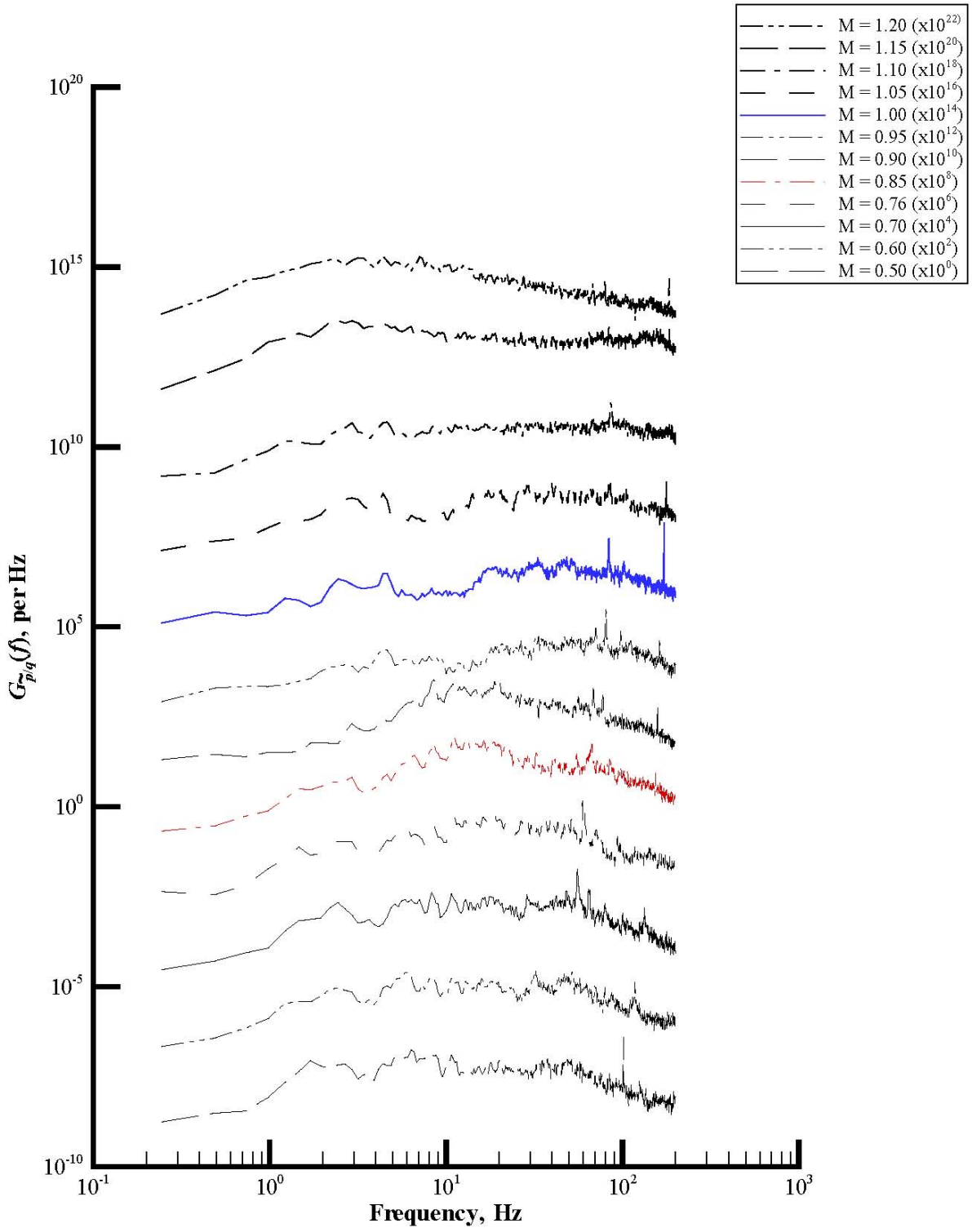
(b) Rake starboard total pressure.

Figure 29. Continued.



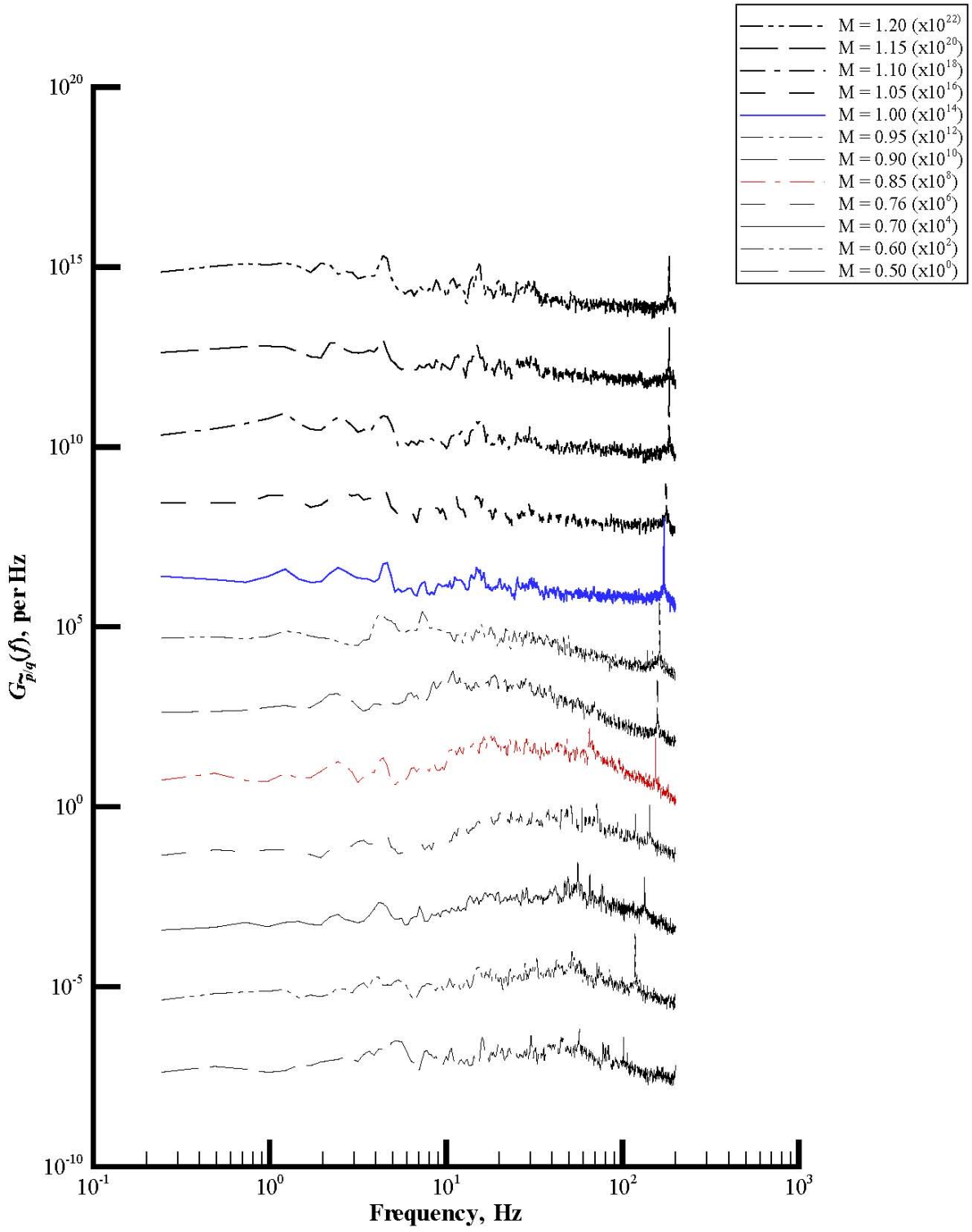
(c) Rake static pressure.

Figure 29. Continued.



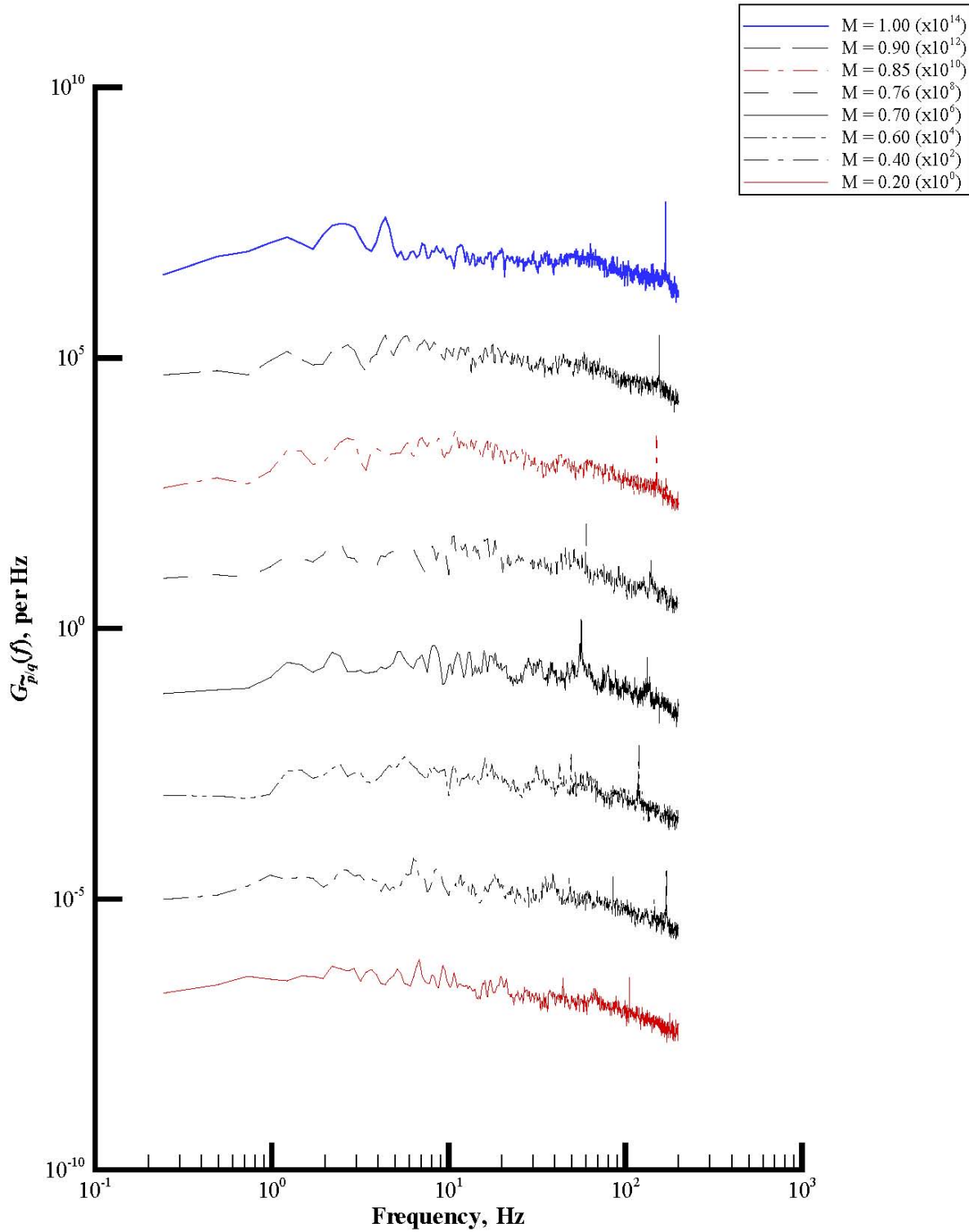
(d) Rake acoustic pressure.

Figure 29. Continued.



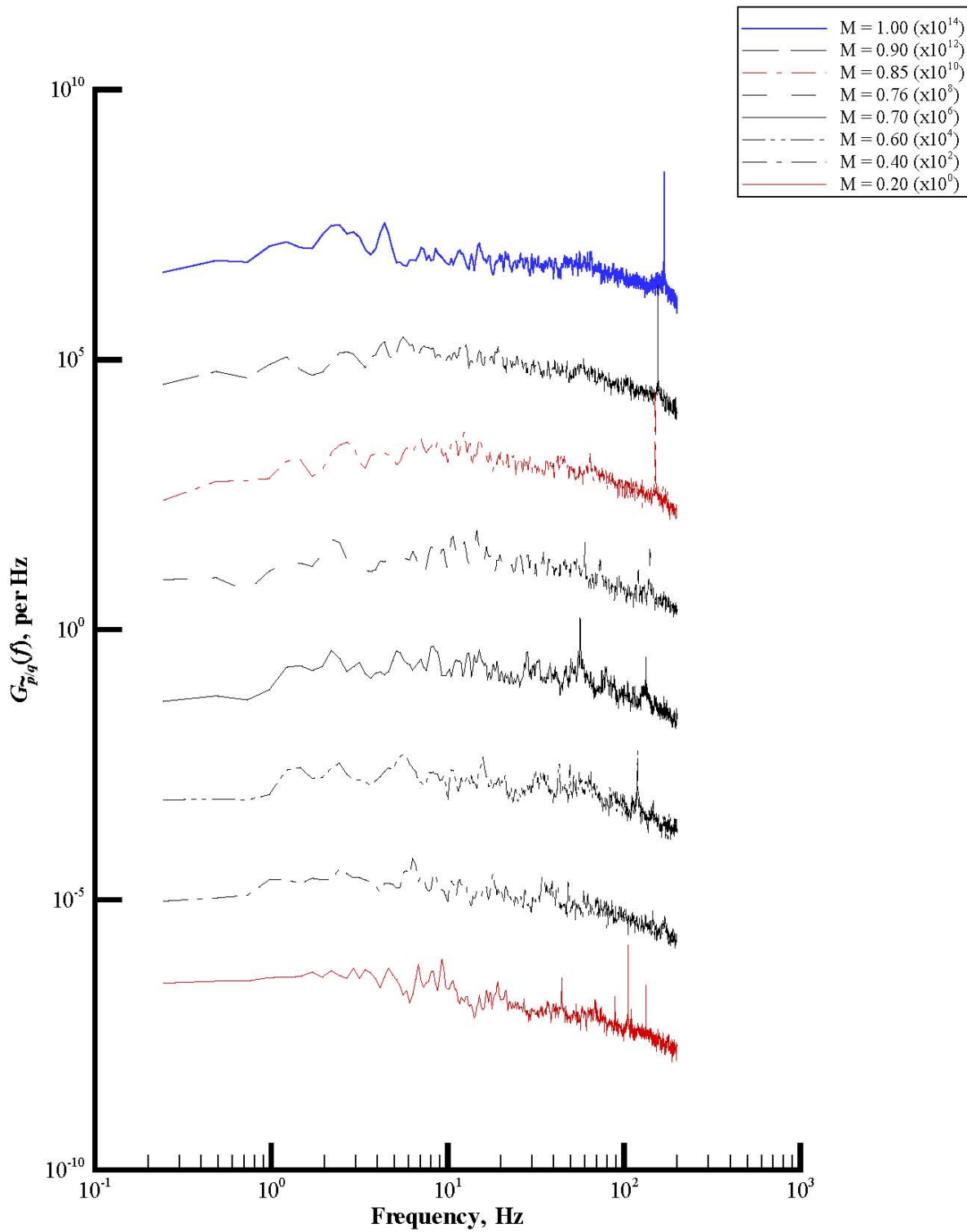
(e) Wall static pressure.

Figure 29. Concluded.



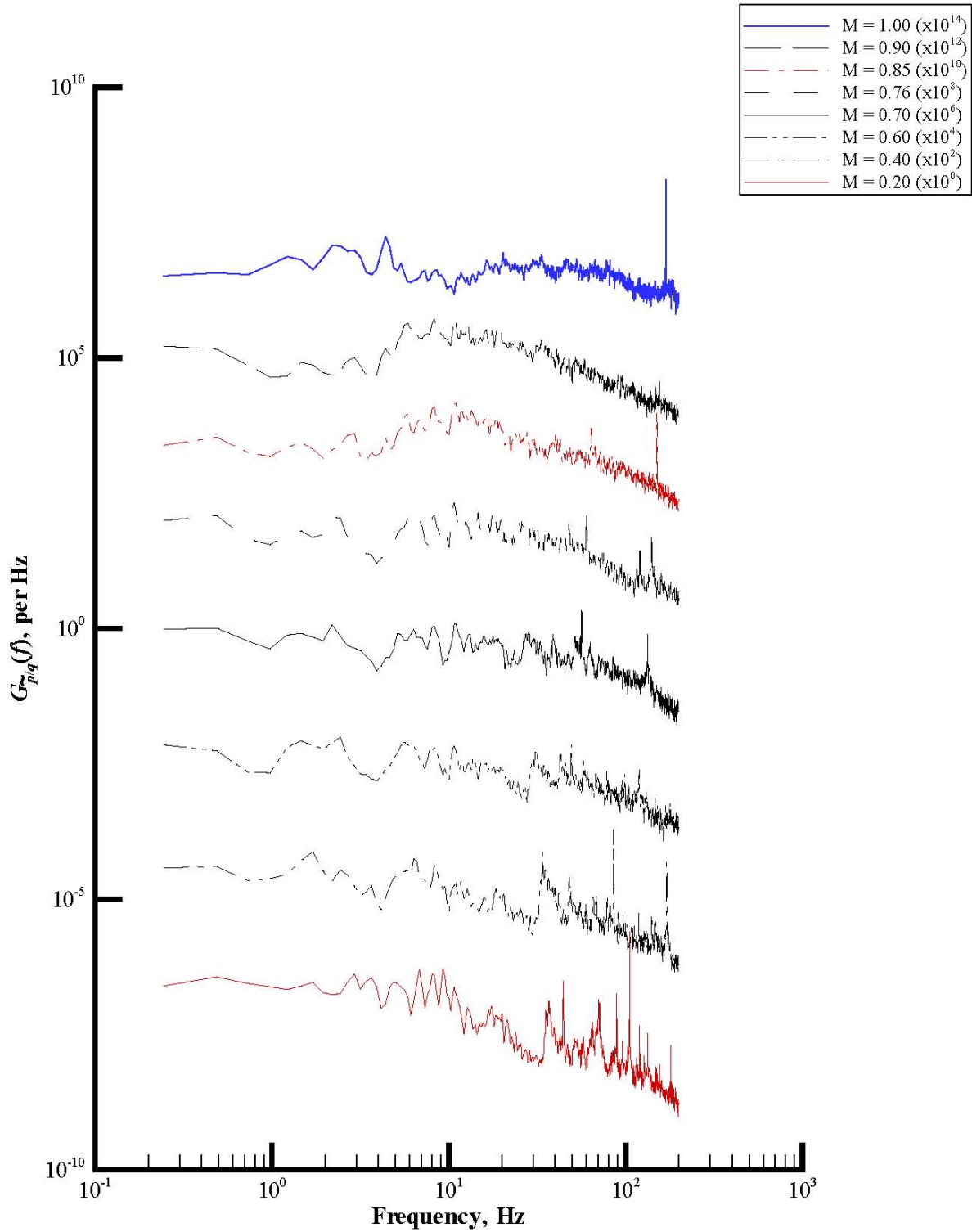
(a) Rake port total pressure.

Figure 30. Plots of power spectral density functions of set 9.



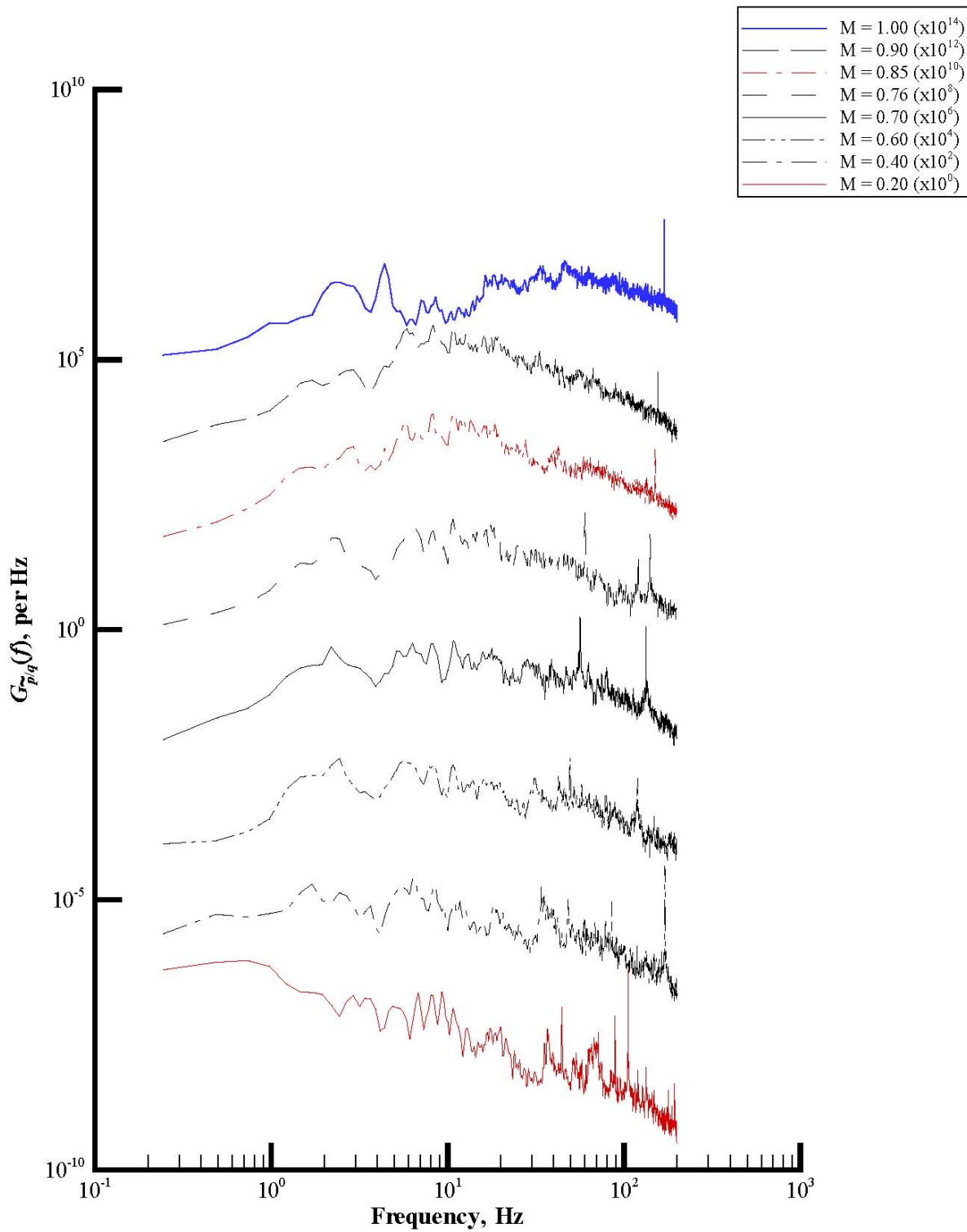
(b) Rake starboard total pressure.

Figure 30. Continued.



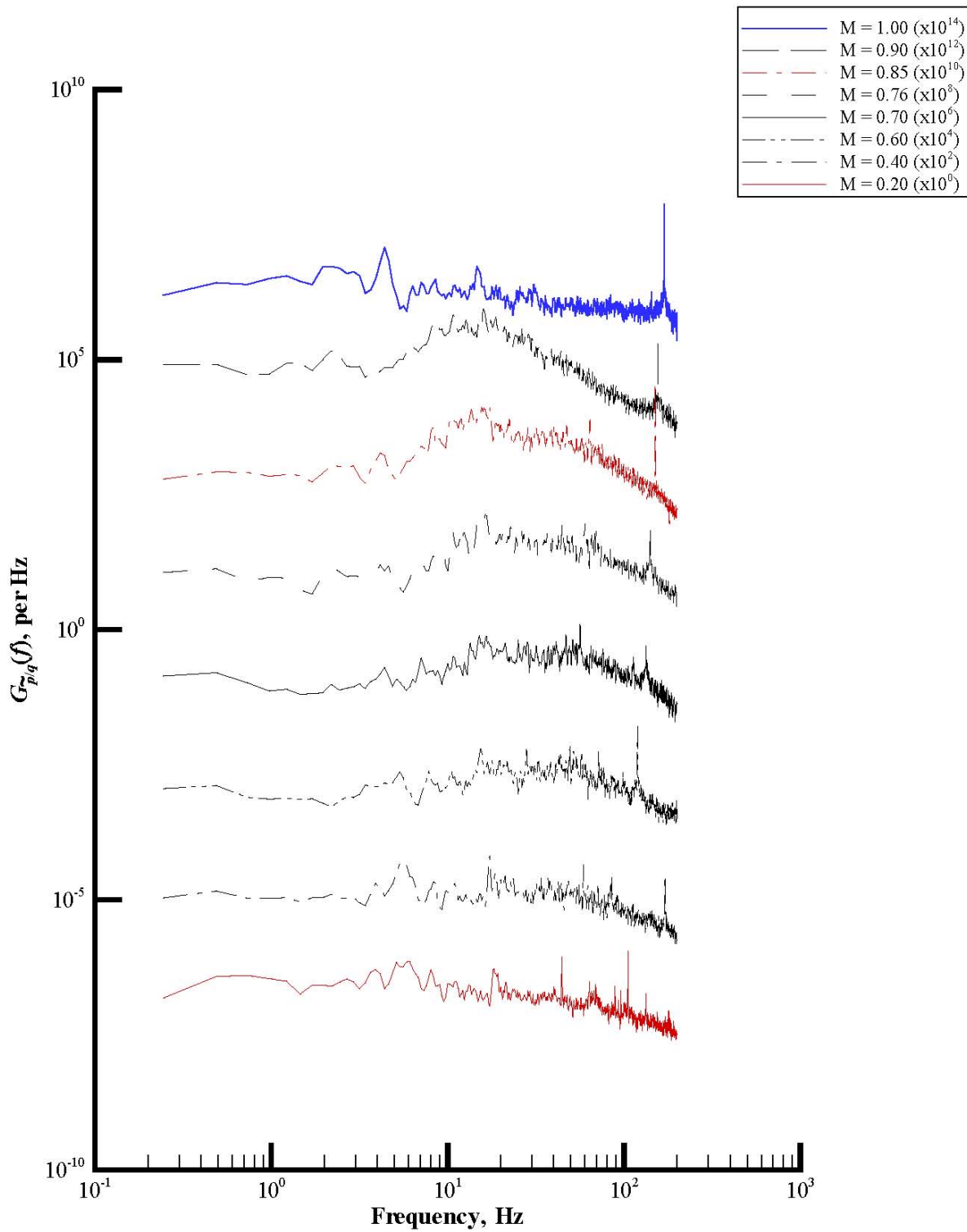
(c) Rake static pressure.

Figure 30. Continued.



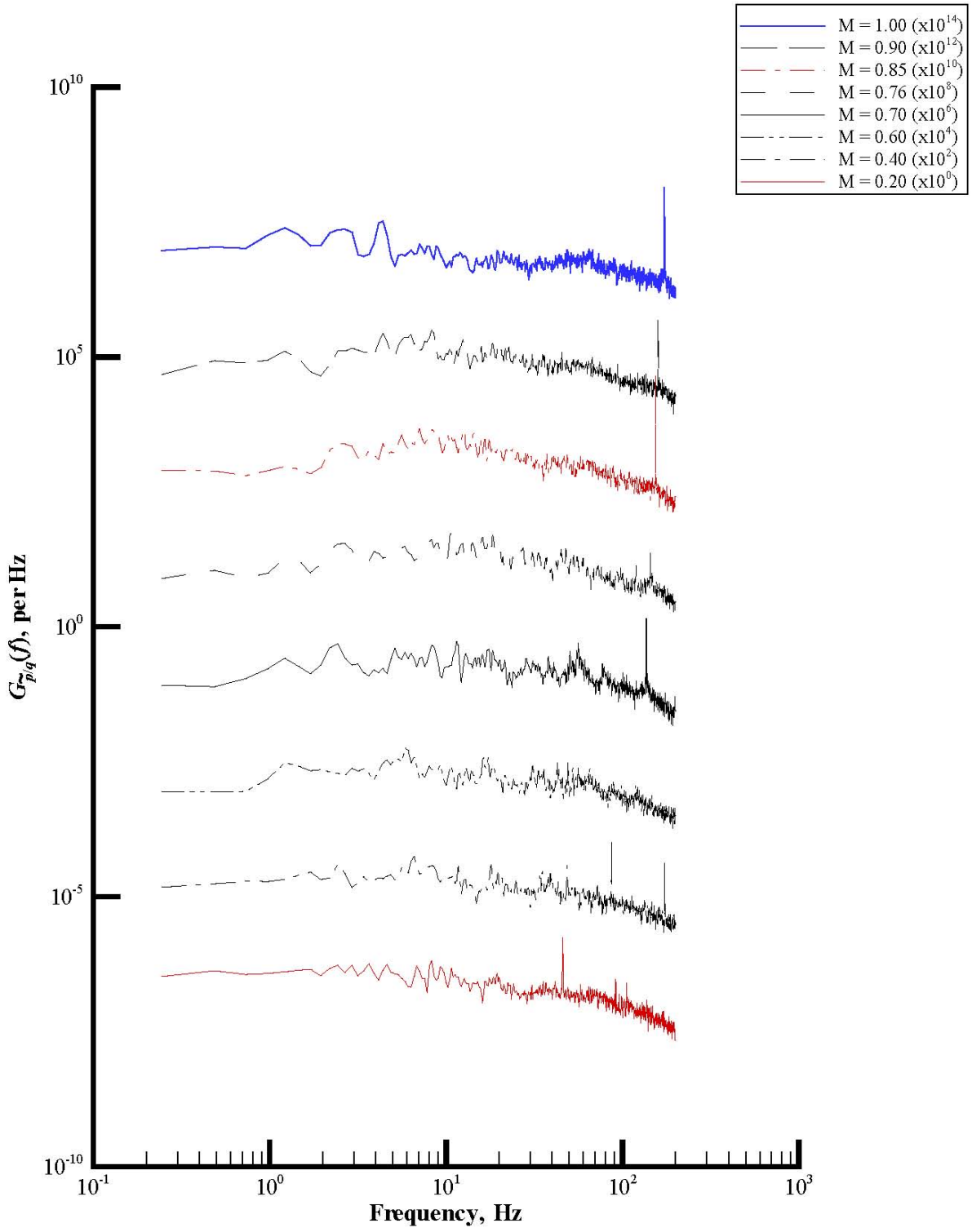
(d) Rake acoustic pressure.

Figure 30. Continued.



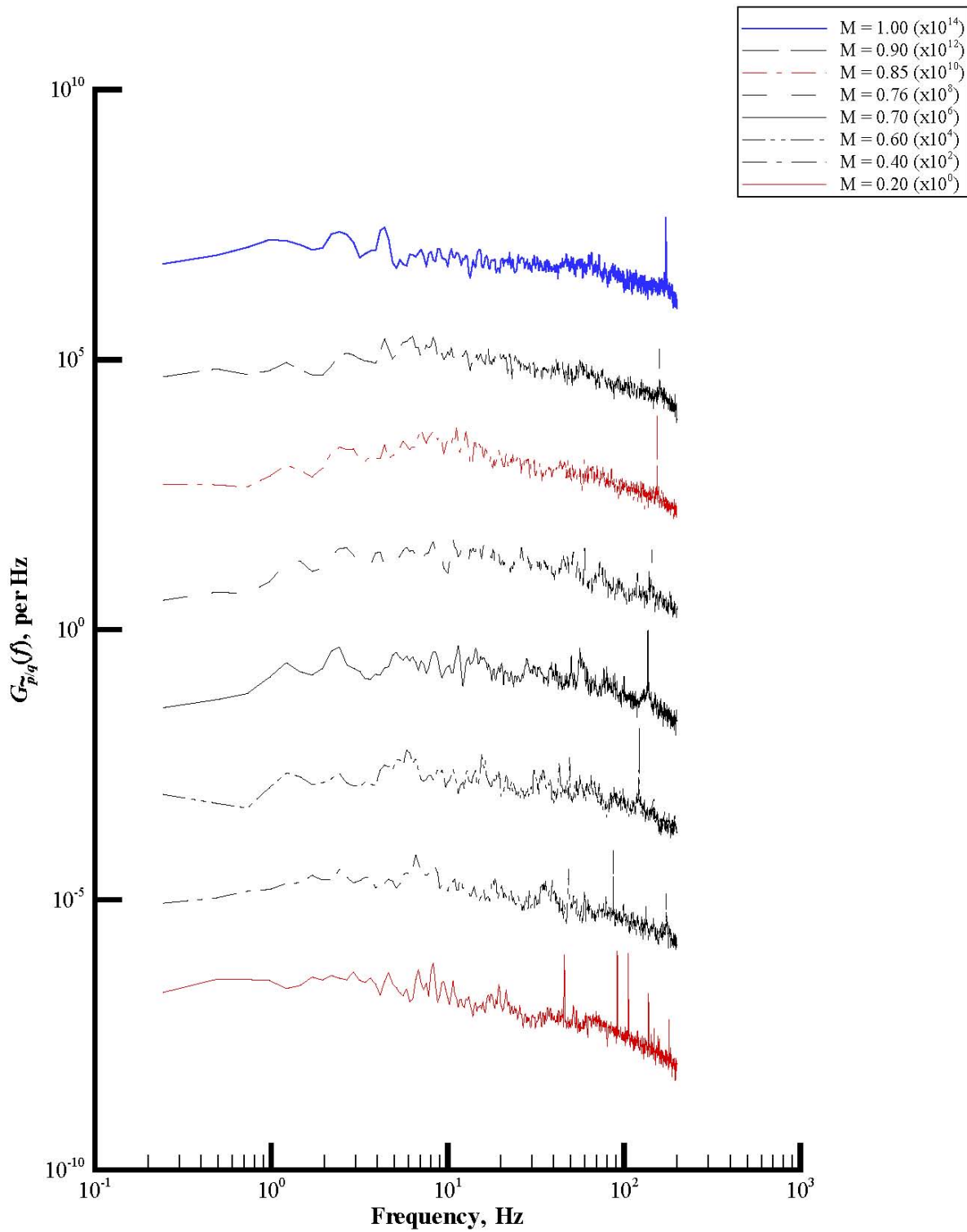
(e) Wall static pressure.

Figure 30. Concluded.



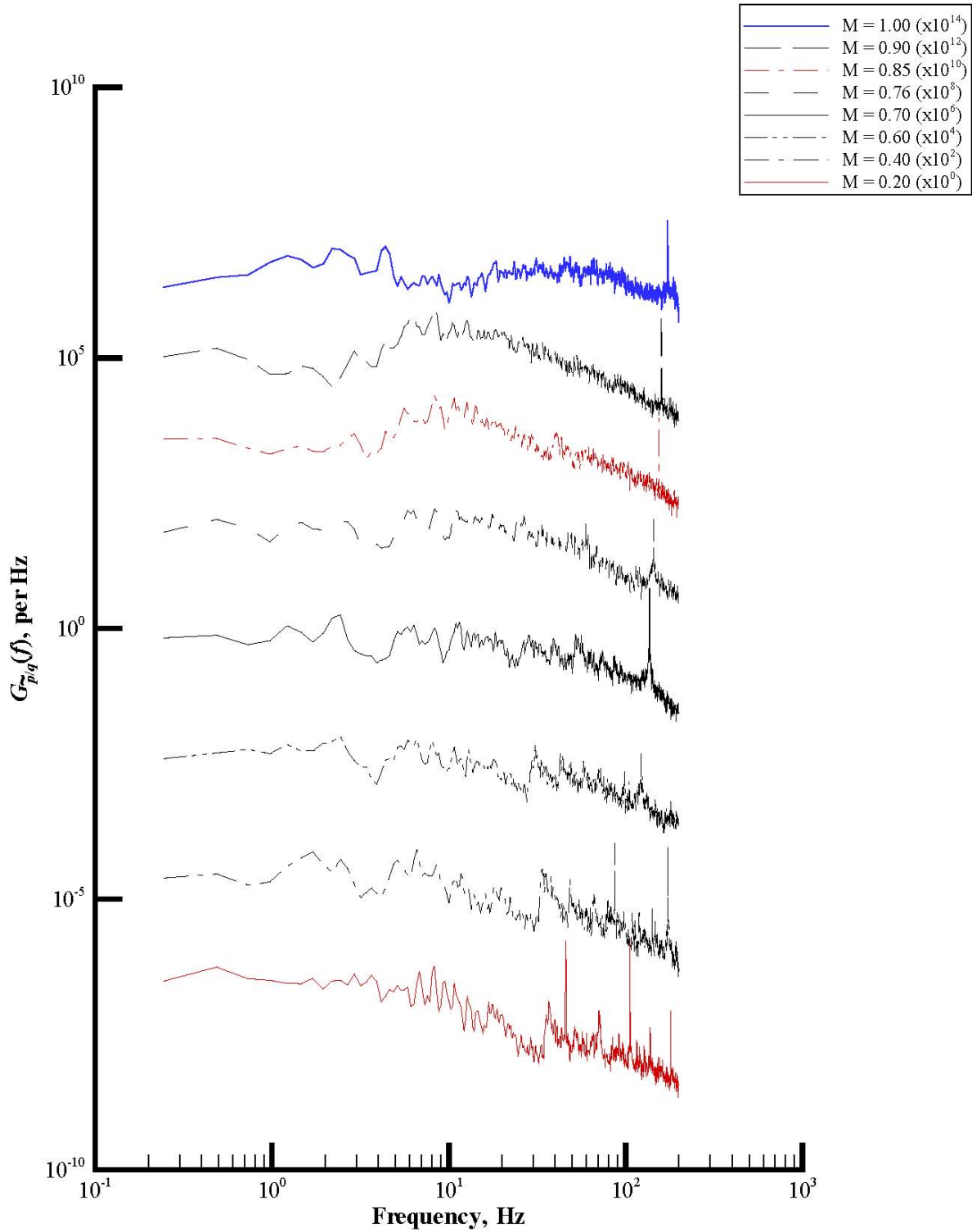
(a) Rake port total pressure.

Figure 31. Plots of power spectral density functions of set 10.



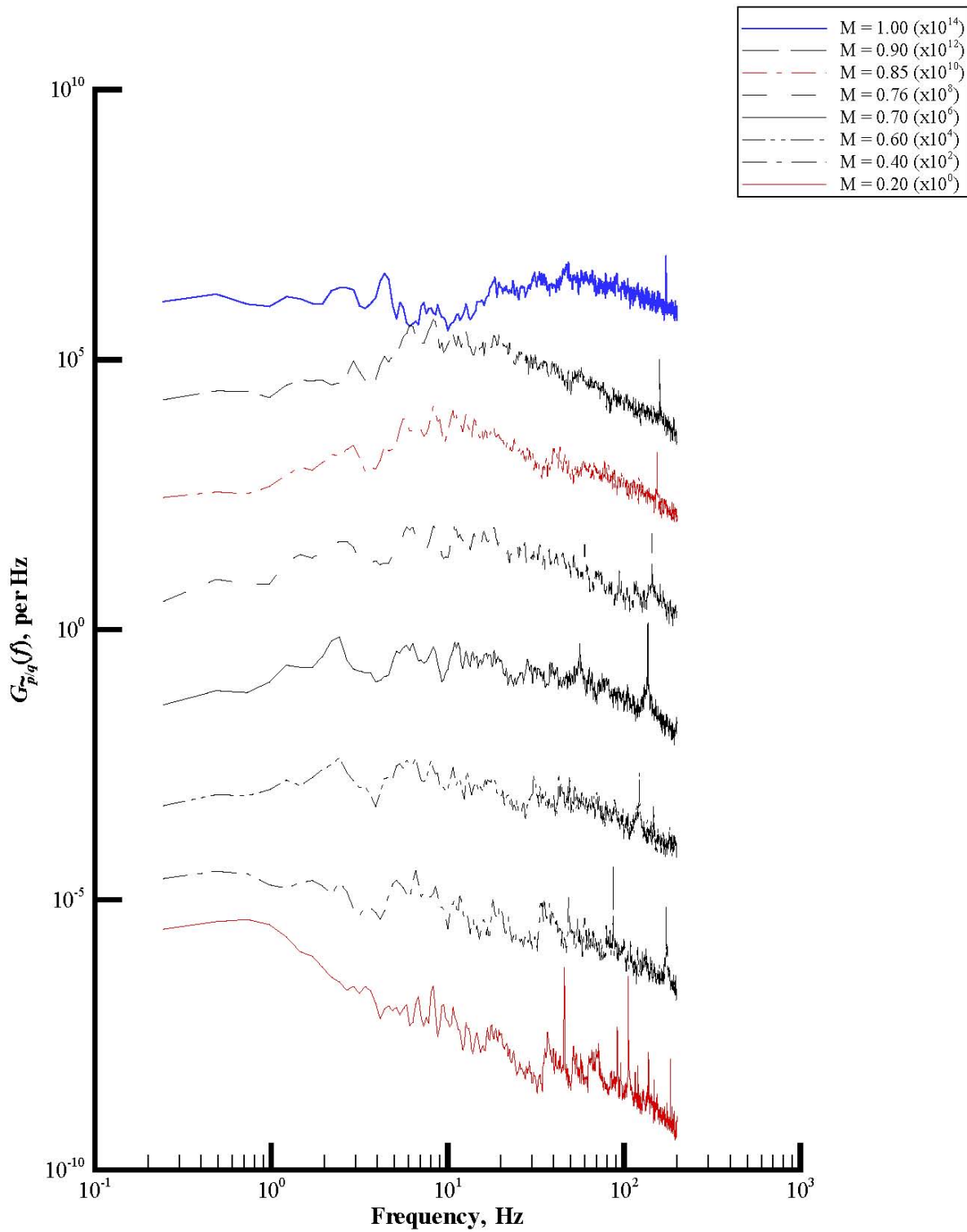
(b) Rake starboard total pressure.

Figure 31. Continued.



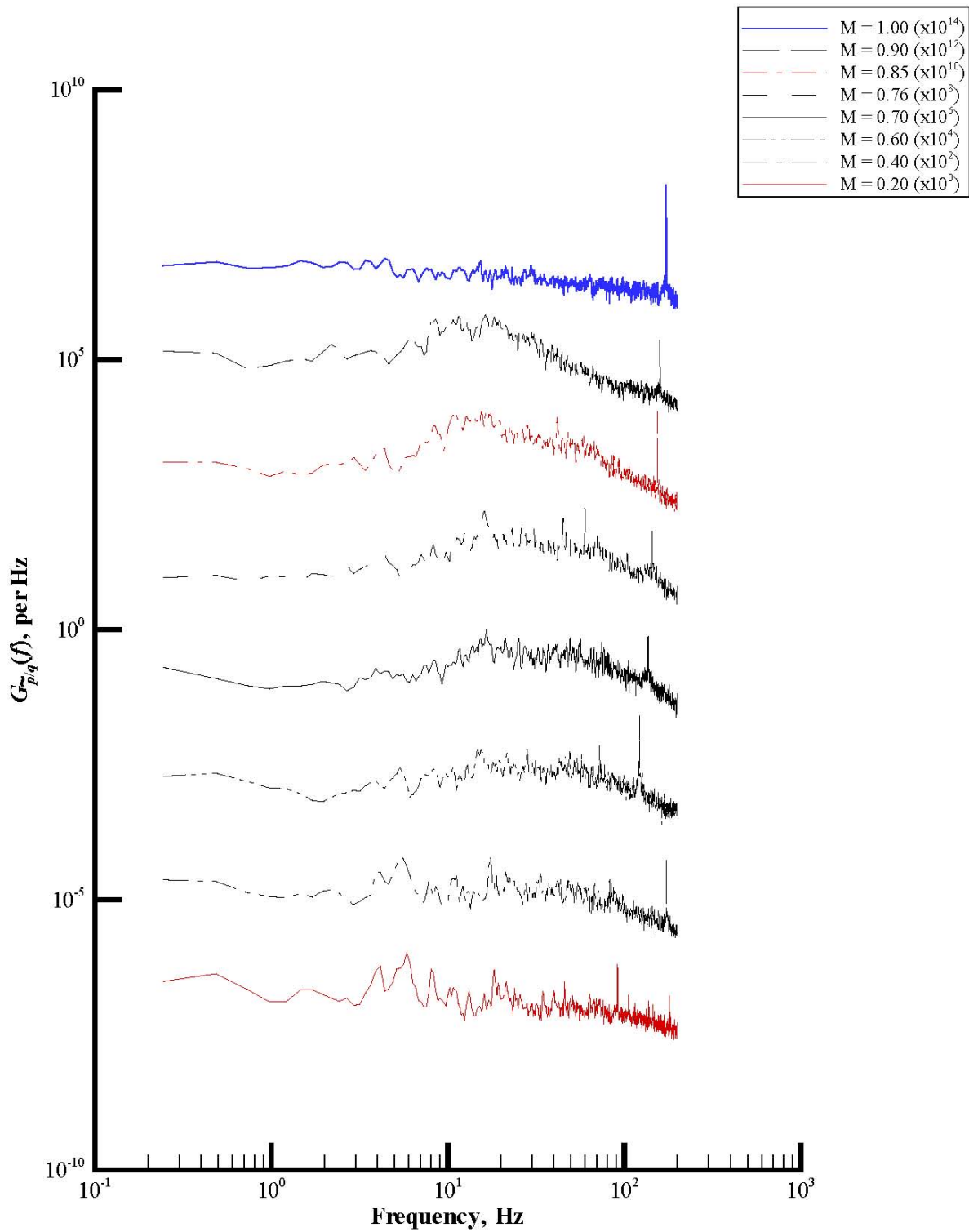
(c) Rake static pressure.

Figure 31. Continued.



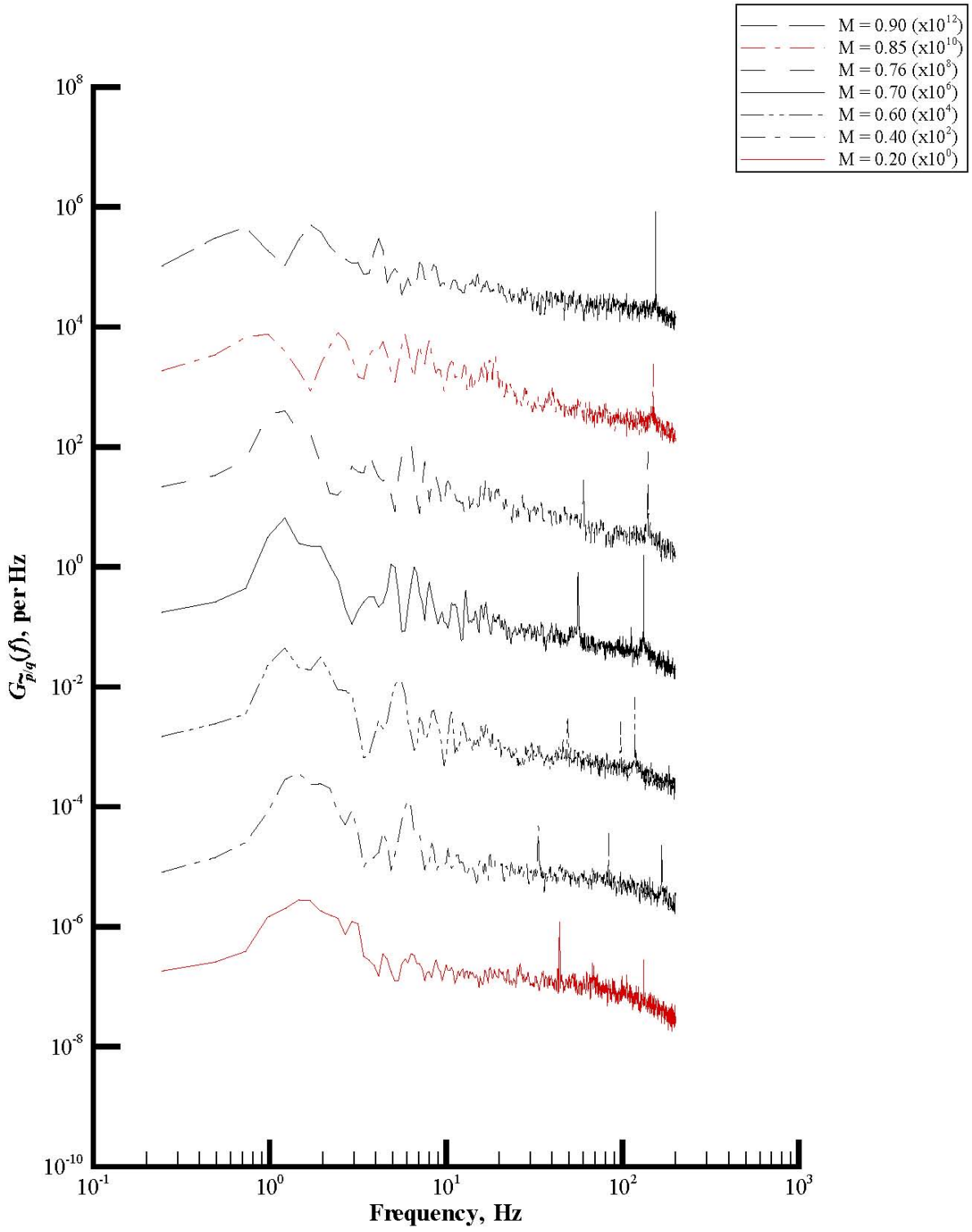
(d) Rake acoustic pressure.

Figure 31. Continued.



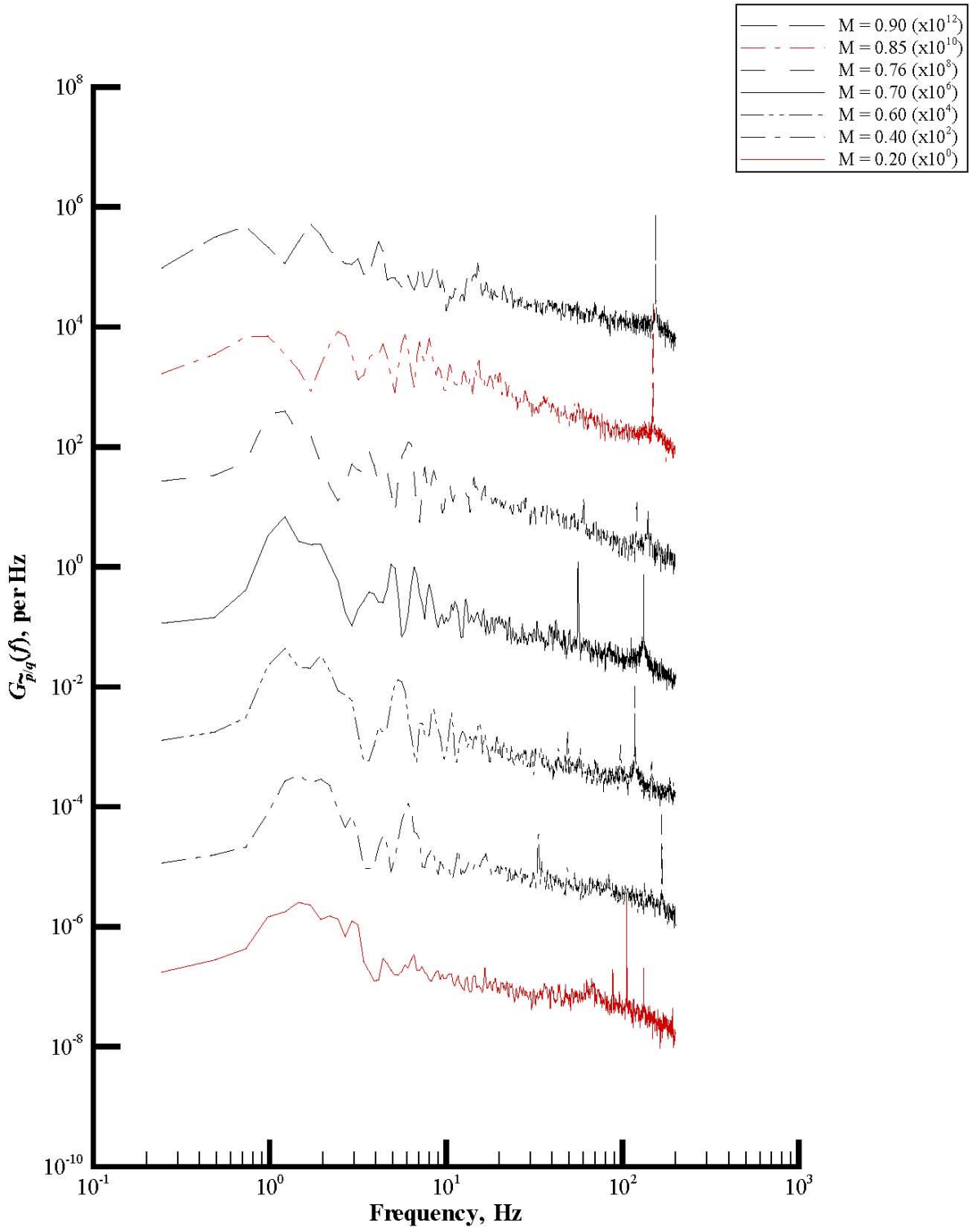
(e) Wall static pressure.

Figure 31. Concluded.



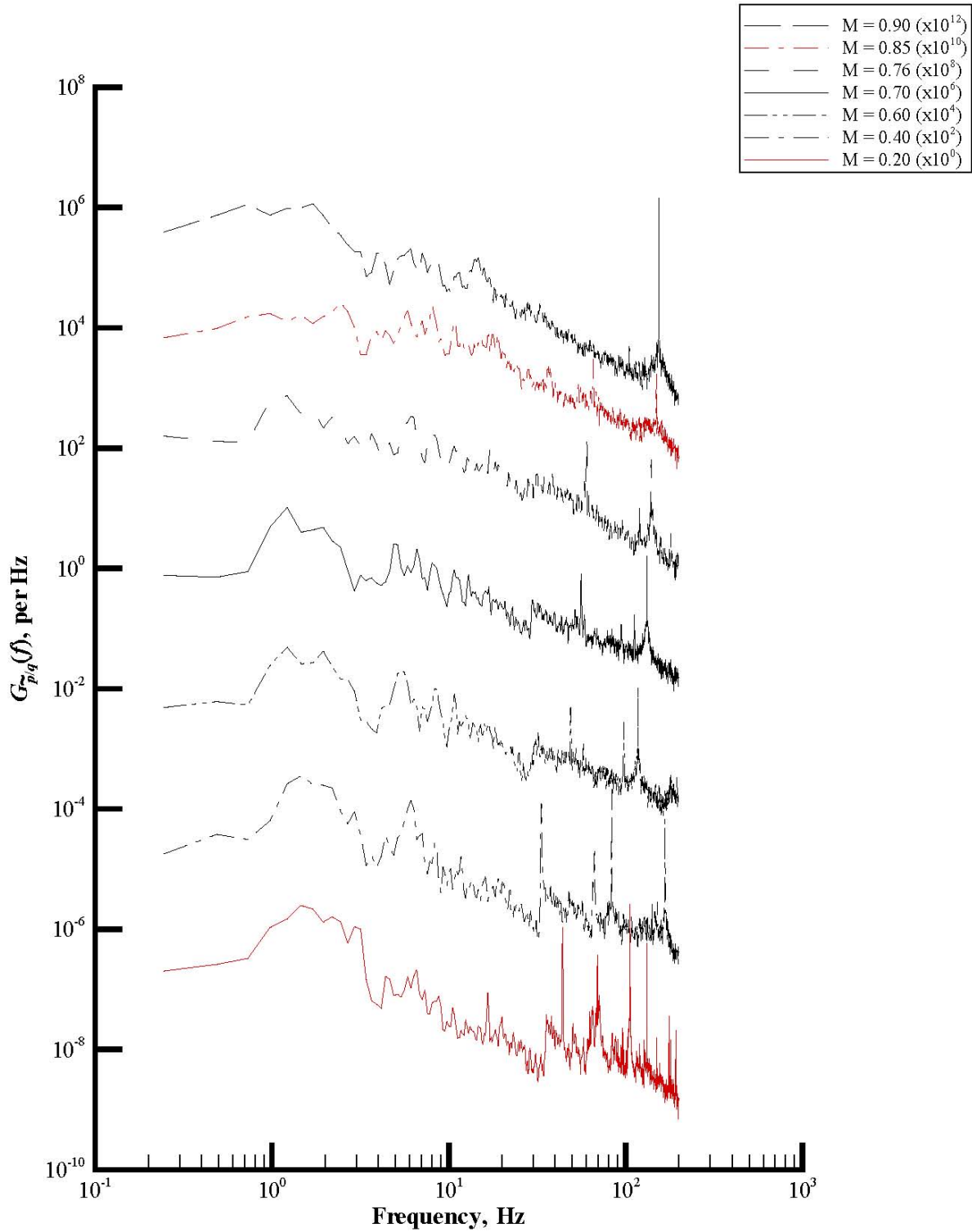
(a) Rake port total pressure.

Figure 32. Plots of power spectral density functions of set 11.



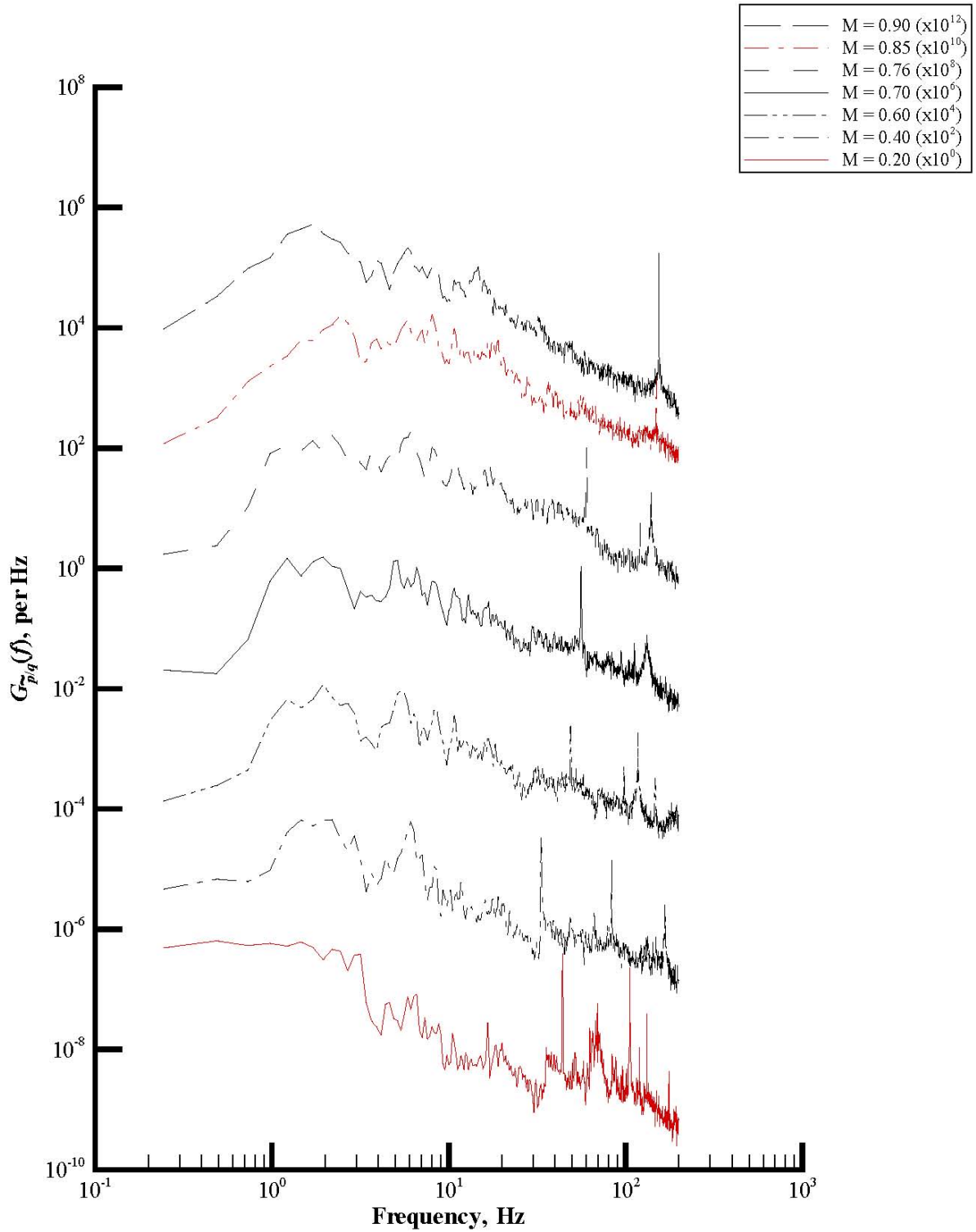
(b) Rake starboard total pressure.

Figure 32. Continued.



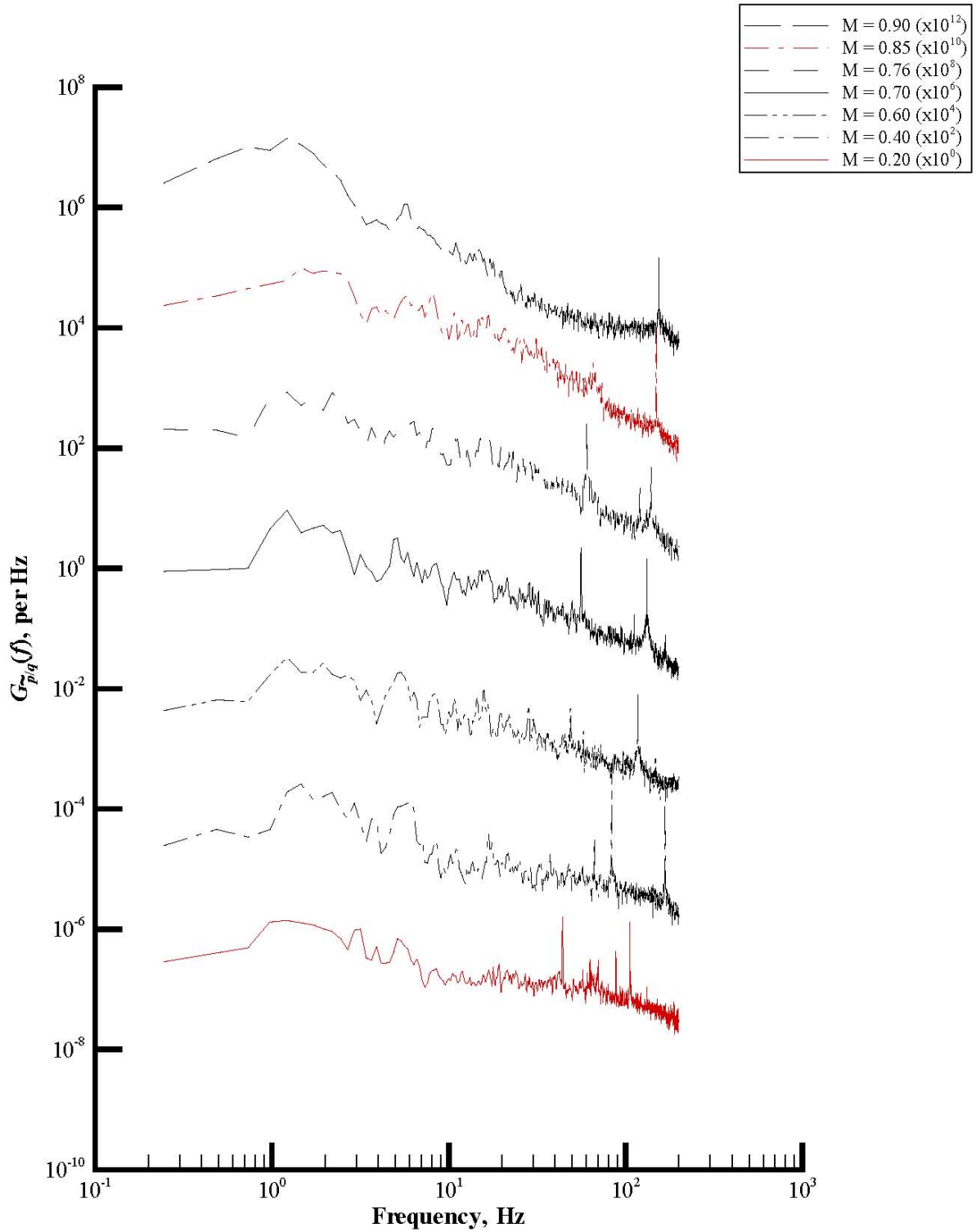
(c) Rake static pressure.

Figure 32. Continued.



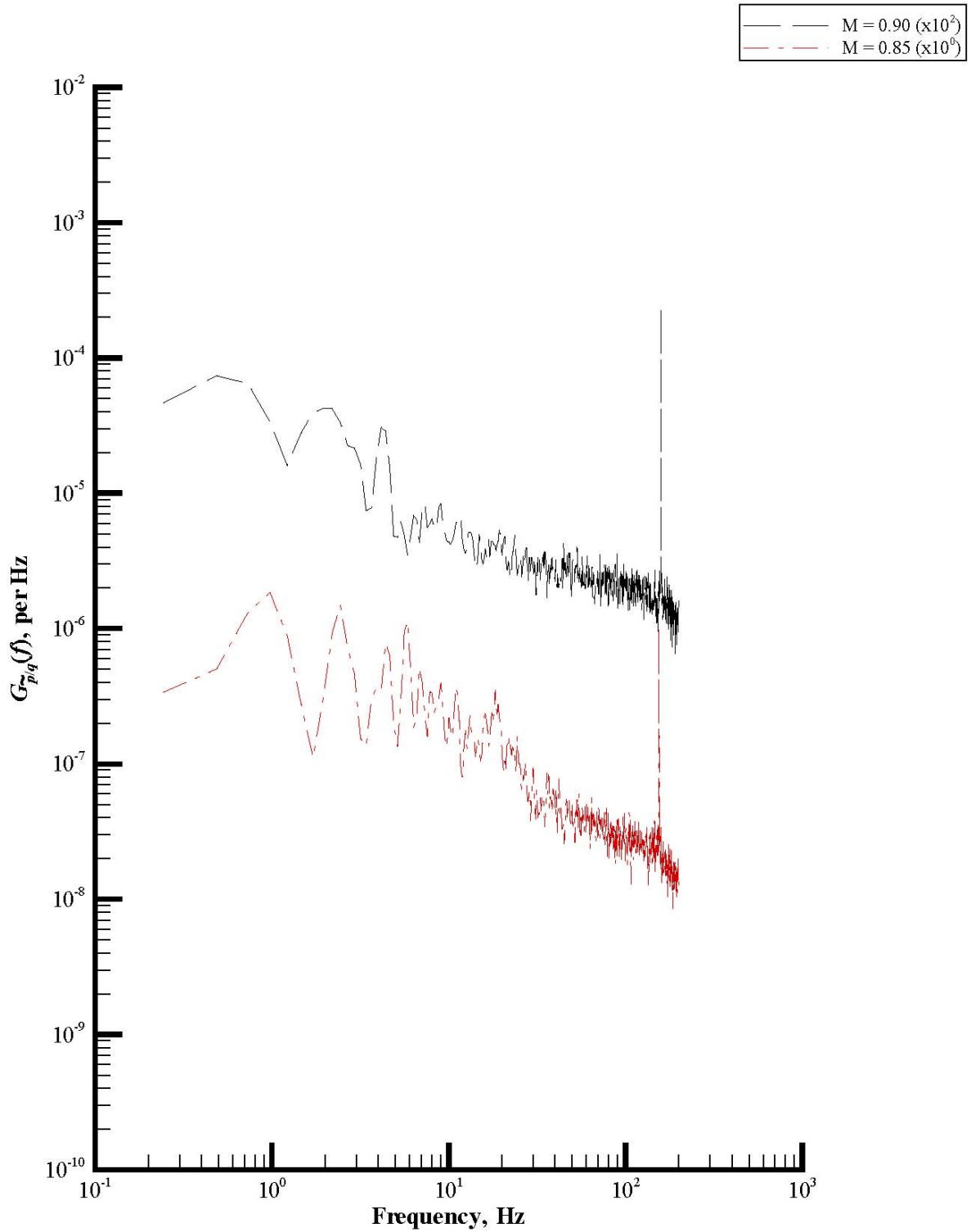
(d) Rake acoustic pressure.

Figure 32. Continued.



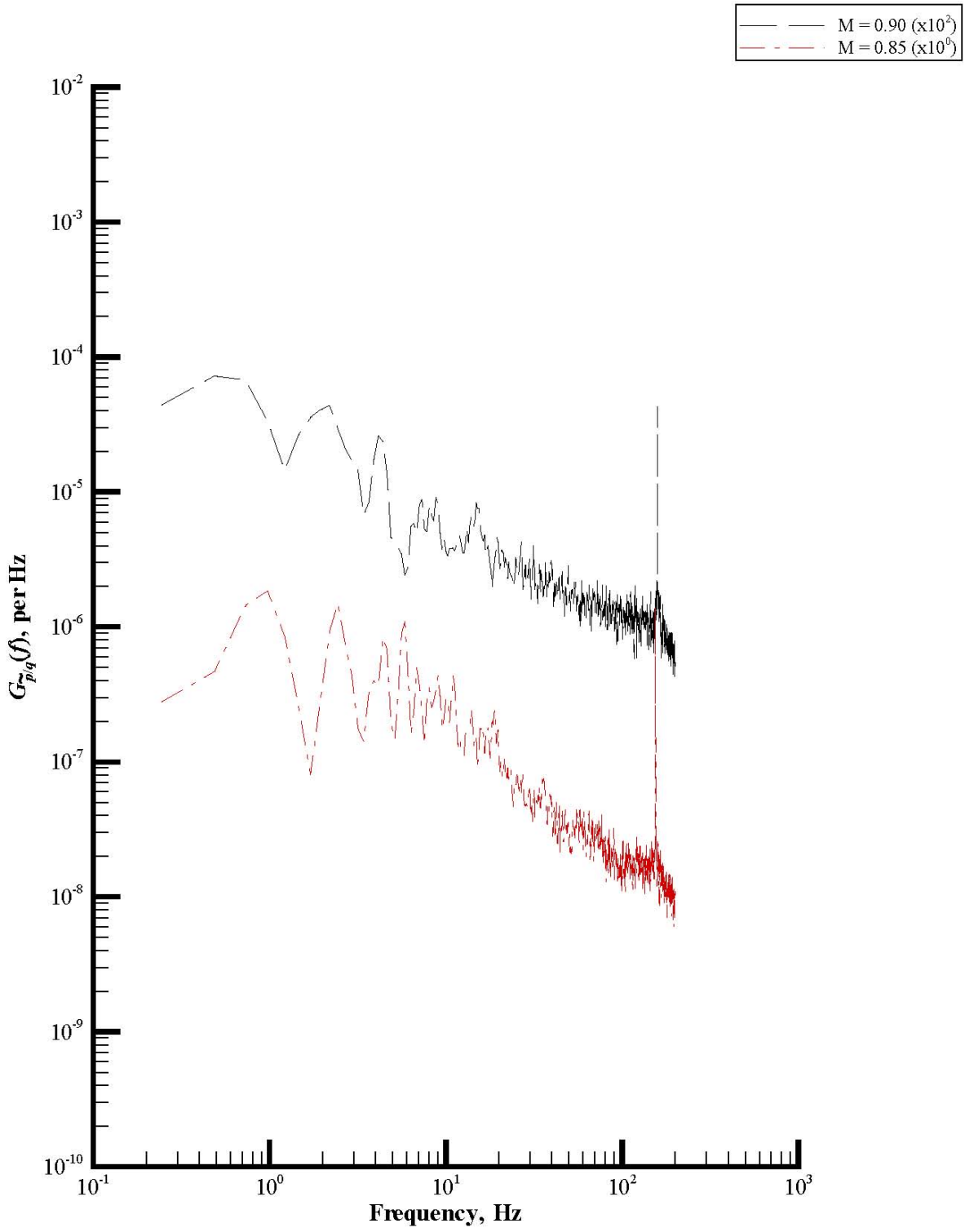
(e) Wall static pressure.

Figure 32. Concluded.



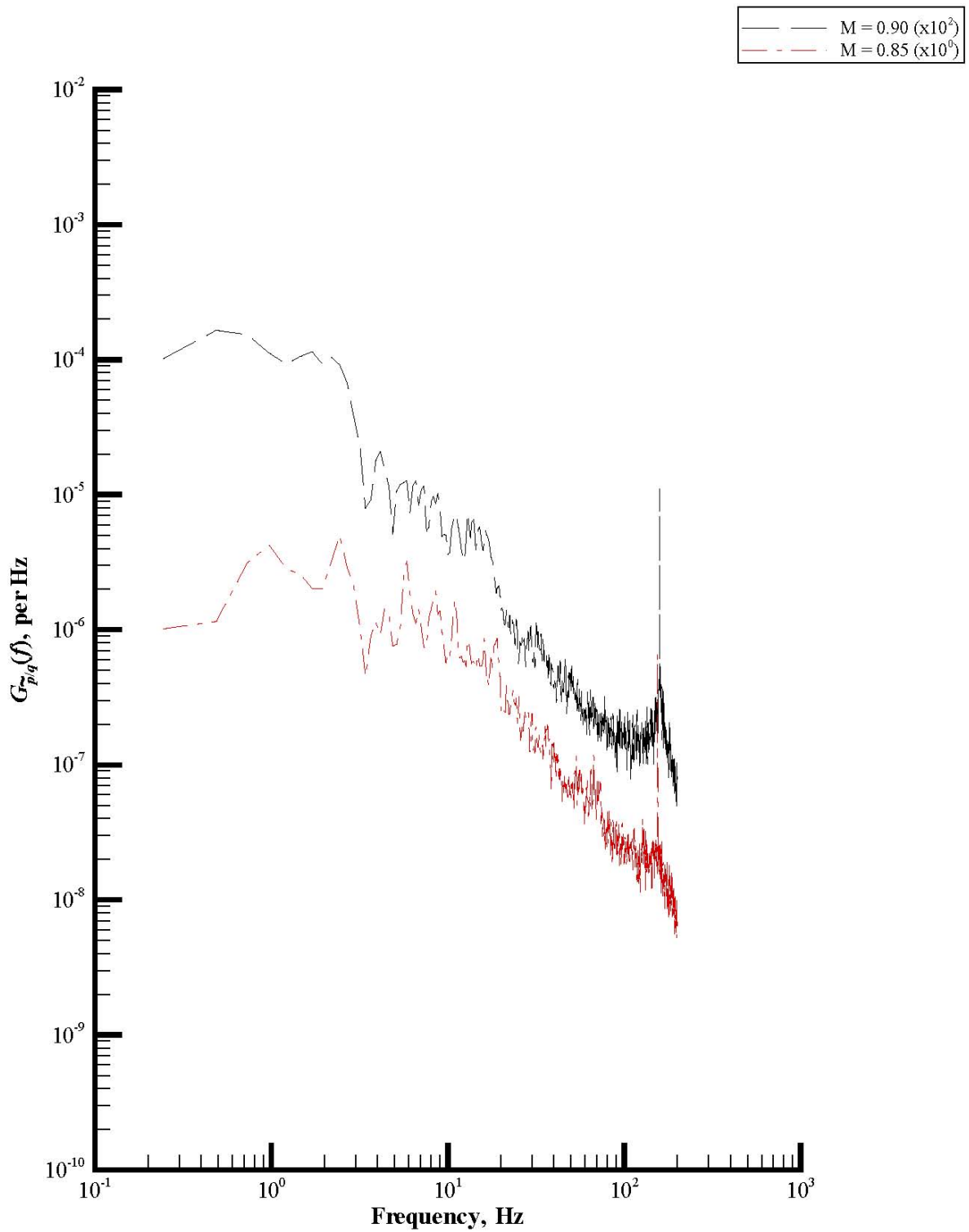
(a) Rake port total pressure.

Figure 33. Plots of power spectral density functions of set 12.



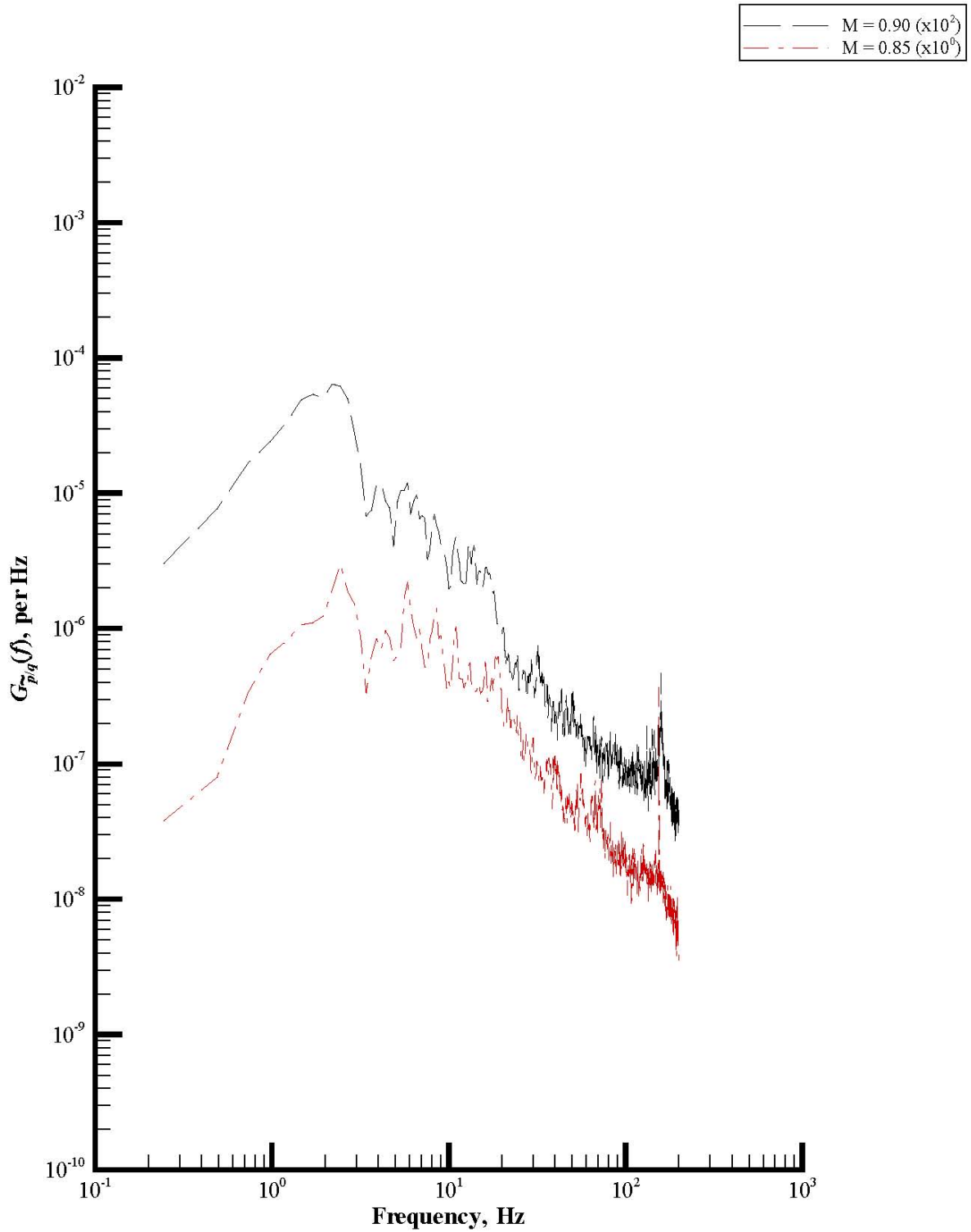
(b) Rake starboard total pressure.

Figure 33. Continued.



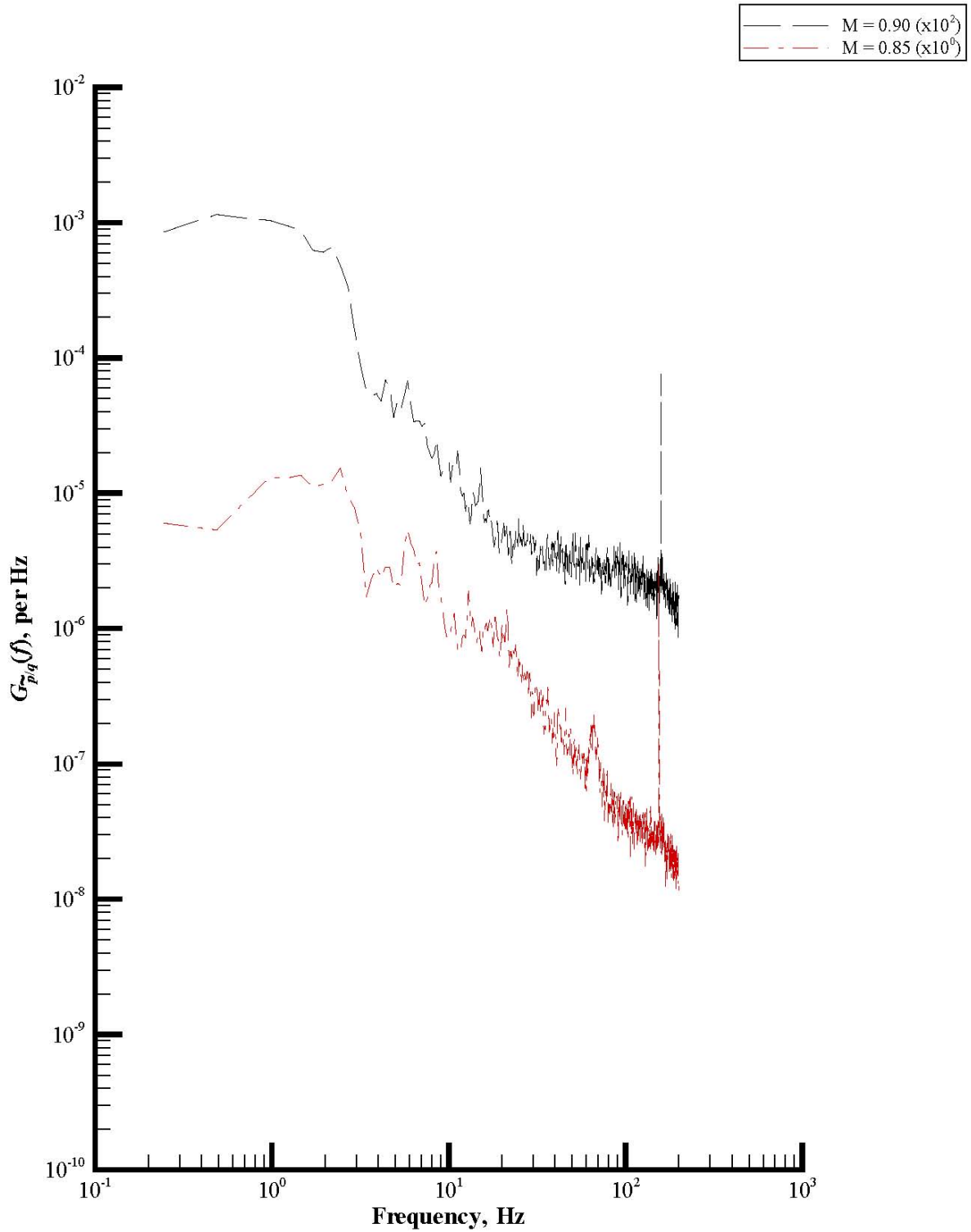
(c) Rake static pressure.

Figure 33. Continued.



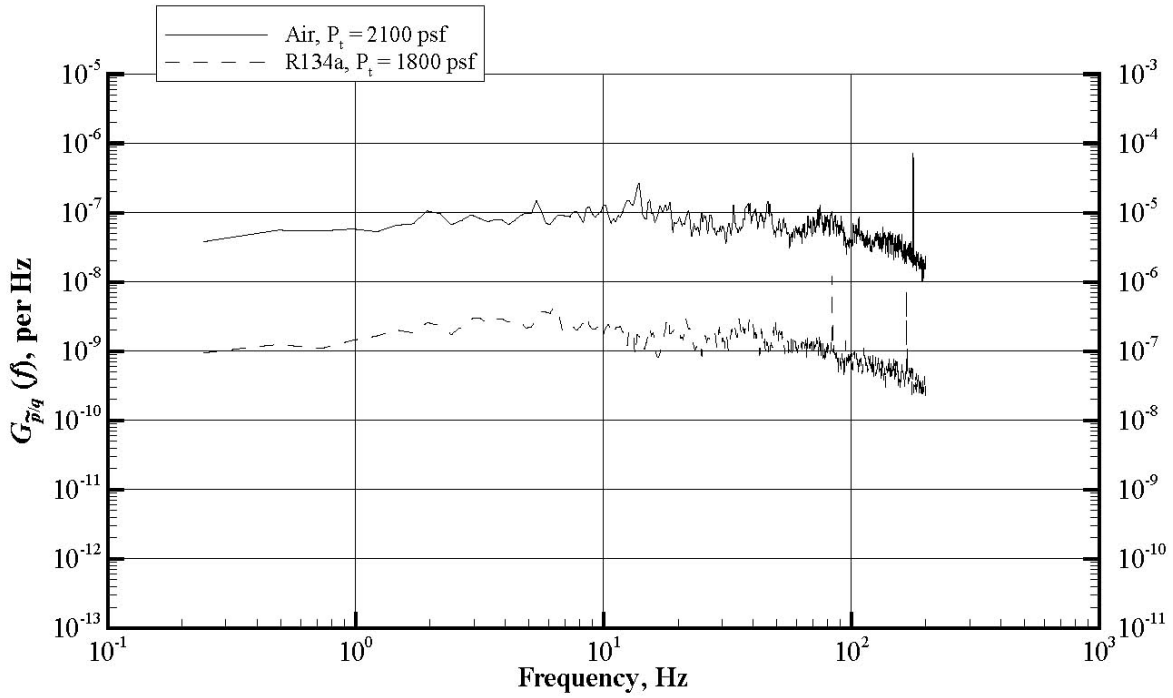
(d) Rake acoustic pressure.

Figure 33. Continued.

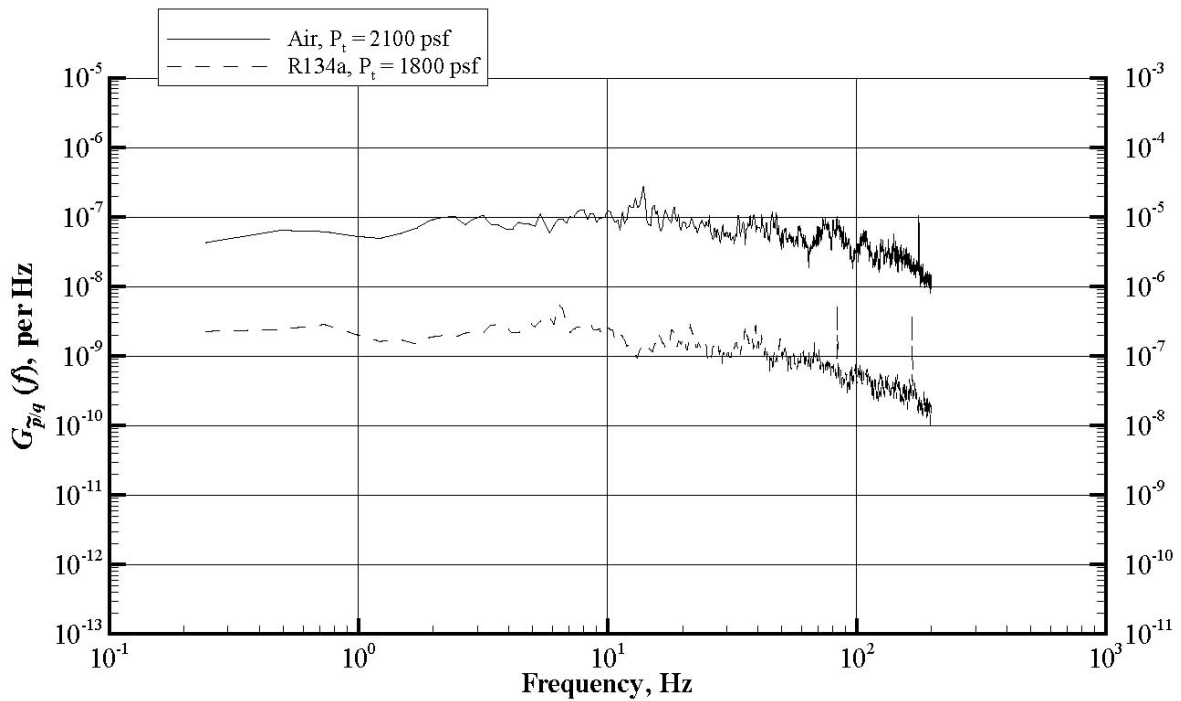


(e) Wall static pressure.

Figure 33. Concluded.

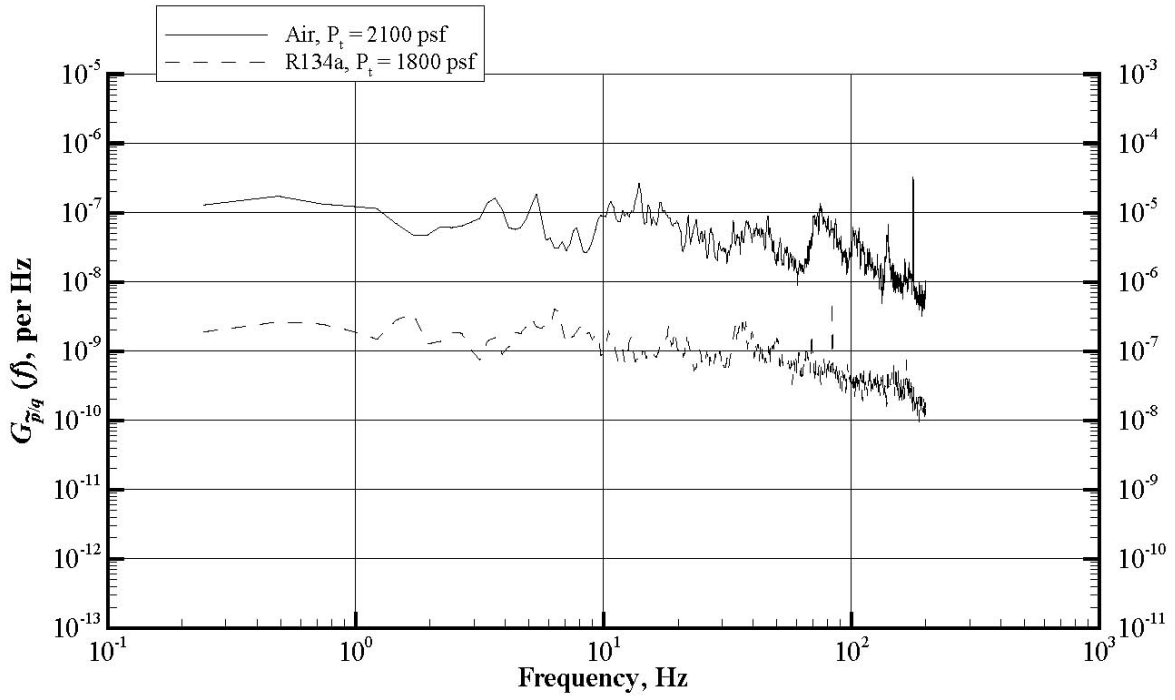


(a) Rake port total pressure.

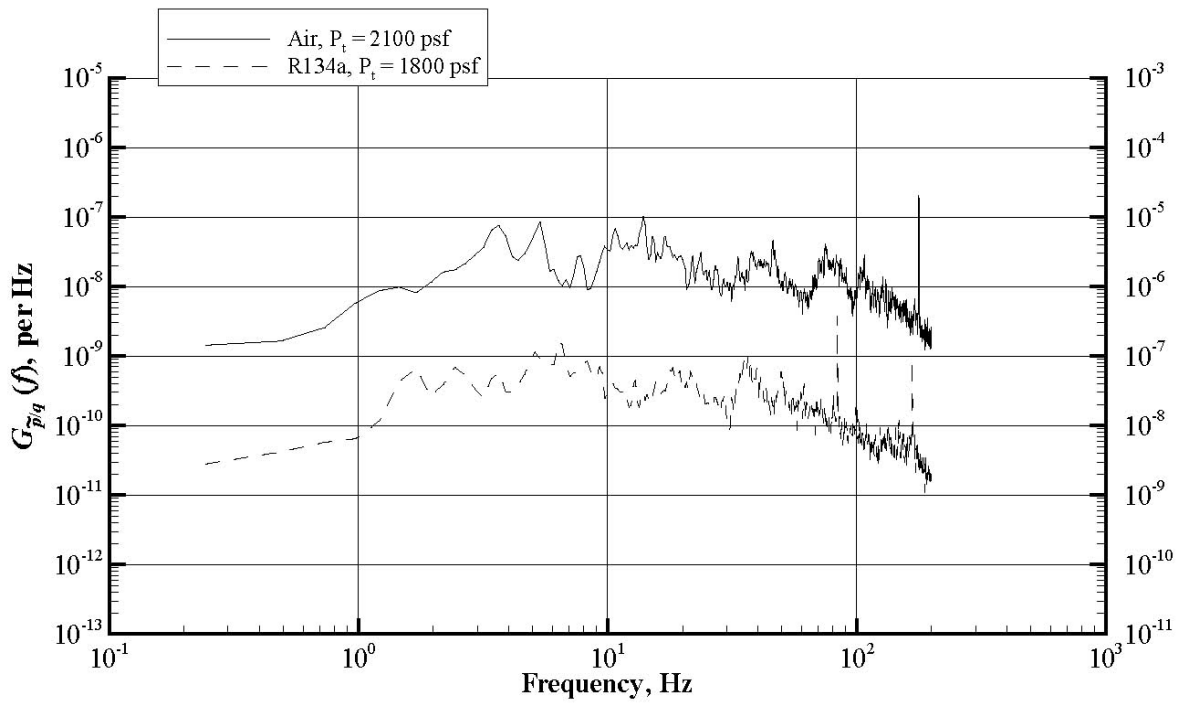


(b) Rake starboard total pressure.

Figure 34. Comparison of low-frequency spectra in air ($P_t = 2100$ psf) and R134a ($P_t = 1800$ psf), $M = 0.4$.

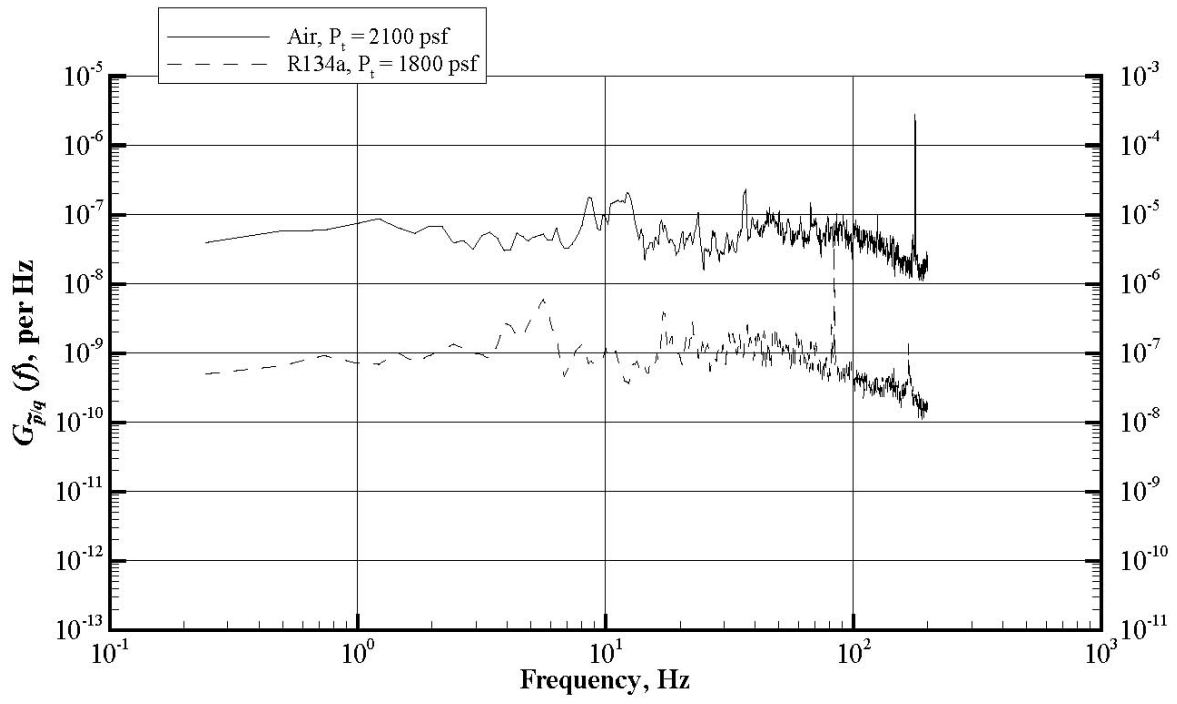


(c) Rake static pressure.



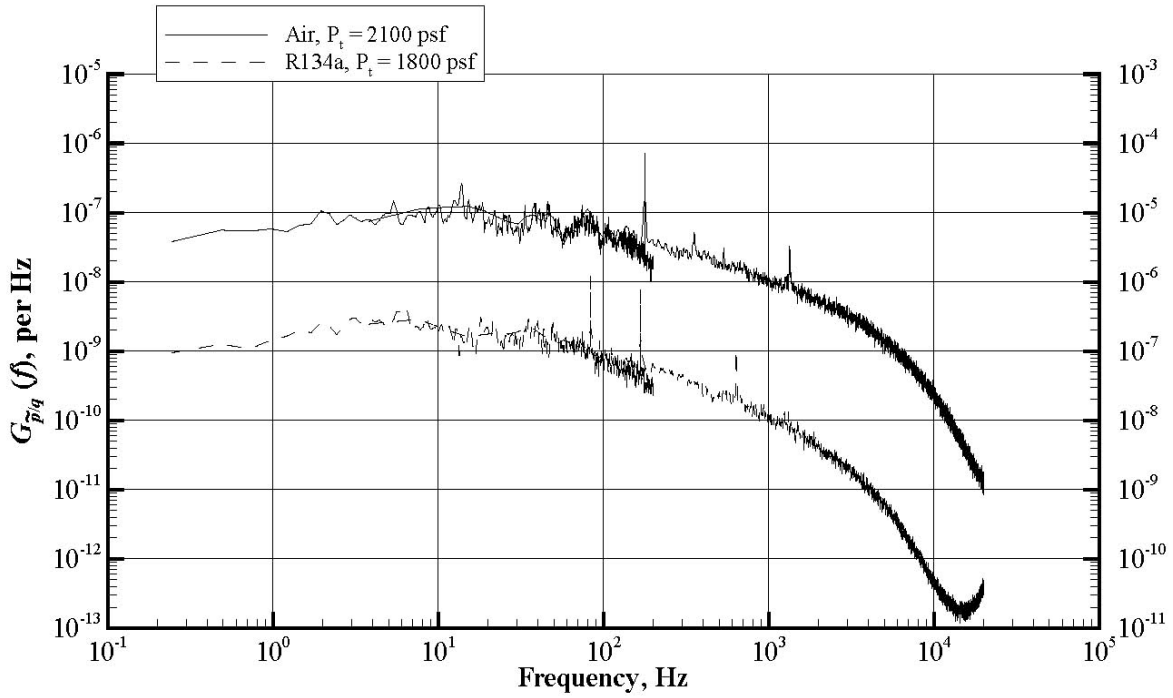
(d) Rake acoustic pressure.

Figure 34. Continued.

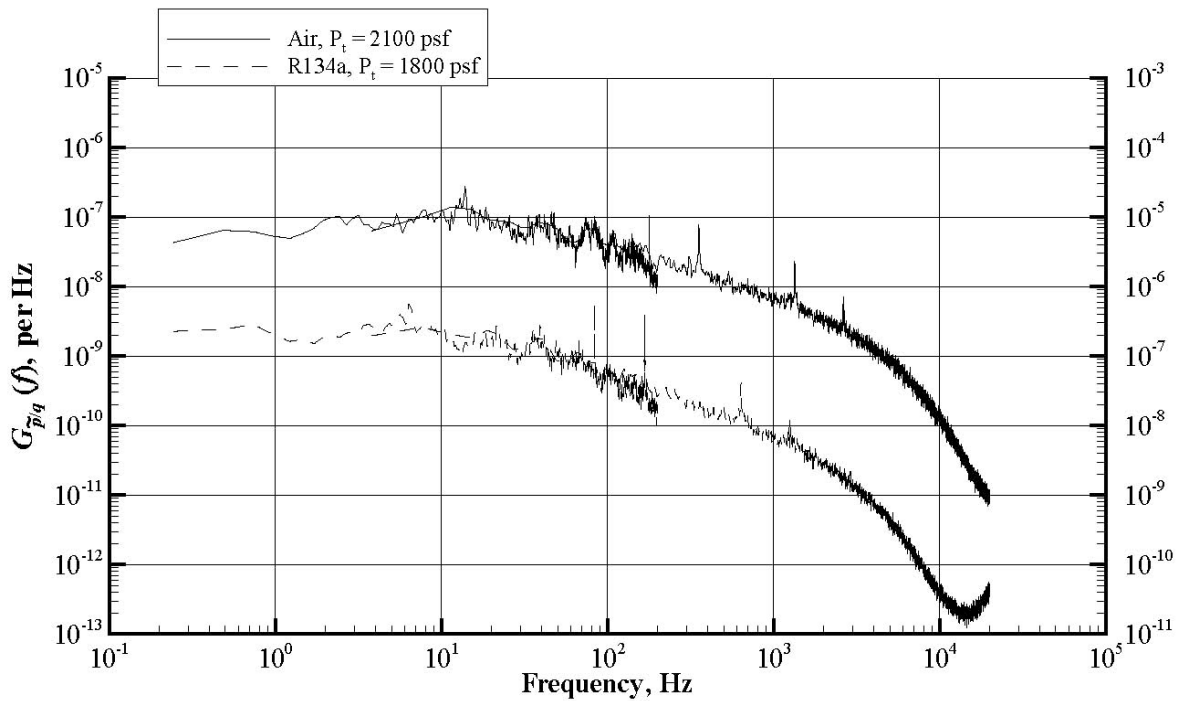


(e) Wall static pressure.

Figure 34. Concluded.

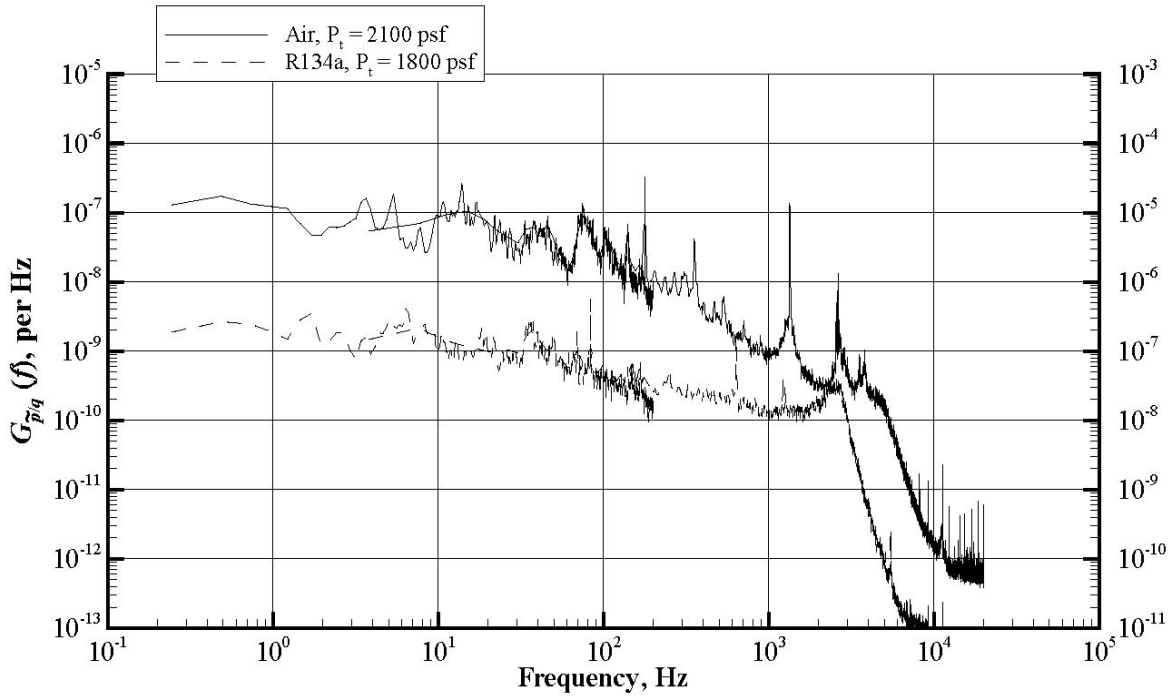


(a) Rake port total pressure.

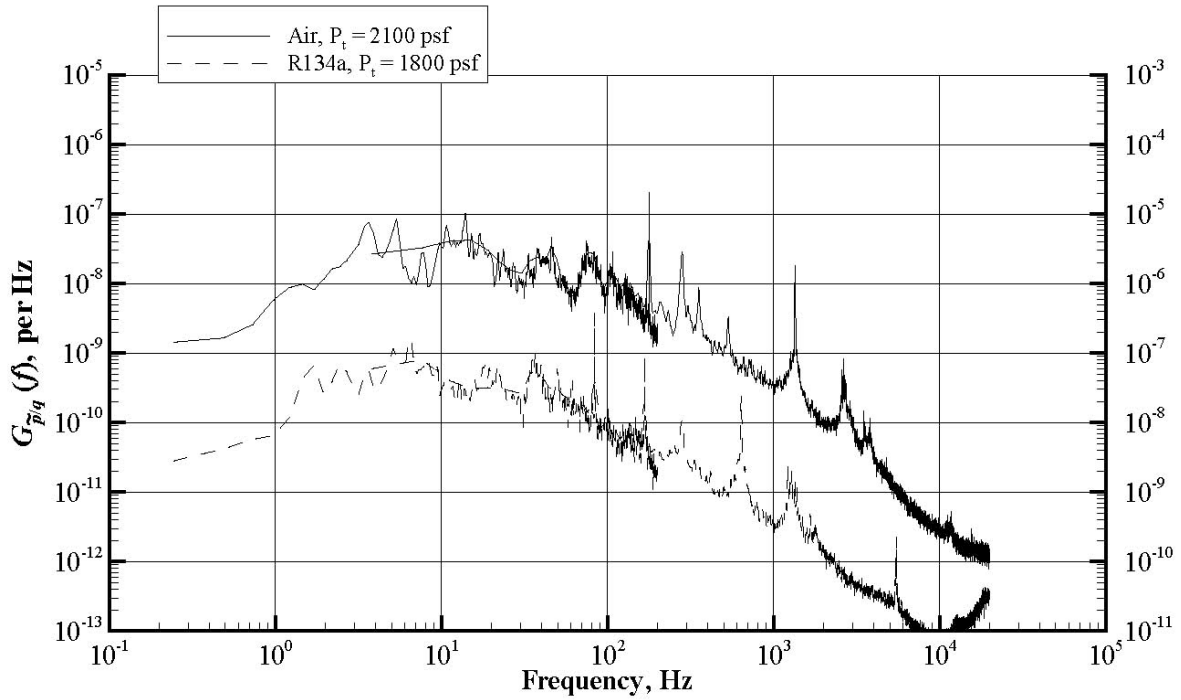


(b) Rake starboard total pressure.

Figure 35. Comparison of extended spectra in air ($P_t = 2100$ psf) and R134a ($P_t = 1800$ psf), $M = 0.4$.

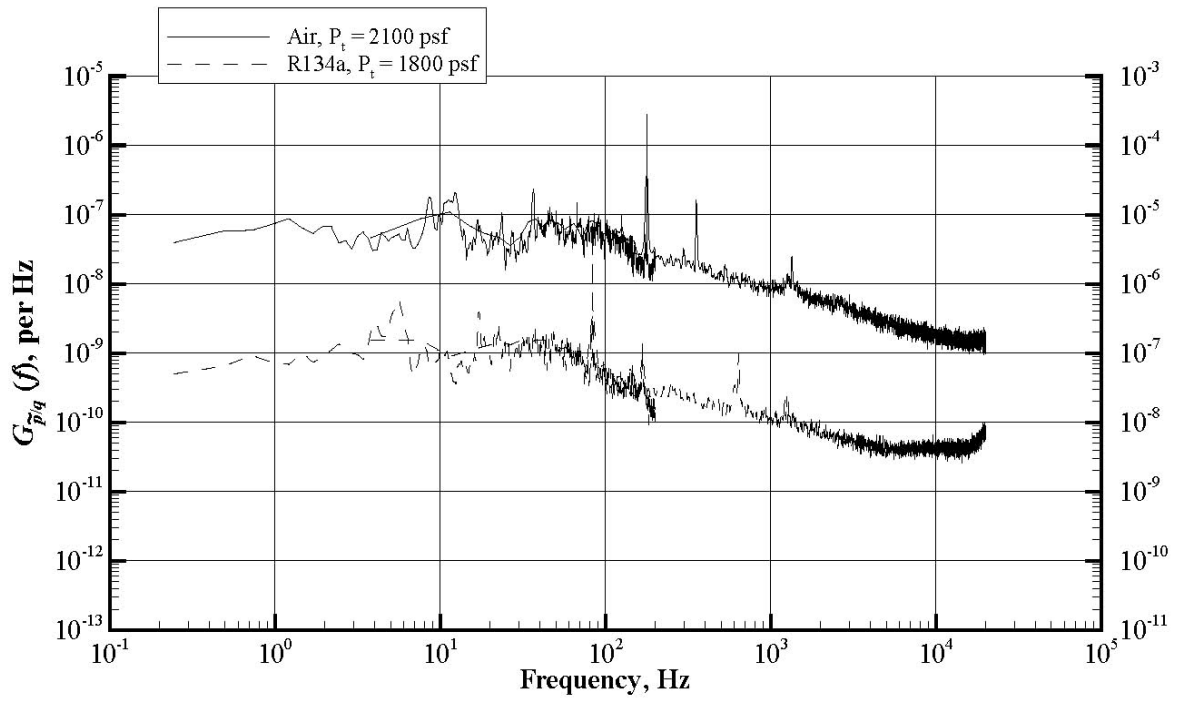


(c) Rake static pressure.



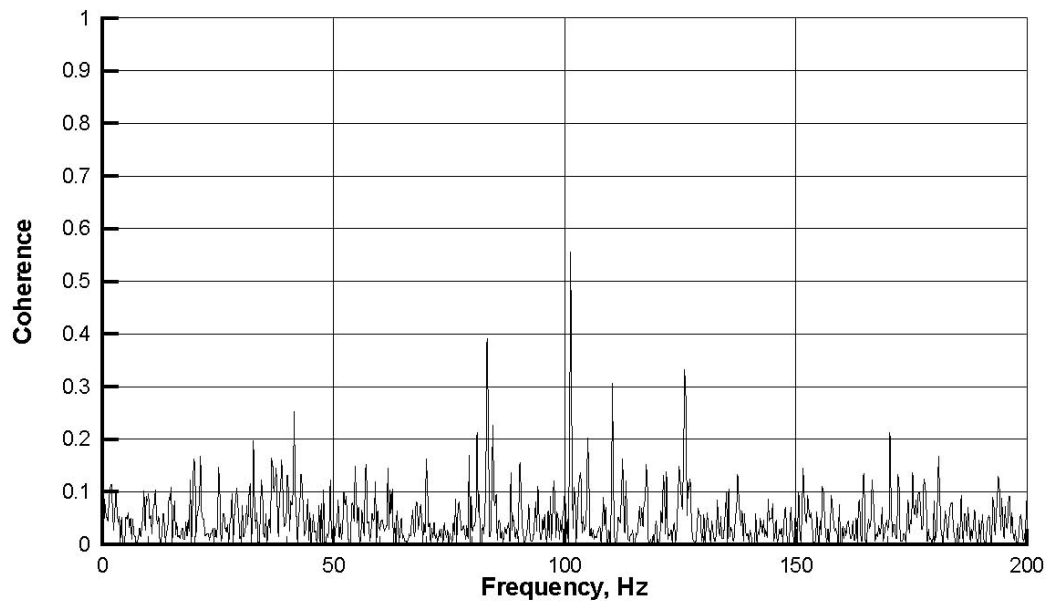
(d) Rake acoustic pressure.

Figure 35. Continued.

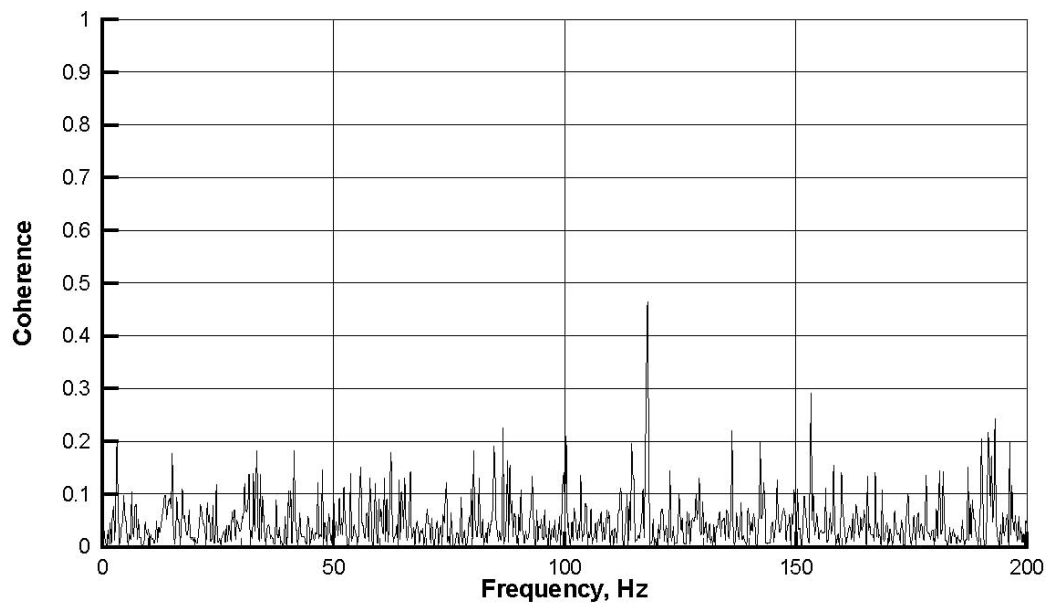


(e) Wall static pressure.

Figure 35. Concluded.

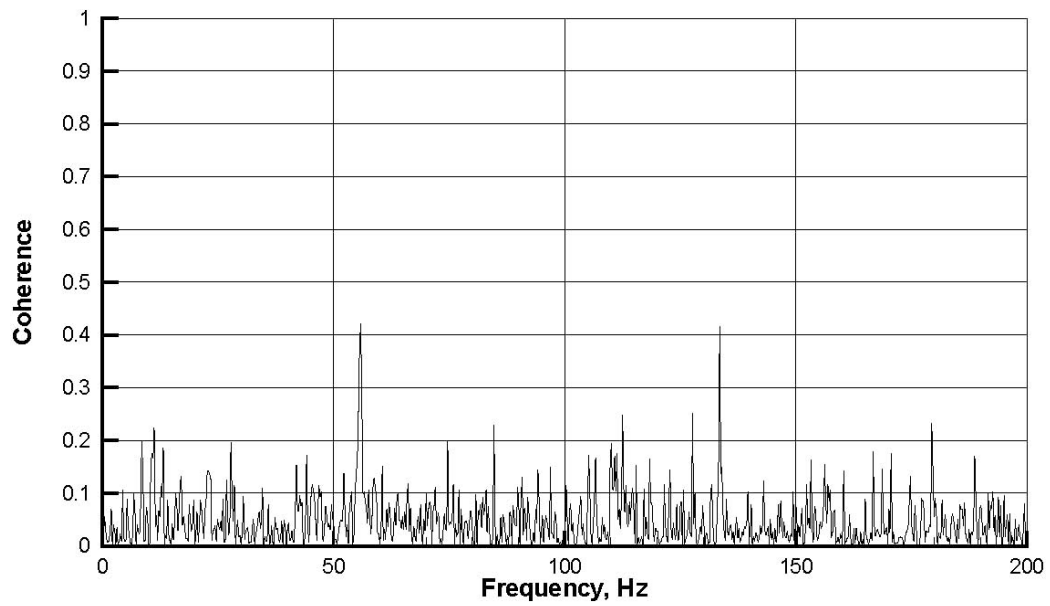


(a) Mach = 0.5.

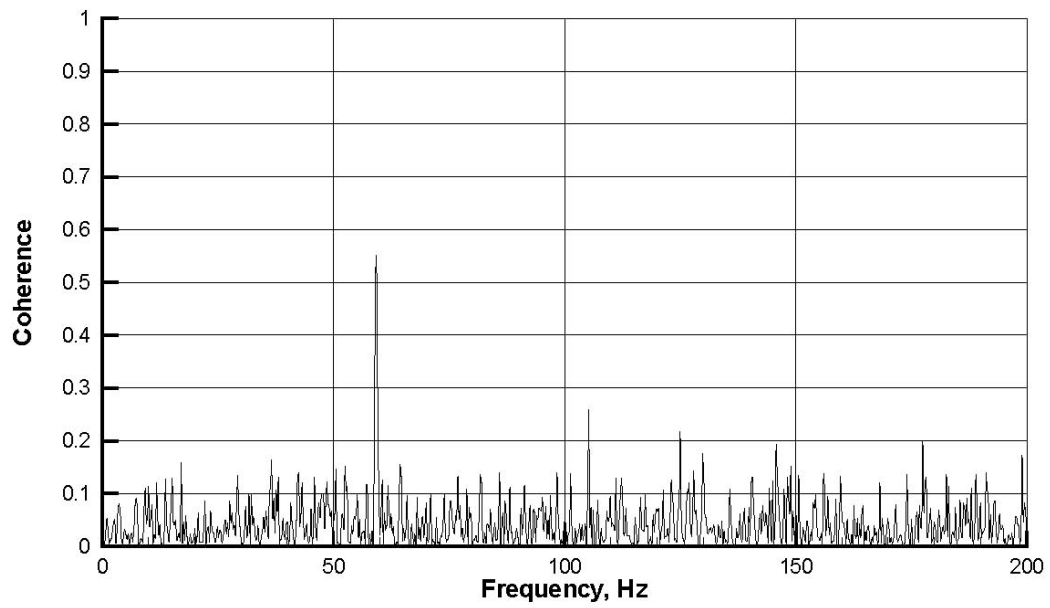


(b) Mach = 0.6.

Figure 36. Coherence between rake acoustic pressure and rake port vertical acceleration, set 8, open slots, R134a, $q = 225$ psf.

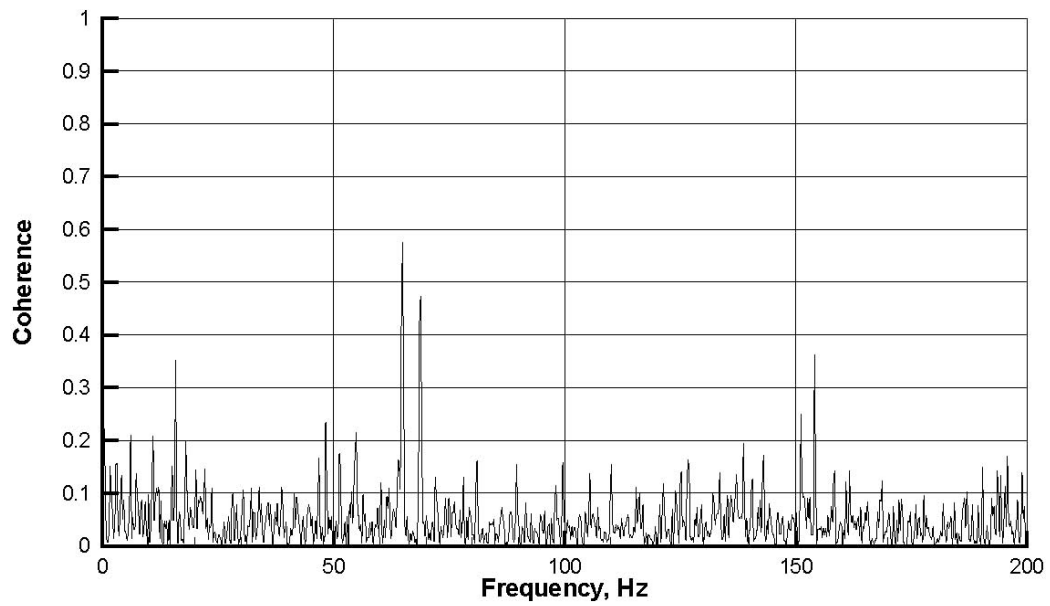


(c) Mach = 0.7.

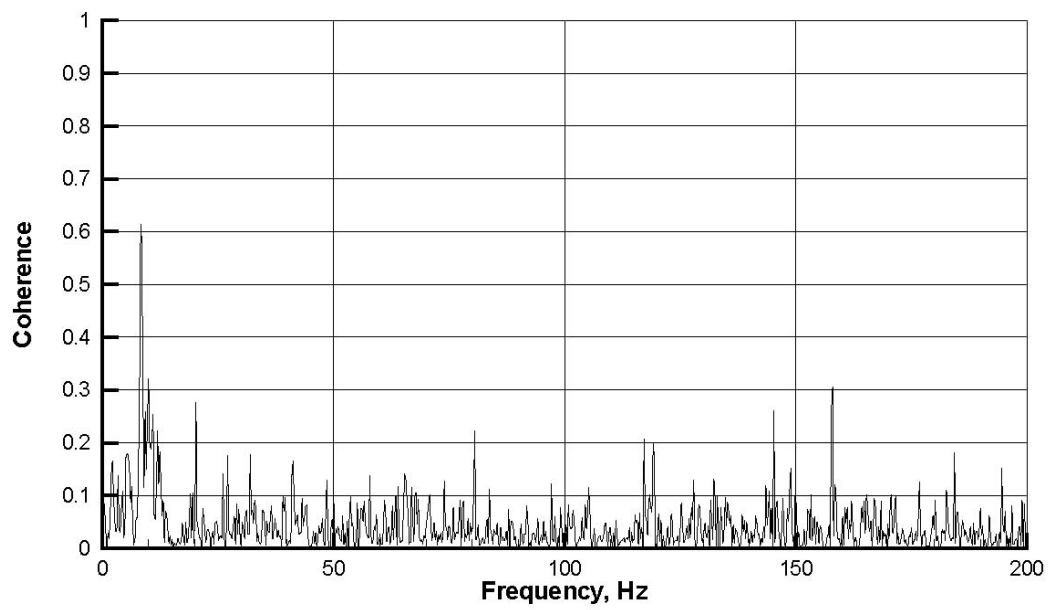


(d) Mach = 0.76.

Figure 36. Continued.

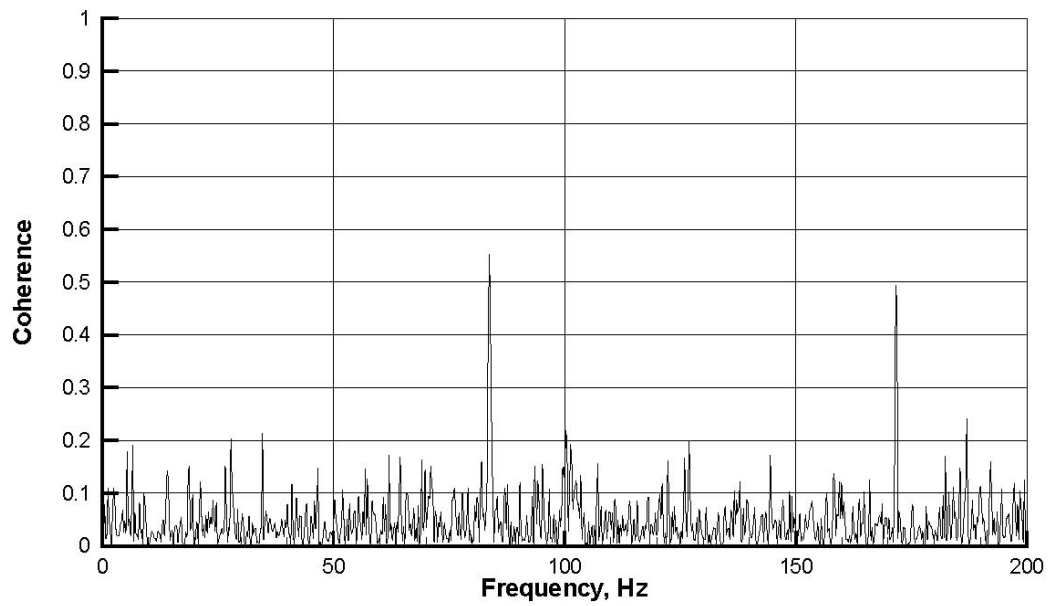


(e) Mach = 0.85.

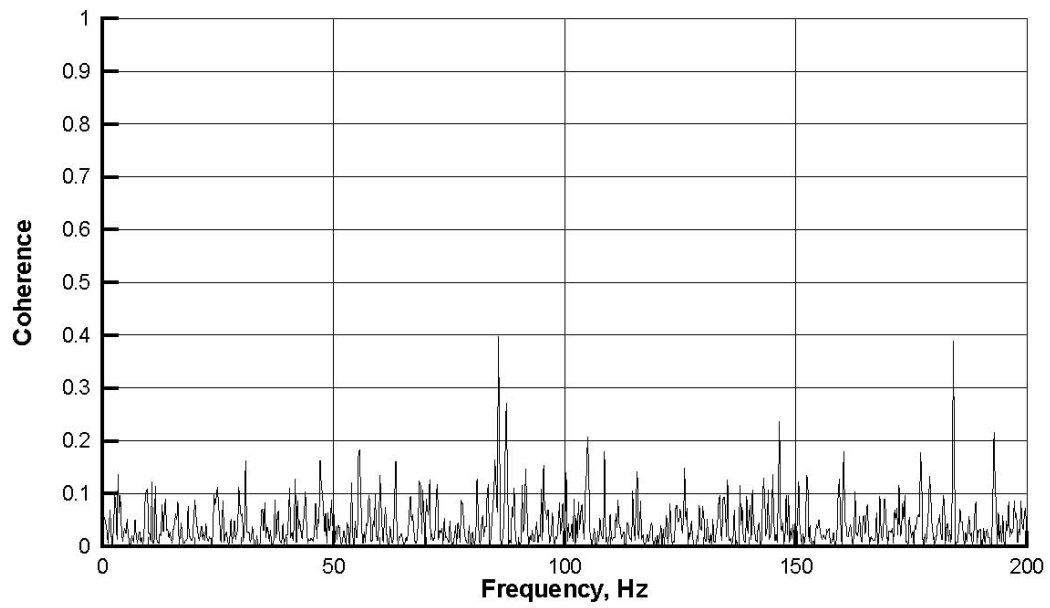


(f) Mach = 0.9.

Figure 36. Continued.

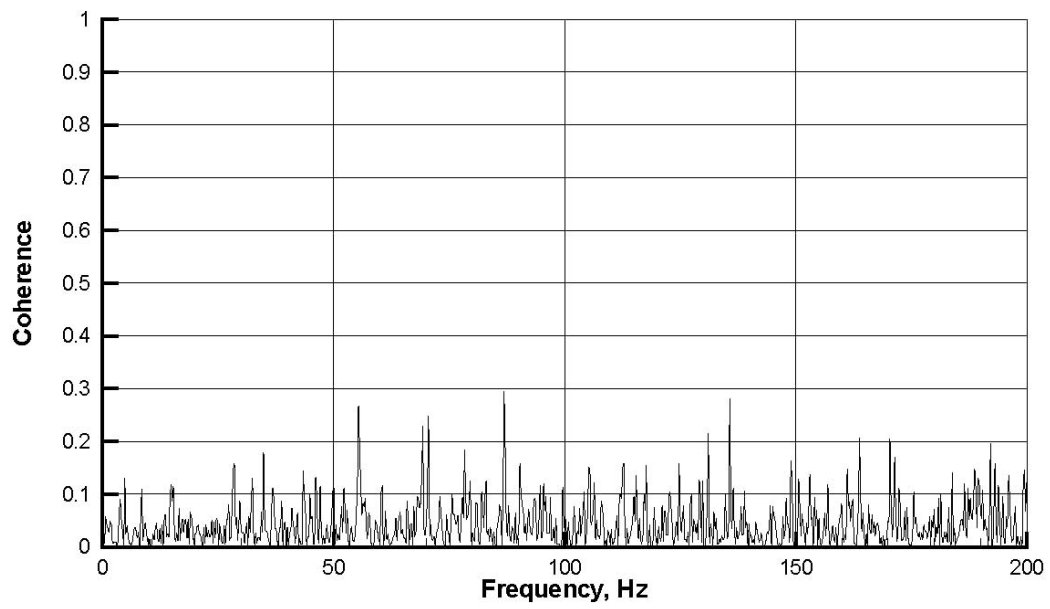


(g) Mach = 1.0.



(h) Mach = 1.1.

Figure 36. Continued.



(i) Mach = 1.2.

Figure 36. Concluded.

Appendix

Extended Spectra

This appendix includes extended spectra for all the sets described in table 2. Short descriptions of the sets are shown in table A1. Both the low-frequency (up to 200 Hz) and the high-frequency (up to 20 000 Hz) spectra are superimposed on the same plot. The high-frequency spectra have a frequency resolution of 3.81 Hz, were filtered to 50 000 Hz, and truncated to 20 000 Hz.

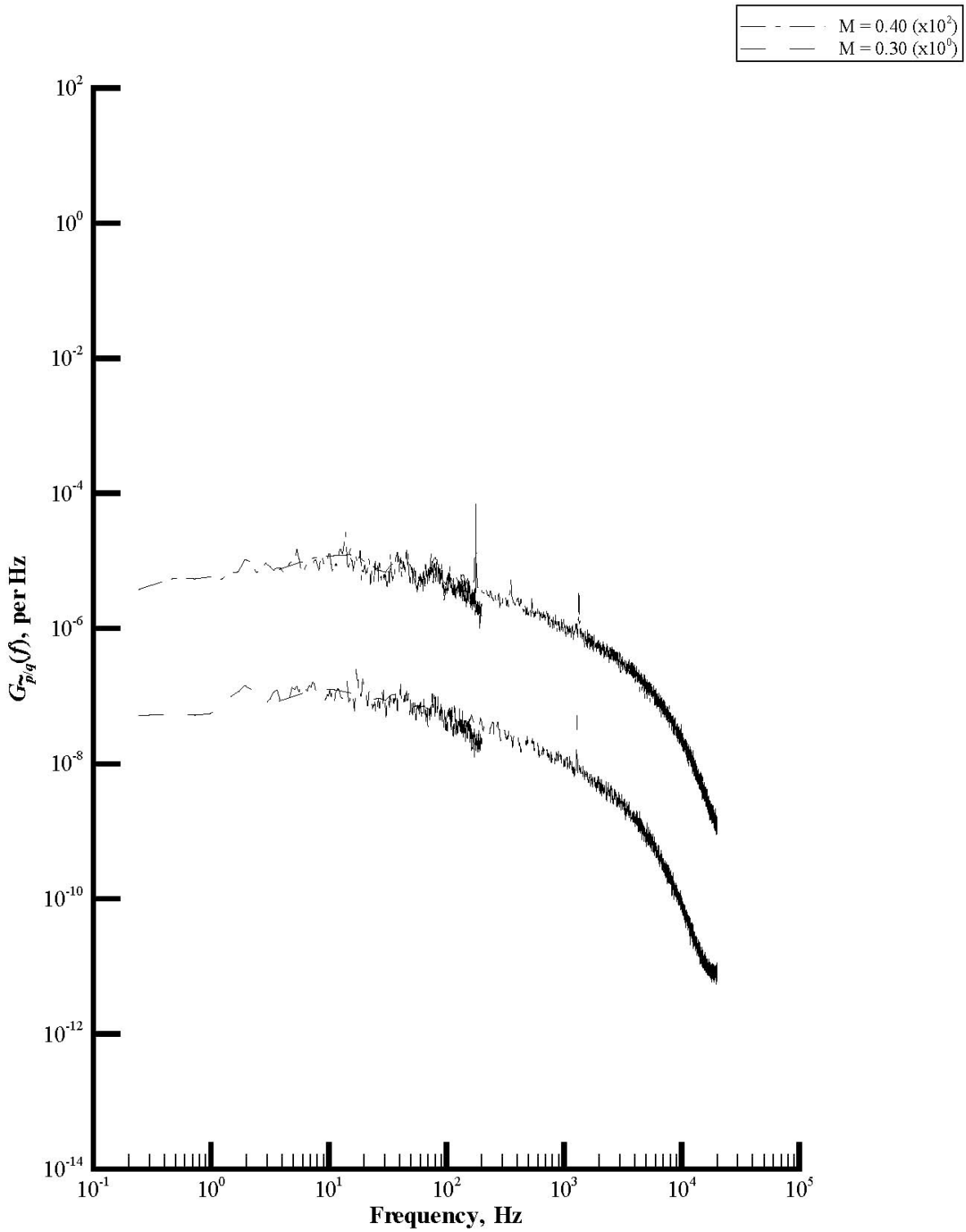
Figures A1 through A12 contain plots of power spectral densities (PSDs) for data acquired for each sensor and for each of the 76 unique test conditions identified in table 2. Each figure pertains to a different data set, beginning with data set 1 for figure A1 and ending with data set 12 for figure A12. Each figure has five parts, (a) through (e), with each pertaining to data acquired by a different fluctuating pressure transducer: rake port total pressure, rake starboard total pressure, rake static pressure, rake acoustic pressure, and wall static pressure at tunnel station 43. Within each part, PSD plots are presented by Mach number. Thus data set 1, with only two Mach numbers, contains two PSDs per part, while data set 7, with 12 Mach numbers, contains 12 PSDs per part.

In order to present many PSDs on a single plot without the confusion of overlapping PSDs, a multiplication-factor scheme has been employed. Each PSD has been multiplied by a different even power of 10 so that there is sufficient separation of the PSDs in the figure to avoid overlap. In the key for each figure, the numbers in parentheses following the Mach number indicate the multiplication factor which must be removed from that particular PSD in order to determine its correct magnitude at any given frequency.

The blade passing frequency (BPF) and its harmonics (multiples of the BPF) can be seen on all sensors to a greater or lesser degree. There are a few test points for which high-frequency data were not obtained and these PSDs are therefore missing on the plots. Within the region of frequency overlap (from high-frequency end of low-frequency spectra to the low-frequency end of extended spectra), the values of the two spectra are in good agreement as they should be with a few exceptions. At the highest frequencies, there appears to be aliasing, but the authors are convinced that anti-aliasing filters were implemented properly.

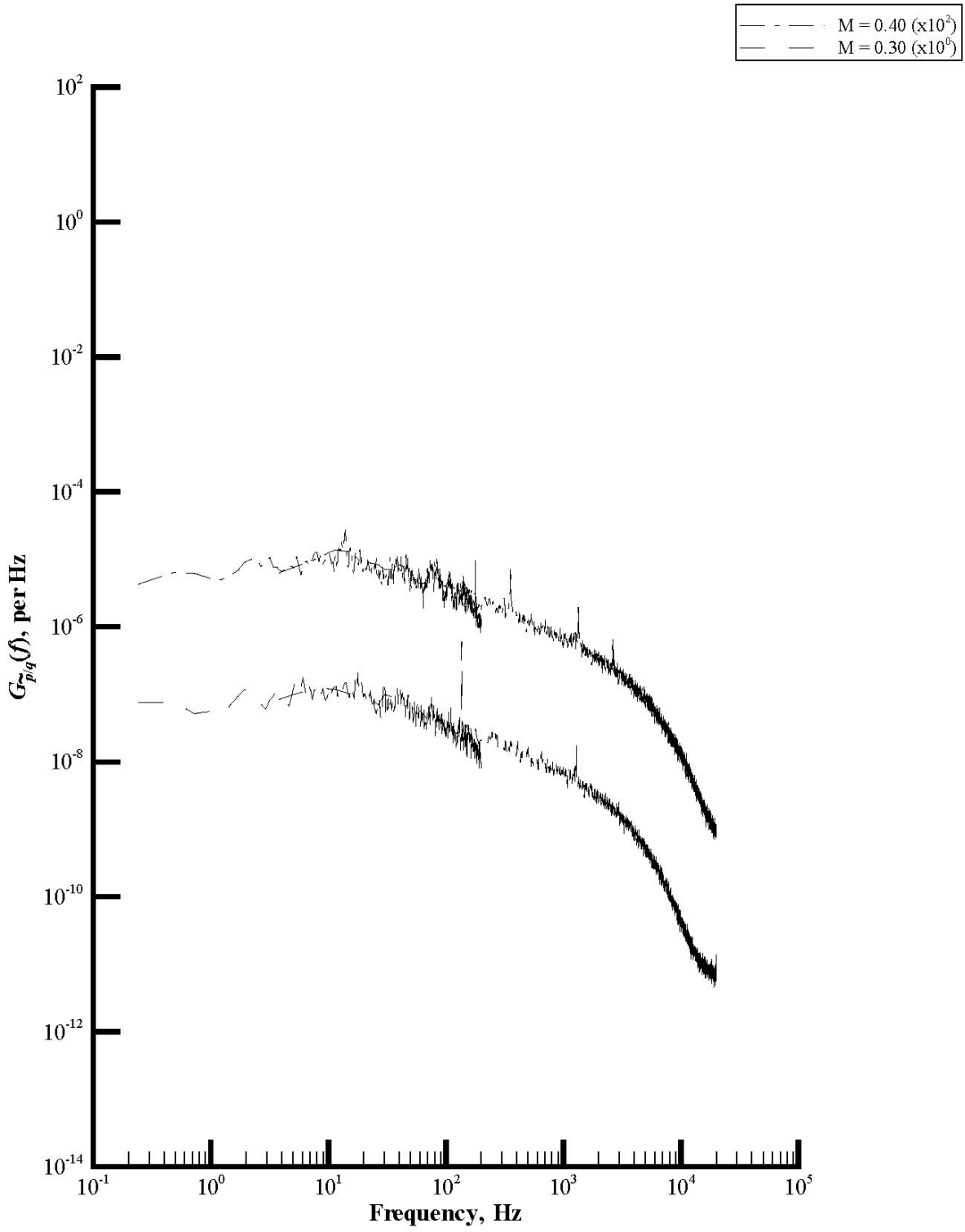
Table A1. Brief Description of Sets

Set	Description
1	Air, open slots, $P_t = 2100$ psf
2	Air, open slots, $P_t = 400$ psf
3	Air, open slots, $P_t = 100$ psf
4	R134a, open slots, $P_t = 1800$ psf
5	R134a, open slots, $P_t = 500$ psf
6	R134a, open slots, $P_t = 500$ psf, repeat
7	R134a, open slots, $P_t = 200$ psf
8	R134a, open slots, $q = 225$ psf
9	R134a, wall slots closed, $P_t = 500$ psf
10	R134a, wall slots closed, $P_t = 200$ psf
11	R134a, all slots closed, $P_t = 500$ psf
12	R134a, all slots closed, $P_t = 200$ psf



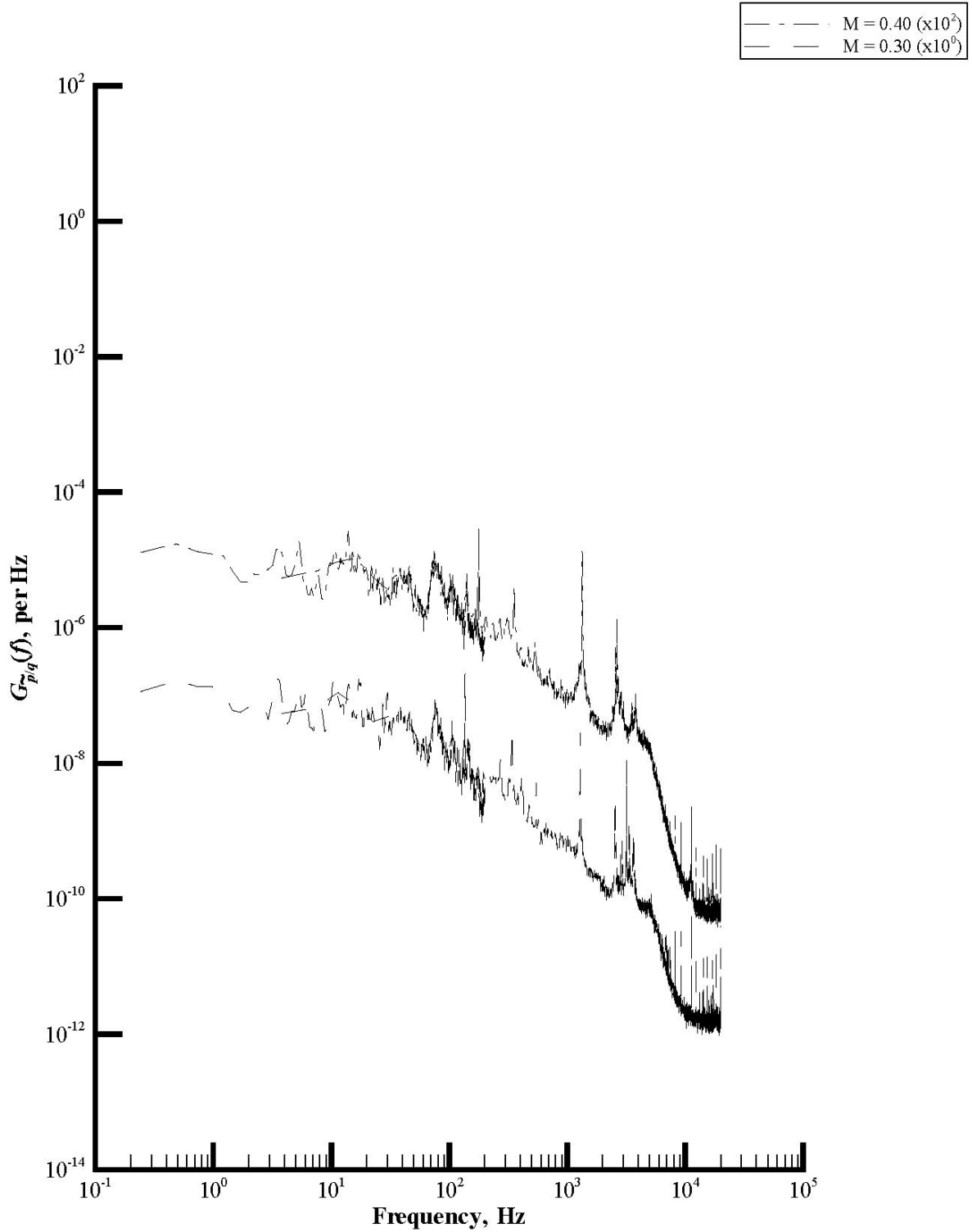
(a) Rake port total pressure.

Figure A1. Extended spectra plots of power spectral density functions of set 1.



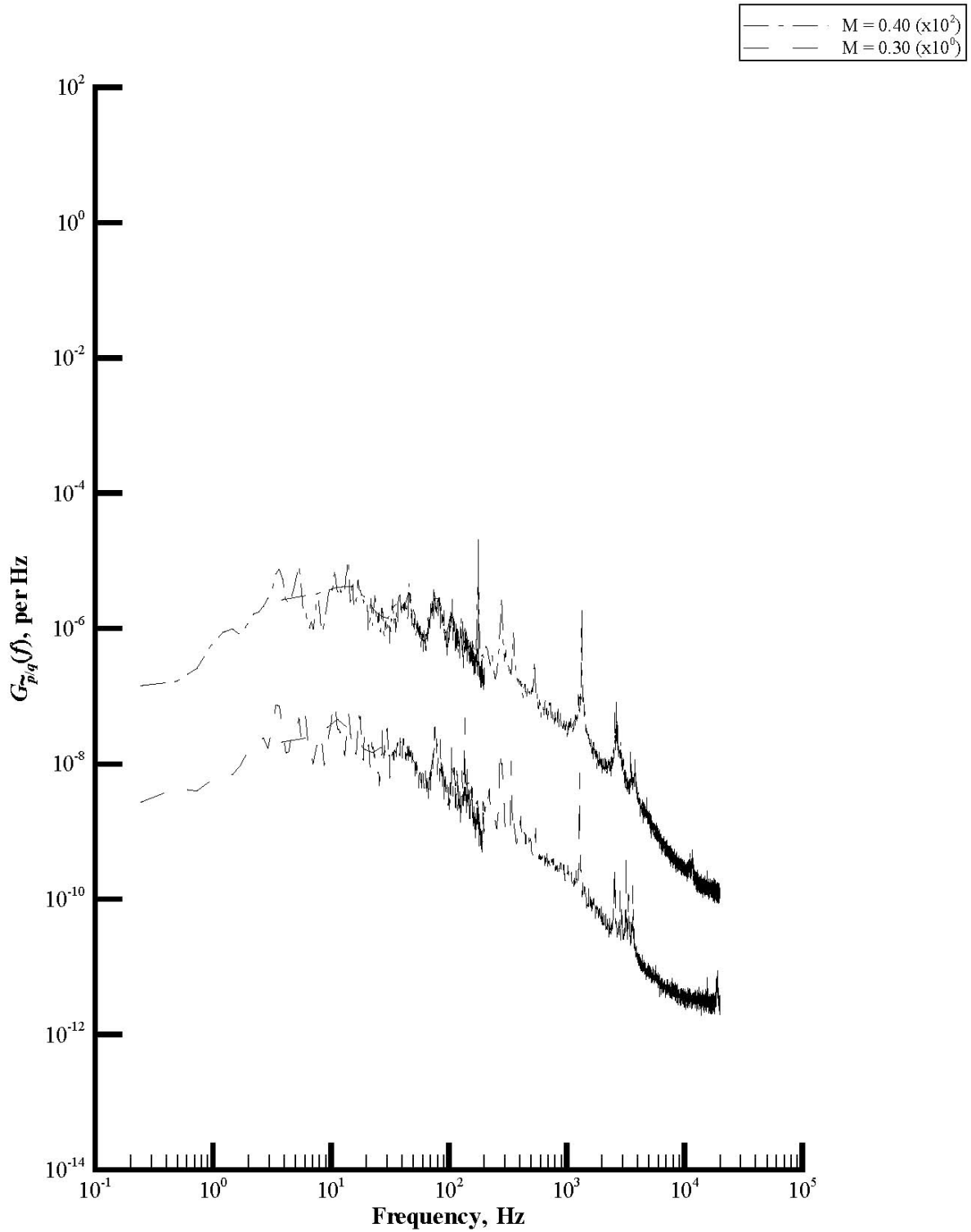
(b) Rake starboard total pressure.

Figure A1. Continued.



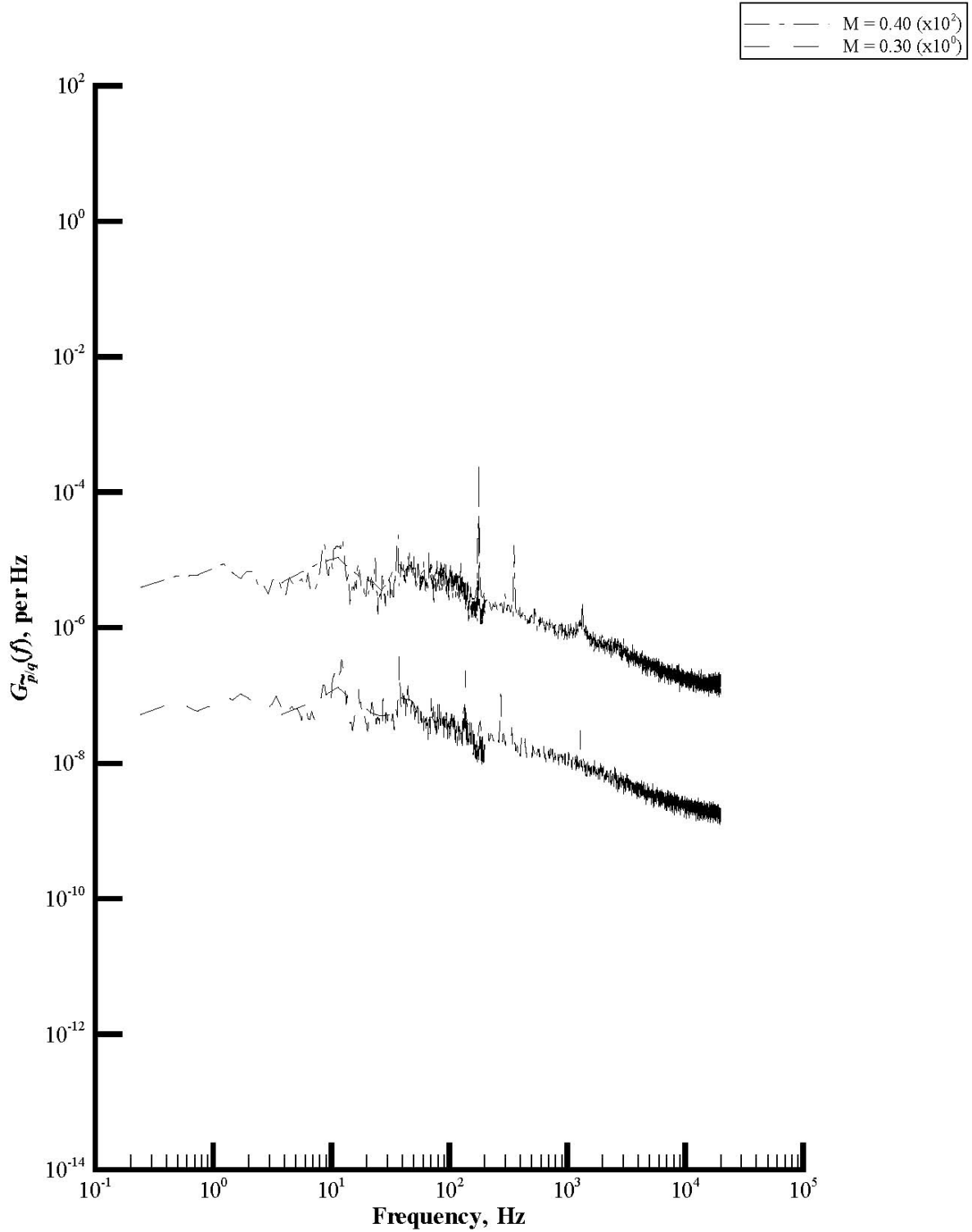
(c) Rake static pressure.

Figure A1. Continued.



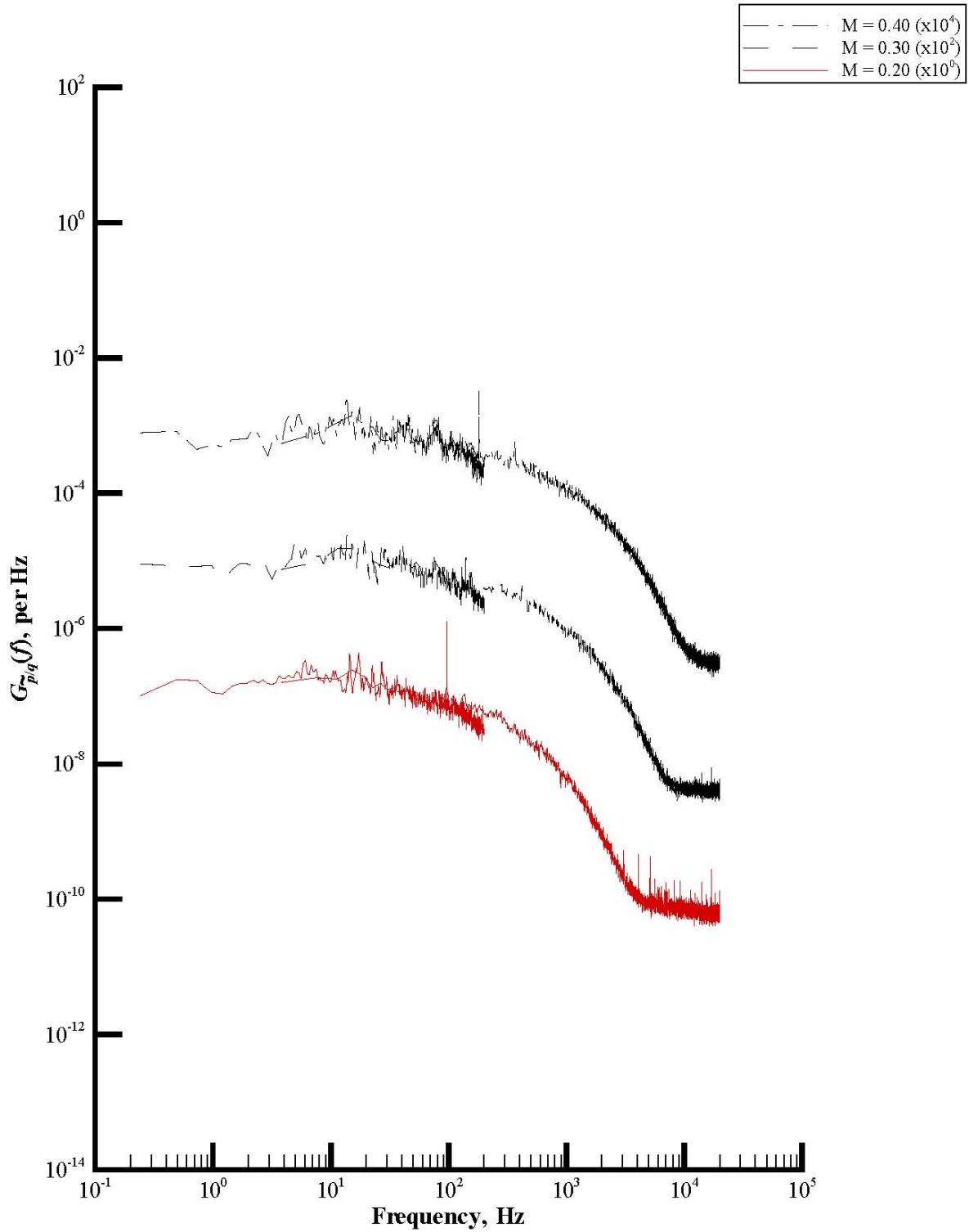
(d) Rake acoustic pressure.

Figure A1. Continued.



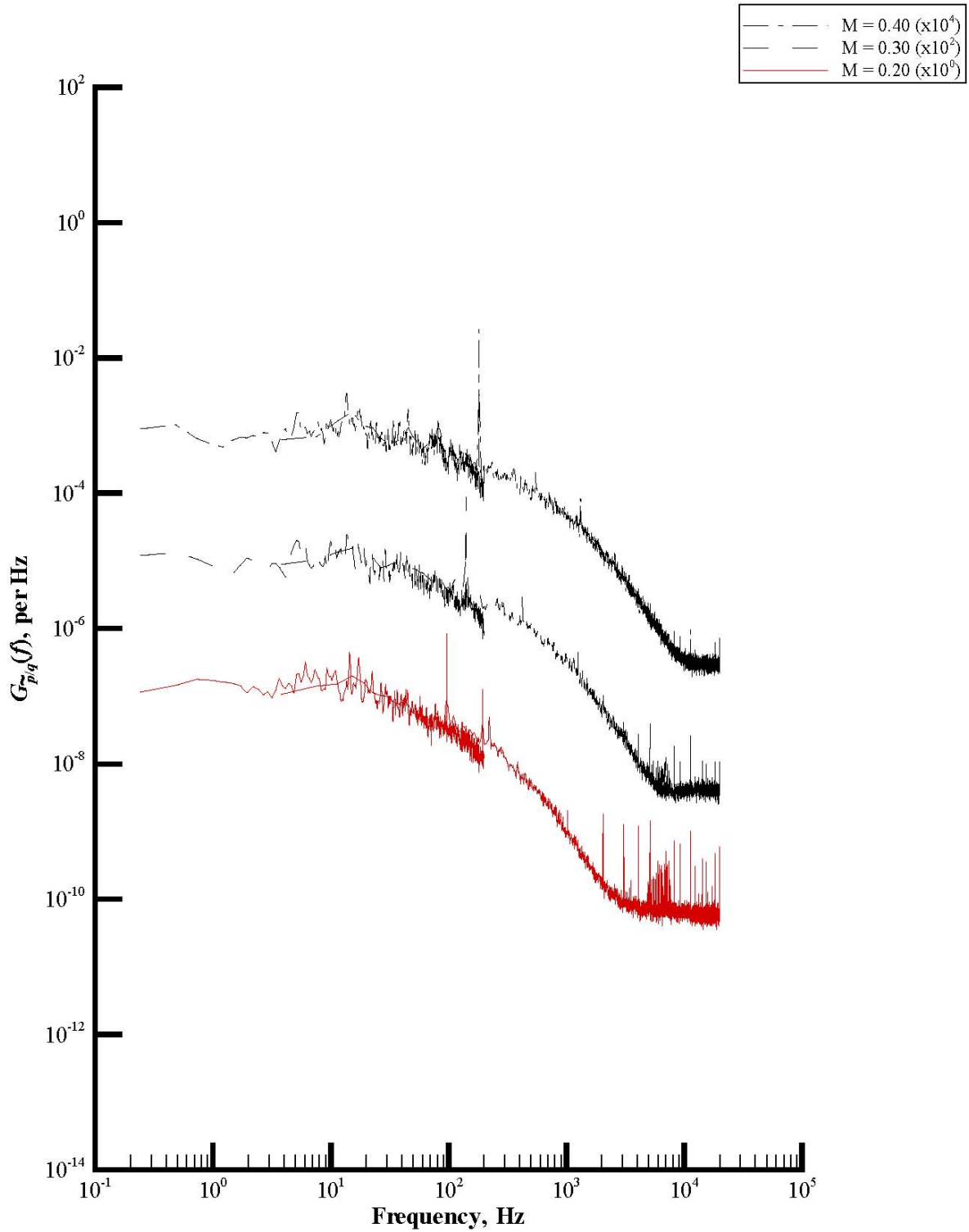
(e) Wall static pressure.

Figure A1. Concluded.



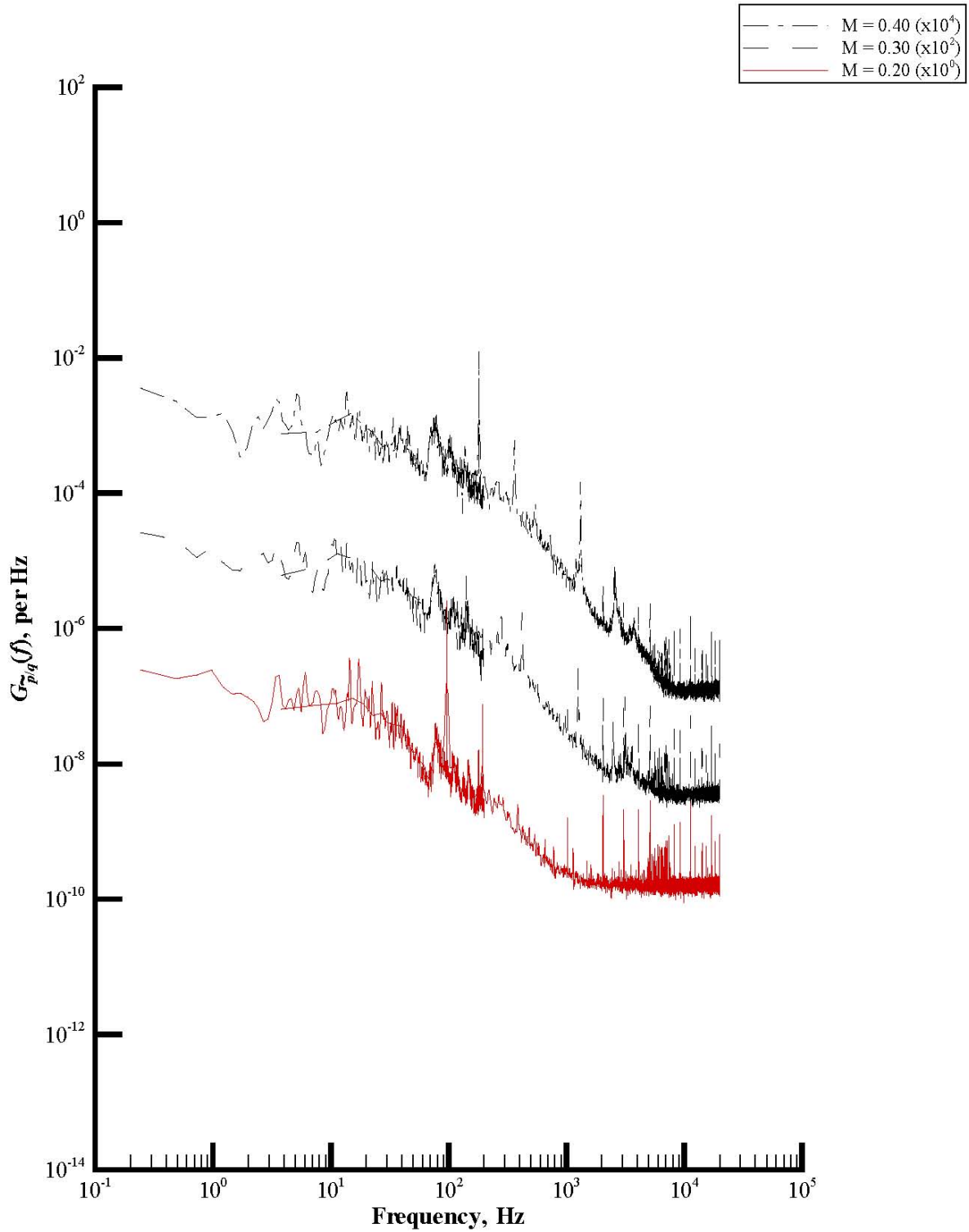
(a) Rake port total pressure.

Figure A2. Extended spectra plots of power spectral density functions of set 2.



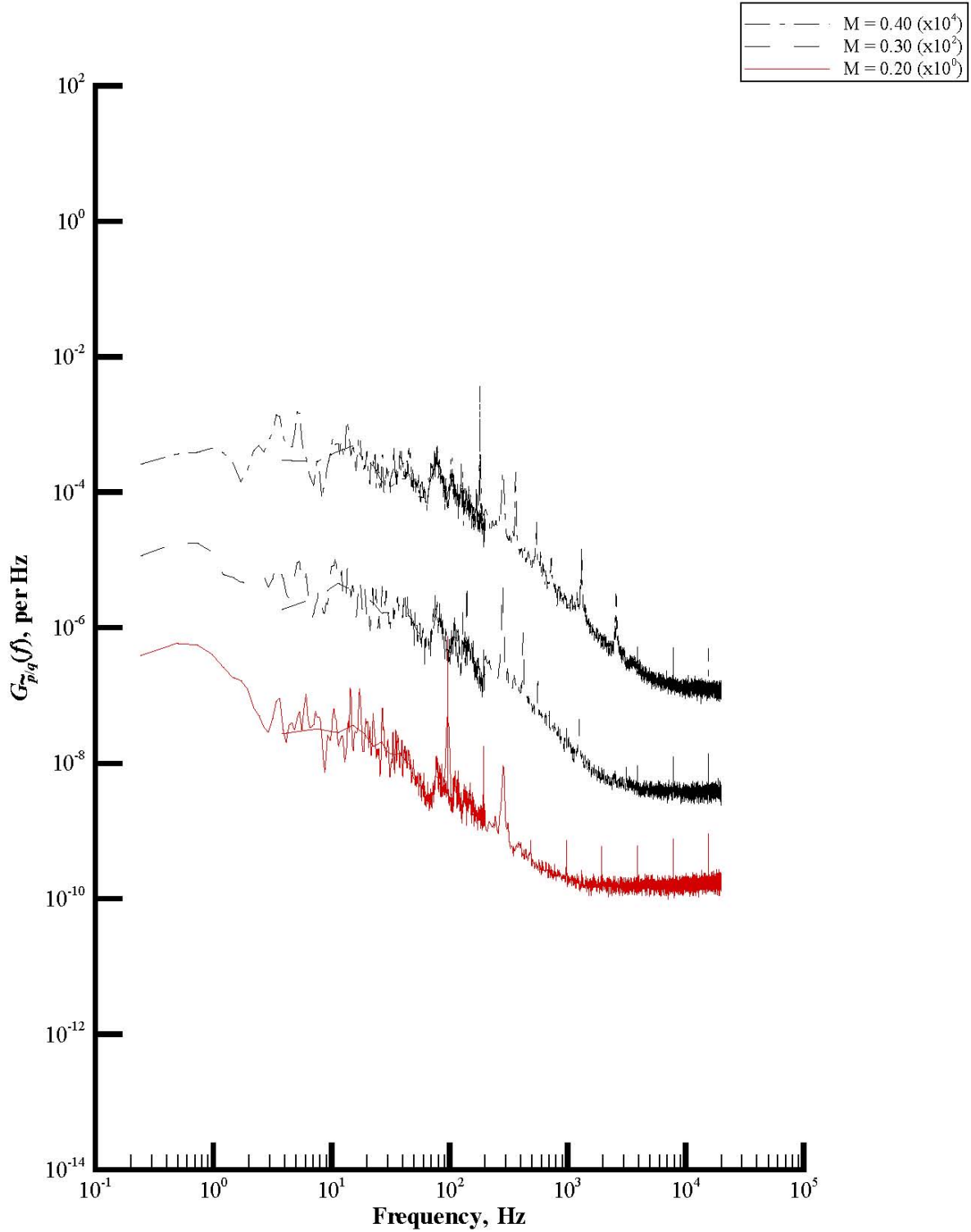
(b) Rake starboard total pressure.

Figure A2. Continued.



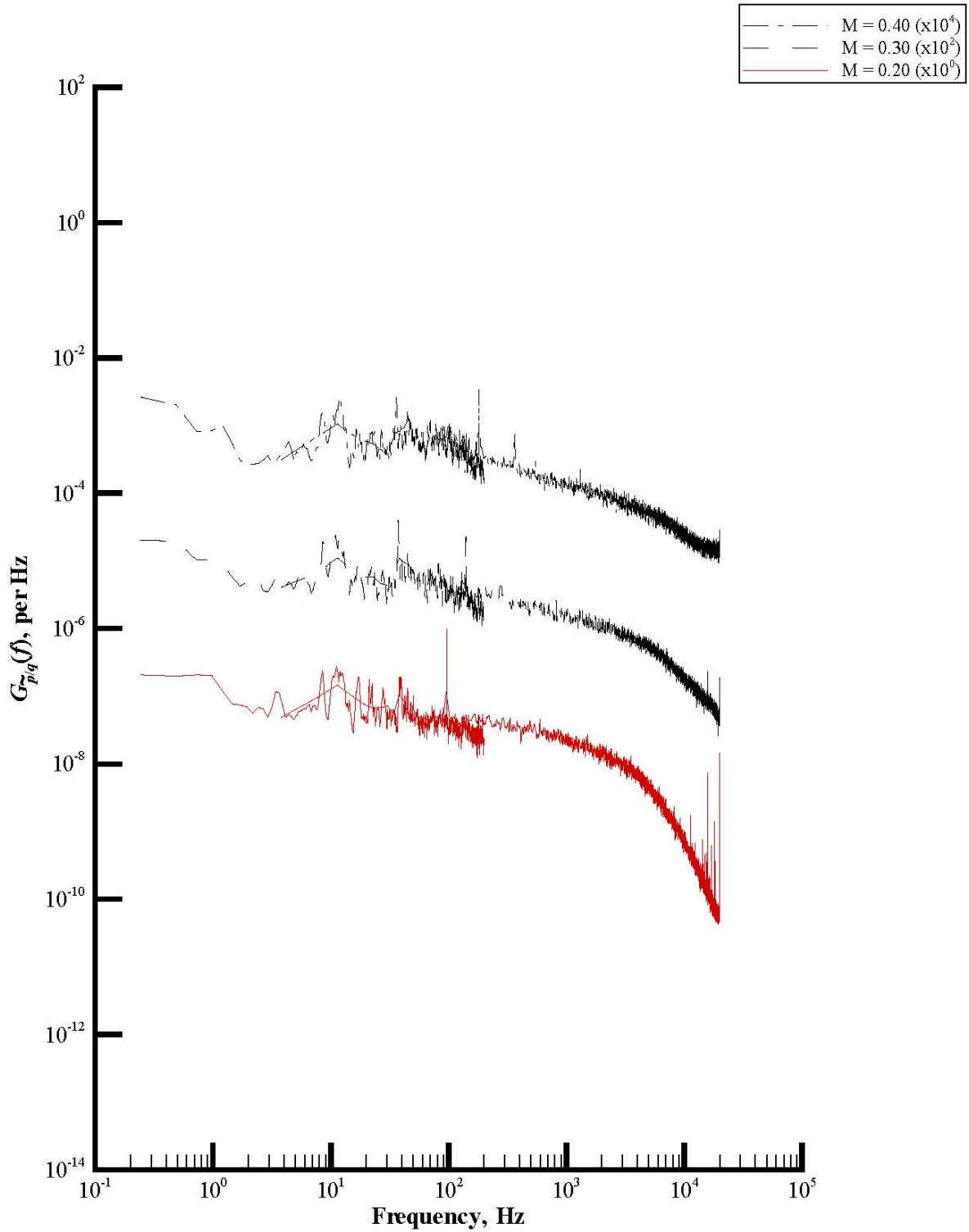
(c) Rake static pressure.

Figure A2. Continued.



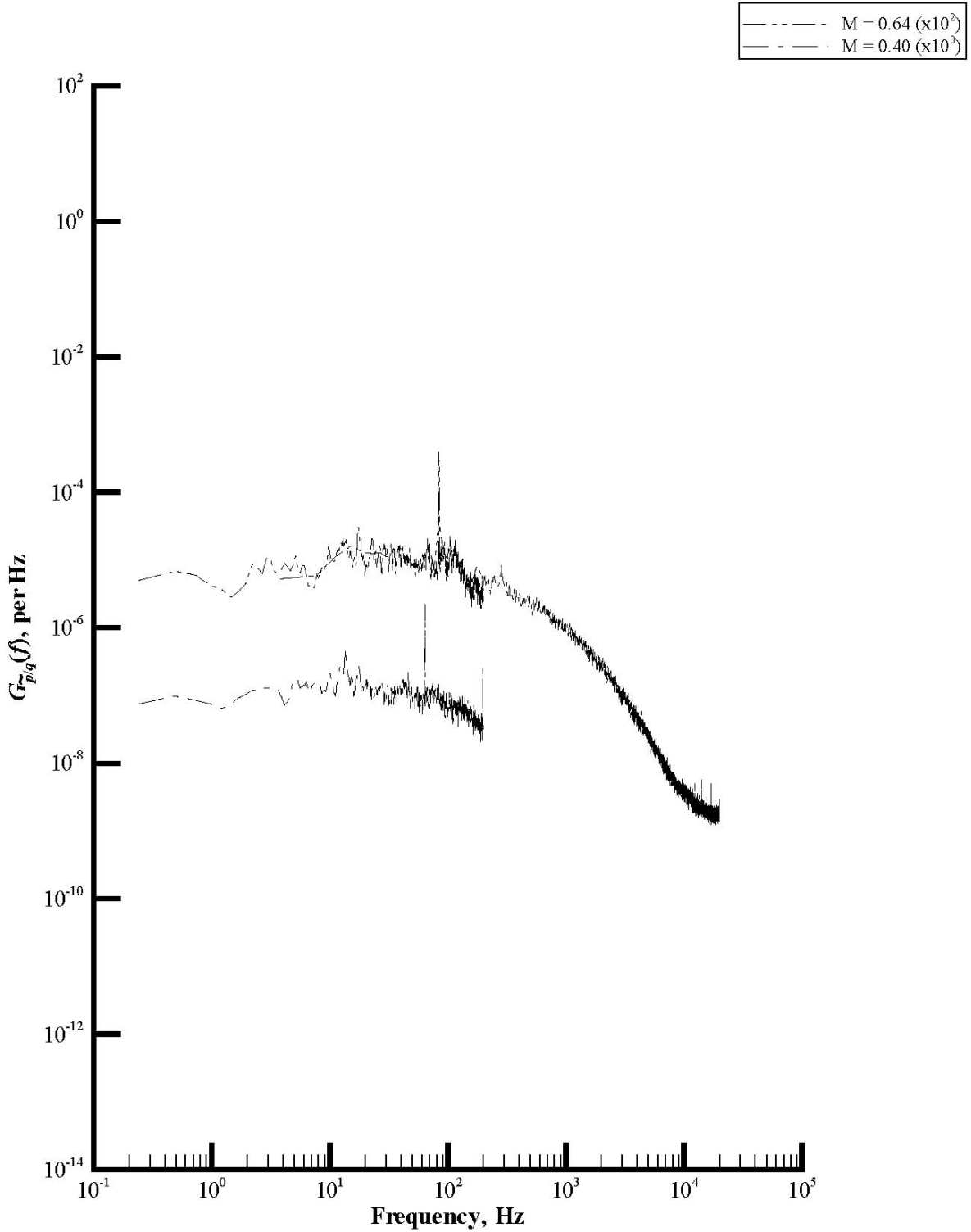
(d) Rake acoustic pressure.

Figure A2. Continued.



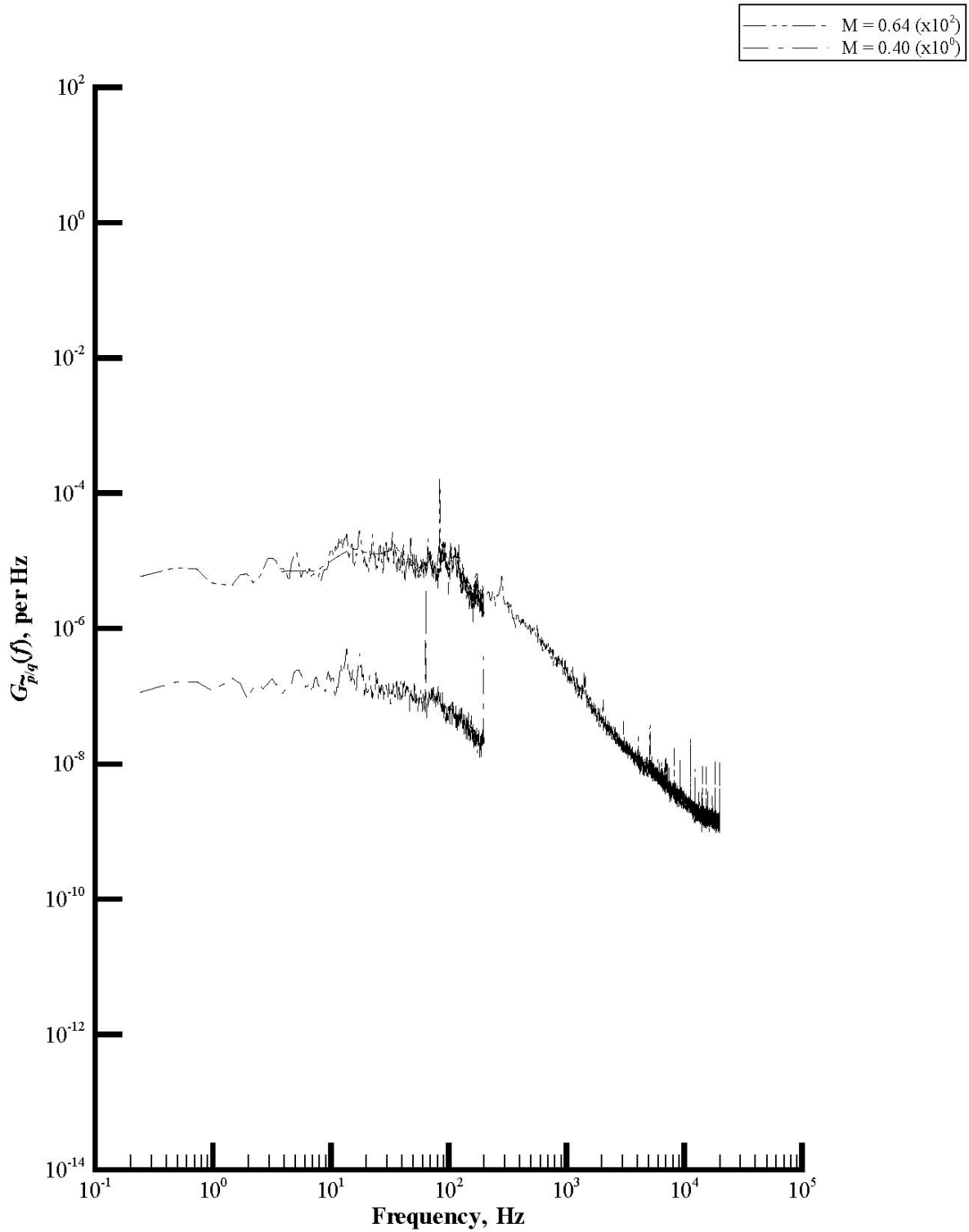
(e) Wall static pressure.

Figure A2. Concluded.



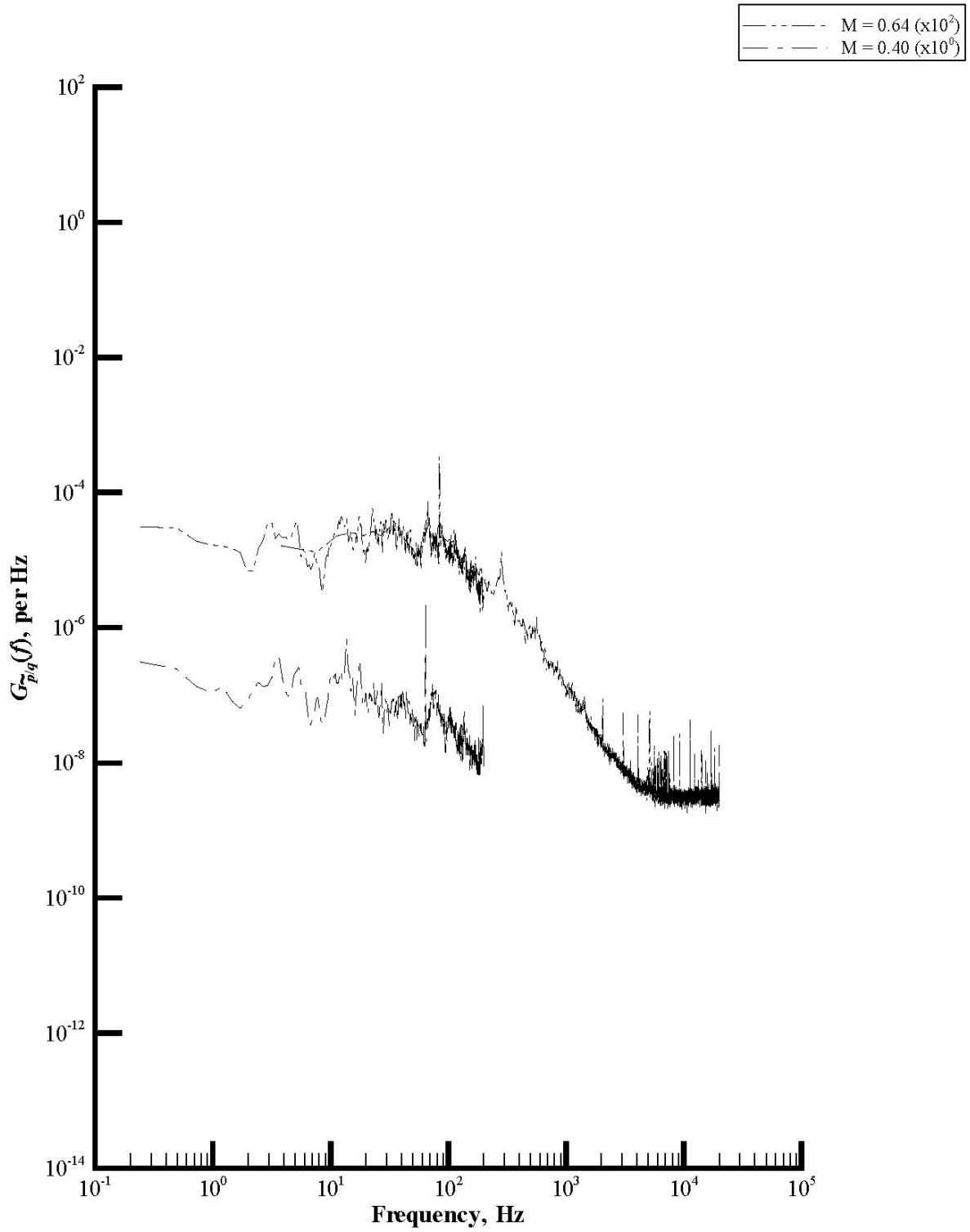
(a) Rake port total pressure.

Figure A3. Extended spectra plots of power spectral density functions of set 3.



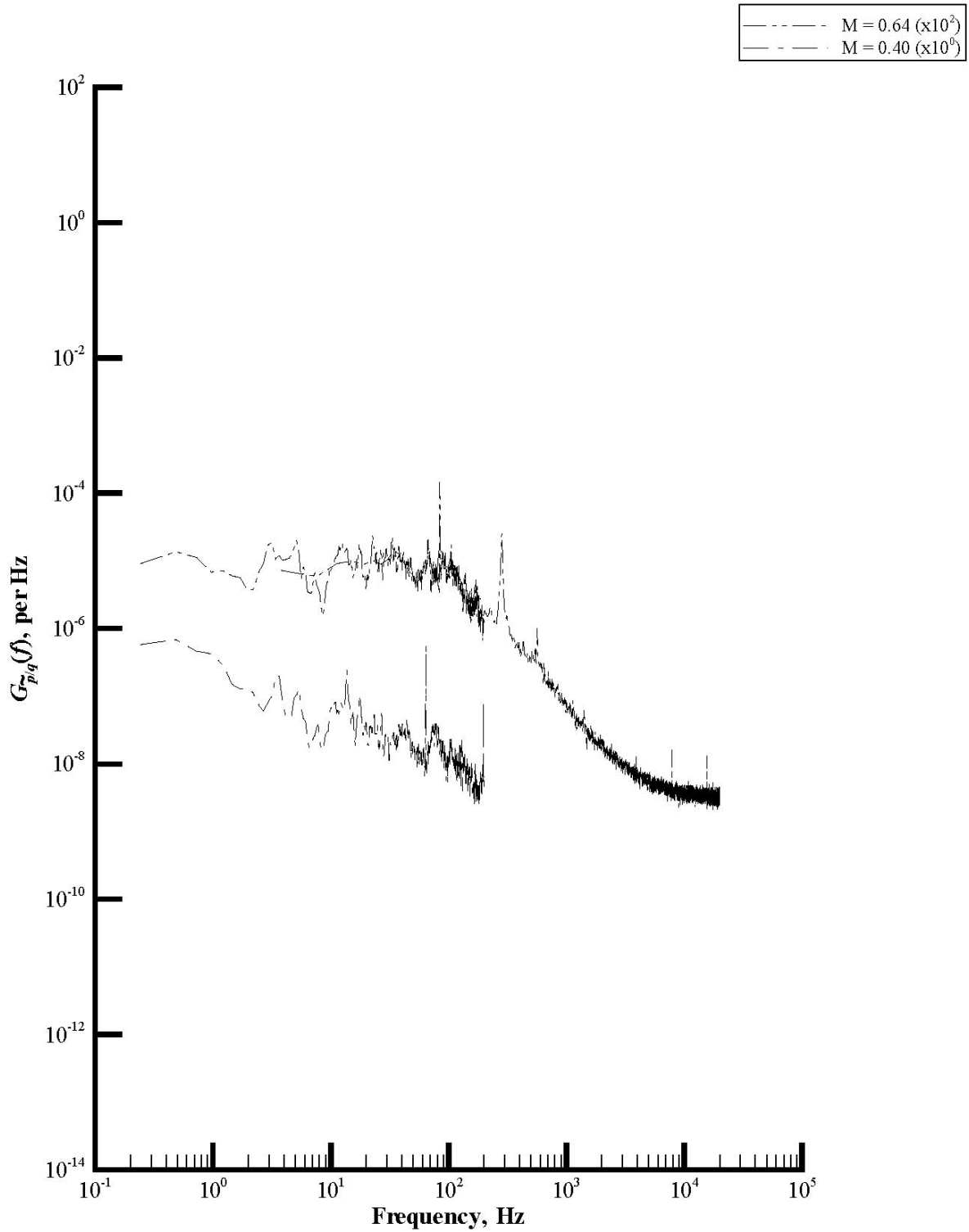
(b) Rake starboard total pressure.

Figure A3. Continued.



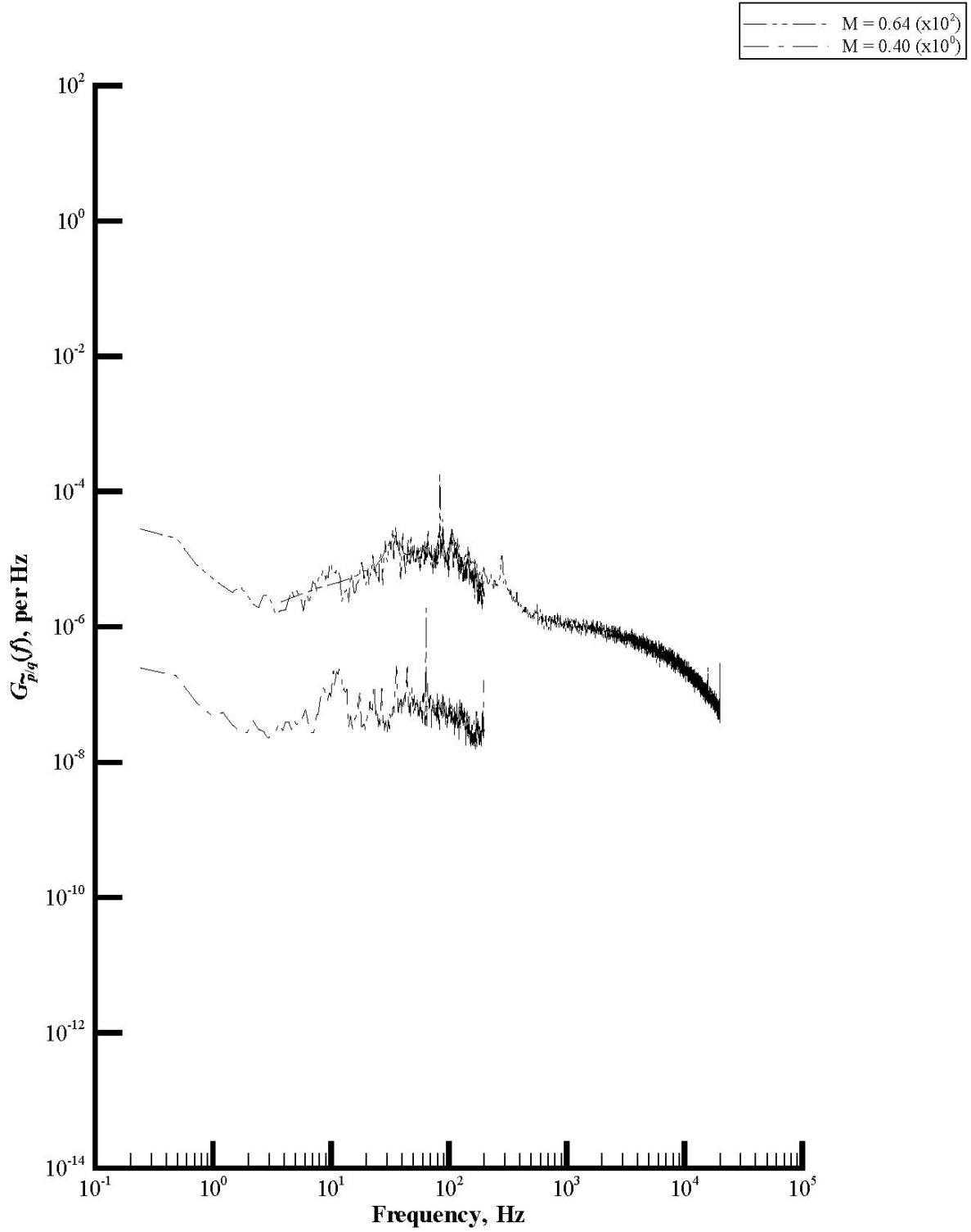
(c) Rake static pressure.

Figure A3. Continued.



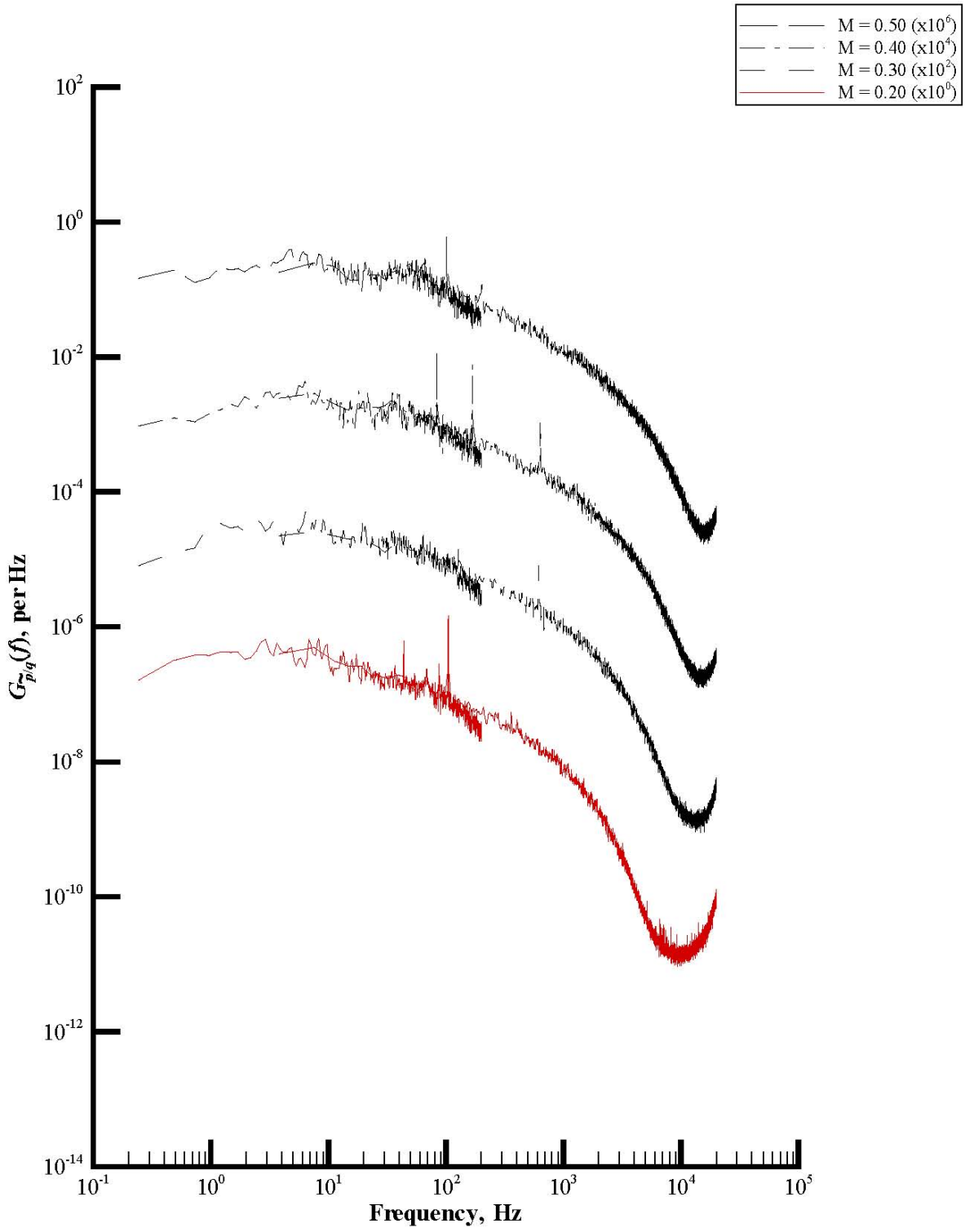
(d) Rake static pressure.

Figure A3. Continued.



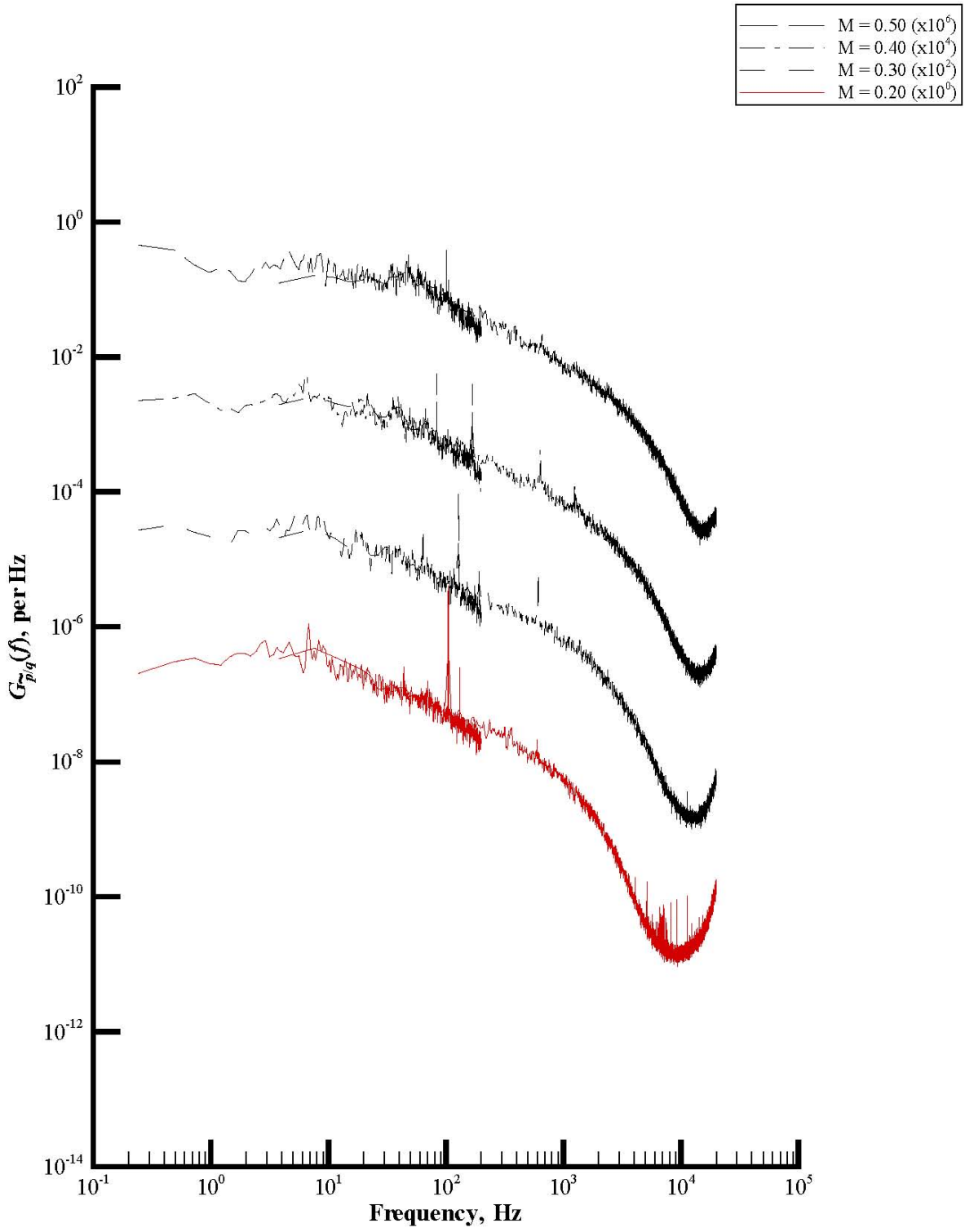
(e) Wall static pressure.

Figure A3. Concluded.



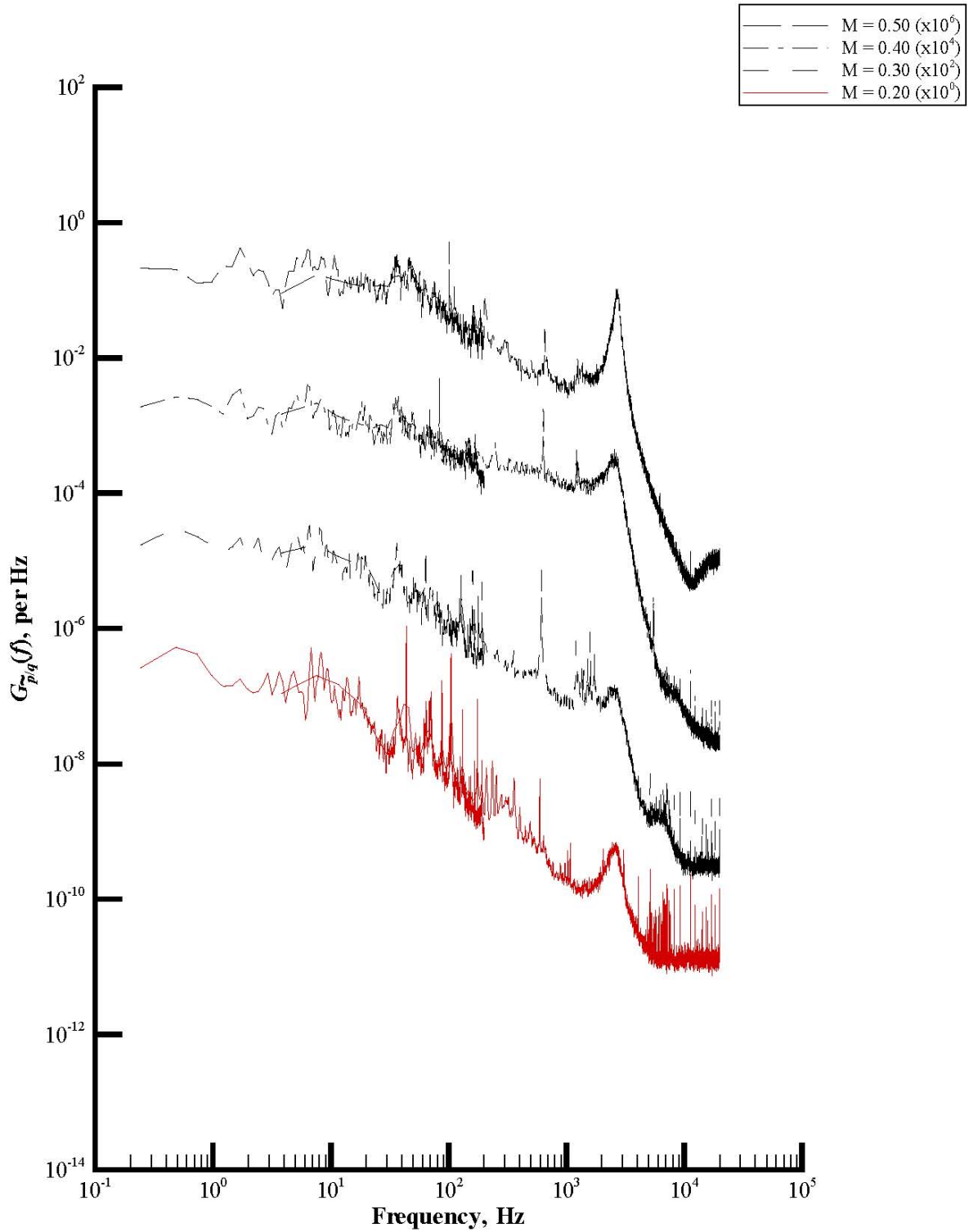
(a) Rake port total pressure.

Figure A4. Extended spectra plots of power spectral density functions of set 4.



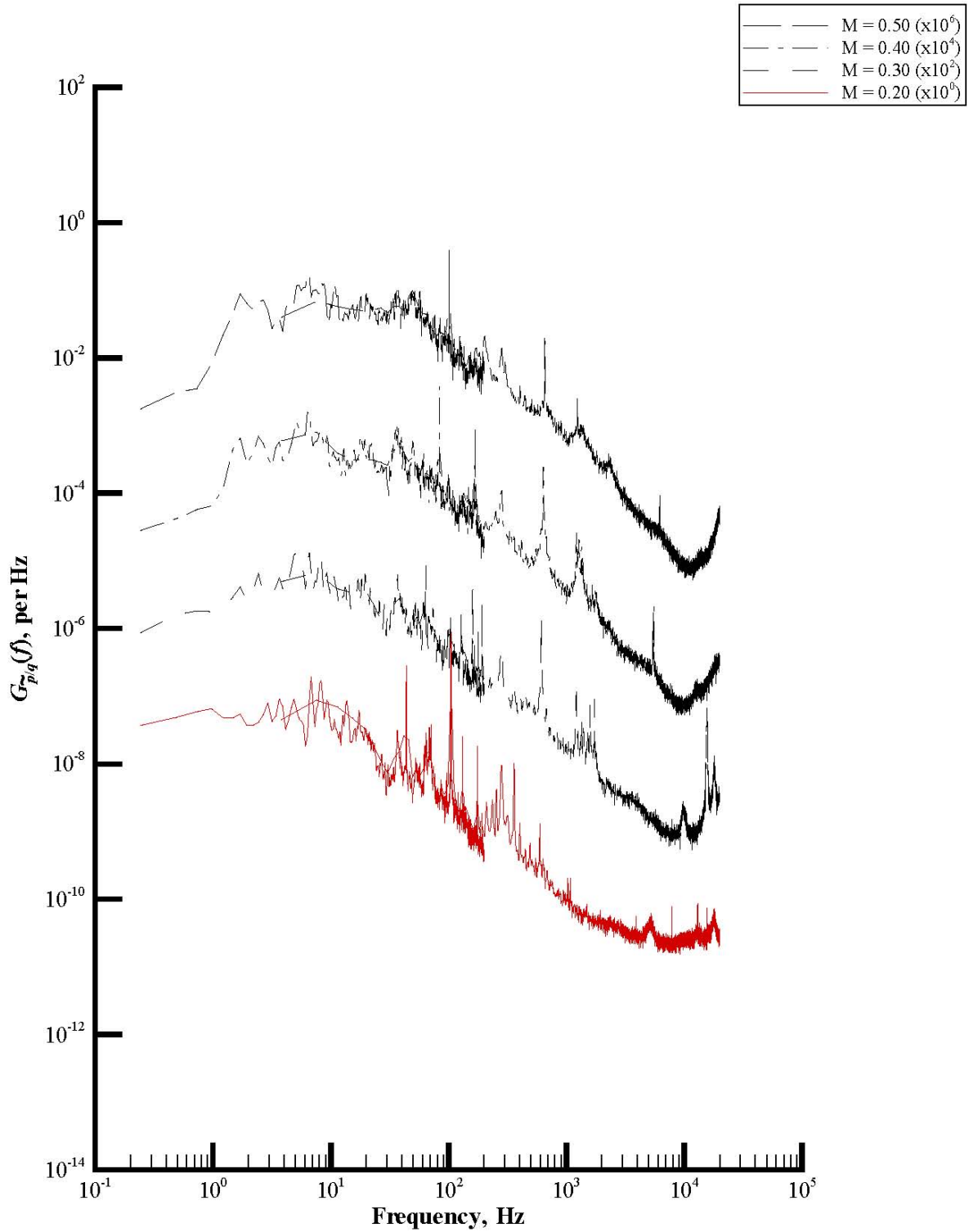
(b) Rake starboard total pressure.

Figure A4. Continued.



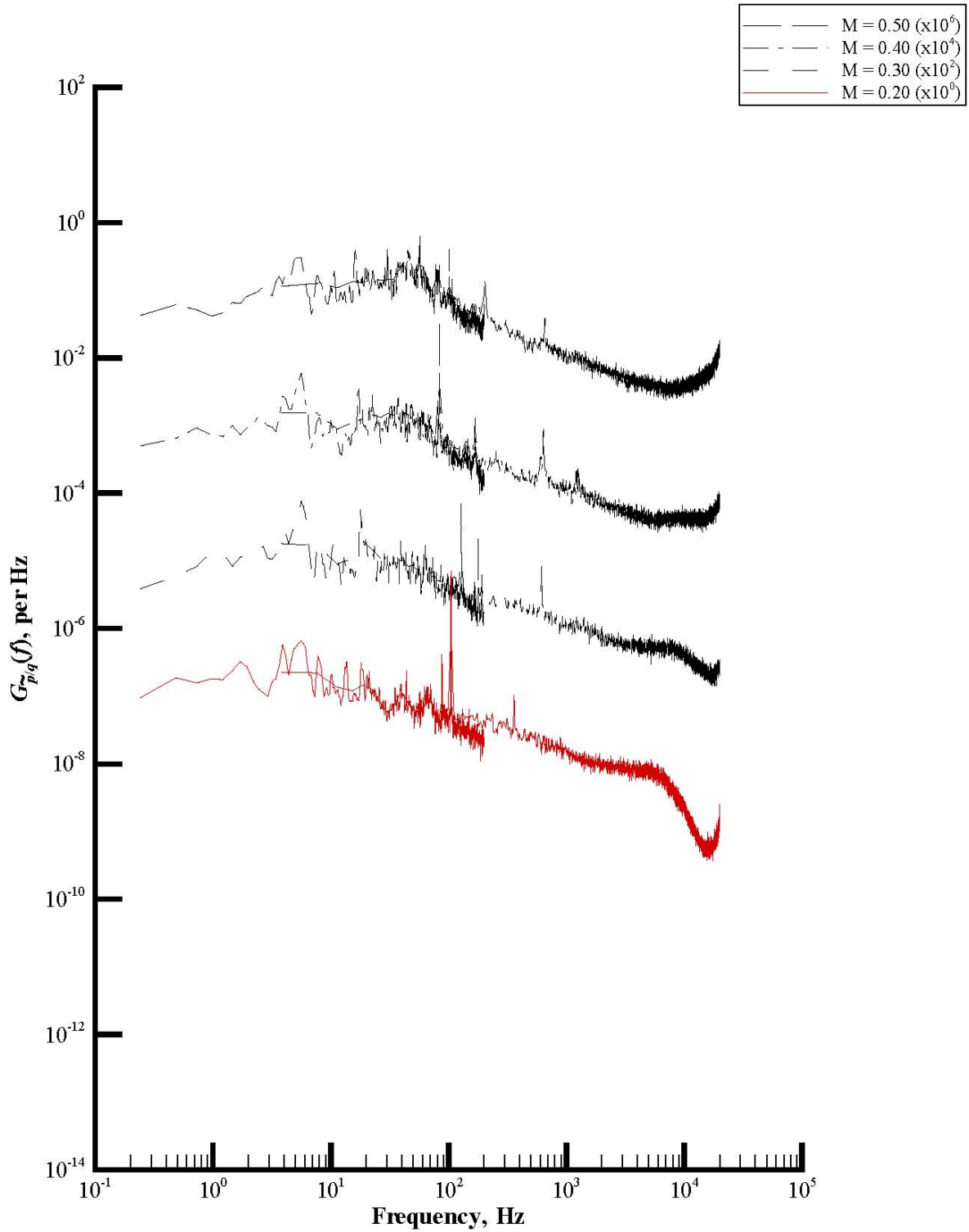
(c) Rake static pressure.

Figure A4. Continued.



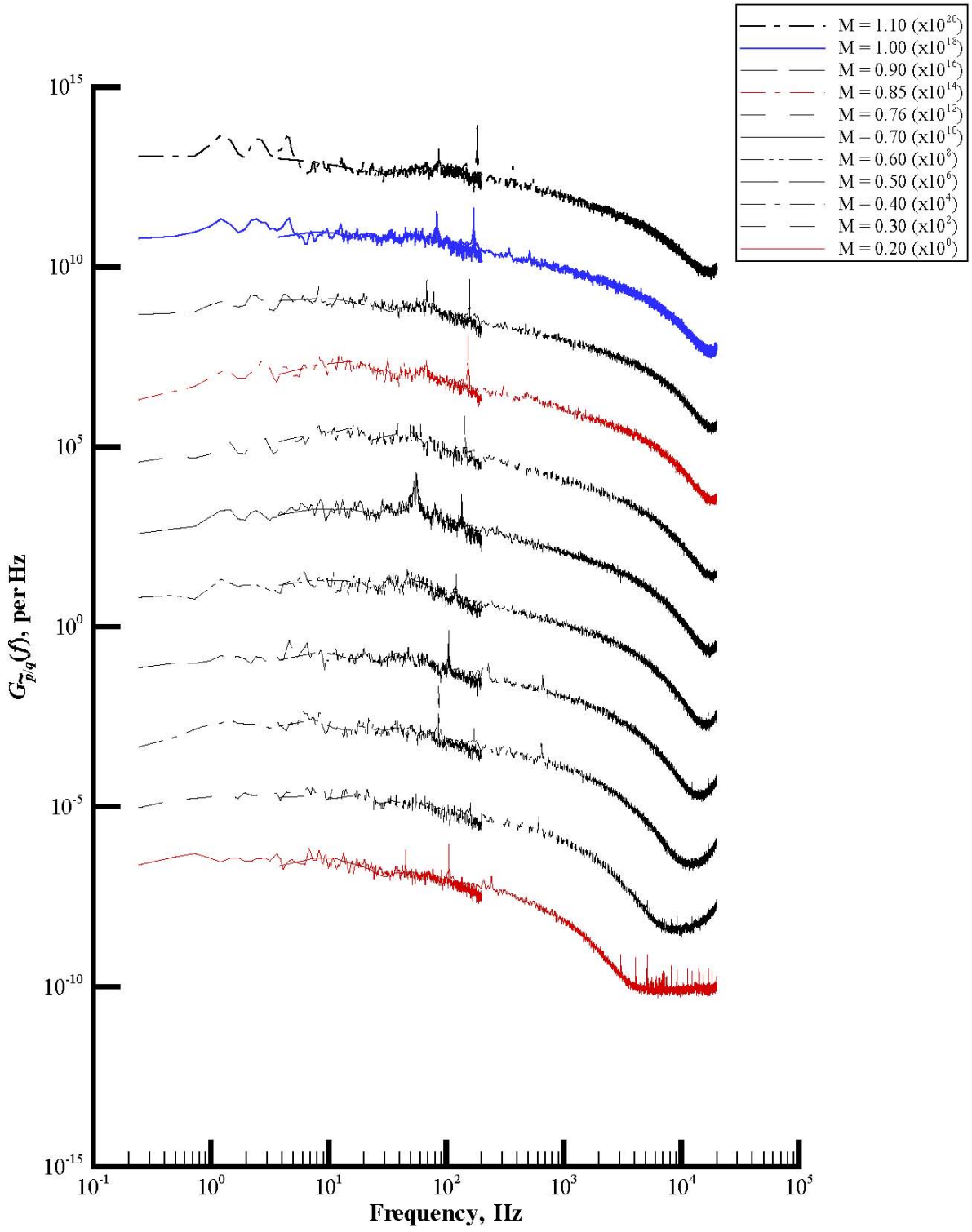
(d) Rake acoustic pressure.

Figure A4. Continued.



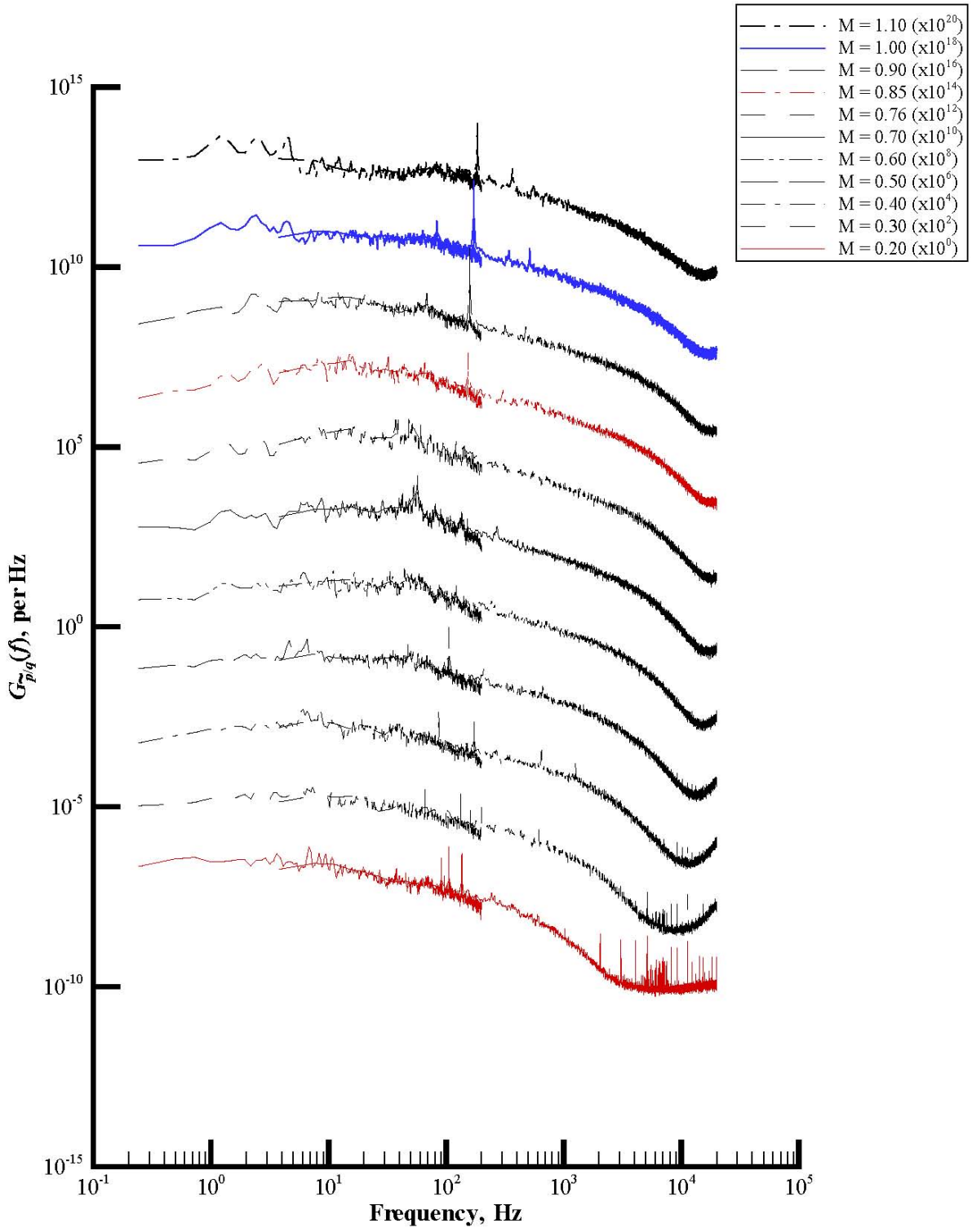
(e) Wall static pressure.

Figure A4. Concluded.



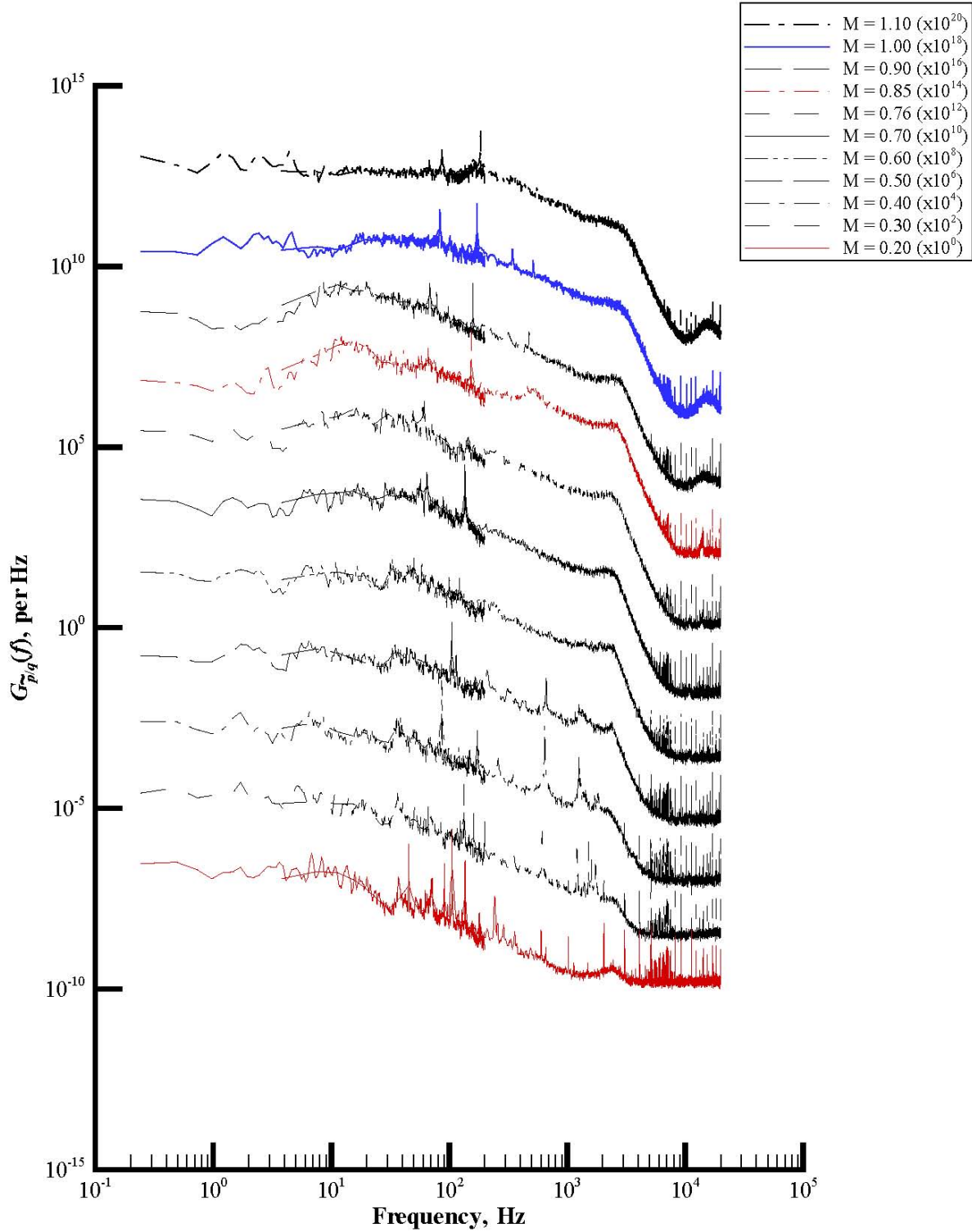
(a) Rake port total pressure.

Figure A5. Extended spectra plots of power spectral density functions of set 5.



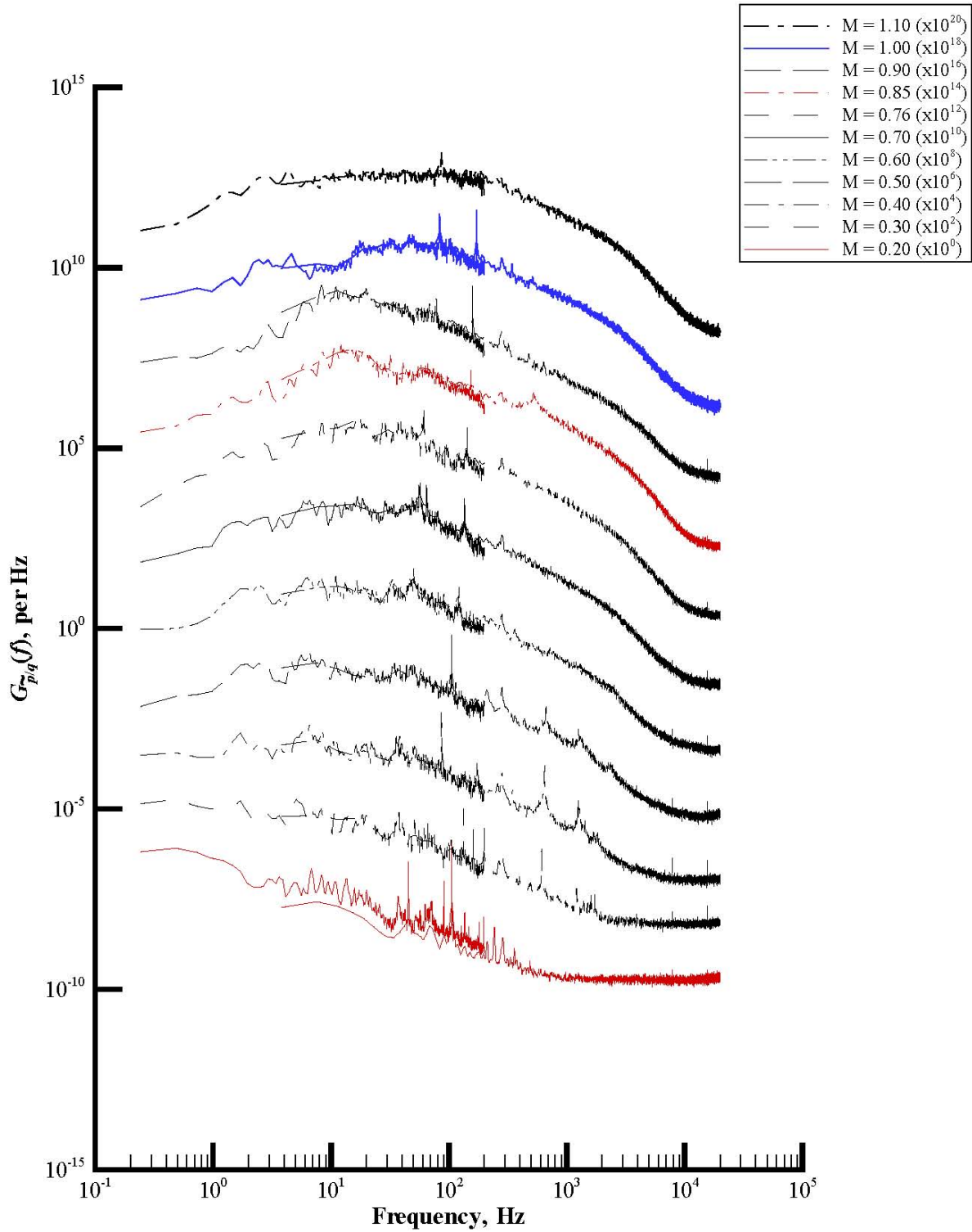
(b) Rake starboard total pressure.

Figure A5. Continued.



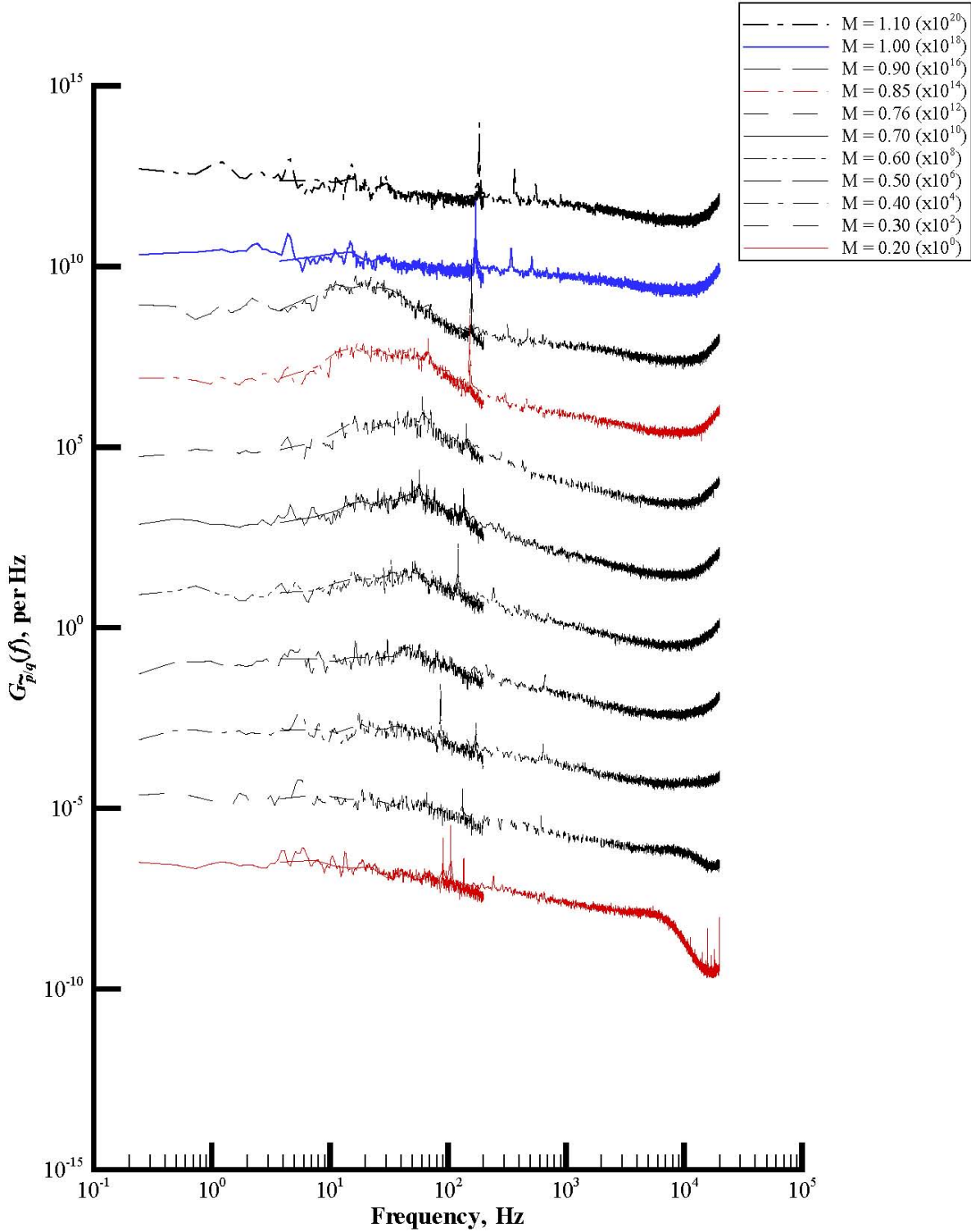
(c) Rake static pressure.

Figure A5. Continued.



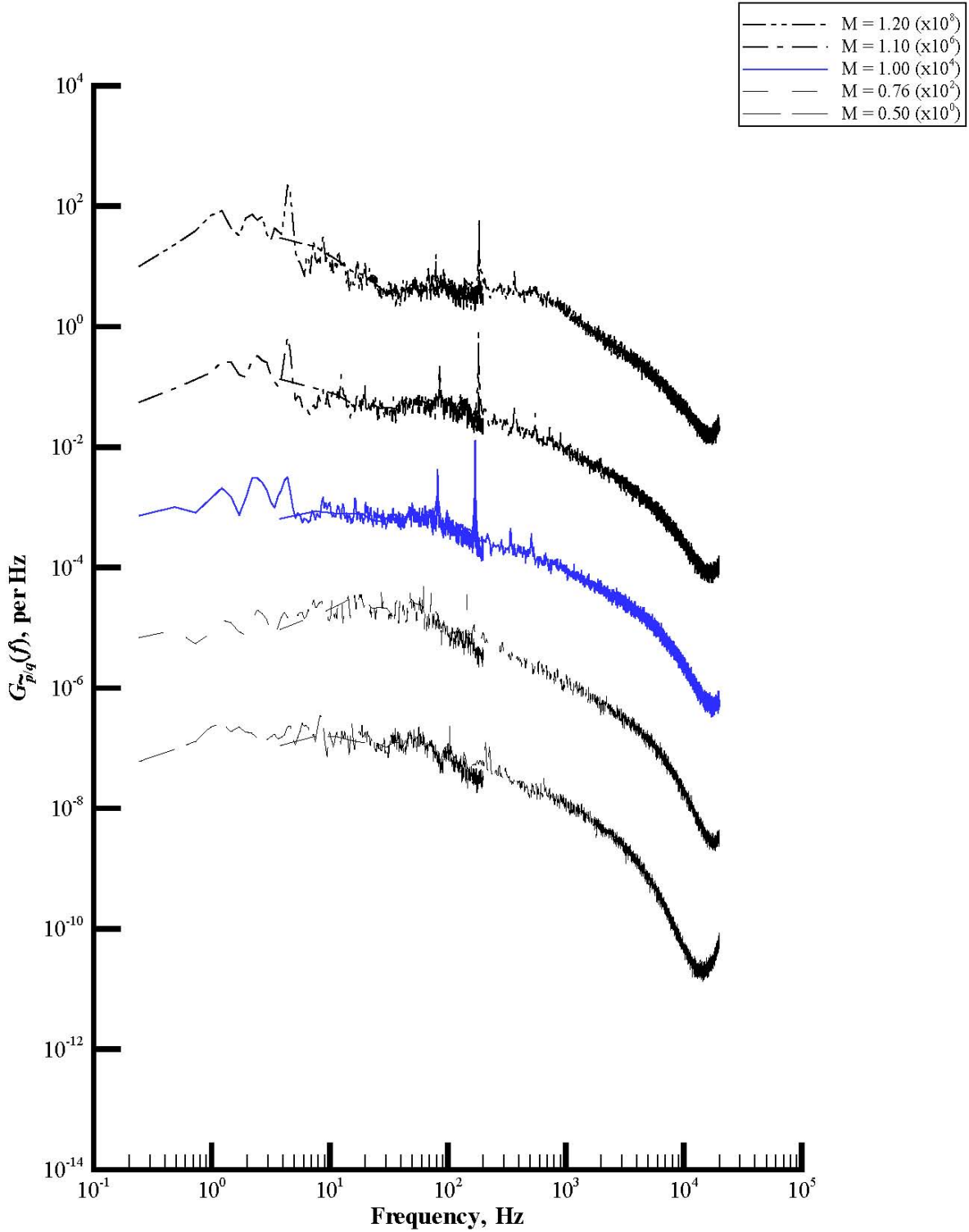
(d) Rake acoustic pressure.

Figure A5. Continued.



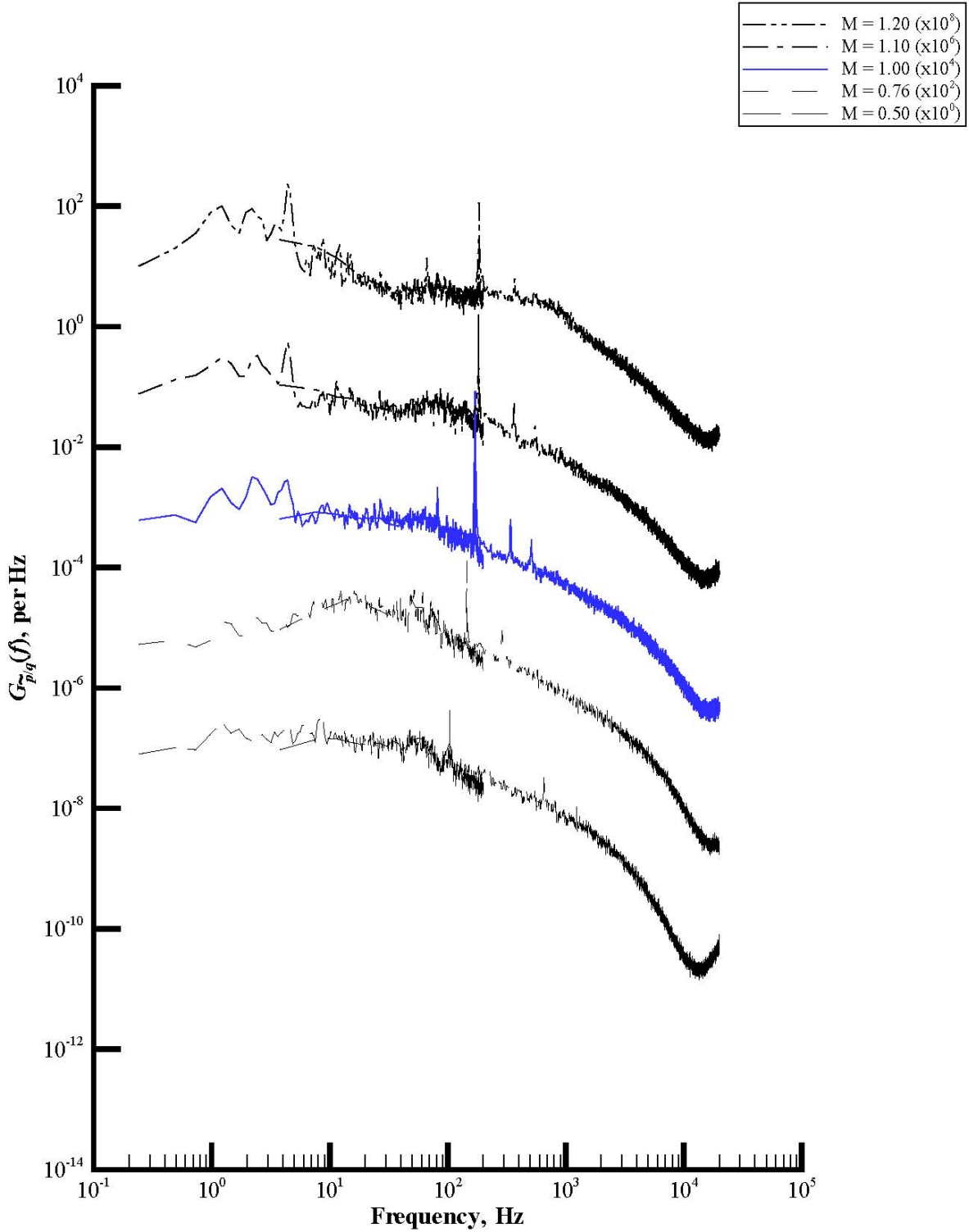
(e) Wall static pressure.

Figure A5. Concluded.



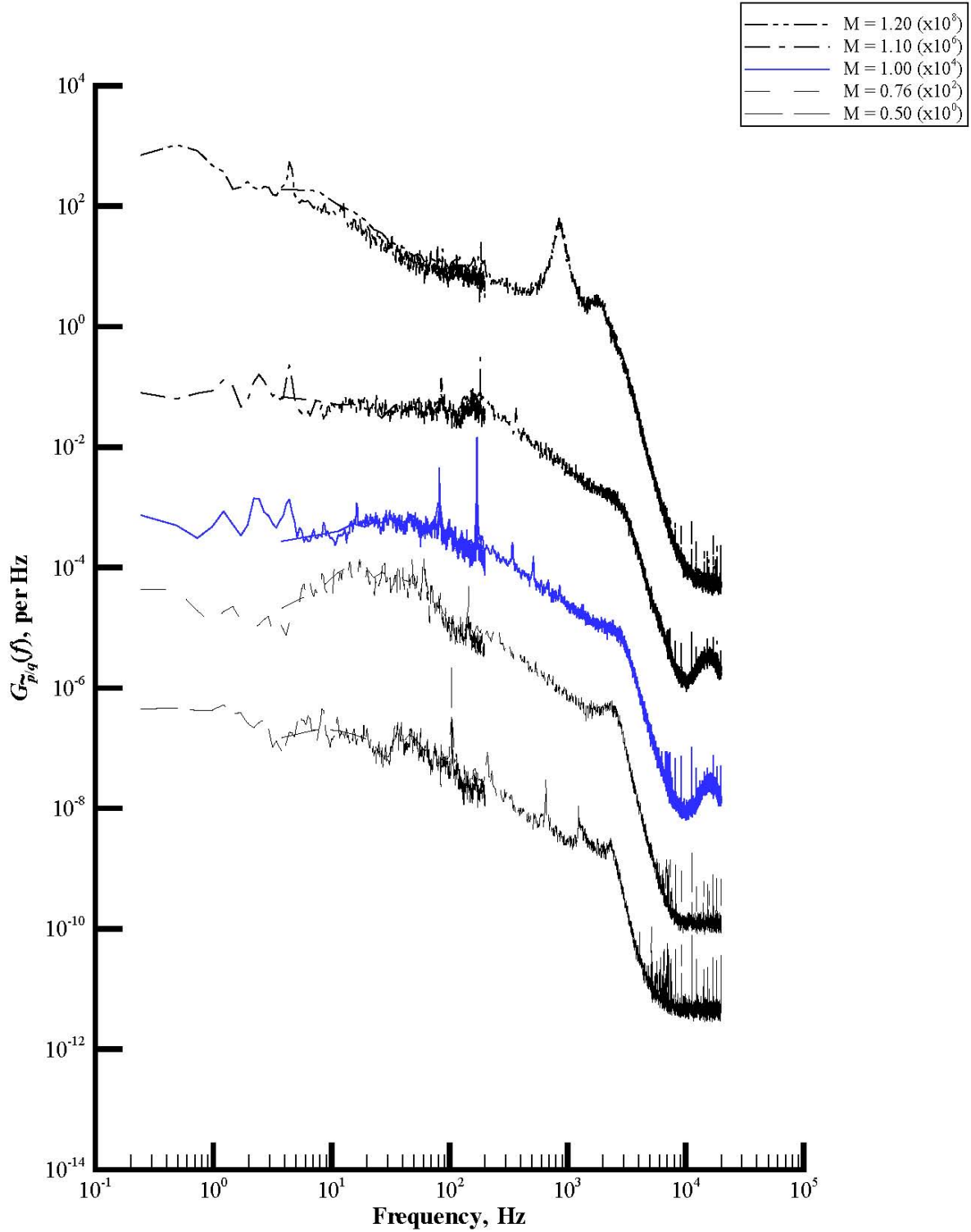
(a) Rake port total pressure.

Figure A6. Extended spectra plots of power spectral density functions of set 6.



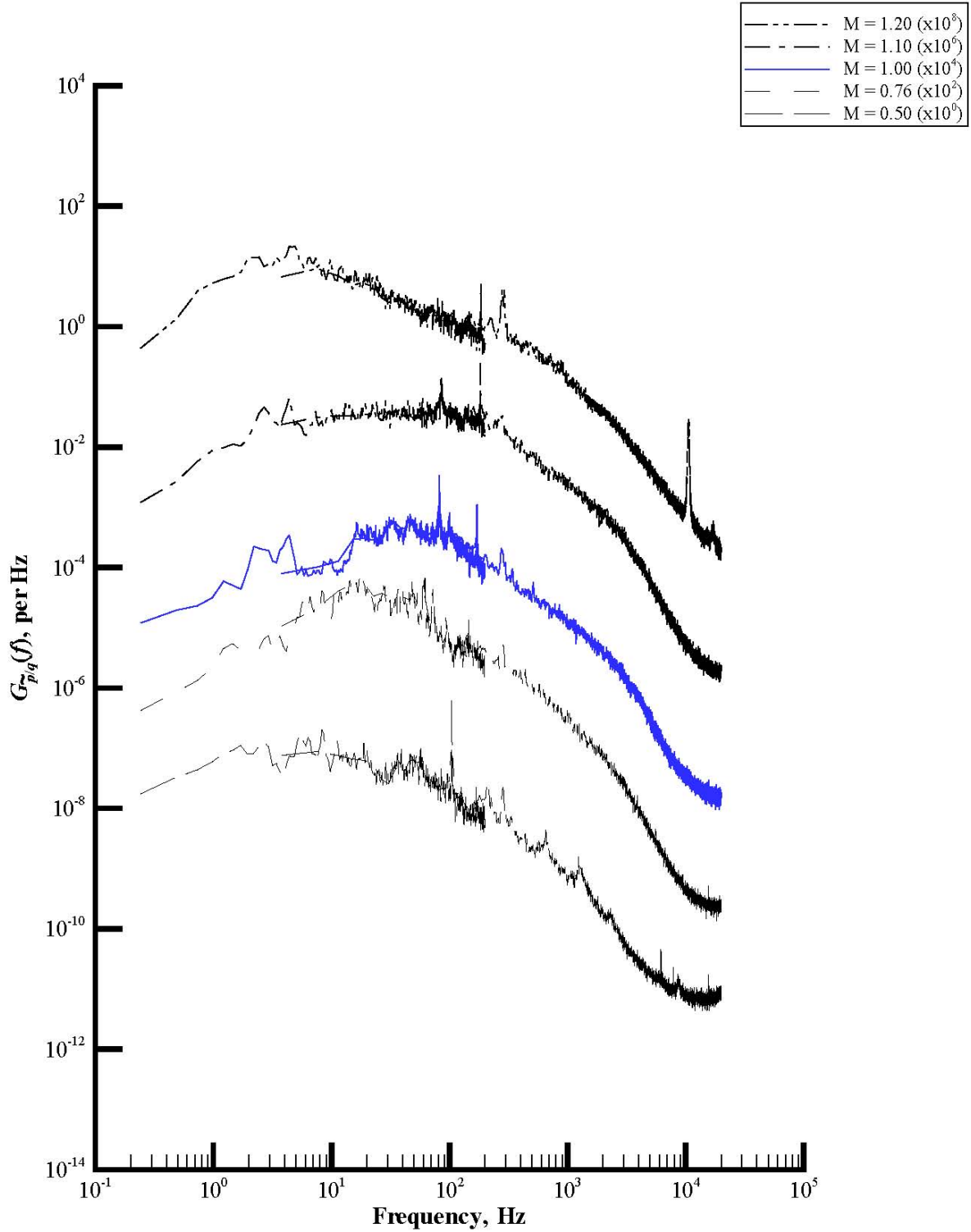
(b) Rake starboard total pressure.

Figure A6. Continued.



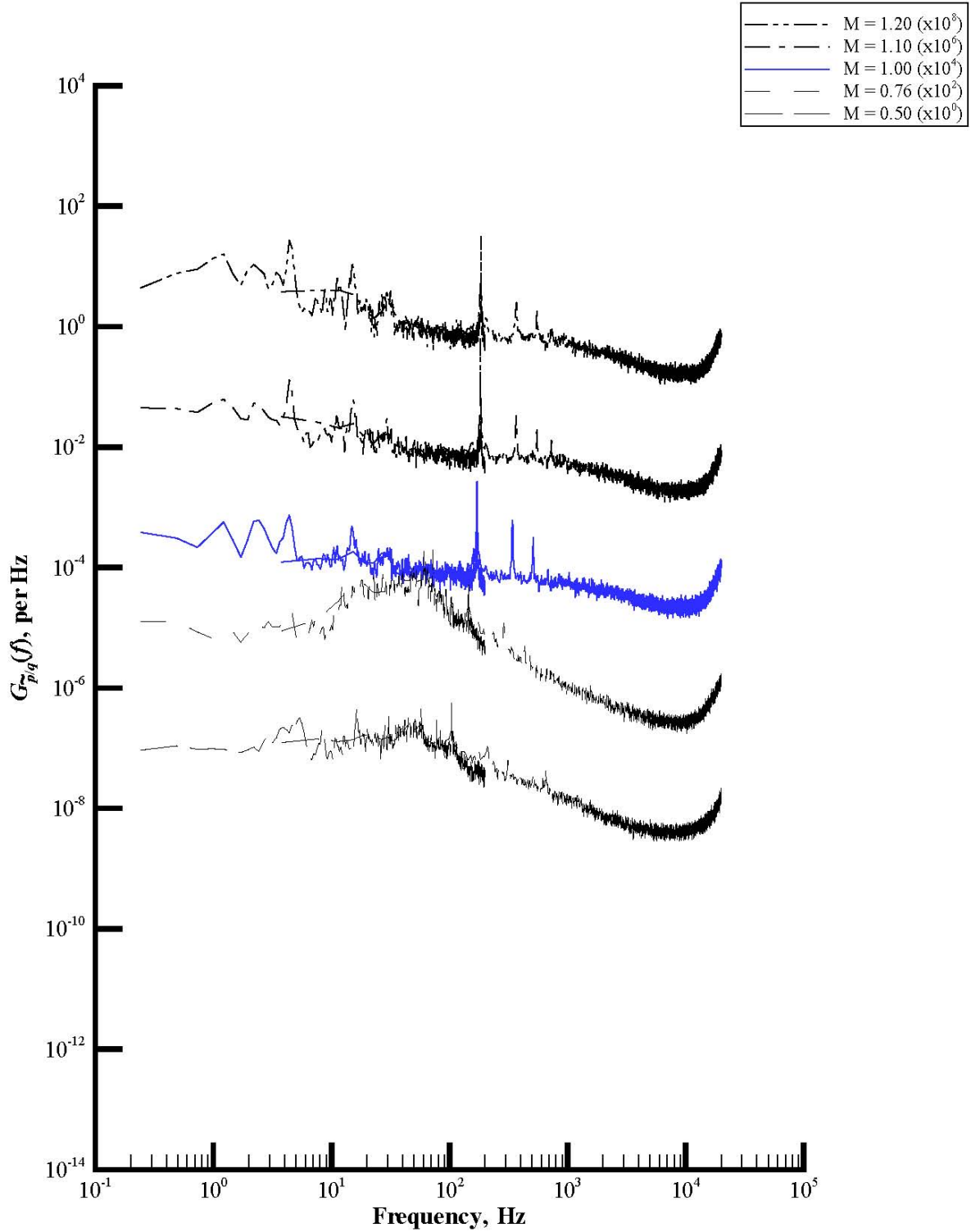
(c) Rake static pressure.

Figure A6. Continued.



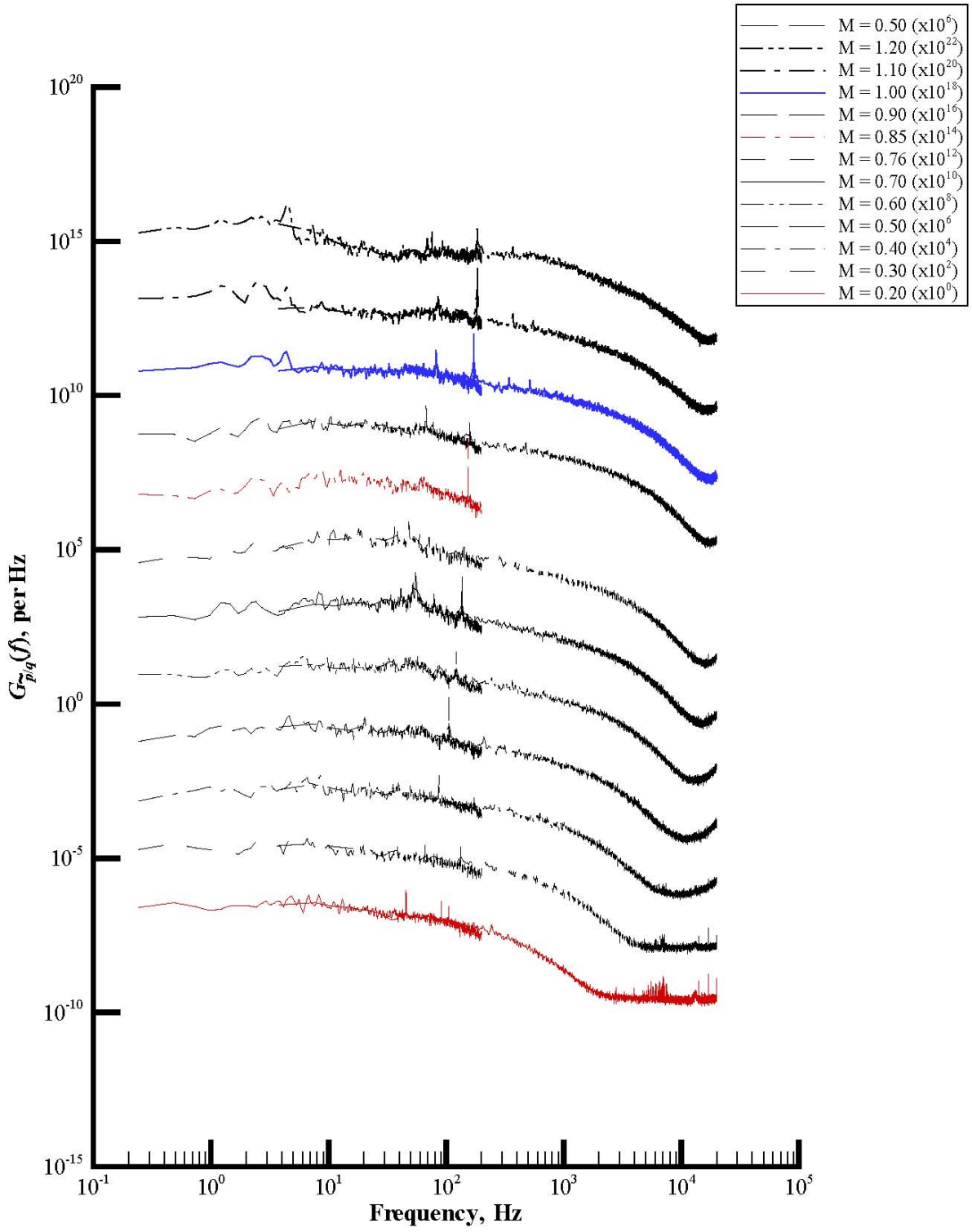
(d) Rake acoustic pressure.

Figure A6. Continued.



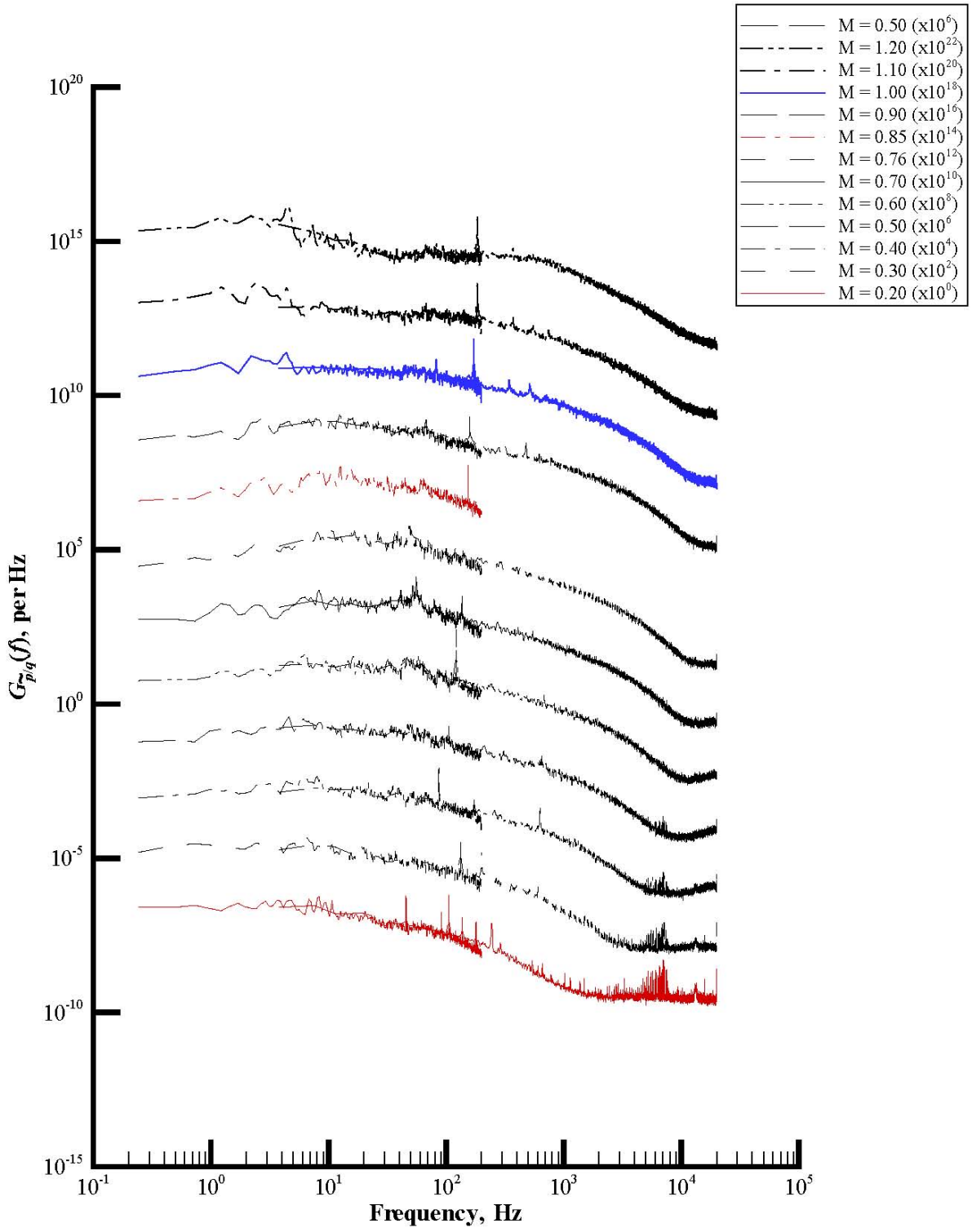
(e) Wall static pressure.

Figure A6. Concluded.



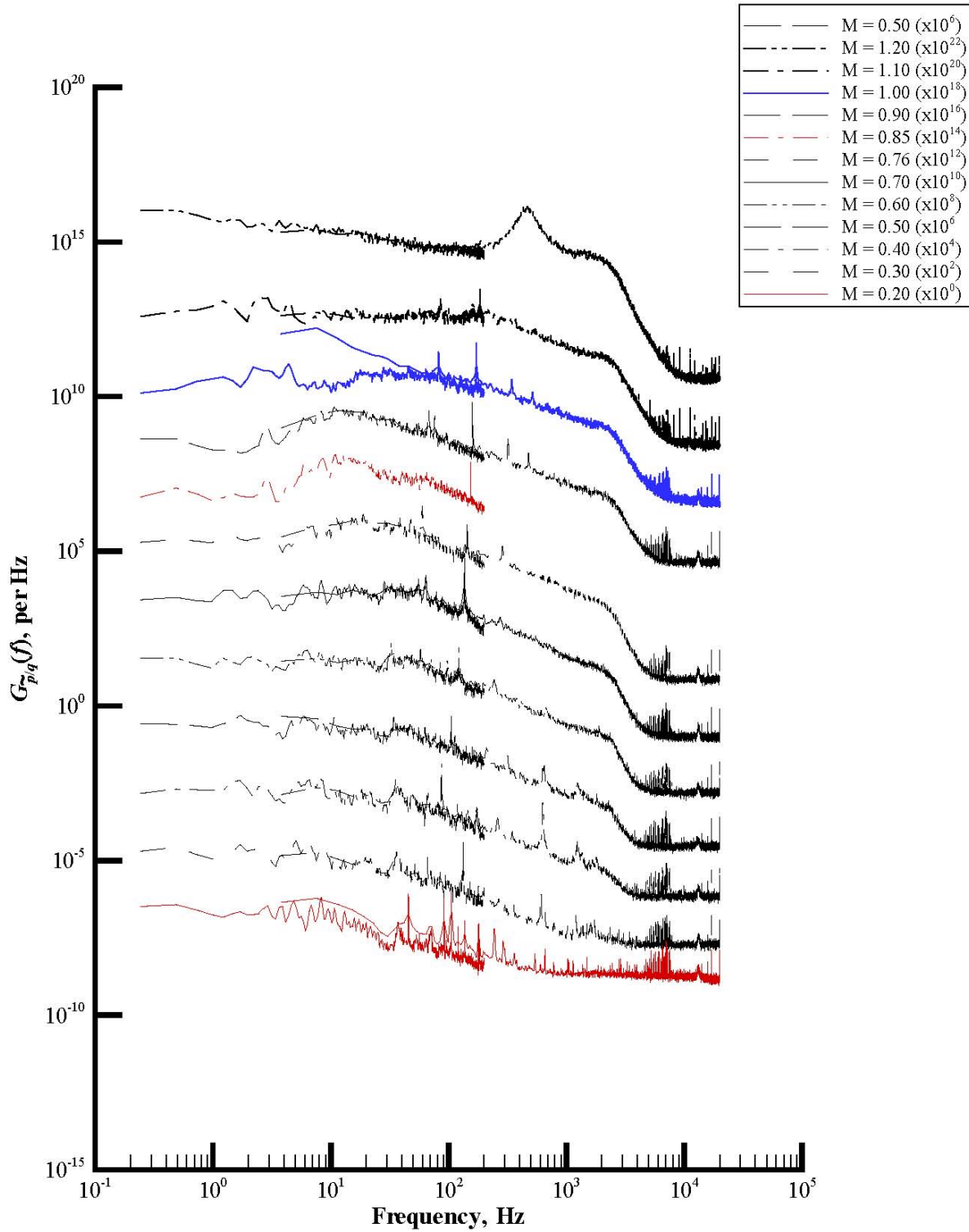
(a) Rake port total pressure.

Figure A7. Extended spectra plots of power spectral density functions of set 7.



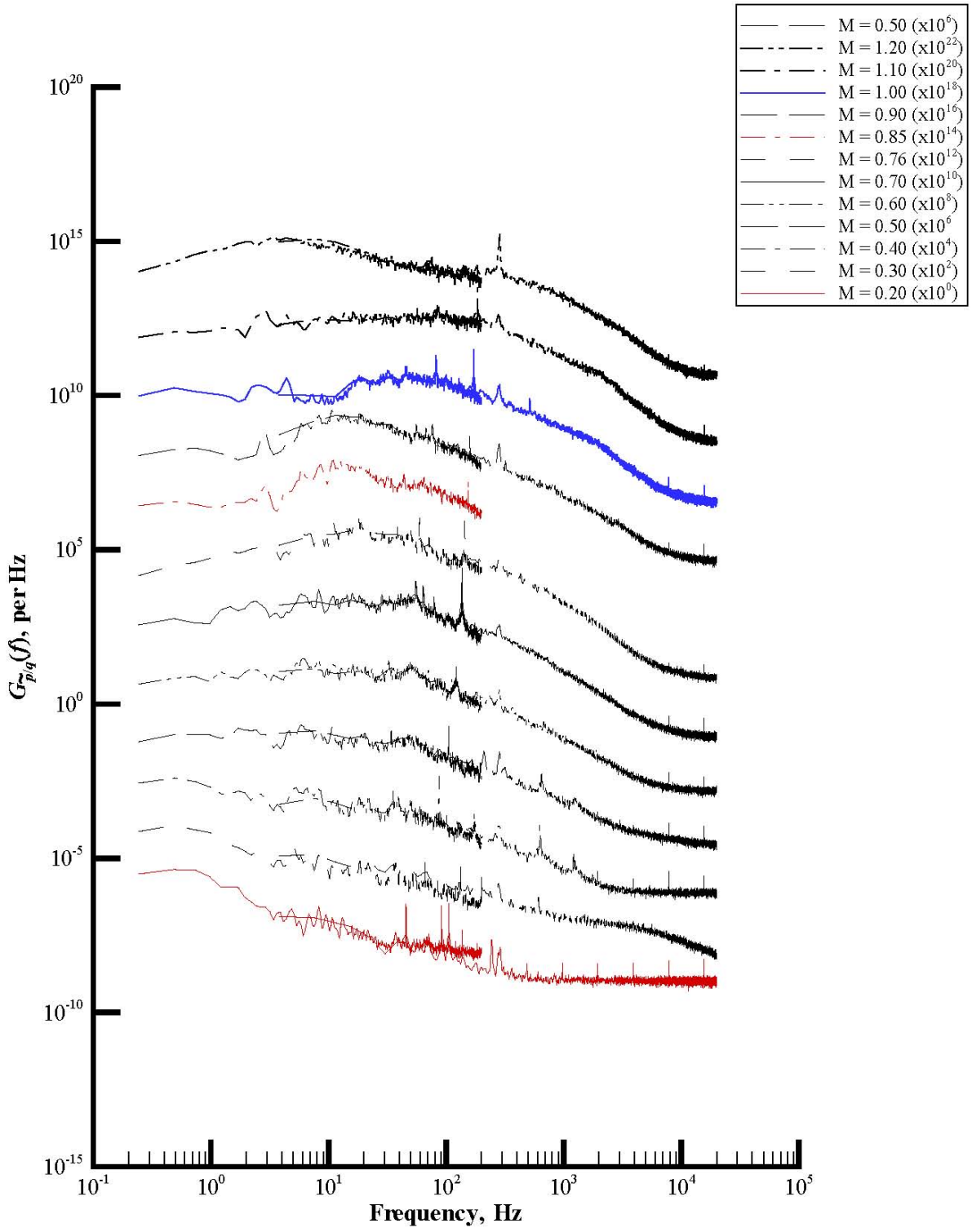
(b) Rake starboard total pressure.

Figure A7. Continued.



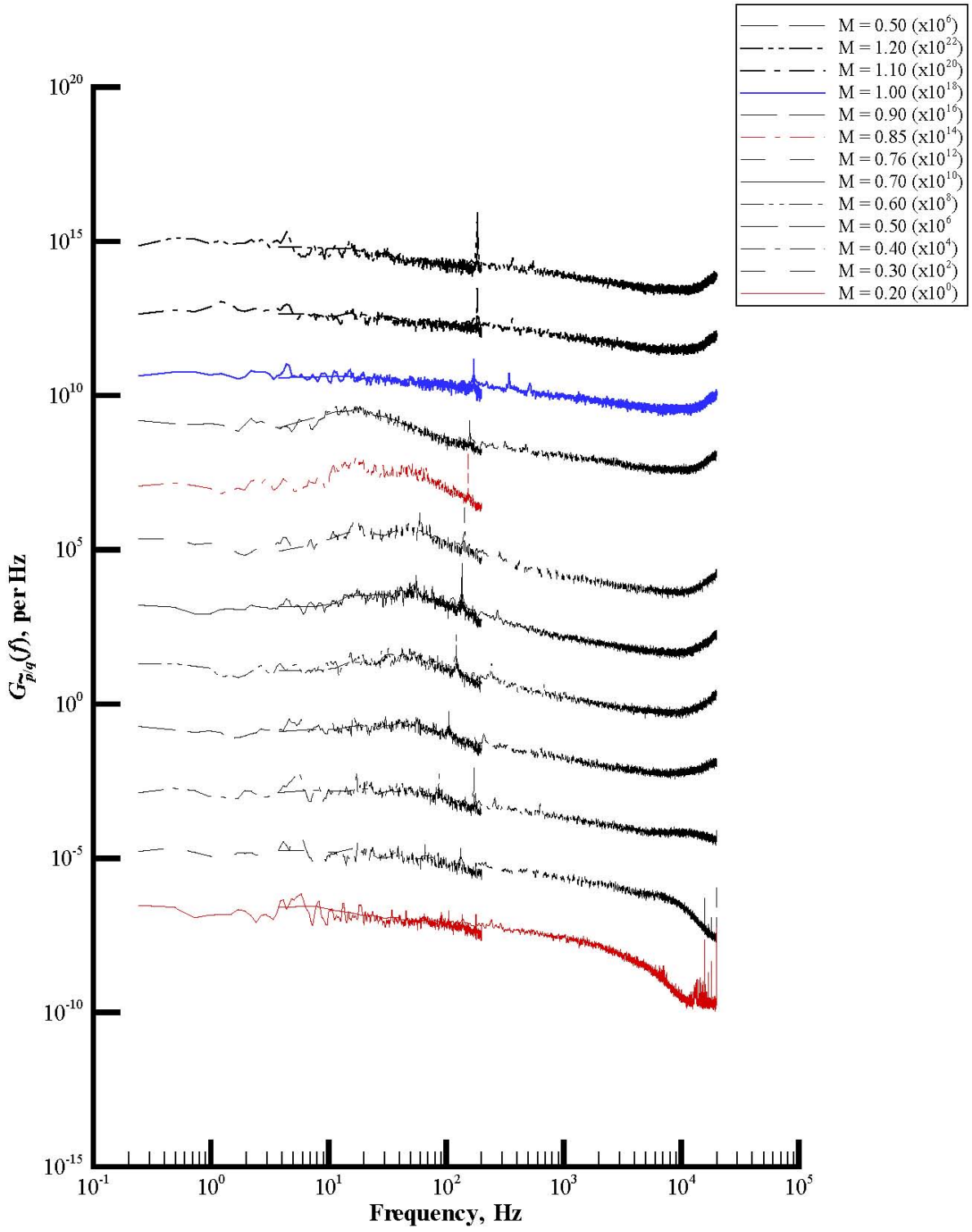
(c) Rake static pressure.

Figure A7. Continued.



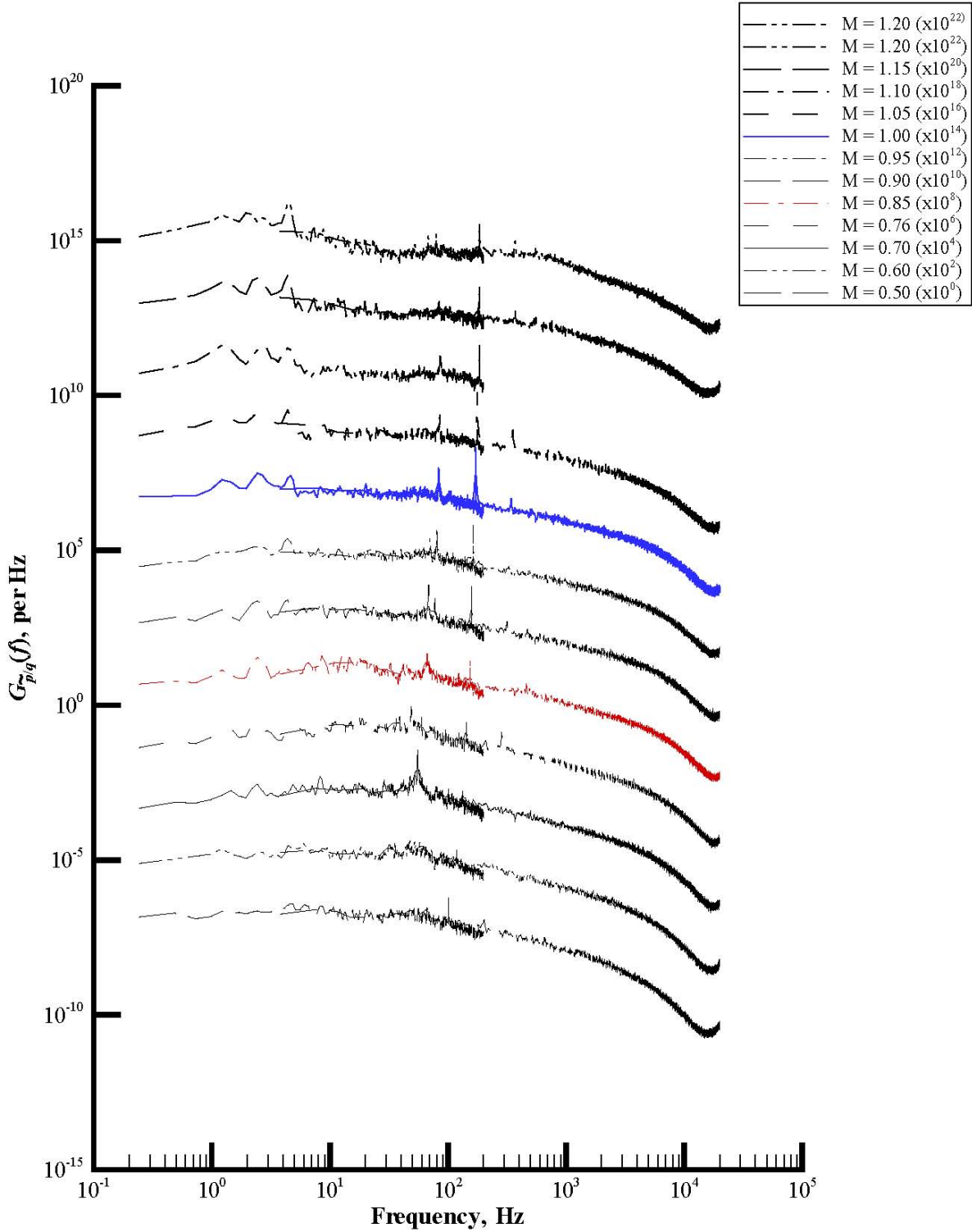
(d) Rake acoustic pressure.

Figure A7. Continued.



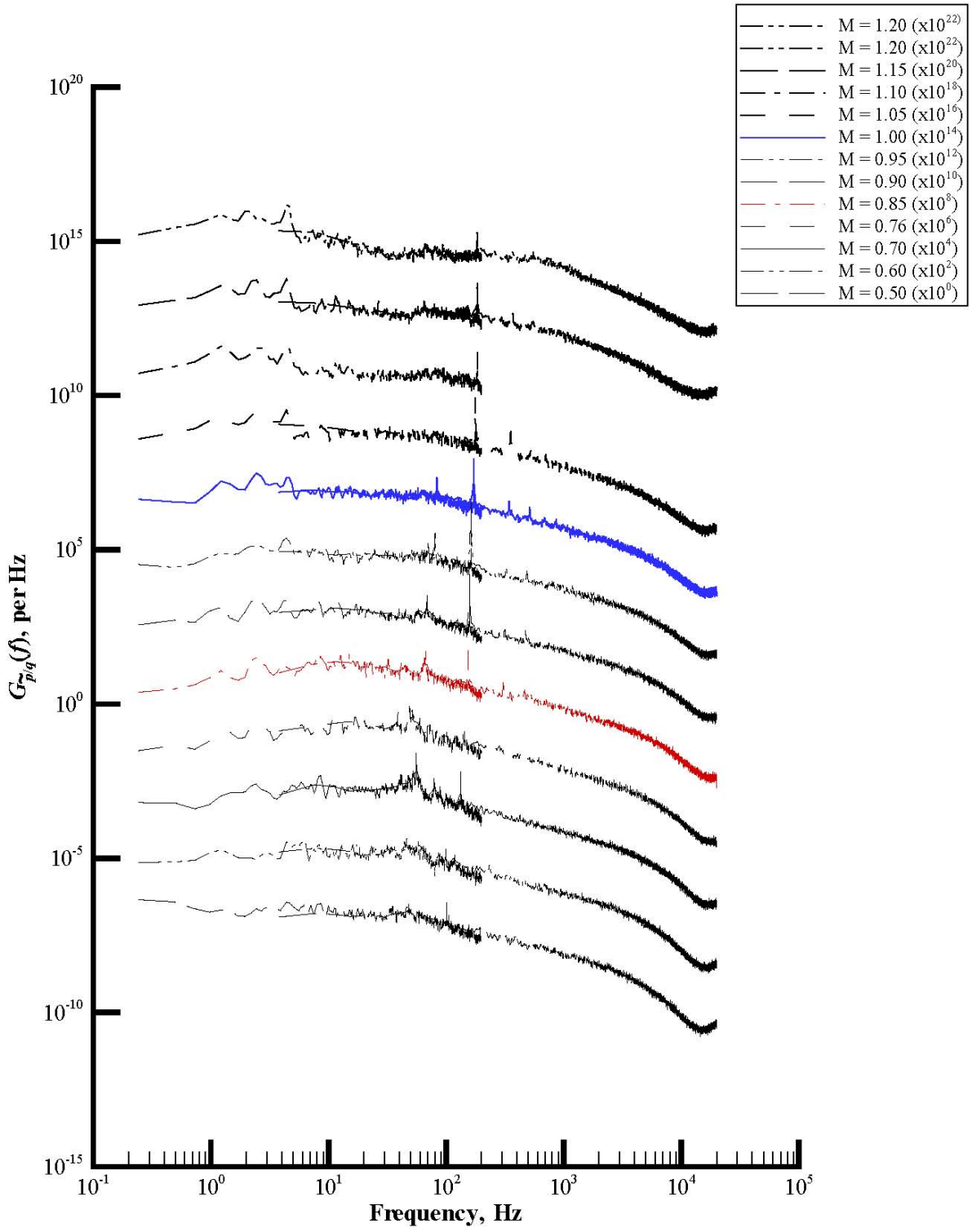
(e) Wall static pressure.

Figure A7. Concluded.



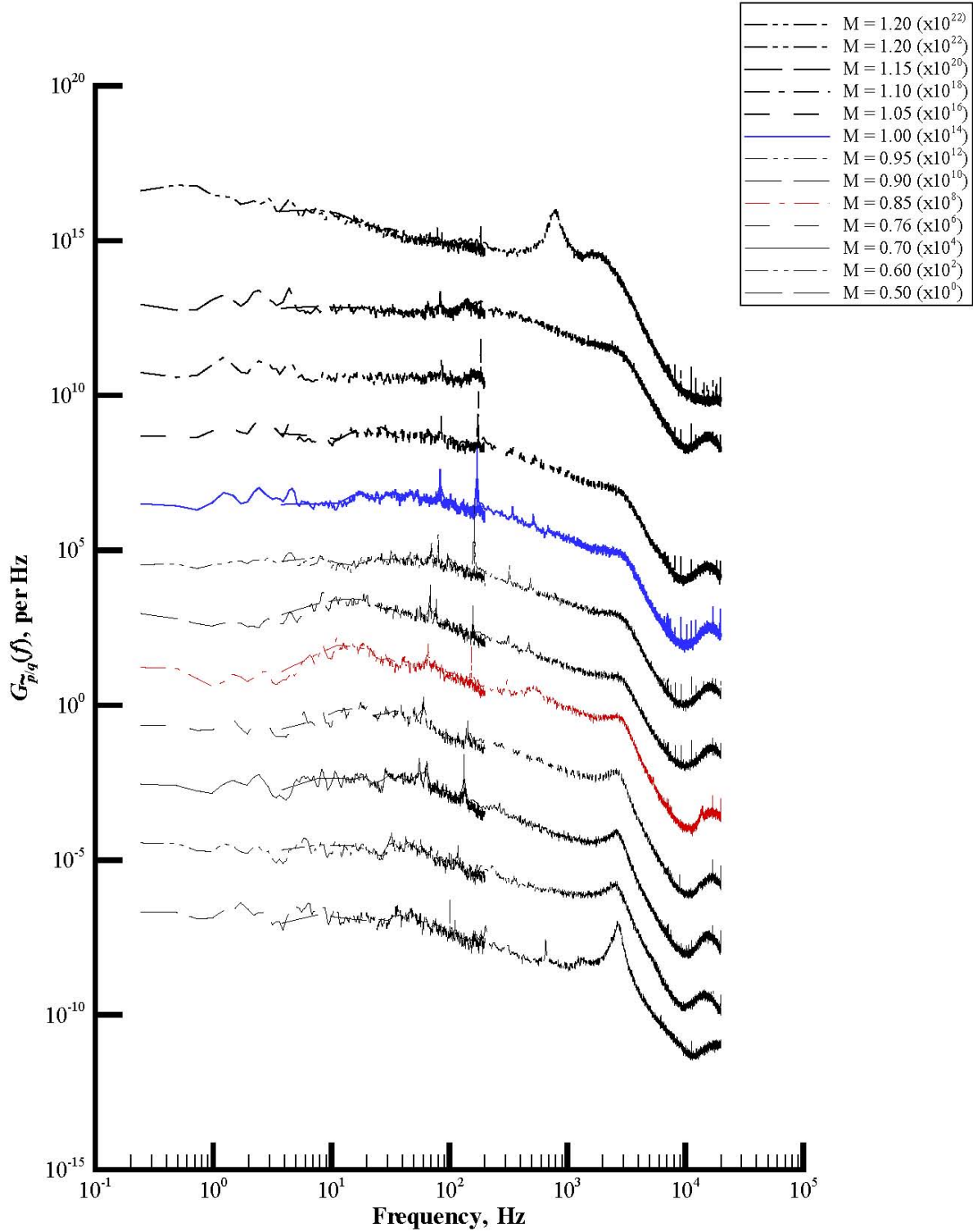
(a) Rake port total pressure.

Figure A8. Extended spectra plots of power spectral density functions of set 8.



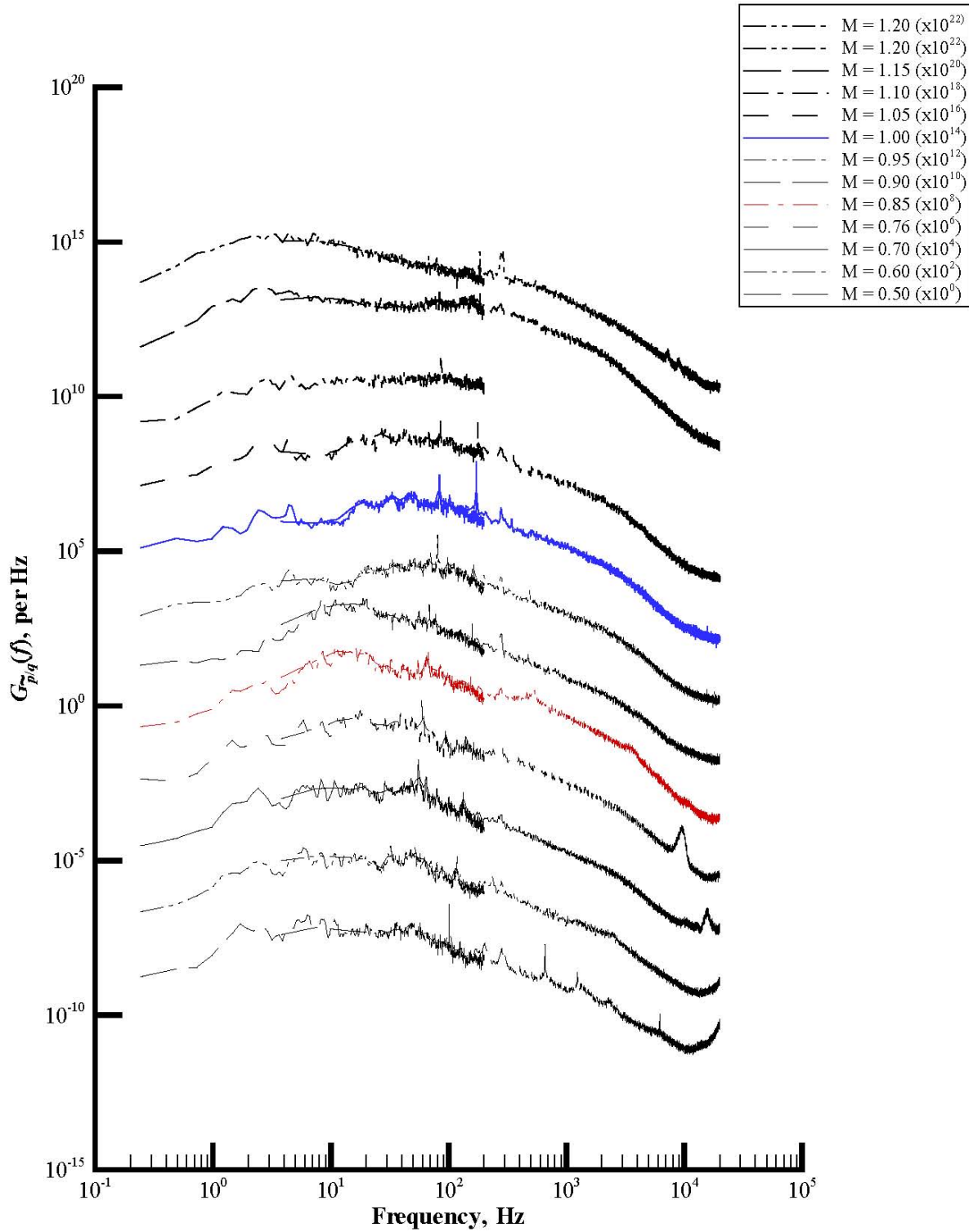
(b) Rake starboard total pressure.

Figure A8. Continued.



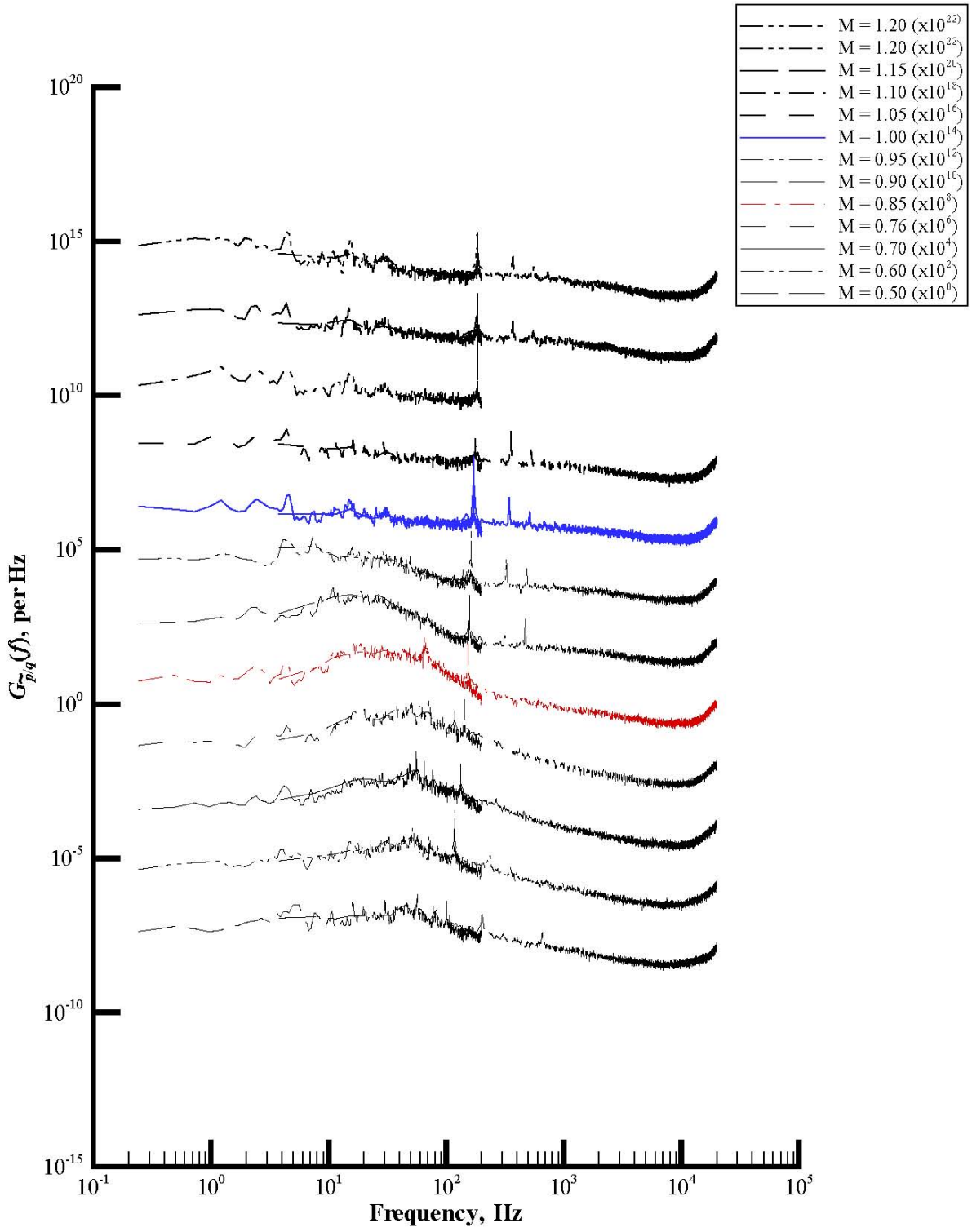
(c) Rake static pressure.

Figure A8. Continued.



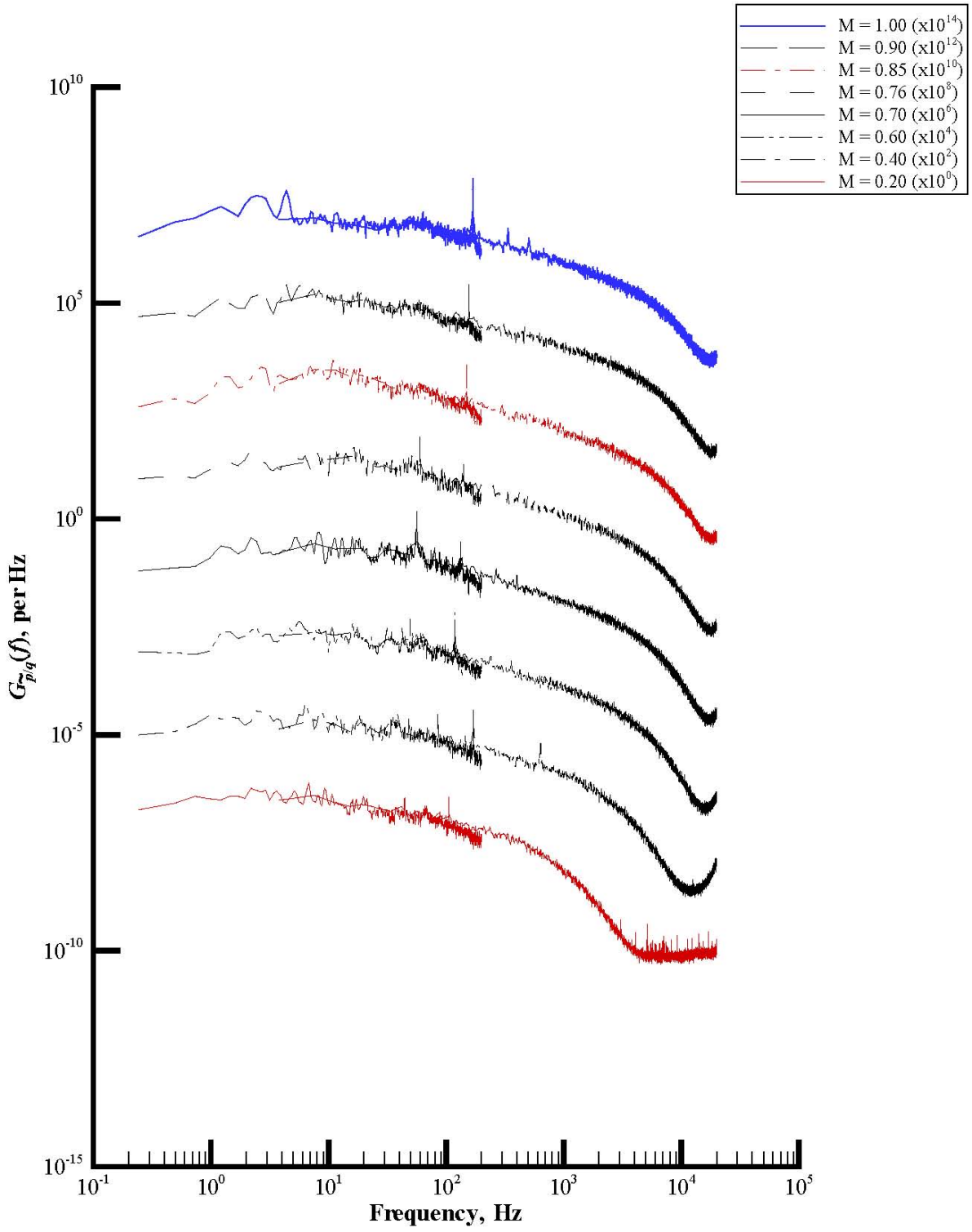
(d) Rake acoustic pressure.

Figure A8. Continued.



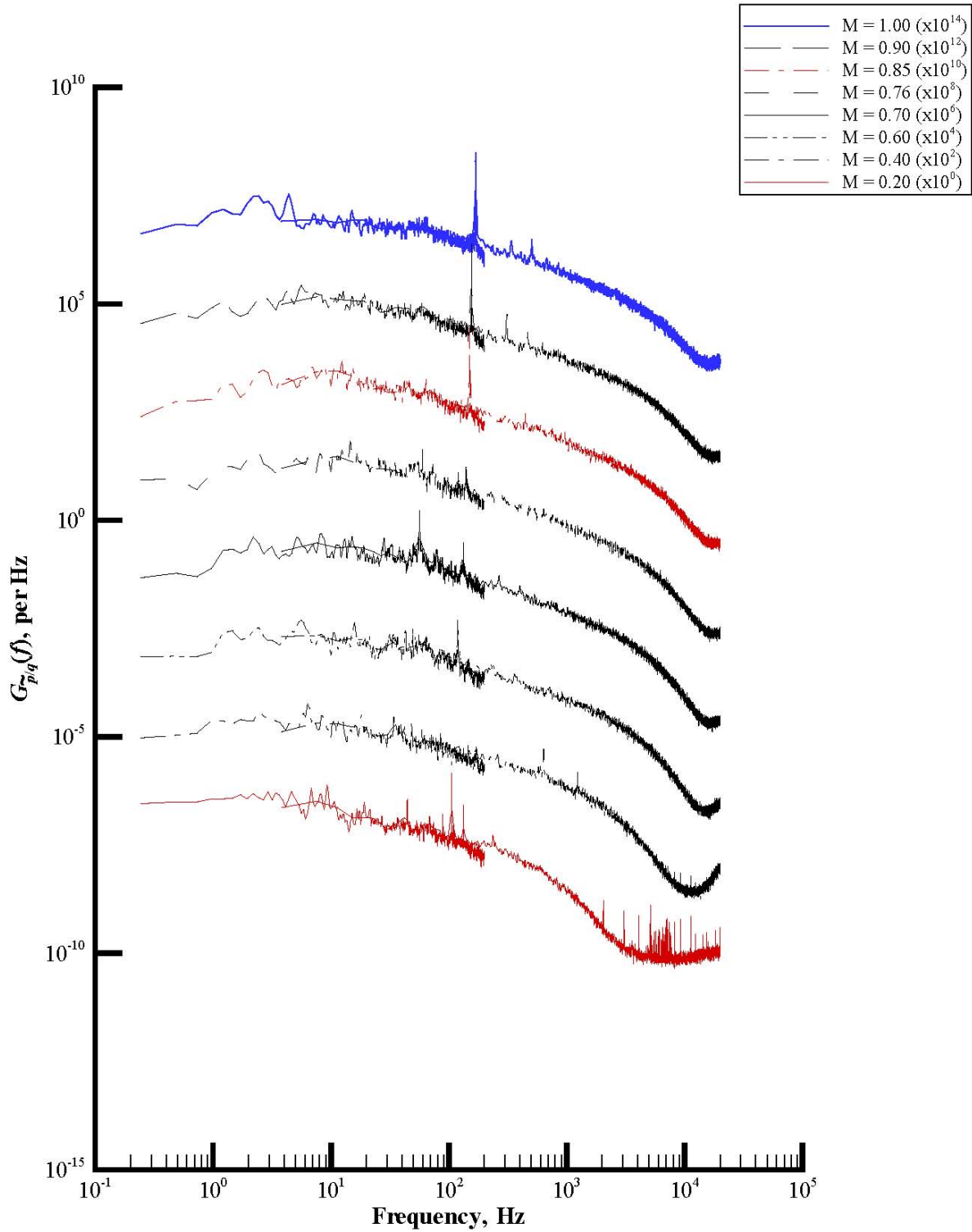
(e) Wall static pressure.

Figure A8. Concluded.



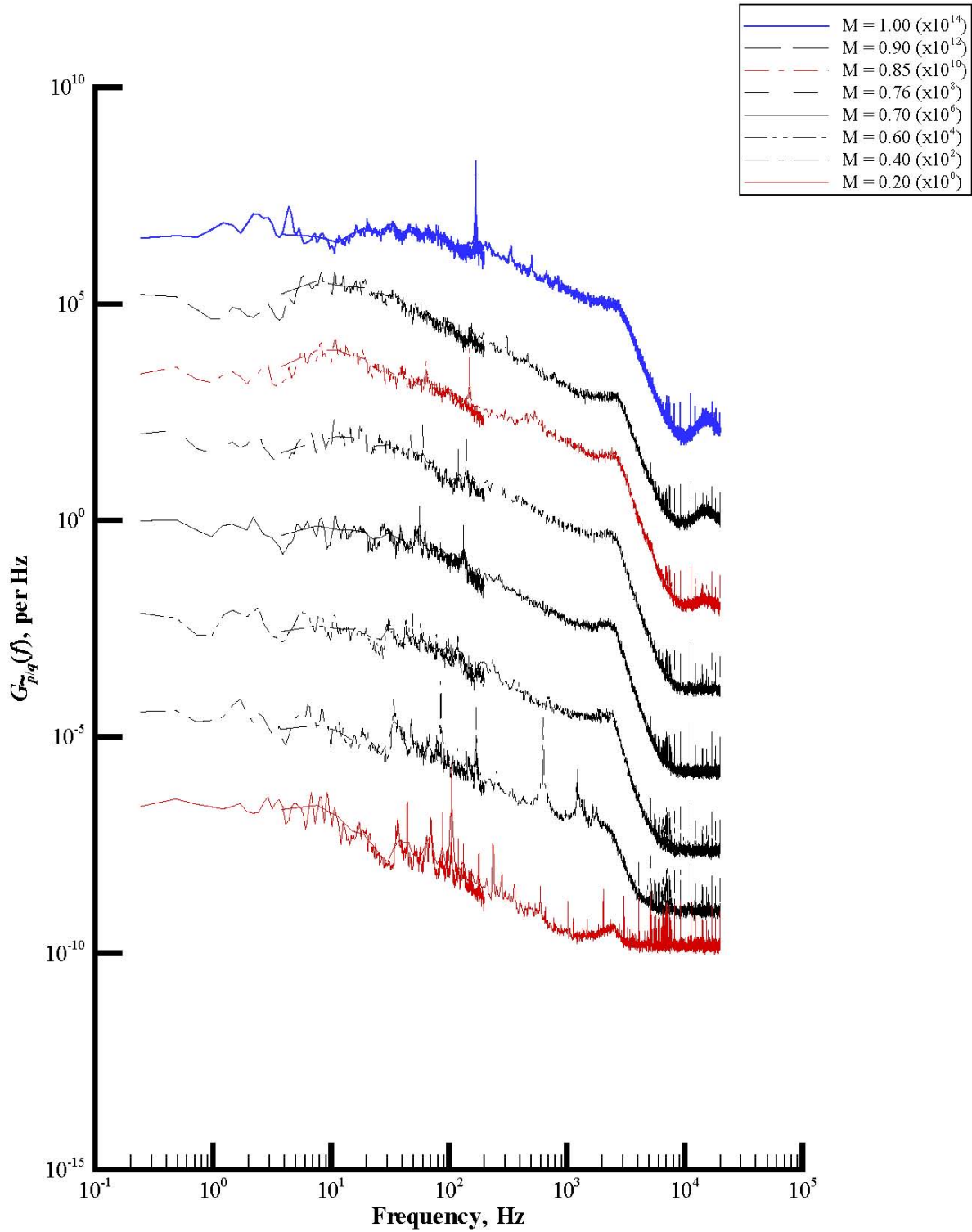
(a) Rake port total pressure.

Figure A9. Extended spectra plots of power spectral density functions of set 9.



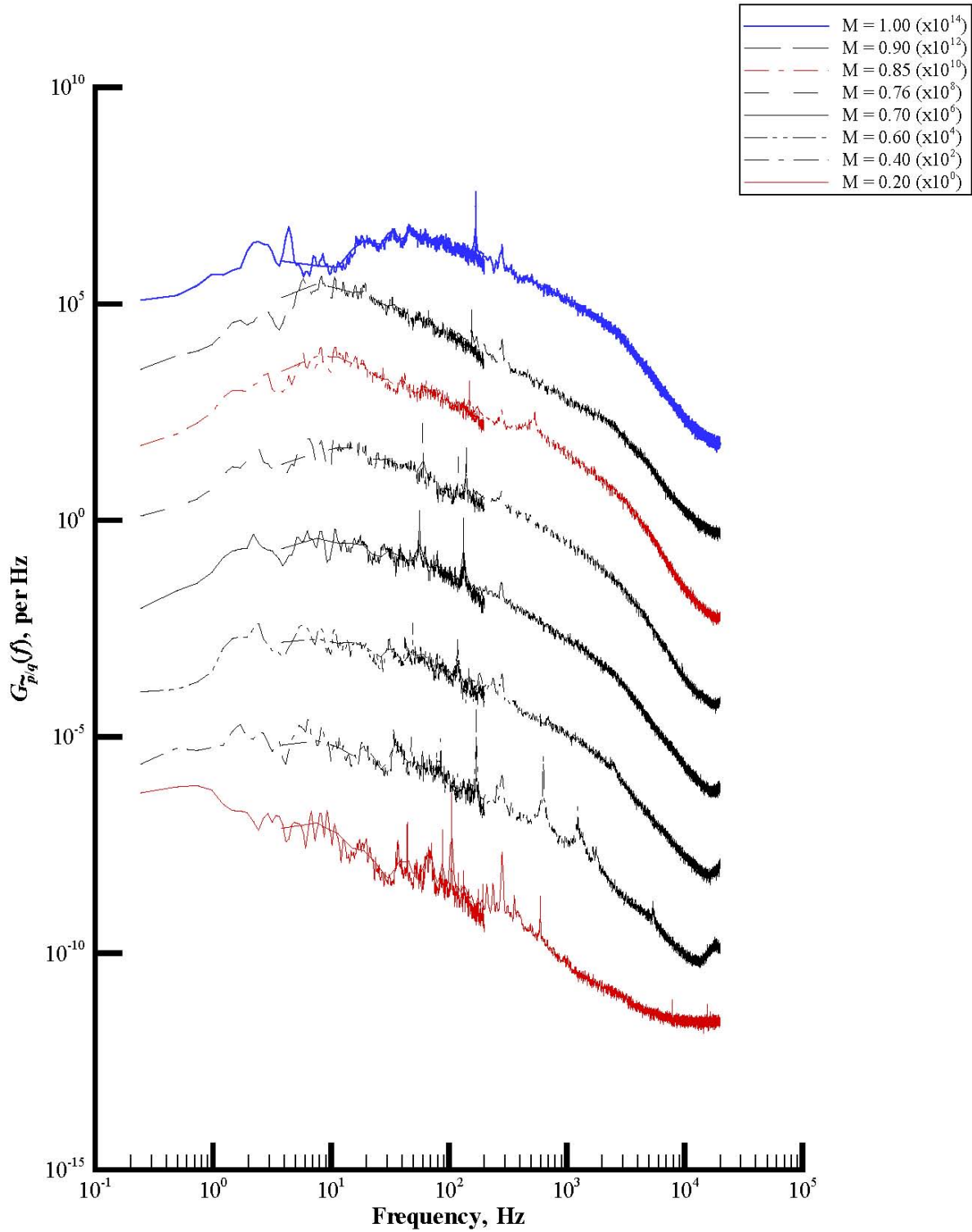
(b) Rake starboard total pressure.

Figure A9. Continued.



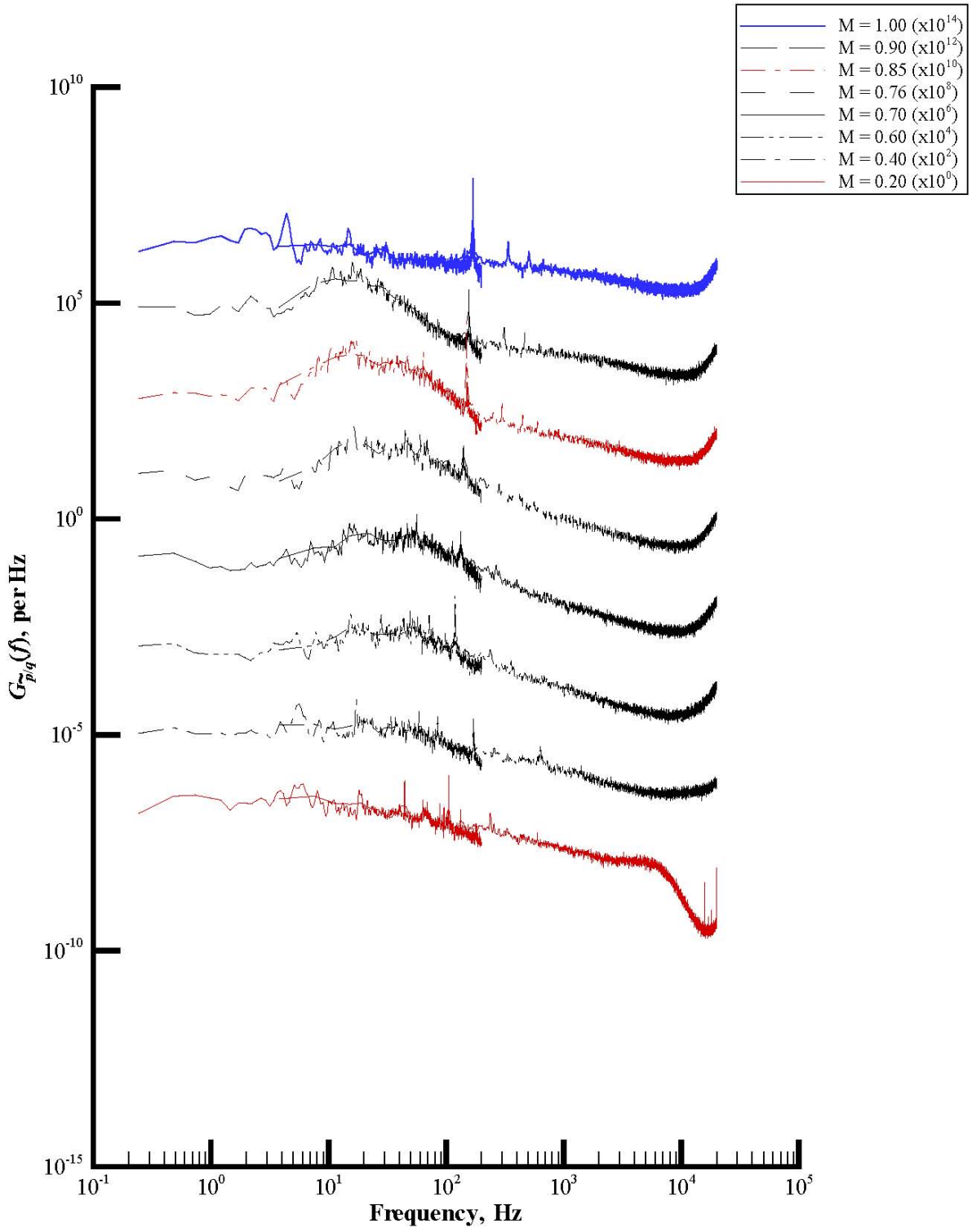
(c) Rake static pressure.

Figure A9. Continued.



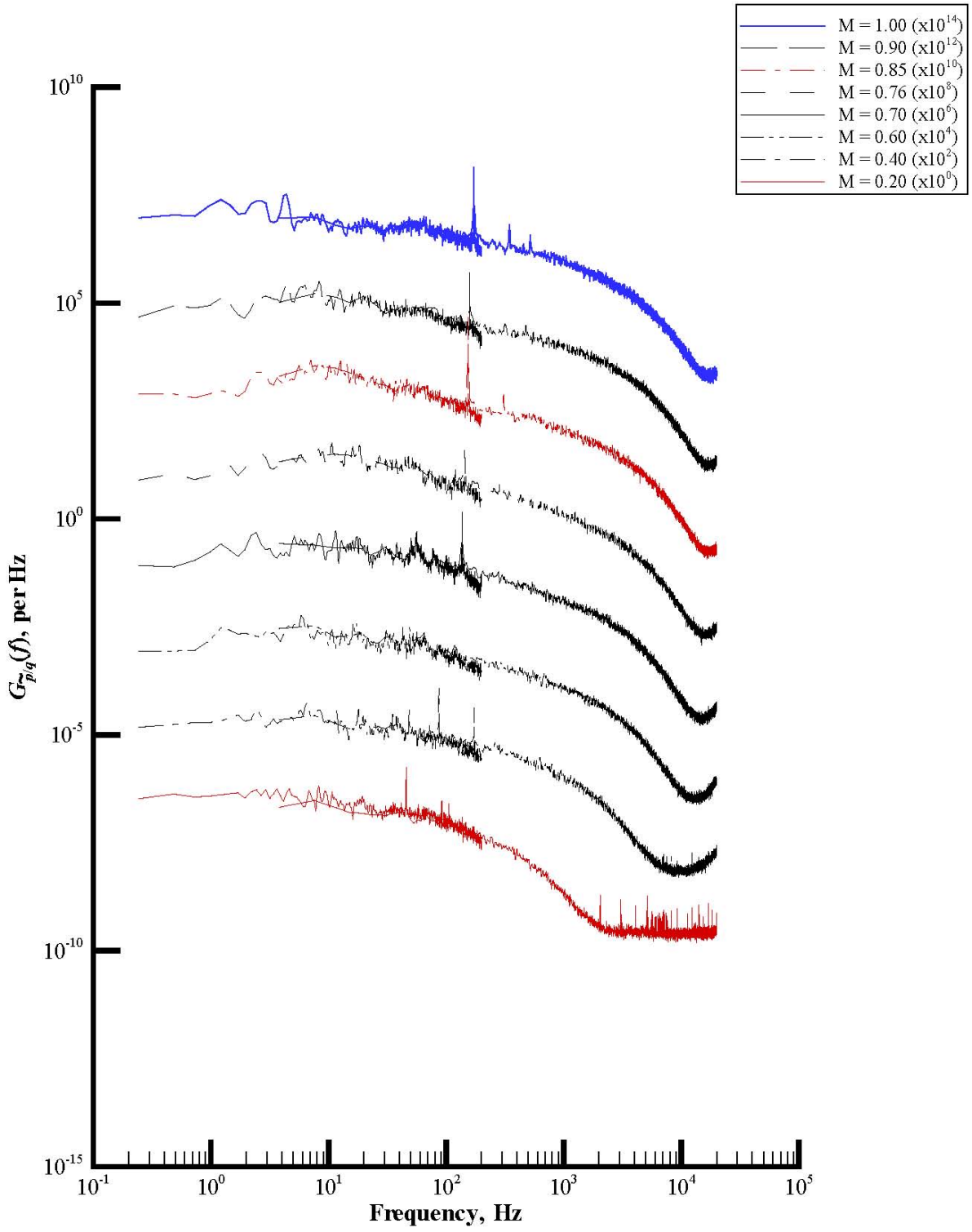
(d) Rake acoustic pressure.

Figure A9. Continued.



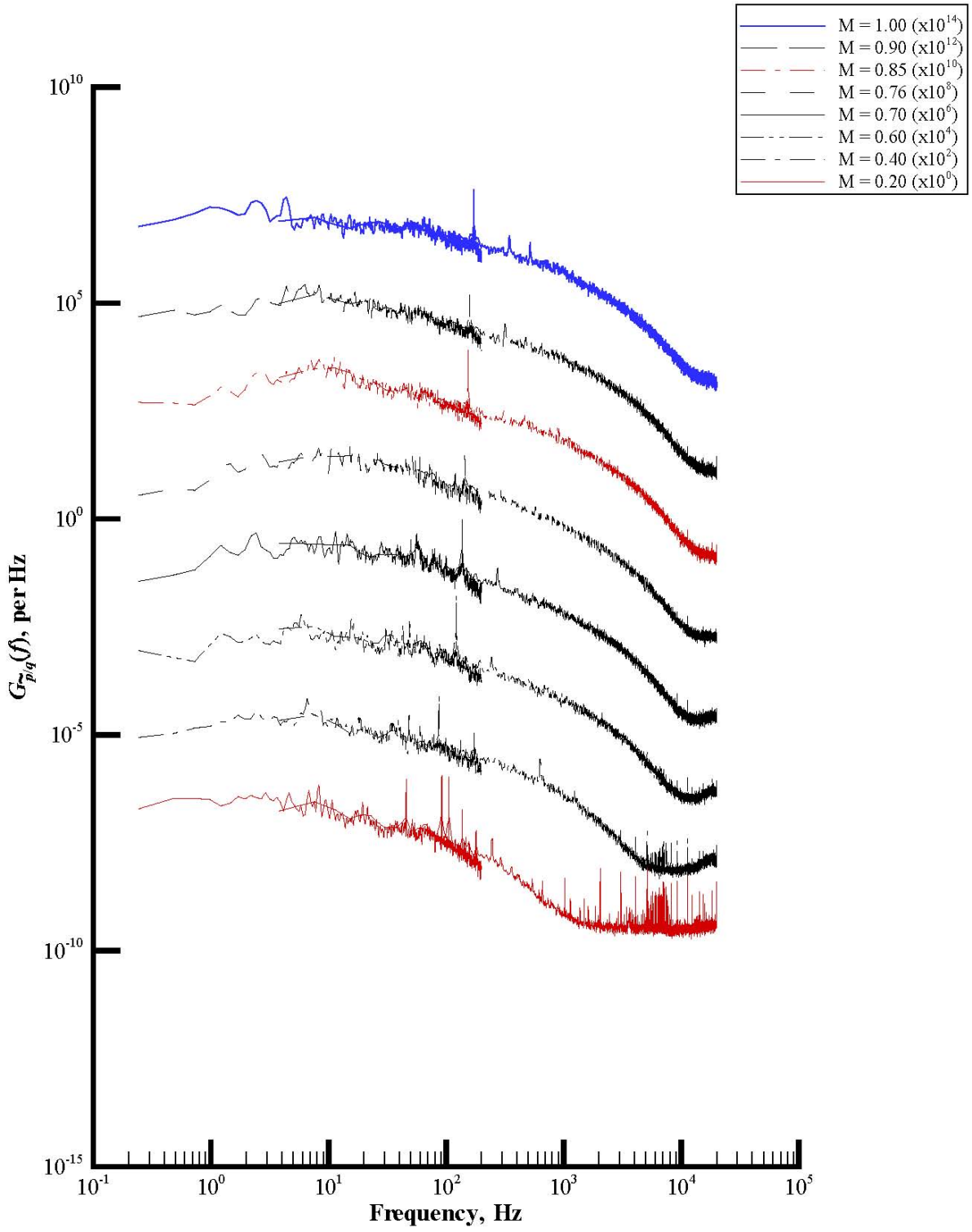
(e) Wall static pressure.

Figure A9. Concluded.



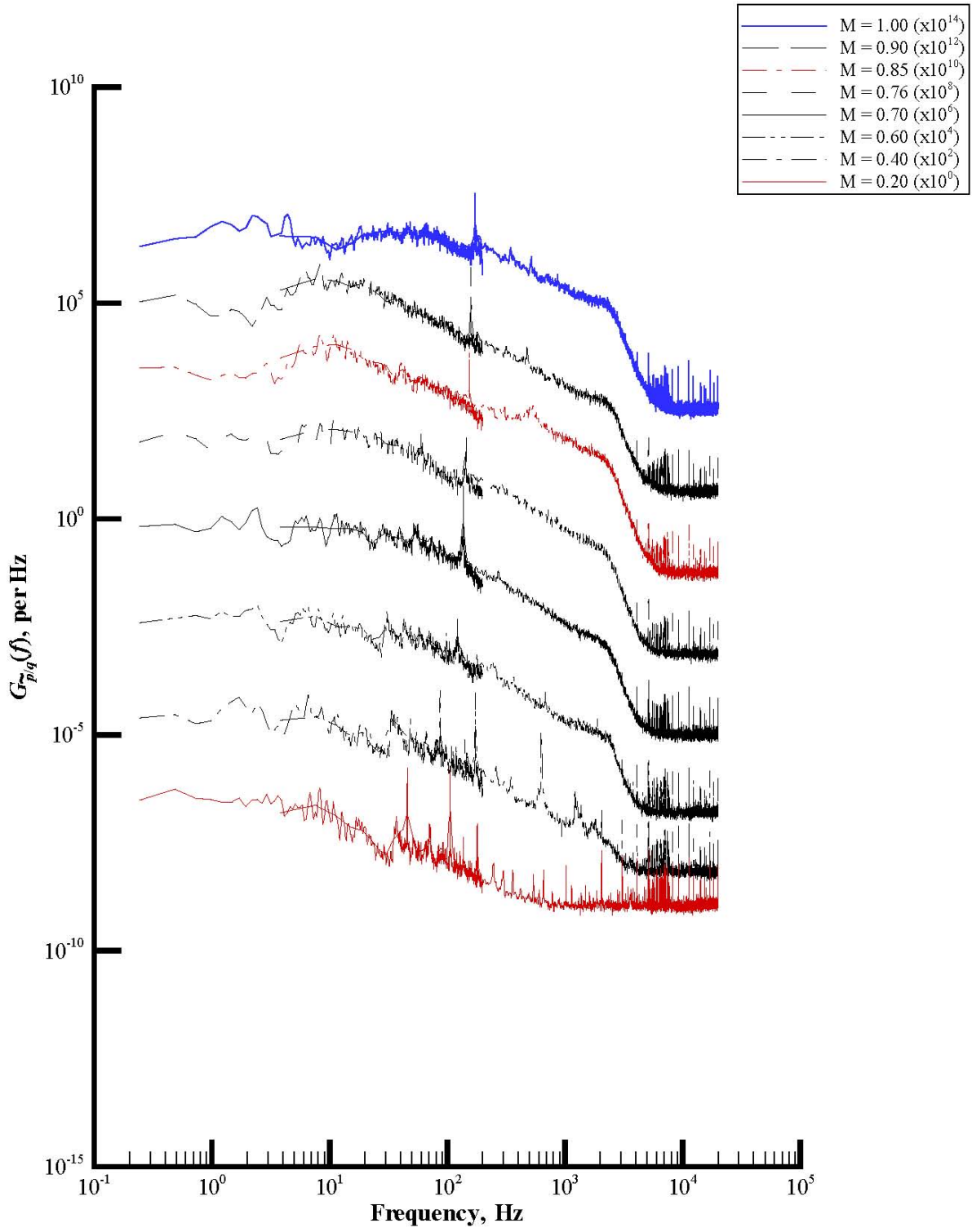
(a) Rake port total pressure.

Figure A10. Extended spectra plots of power spectral density functions of set 10.



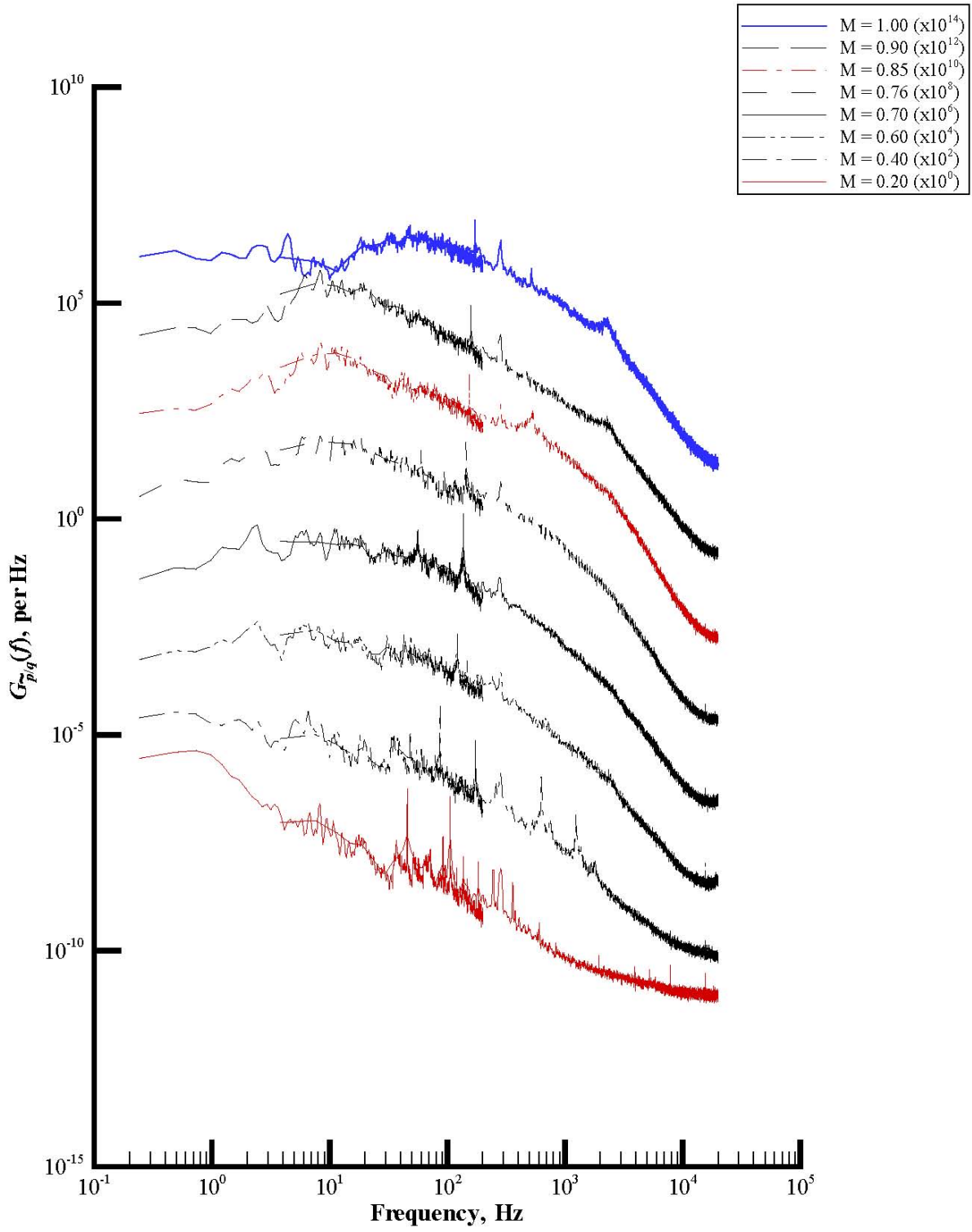
(b) Rake starboard total pressure.

Figure A10. Continued.



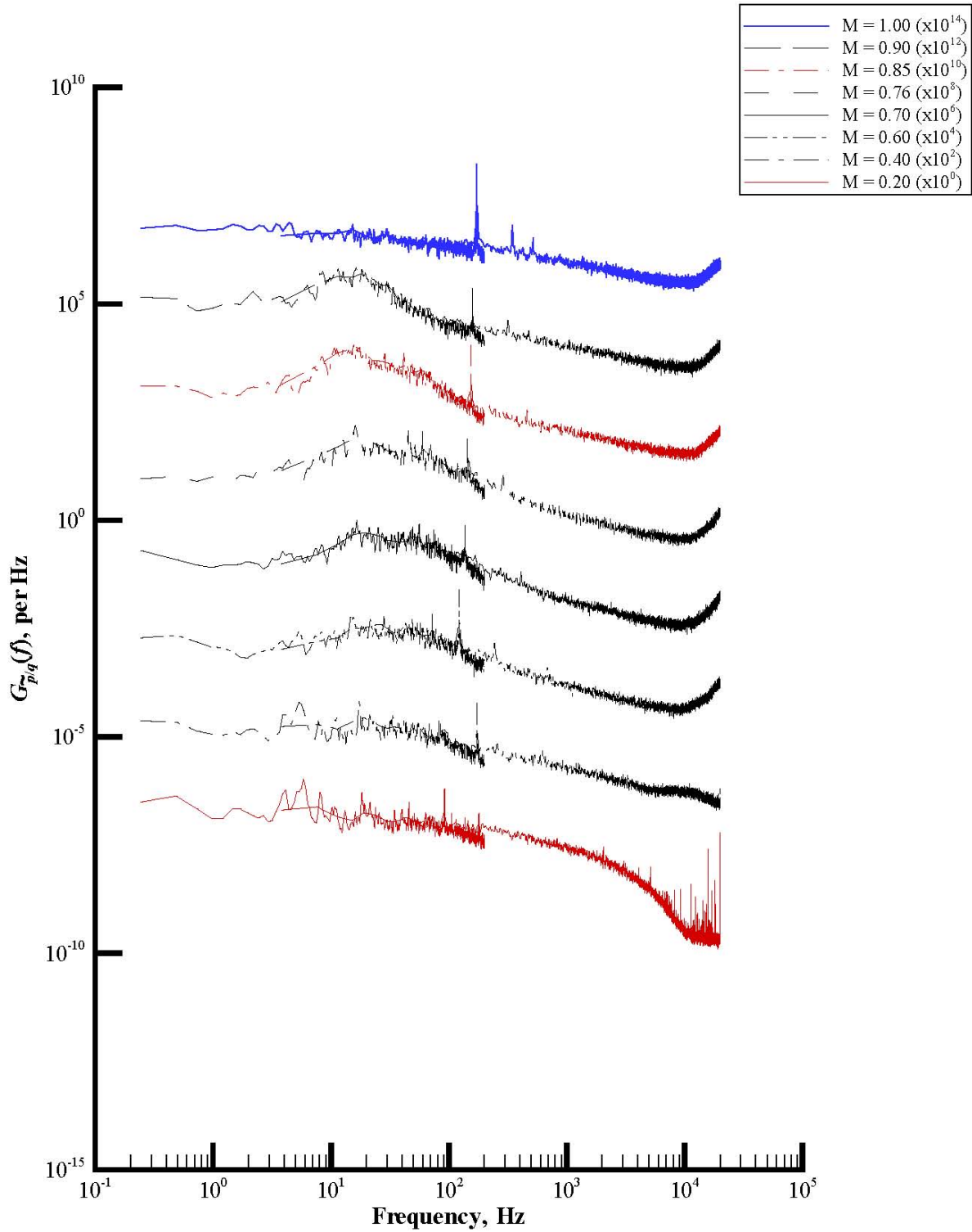
(c) Rake static pressure.

Figure A10. Continued.



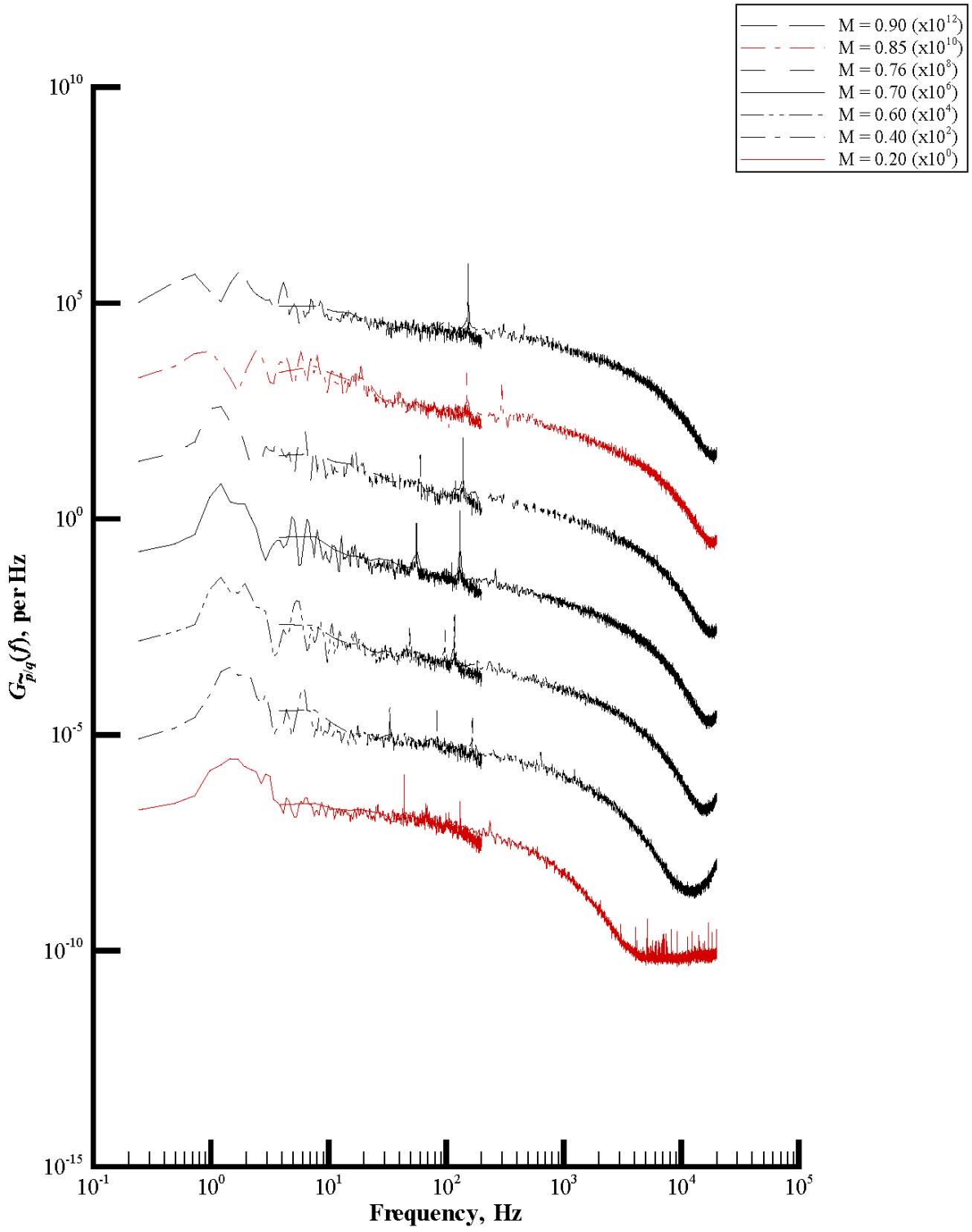
(d) Rake acoustic pressure.

Figure A10. Continued.



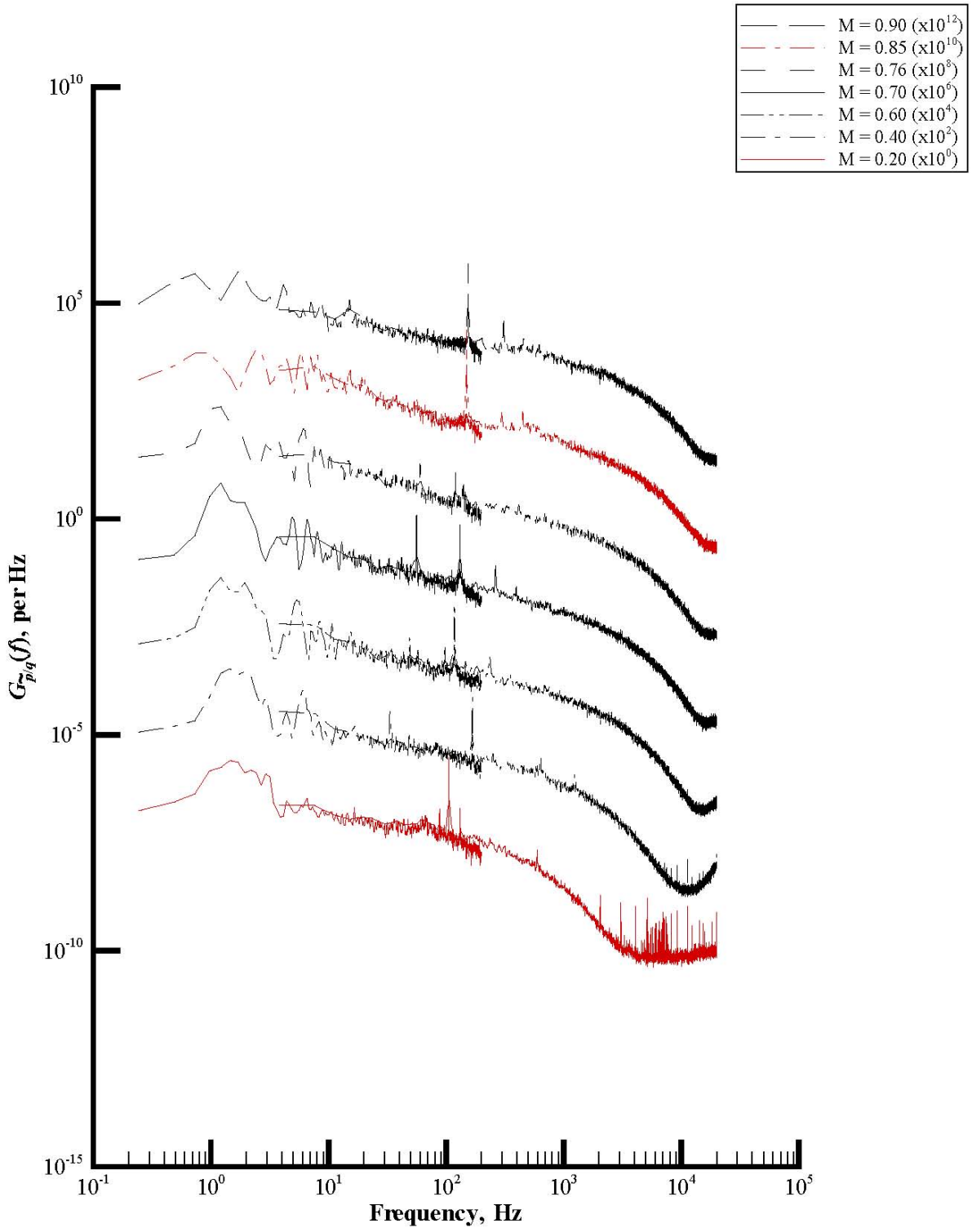
(e) Wall static pressure.

Figure A10. Concluded.



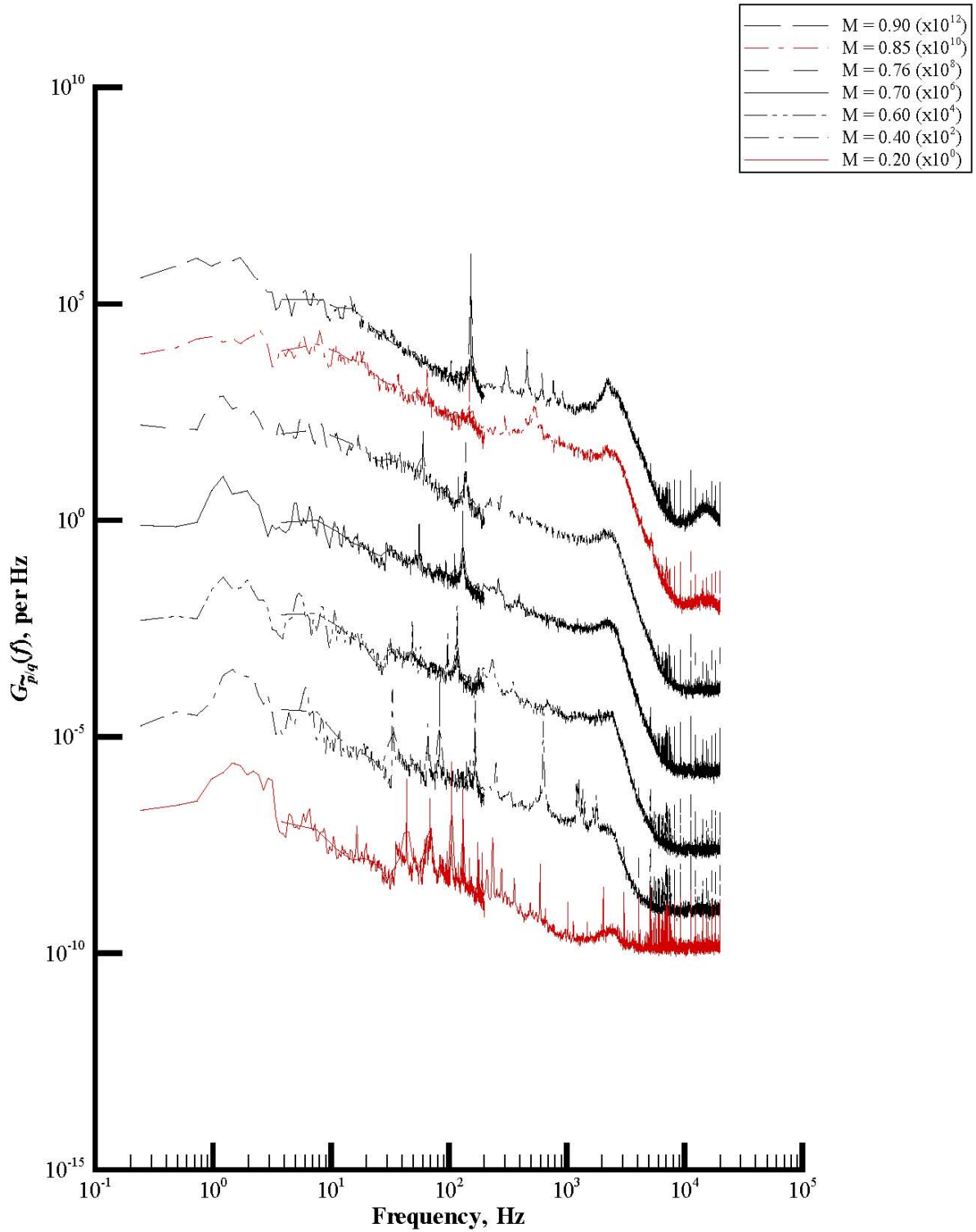
(a) Rake port total pressure.

Figure A11. Extended spectra plots of power spectral density functions of set 11.



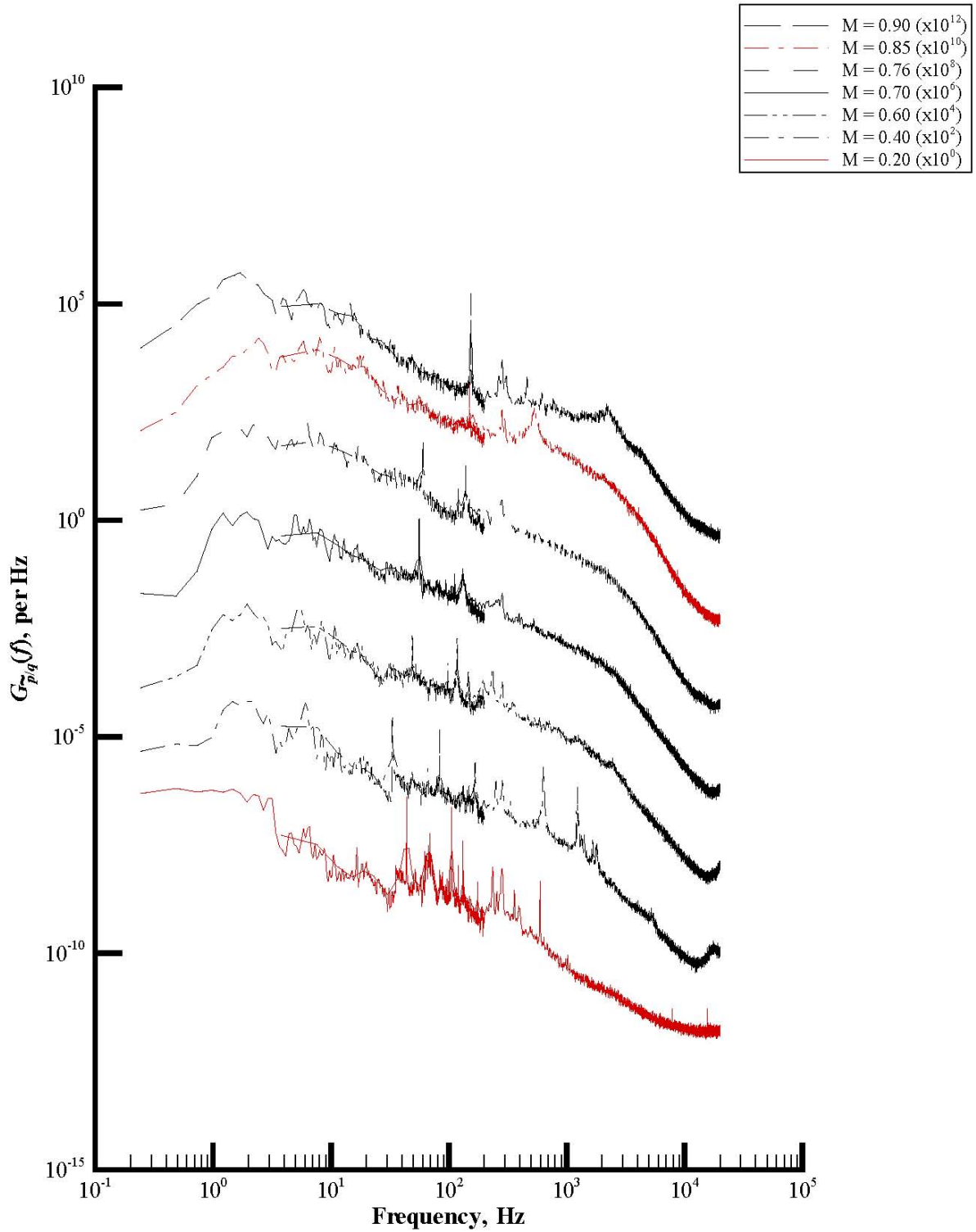
(b) Rake starboard total pressure.

Figure A11. Continued.



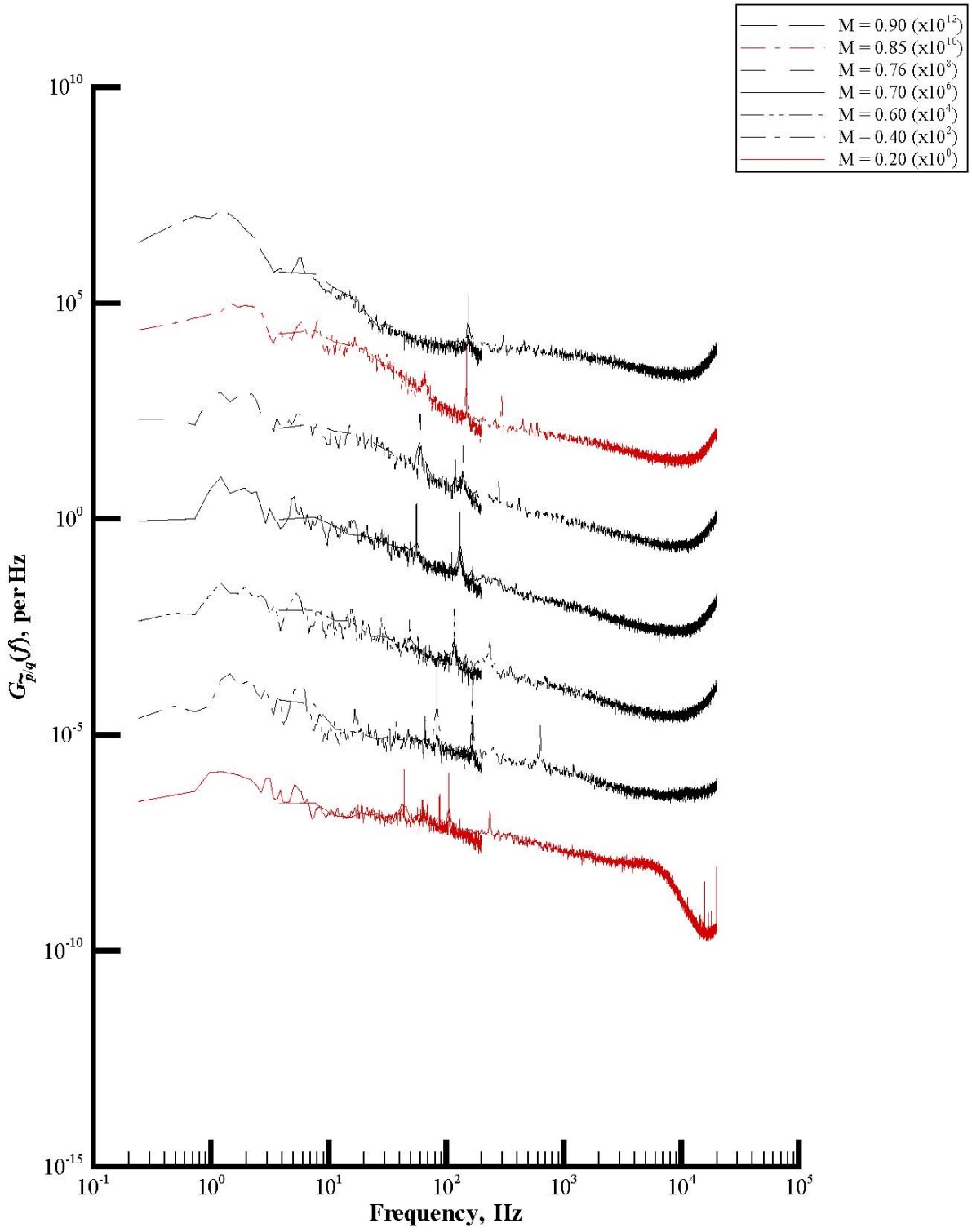
(c) Rake static pressure.

Figure A11. Continued.



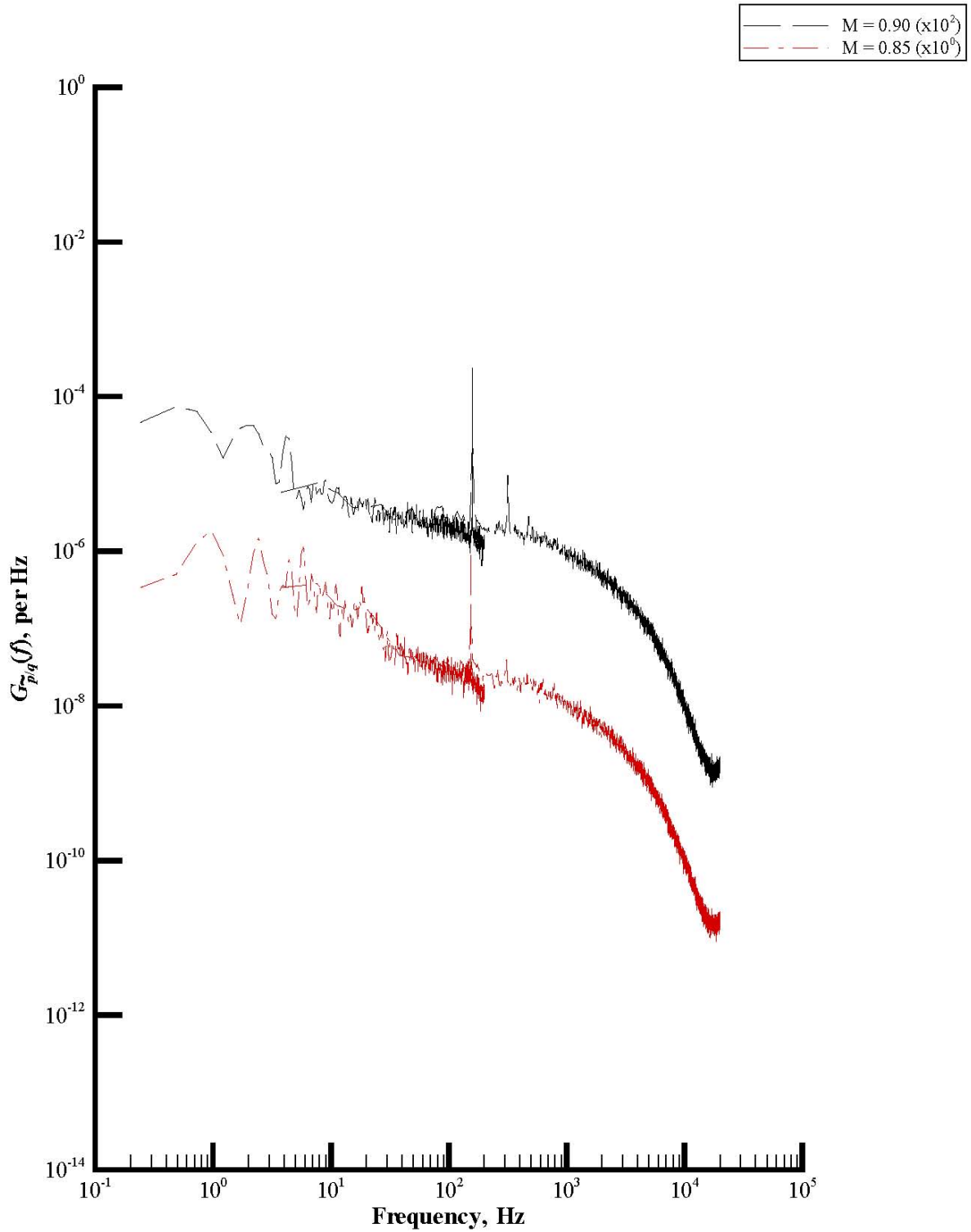
(d) Rake acoustic pressure.

Figure A11. Continued.



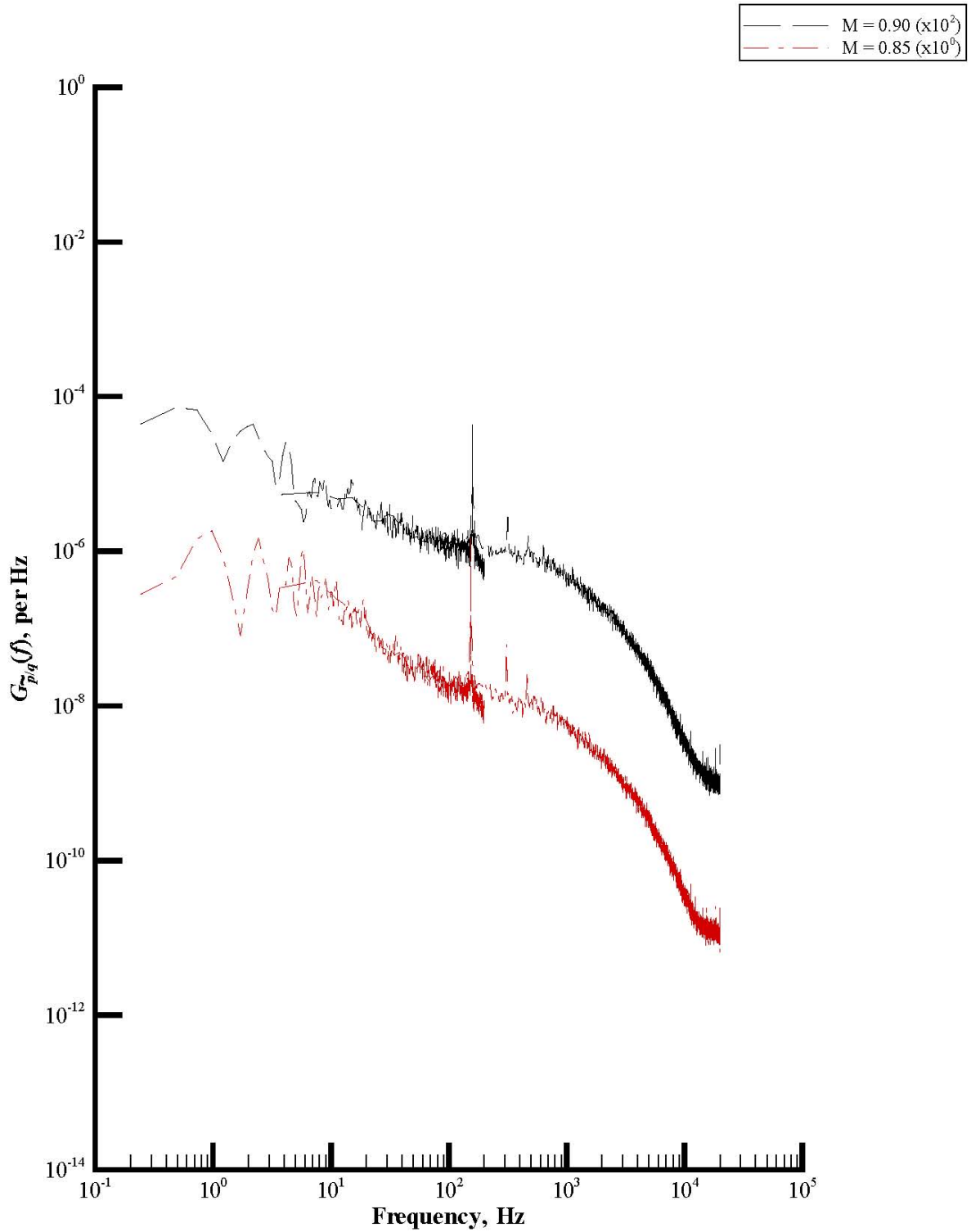
(e) Wall static pressure.

Figure A11. Concluded.



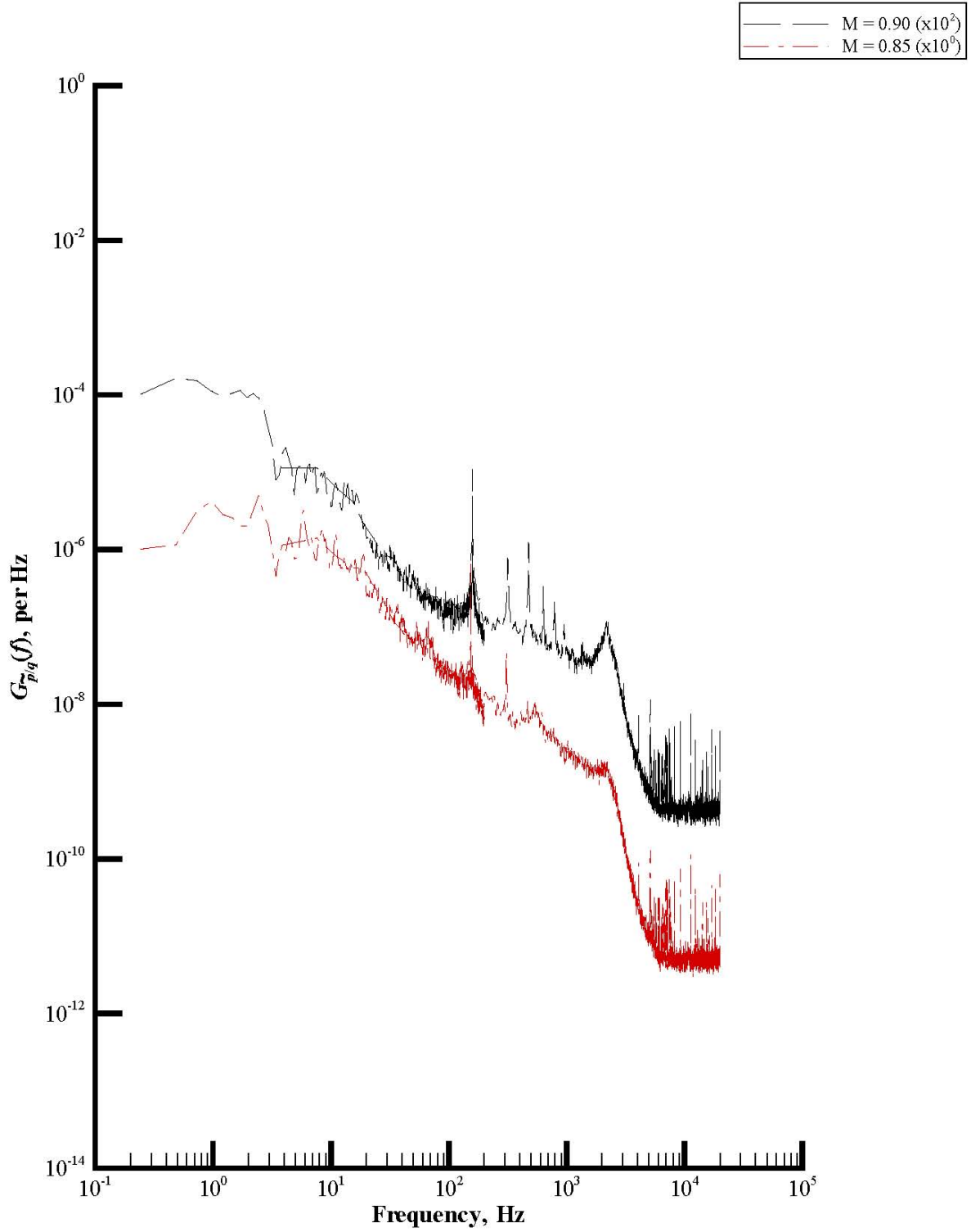
(a) Rake port total pressure.

Figure A12. Extended spectra plots of power spectral density functions of set 12.



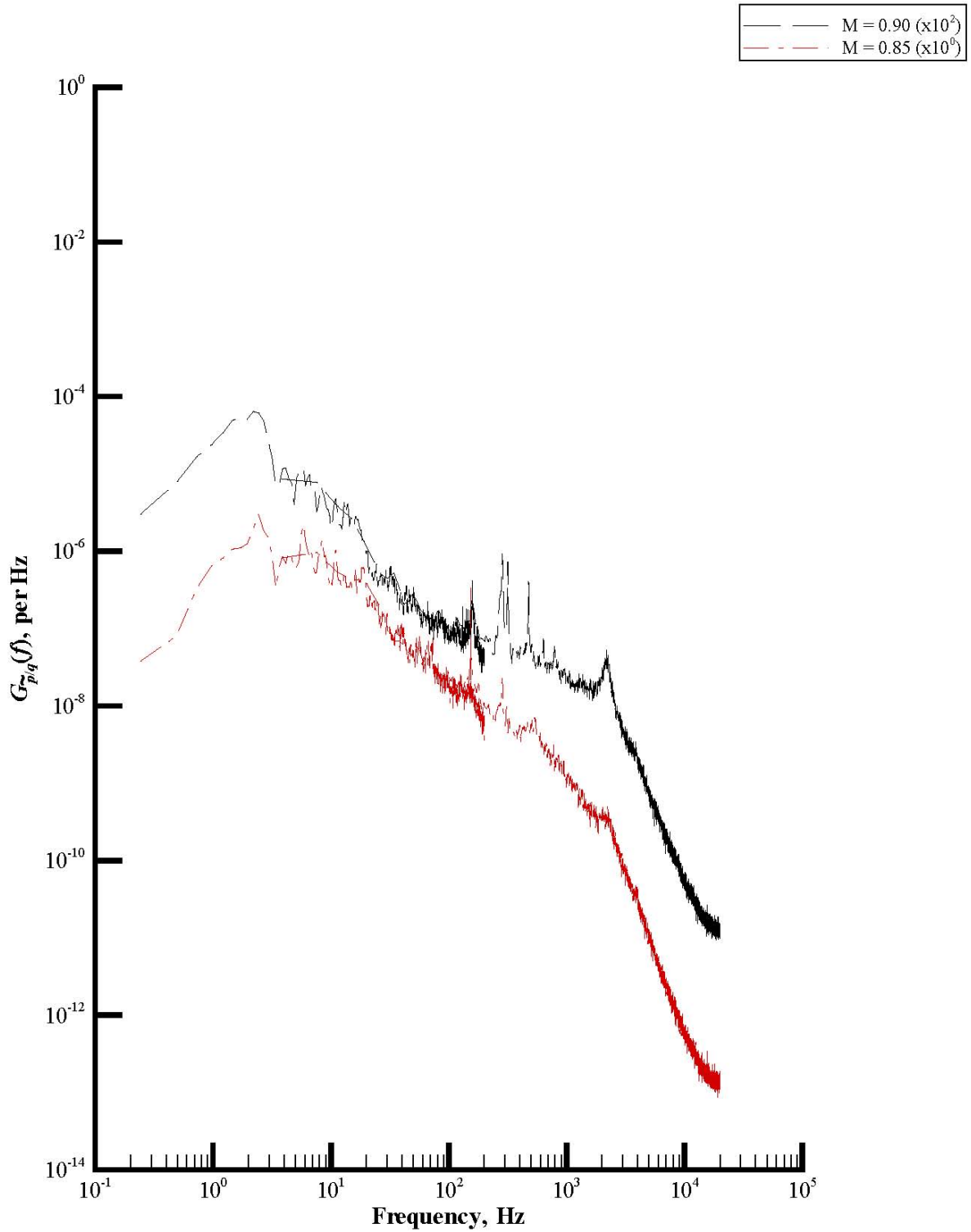
(b) Rake starboard total pressure.

Figure A12. Continued.



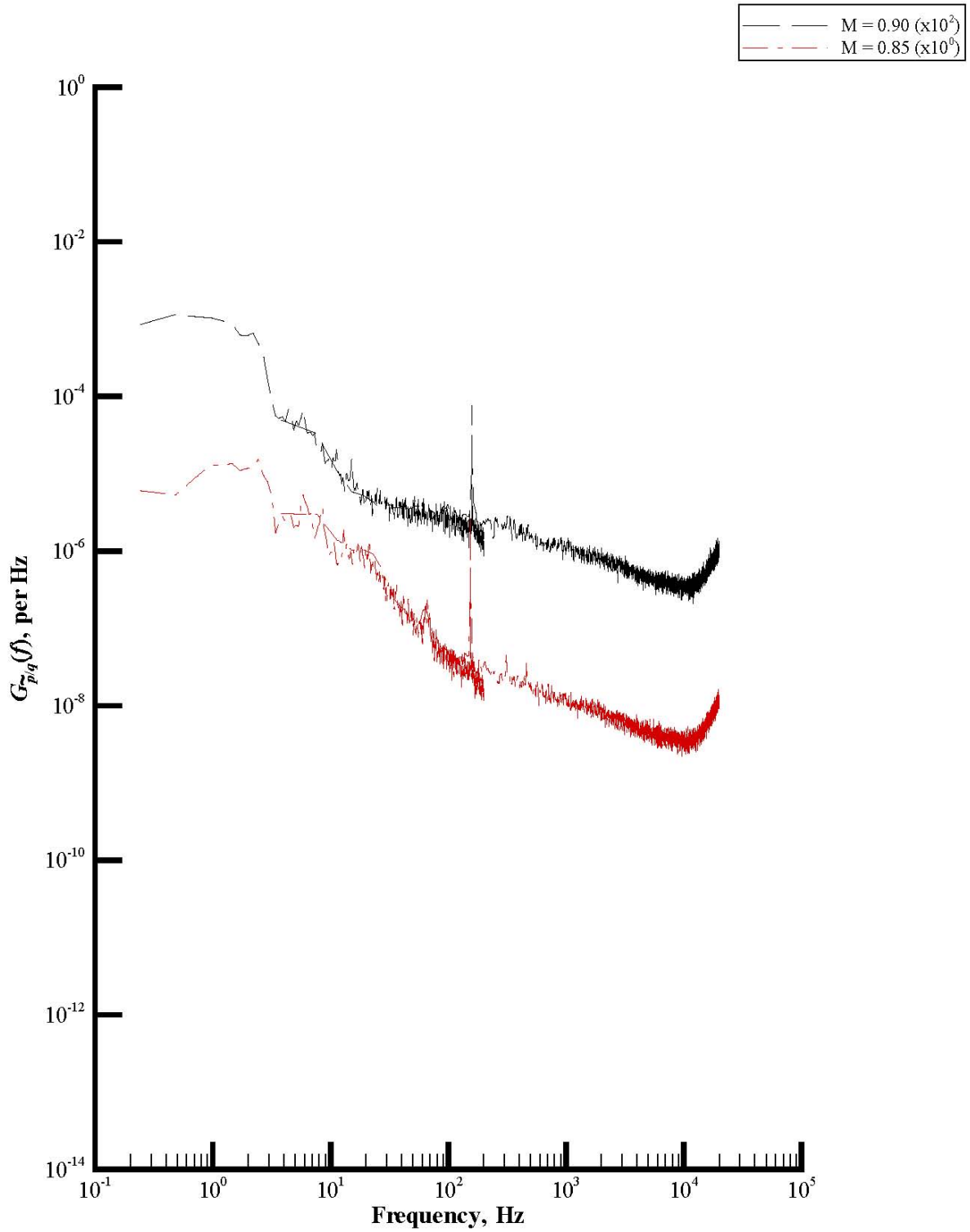
(c) Rake static pressure.

Figure A12. Continued.



(d) Rake acoustic pressure.

Figure A12. Continued.



(e) Wall static pressure.

Figure A12. Concluded.

REPORT DOCUMENTATION PAGE

*Form Approved
OMB No. 0704-0188*

The public reporting burden for this collection of information is estimated to average 1 hour per response, including the time for reviewing instructions, searching existing data sources, gathering and maintaining the data needed, and completing and reviewing the collection of information. Send comments regarding this burden estimate or any other aspect of this collection of information, including suggestions for reducing this burden, to Department of Defense, Washington Headquarters Services, Directorate for Information Operations and Reports (0704-0188), 1215 Jefferson Davis Highway, Suite 1204, Arlington, VA 22202-4302. Respondents should be aware that notwithstanding any other provision of law, no person shall be subject to any penalty for failing to comply with a collection of information if it does not display a currently valid OMB control number.
PLEASE DO NOT RETURN YOUR FORM TO THE ABOVE ADDRESS.

1. REPORT DATE (DD-MM-YYYY) 01- 02 - 2005		2. REPORT TYPE Technical Memorandum		3. DATES COVERED (From - To)	
4. TITLE AND SUBTITLE Measurements of Flow Turbulence in the NASA Langley Transonic Dynamics Tunnel				5a. CONTRACT NUMBER	
				5b. GRANT NUMBER	
				5c. PROGRAM ELEMENT NUMBER	
6. AUTHOR(S) Wieseman, Carol D.; and Sleeper, Robert K.				5d. PROJECT NUMBER	
				5e. TASK NUMBER	
				5f. WORK UNIT NUMBER 23-762-55-MN	
7. PERFORMING ORGANIZATION NAME(S) AND ADDRESS(ES) NASA Langley Research Center Hampton, VA 23681-2199				8. PERFORMING ORGANIZATION REPORT NUMBER L-19024	
9. SPONSORING/MONITORING AGENCY NAME(S) AND ADDRESS(ES) National Aeronautics and Space Administration Washington, DC 20546-0001				10. SPONSOR/MONITOR'S ACRONYM(S) NASA	
				11. SPONSOR/MONITOR'S REPORT NUMBER(S) NASA/TM-2005-213529	
12. DISTRIBUTION/AVAILABILITY STATEMENT Unclassified - Unlimited Subject Category 05 Availability: NASA CASI (301) 621-0390					
13. SUPPLEMENTARY NOTES Wieseman and Sleeper, Langley Reserach Center, Hampton, VA. An electronic version can be found at http://ntrs.nasa.gov					
14. ABSTRACT An assessment of the flow turbulence in the NASA Langley Transonic Dynamics Tunnel (TDT) was conducted during calibration activities following the facility conversion from a Freon-12 heavy-gas test medium to an R134a heavy-gas test medium. Total pressure, static pressure, and acoustic pressure levels were measured at several locations on a sting-mounted rake. The test measured wall static pressures at several locations although this paper presents only those from one location. The test used two data acquisition systems, one sampling at 1000 Hz and the second sampling at 125000 Hz, for acquiring time-domain data. This paper presents standard deviations and power spectral densities of the turbulence points throughout the wind tunnel envelope in air and R134a. The objective of this paper is to present the turbulence characteristics for the test section. No attempt is made to assess the causes of the turbulence. The present paper looks at turbulence in terms of pressure fluctuations. Reference 1 looked at tunnel turbulence in terms of velocity fluctuations.					
15. SUBJECT TERMS Turbulence; Transonic flow; Wind tunnel; Flow quality; Measurements					
16. SECURITY CLASSIFICATION OF:			17. LIMITATION OF ABSTRACT	18. NUMBER OF PAGES	19a. NAME OF RESPONSIBLE PERSON
a. REPORT	b. ABSTRACT	c. THIS PAGE			STI Help Desk (email: help@sti.nasa.gov)
U	U	U	UU	176	19b. TELEPHONE NUMBER (Include area code) (301) 621-0390